

# Testing of multidimensional tectonomagmatic discrimination diagrams on fresh and altered rocks

M. ABDELALY RIVERA-GÓMEZ<sup>1</sup> and SURENDRA P. VERMA<sup>2</sup>✉

<sup>1</sup>Posgrado en Ingeniería, Instituto de Energías Renovables, Universidad Nacional Autónoma de México, Temixco, Mor., 62580, Mexico; marig@ier.unam.mx

<sup>2</sup>Departamento de Sistemas Energéticos, Instituto de Energías Renovables, Universidad Nacional Autónoma de México, Temixco, Mor. 62580, Mexico; spv@ier.unam.mx

(Manuscript received January 18, 2015; accepted in revised form March 10, 2016)

**Abstract:** We evaluated 55 multidimensional diagrams proposed during 2004–2013 for the tectonic discrimination of ultrabasic, basic, intermediate, and acid magmas. The Miocene to Recent rock samples for testing the diagrams had not been used for constructing them. Eighteen test studies (2 from ocean island; 2 from ocean island/continental rift; 6 from continental rift; 4 from continental arc; 2 from island arc; 1 from mid-ocean ridge, and 1 from collision) of relatively fresh rocks fully confirmed the satisfactory functioning of these diagrams for all tectonic fields for which they were proposed. Eight additional case studies on hydrothermally altered or moderately to highly weathered rocks were also presented to achieve further understanding of the functioning of these diagrams. For these rocks as well, the diagrams indicated the expected tectonic setting. We also show that for testing or using these diagrams the freely-available geochemistry databases should be used with caution but certainly after ascertaining the correct magma types to select the appropriate diagram sets. The results encourage us to recommend these diagrams for deciphering the tectonic setting of older terranes or areas with complex or transitional tectonic settings.

**Key words:** tectonic setting, discriminant function diagrams, arc, within-plate, rift, collision.

## Introduction

The idea of trying to chemically fingerprint magmas from different tectonic settings is probably best attributed to the pioneer work of Pearce & Cann (1971, 1973). In these papers, the authors identified differences in the geochemical signature of rocks from volcanic arc, ocean floor, and within-plate settings. Since then, numerous bivariate (x-y-type; e.g. Pearce & Gale 1977; Pearce & Norry 1979; Pearce 1982; Shervais 1982), ternary (e.g. Pearce et al. 1977; Wood 1980; Mullen 1983; Meschede 1986; Cabanis & Lecolle 1989), and old multivariate tectonomagmatic discrimination diagrams (Pearce 1976; Butler & Woronow 1986), as well as 20 new multidimensional diagrams (Agrawal et al. 2004, 2008; Verma et al. 2006; Verma & Agrawal 2011) have appeared in the literature for basic and ultrabasic igneous rocks (with  $(\text{SiO}_2)_{\text{adj}} < 52\%$ ; where the subscript  $\text{adj}$  refers to the adjusted data on an anhydrous 100 % adjusted basis; Le Bas et al. 1986; Verma et al. 2002). The diagrams of the older bivariate or ternary types for the tectonic discrimination of magmas with higher silica (with  $(\text{SiO}_2)_{\text{adj}} > 52\%$ ) are less numerous (Bailey 1981; Pearce et al. 1984; Gorton & Schandl 2000) although, more recently, 35 diagrams have now been proposed (three sets of five diagrams each, i.e., 15 for intermediate magmas by Verma & Verma 2013; and four sets of five diagrams each, i.e., 20 for acid or felsic magmas by Verma et al. 2012, 2013).

From an extensive database of samples from known tectonic settings, Verma (2010) evaluated most of the tectonomagmatic discrimination diagrams for basic and ultrabasic rocks and concluded that only the multidimensional dia-

grams, particularly the newer ones, worked satisfactorily with high percent success (Agrawal et al. 2004, 2008; Verma et al. 2006). Similarly, Verma et al. (2012) evaluated the highly used Pearce et al. (1984) diagrams for acid or felsic magmas and found them to perform unsatisfactorily, particularly for the collision setting.

Although most of the older bivariate and ternary diagrams have already been extensively evaluated, especially by Verma (2010), this is not the case of the newer multidimensional diagrams, particularly those published after 2010 (Verma & Agrawal 2011; Verma et al. 2012, 2013; Verma & Verma 2013). It is, therefore, worthwhile to evaluate all 55 such diagrams (Agrawal et al. 2004, 2008; Verma et al. 2006, 2012, 2013; Verma & Agrawal 2011; Verma & Verma 2013) using geochemical data from fresh as well as hydrothermally altered or highly weathered rocks from known tectonic settings. The evaluation from fresh rock data will provide an independent test on the functioning of these diagrams. The use of hydrothermally altered or weathered rocks for such an independent evaluation will likely render these diagrams appropriate for older terrains. Recently, Pandarinath (2014a) showed good functioning of these diagrams for hydrothermally altered rocks from seven geothermal wells. We will not present here the application to older terrains such as Precambrian belts; this has been extensively reported recently by Verma & Oliveira (2013, 2015), Pandarinath (2014b), Armstrong (2015), Bora & Kumar (2015), Kaur et al. (2015), Rahman & Mondal (2015), Srivastava et al. (2015), and Verma et al. (2015a,b).

This testing exercise is not trivial for at least four reasons: (1) such an evaluation of the older x-y (where x and y are

simple concentration or element ratio variables) or ternary (generally of three concentration variables) types of diagrams has shown them to perform unsatisfactorily in both igneous and sedimentary rock geochemistry (Armstrong-Altrin & Verma 2005; Verma 2010, 2015a; Verma et al. 2012, 2016; Verma & Armstrong-Altrin 2013, 2016; Armstrong, 2015); (2) the evaluation of the newer multidimensional diagrams can provide statistical information on percent success for the relatively older diagrams (proposed during 2004–2011) and total percent probability values for the newer ones (proposed during 2012–2013); and (3) a routine use of well-known databases, such as GERM, GEOROC-Mainz, and EGDB-USGS, for testing of our diagrams is to be viewed with caution.

### Available multidimensional diagrams

These diagrams were proposed from statistical analysis of a large number of Miocene to Recent igneous rock samples from known tectonic settings. Thus, for the tectonic discrimination of basic and ultrabasic rocks from island arc, continental rift, ocean island, and mid-ocean ridge settings, Agrawal et al. (2004, 2008), Verma et al. (2006), and Verma & Agrawal (2011) used geochemical data for 1159, 1645, 2732, and 1877 samples, respectively, and proposed 5 diagrams in each paper. Verma et al. (2012) proposed 5 diagrams for the discrimination of four tectonic settings (island arc, continental arc, combined continental rift and ocean island as within-plate, and collision) from a compilation of 1132 acid rock samples. Similarly, for the proposal of the 15 diagrams each, Verma et al. (2013) and Verma & Verma (2013) employed compositional data for 3056 acid and 3664 intermediate rock samples, respectively, from island arc, continental arc, continental rift, ocean island, and collision tectonic settings.

The diagrams require prior calculations of complex discriminant functions DF1–DF2, whose equations were presented by the respective original authors (Agrawal et al. 2004, 2008; Verma et al. 2006, 2012, 2013; Verma & Agrawal 2011; Verma & Verma 2013). All these equations were also summarized recently by Verma et al. (2015b), which are reproduced here for easy reference as Tables S1–S11 in the Supplementary Material file\* (Table S1 for five diagrams of Agrawal et al. 2004; Table S2 for five diagrams of Verma et al. 2006; Table S3 for five diagrams of Agrawal et al. 2008; Table S4 for five diagrams of Verma & Agrawal 2011; Tables S5–S7 for 15 diagrams of Verma & Verma 2013; Table S8 for five diagrams of Verma et al. 2012; and Tables S9–S11 for 15 diagrams of Verma et al. 2013). The computer program SINCLAS (Verma et al. 2002) or IgRoCS (Verma & Rivera-Gómez 2013a) can be used for obtaining the adjusted data referred to in these equations (see the subscript <sub>adj</sub>) and deciding the magma types (basic, ultrabasic, intermediate, and acid; Le Bas et al. 1986).

We also note that these different sets of diagrams are independent of each other although they require complete datasets for all elements in the respective DF1–DF2 functions. For example, the major element based diagrams would

require that concentrations of all major elements be available in a given sample; if an element is missing from the data, the set of major-element diagrams cannot be used. Unfortunately, sometimes only major elements are available from a particular area, so the inference can be drawn only from one set of diagrams. Thus, any set of diagrams can be used independently of the other sets.

### Database and procedures

The geochemical data were compiled for 1034 samples of Miocene to Holocene relatively fresh as well as hydrothermally altered or weathered igneous rocks from different areas of known, uncontroversial tectonic settings from all over the world (Fig. S1 in the Supplementary Material file; compiled references are in Tables S12 and S13). A synthesis of this compilation for 18 test studies (1 to 18) from fresh rocks is presented in Table S12 and for hydrothermally altered or weathered rocks for 8 application studies (A1 to A8) is provided in Table S13. The cases are arranged according to the expected tectonic setting. The original authors' descriptions of alteration were used to group the samples in application studies as fresh and altered rocks; more details are provided in the relevant sections.

The geochemical data were also examined for the Tonga arc compiled in a freely-available geochemistry database GEOROC-Mainz, which enabled us to show the need for caution in the indiscriminate use of such databases.

We will describe in detail the first Test study under the general heading of "Ocean Island tectonic setting". This (Test study 1) is for the region of the Hawaiian Islands, in which four sub-regions (1a–1d) are separately considered because we wanted to show that these diagrams can be applied and tested with individual datasets. Obviously, if the main objective was to decipher the tectonic setting of a given area or region, all pertinent rock data or evidence should be used. This obviously includes the geological reconstruction of terranes. The approximate coordinates (longitude and latitude) of sample locations are then presented in two columns. The next columns present a subdivision of the compiled samples in terms of basic (B)+ultrabasic (U), intermediate (I), and acid (A) magmas, which allowed the application of appropriate sets of discrimination diagrams (Agrawal et al. 2004, 2008; Verma et al. 2006; Verma & Agrawal 2011 — all these four papers for basic and ultrabasic magmas; Verma & Verma 2013 — for intermediate magmas; and Verma et al. 2012, 2013 — for acid magmas). Thus, for the Mauna Kea area (Test study 1a), complete data were available for 303 basic and 3 ultrabasic rock samples only; no sample proved to be of intermediate or acid magma. Therefore, only diagrams for basic and ultrabasic rocks can be applied and that too for major element based (symbol m1 for Agrawal et al. 2004 and m2 for Verma et al. 2006) and immobile trace element based (symbol t2 for Verma and Agrawal 2011) diagrams; complete data were not available for the other immobile element based diagram set (t1 for Agrawal et al. 2008). Note the table is or tables are also defined where the results of the discrimination diagrams are presented (in this

\* Supplementary Material (Tables S1–S54 and Figs. S1–S52) only in an electronical version on [www.geologicacarpathica.com](http://www.geologicacarpathica.com)

case, Table 1). The next columns show the approximate ages in Ma (or geological epoch or period) and rock types assigned by the original authors (in this case, 0.1–0.4 Ma). The next column synthesizes the tectonic setting indicated by the diagrams (in this case, OIB). The final column lists the references from which the data were compiled (in this case, Rhodes & Vollinger 2004; Rhodes 2012).

For a correct application of the tectonomagmatic discrimination diagrams, the IgRoCS program (Verma & Rivera-Gómez 2013a) was used to obtain the magma types as basic or ultrabasic, intermediate, and acid, following the recommendations of the IUGS (Le Bas et al. 1986; Le Bas & Streckeisen 1991; Le Maitre et al. 2002). It is important to strictly follow the procedure used by the original authors of the diagrams, for example, note the subscript adj in numerous equations listed in Tables S1–S11. These magma names could as well be mafic or ultramafic, intermediate, and felsic, respectively, but because we are using the chemical criterion of adjusted SiO<sub>2</sub> for this distinction and not the contents of Mg, Fe, and Si, we continue to use the nomenclature of the IUGS. Depending on the magma types, appropriate sets of diagrams were used to test if they provided the expected results of the tectonic setting.

To infer the tectonic setting for basic and ultrabasic magmas, we used the software TecD (Verma & Rivera-Gómez 2013b), which allows the application of the diagrams by

Agrawal et al. (2004, 2008), Verma et al. (2006), and Verma & Agrawal (2011). The four tectonic settings that can be discriminated from the diagrams contained in this software are as follows: IAB (island arc basic rocks), CRB (continental rift basic rocks), OIB (ocean-island basic rocks), and MORB (mid-ocean ridge basic rocks). TecD automatically counts the samples that plot in a given tectonic setting and provides a synthesis of the counting results of all five diagrams of a given set, both as the number of samples as well as the corresponding percentage values (called percent success for the expected or inferred tectonic setting). Because a given tectonic setting will be missing from one of the five diagrams in any set, the total percentage for any of the four settings will never be 100 %; it will be around 80 % as a maximum value. Further, because of this automatic procedure programmed in TecD, it is not necessary to actually plot the samples in diagrams. Nevertheless, following the suggestion of reviewers we provided the corresponding diagrams for almost all studies, so one can better understand the functioning of TecD.

Another program TecDIA (Verma et al. 2015c) was used for the application of all diagrams for intermediate (Verma & Verma 2013) and acid magmas (Verma et al. 2012, 2013). TecDIA also computes the probabilities of samples for the different tectonic settings and provides a synthesis of these probability values. The tectonic settings that can be discriminated from the diagrams for intermediate and acid magmas

**Table 1:** Testing of multidimensional diagrams from Quaternary (0.1–0.4 Ma) basic and ultrabasic rocks of Mauna Kea, Hawaii (Rhodes and Vollinger, 2004; Rhodes et al. 2012; Test study 1a).

Figure reference; figure type	Discrimination diagram	Total no. of samples (%)	Predicted tectonic affinity and number of discriminated samples (%)				
			IAB	CRB+OIB	CRB	OIB	MORB
Agrawal et al. (2004); adjusted major element concentrations	IAB-CRB-OIB-MORB	306 (100)	0 (0)	---	0 (0)	306 (100)	0 (0)
	IAB-CRB-OIB	306 (100)	0 (0)	---	0 (0)	306 (100)	---
	IAB-CRB-MORB	306 (100)	0 (0)	---	217 (70.9)	---	89 (29.1)
	IAB-OIB-MORB	306 (100)	0 (0)	---	---	306 (100)	0 (0)
	CRB-OIB-MORB	306 (100)	---	---	0 (0)	306 (100)	0 (0)
<i>Test study 1a. Synthesis of all five diagrams of Agrawal et al. (2004)</i>		<b>1530 (100)</b>	<b>0 (0)</b>	---	<b>217 (14.2)</b>	<b>1224 (80.0)</b>	<b>89 (5.8)</b>
Verma et al. (2006); log-ratios of major elements	IAB-CRB-OIB-MORB	306 (100)	0 (0)	---	4 (1.3)	300 (98)	2 (0.7)
	IAB-CRB-OIB	306 (100)	0 (0)	---	0 (0)	306 (100)	---
	IAB-CRB-MORB	306 (100)	0 (0)	---	36 (11.8)	---	270 (88.2)
	IAB-OIB-MORB	306 (100)	0 (0)	---	---	306 (100)	0 (0)
	CRB-OIB-MORB	306 (100)	---	---	0 (0)	306 (100)	0 (0)
<i>Test study 1a. Synthesis of all five diagrams of Verma et al. (2006)</i>		<b>1530 (100)</b>	<b>0 (0)</b>	---	<b>40 (2.6)</b>	<b>1218 (79.6)</b>	<b>272 (17.8)</b>
Verma and Agrawal (2011); log-ratios of immobile major and trace elements	IAB-CRB+OIB-MORB	306 (100)	2 (0.7)	303 (99)	---	---	1 (0.3)
	IAB-CRB-OIB	306 (100)	3 (1)	---	1 (0.3)	302 (98.7)	---
	IAB-CRB-MORB	306 (100)	2 (0.7)	---	303 (99)	---	1 (0.3)
	IAB-OIB-MORB	306 (100)	2 (0.7)	---	---	303 (99)	1 (0.3)
	CRB-OIB-MORB	306 (100)	---	---	1 (0.3)	303 (99)	2 (0.7)
<i>Test study 1a. Synthesis of all five diagrams of Verma and Agrawal (2011)</i>		<b>1530 (100)</b>	<b>9 (0.6)</b>	<b>303 (---)</b>	<b>381 (24.9)</b>	<b>1135 (74.2)</b>	<b>5(0.3)</b>

IAB- island (or continental) arc basic rock; CRB- continental rift basic rock; OIB- ocean island basic rock; MORB- mid-ocean ridge basic rock; CRB+OIB- combined continental rift and ocean island, i.e., within-plate (WP) basic rocks; IA, CR, OI, and MOR will be the corresponding tectonic settings; --- means no samples; the numbers within the parentheses refer to the percent values for the corresponding number of samples; note, for the calculations of percent synthesis values, the samples plotting in the combined CR+OI field (CRB+OIB column) are proportionately distributed between the CR and OI settings.

are as follows: IA (island arc), CA (continental Arc), CR (continental rift) and OI (Ocean Island) together as within-plate, and Col (collision). As for TecD, TecDIA also provides a complete synthesis of the results of all five diagrams in a given set. In fact, TecDIA additionally gives a synthesis of the probability estimates for each tectonic setting in all diagrams as well as the overall percent probability estimates of each diagram set. Therefore, actual plotting of samples in any diagram is really not required. Nevertheless, we also present one example of all diagram types for intermediate and acid magmas (Verma & Verma 2013; Verma et al. 2012, 2013).

## Results and discussion

The results of the evaluation are presented in two subsections. The first part corresponds to relatively fresh rocks from known tectonic settings, whereas the second part shows the results for hydrothermally altered and weathered rocks. A lower limit of five samples with complete data for a given diagram set was arbitrarily established for using them for testing or application purposes. Similarly, results are also presented even if the data were available for only one or two sets of diagrams because the evaluation is independently achieved for all diagram sets.

### *Testing of the diagrams from “fresh” volcanic rocks of ocean island tectonic settings*

The first test study of the Hawaiian Islands will be described in greater detail. All other studies will simply be mentioned with the statistical information in order to keep the paper short and avoid excessive repetition.

#### *Test study 1a: Mauna Kea*

For the Mauna Kea area, 303 samples of basic and 3 ultrabasic rocks (Table S12; Rhodes and Vollinger 2004; Rhodes 2012) had complete dataset for major-element based diagrams of Agrawal et al. (2004) and Verma et al. (2006) and for only one set of immobile trace element based diagrams (Verma & Agrawal 2011). No samples had complete data for the other set of immobile trace element based diagrams (Agrawal et al. 2008), which could not be used. Similarly, none of the diagrams for intermediate and acid rocks (Verma & Verma 2013; Verma et al. 2012, 2013) could be used for this case because no samples proved to be of these types (missing data shown by — in the “I” and “A” columns in Table S12).

Thus, three sets of diagrams (Agrawal et al. 2004; Verma et al. 2006; Verma & Agrawal 2011) could be tested from the Mauna Kea data; and the results are shown in Table 1. The actual diagrams of Agrawal et al. (2004) for the Mauna Kea samples do not really need to be shown for three reasons: (i) these diagrams are based on only major element concentrations and not on log-ratios; (ii) TecD provides complete summary of all the plots (the first part of Table 1); and (iii) we wanted to conserve journal space by presenting only one set of diagrams based on log-ratios (Fig. 1) in the

main part of the paper. Nevertheless, for the sake of completeness and considering that most readers of the journal would like to see the diagrams along with the synthesis in tables, we have added these diagrams (Figs. S2 and S3 for this case study as well as in other figures for other case studies) in the Supplementary file.

In the first set of five diagrams (Fig. S2), all Mauna Kea samples plotted in the OIB fields in four of the five diagrams in which this setting is present. In the diagram (IAB-CRB-MORB) from which OIB is absent, the samples will plot in any other fields; in this case, most of them plotted in the CRB field, followed by the MORB field (Table 1). The synthesis of all diagrams is then presented in Table 1, which shows that the overall percent success for the OIB setting is 80.0 % being the maximum value for such a synthesis provided by TecD. Therefore, these diagrams clearly showed the expected OIB setting for the Mauna Kea samples.

In the other set of diagrams based on log-ratios of major elements (Verma et al. 2006), the Mauna Kea samples are actually plotted in Fig. 1a-e (DF1-DF2 equations from Table S2 were used for the calculations of the x and y coordinates in each diagram) and the results from TecD are also summarized in Table 1. In the first diagram (Fig. 1a), 300 (out of 306) samples plotted in the OIB field, whereas in the other three diagrams (Fig. 1b,d,e) all samples plotted in the OIB field. In the diagram from which the OIB field is missing (Fig. 1c), the samples plotted in the MORB and CRB fields. The overall synthesis of all five diagrams of Verma et al. (2006) also showed a clear result of the OIB tectonic setting with the percent success of 79.6 % (Table 1), very close to the maximum value of 80 %.

Finally, the set of diagrams based on log-ratios of immobile elements (Verma & Agrawal 2011) also showed an OIB setting for the Mauna Kea samples with the percent success of about 74.2 % (Fig. S3; Table 1). In this diagram set, the first diagram has a combined CRB+OIB setting, only three diagrams have an OIB setting, and from one diagram this setting is totally missing. Therefore, the percent success for the OIB can seldom reach the maximum value of 80 %.

Thus, a satisfactory functioning of all three diagram sets for the OIB setting was confirmed from the Mauna Kea data (Test study 1a).

#### *Test study 1b: Mauna Loa*

Forty-five (43 basic and 2 ultrabasic) samples from Mauna Loa (Table S12; Rhodes & Vollinger 2004) allowed the testing of three sets of diagrams. Most of the samples plotted in the OIB field in the three sets for major elements (two sets for basic rocks as Figs. S4 and S5 and one set for acid rocks as Fig. S6; percent success amounting to about 75–76 %; Table S14), thus confirming the good functioning of all three sets of diagrams for the OIB setting.

#### *Test study 1c: Maui Island*

Only 10 basic rock samples available from the Maui Island (Table S12; Sherrod et al. 2007) allowed the testing of three sets of diagrams. Most of the samples plotted in the OIB field in the three sets (overall percent success of about

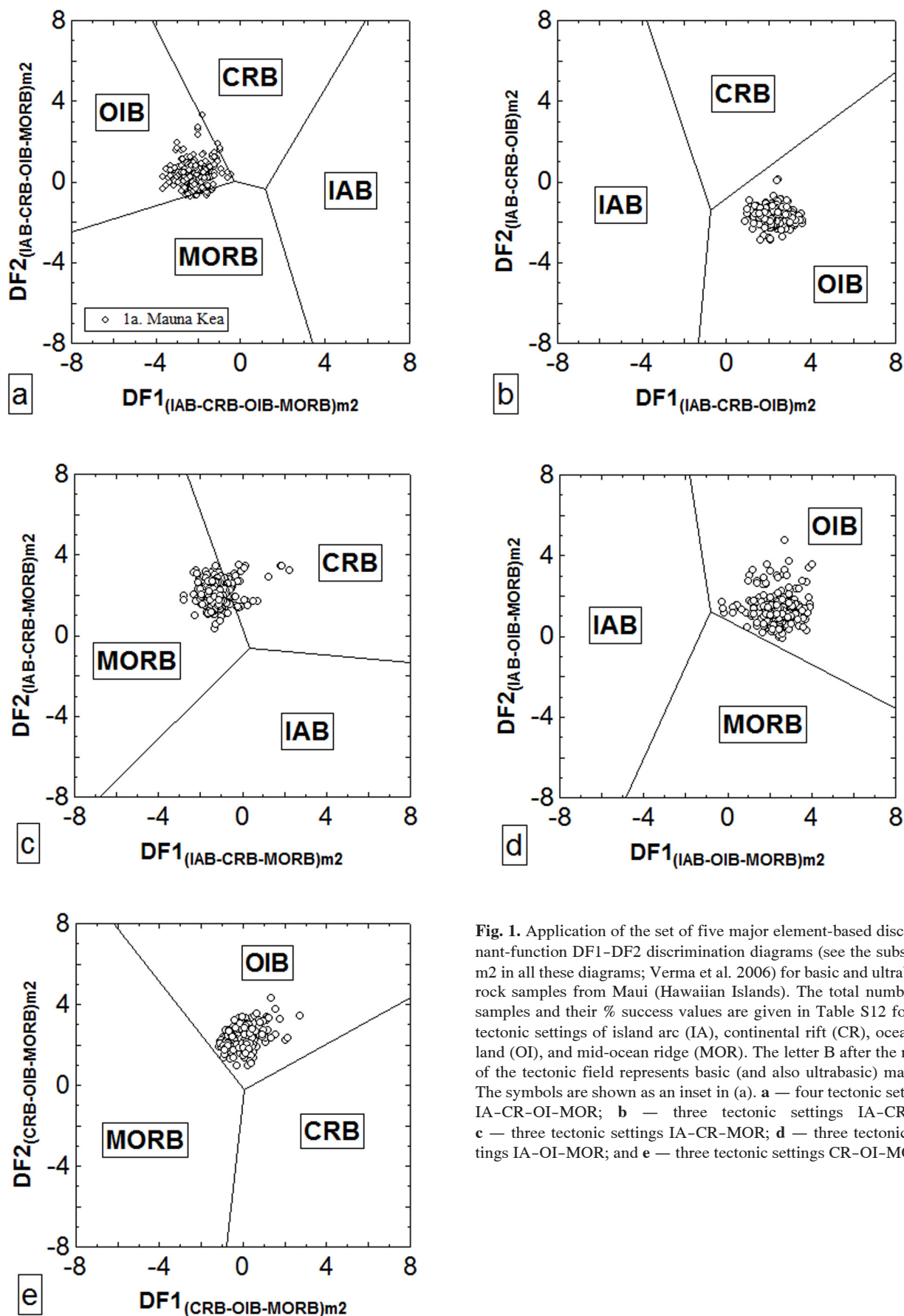


**Fig. 1.** Application of the set of five major element-based discriminant-function DF1-DF2 discrimination diagrams (see the subscript m2 in all these diagrams; Verma et al. 2006) for basic and ultrabasic rock samples from Maui (Hawaiian Islands). The total number of samples and their % success values are given in Table S12 for the tectonic settings of island arc (IA), continental rift (CR), ocean island (OI), and mid-ocean ridge (MOR). The letter B after the name of the tectonic field represents basic (and also ultrabasic) magma. The symbols are shown as an inset in (a). **a** — four tectonic settings IA-CR-OI-MOR; **b** — three tectonic settings IA-CR-OI; **c** — three tectonic settings IA-CR-MOR; **d** — three tectonic settings IA-OI-MOR; and **e** — three tectonic settings CR-OI-MOR.

62–80 %; Figs. S7–S9; Table S15) and confirmed good functioning of all three sets of diagrams for the OIB setting.

#### *Test study 1d: Oahu Island*

Twenty-four samples from the Oahu Island were used (Table S12; Jackson et al. 1999). Nine samples of basic rocks had complete datasets for Agrawal et al. (2004), Verma et al. (2006) and Verma and Agrawal (2011). The set of trace element based diagram (Agrawal et al. 2008) were not used, because the samples with complete data were only four (Table S12) and we had decided to report only the results of at least five samples. The nine basic rock samples indicated the OIB setting in the three sets of diagrams with percent success from 67 % to 78 % (Figs. S10–S12; Table S16).

Complete data for 15 intermediate rock samples were available for two diagram sets (Verma & Verma 2013). For both sets, these samples indicated a within-plate (CR+OI) setting, with about 81 % and 87 % percent probability values (for explanation of probability estimates, see Verma & Verma 2013), respectively, for the complete major and selected immobile element based diagrams (Figs. S13 and S14; Table S17). This inference can be considered consistent with that of the basic rock diagrams, because those for intermediate rocks are incapable of discriminating these two very similar tectonic settings; the distinction between continental rift and ocean island settings can only be made at present from basic and ultrabasic rocks. The testing of the third set is not reported because only three samples with complete data were available (Table S12).

#### *Test study 2: Trindade Island*

The compiled rocks from the Trindade Island (Table S12; Marques et al. 1999) included 14 (2 basic and 12 ultrabasic) samples for testing of three sets of diagrams (Agrawal et al. 2004, 2008; Verma et al. 2006) and 24 intermediate rock samples for two sets of diagrams (24 for the major element based and 13 for immobile trace element based diagrams; Verma & Verma 2013).

The testing of the diagrams for basic and ultrabasic rocks was satisfactory because most of the 14 samples plotted in the OIB field, with percent success of 70 %, 70 %, and 62 %, respectively, for Agrawal et al. (2004), Verma et al. (2006), and Agrawal et al. (2008) diagrams (Figs. S15–S17; Table S18). Similarly, the two sets of diagrams for intermediate rocks (major elements and immobile trace elements) were also satisfactorily tested for the within-plate setting, with percent probability values of about 76 % and 80 %, respectively (Figs. S18 and S19; Table S19).

#### *Testing of the diagrams from “fresh” volcanic rocks of ocean island or continental rift tectonic setting*

#### *Test study 3: White Island, Ross Sea, Antarctica*

Cooper et al. (2007) suggested that rocks from the White Island resulted from rift-related decompression melting rather than the action of a mantle plume earlier suggested by Behrendt et al. (1991, 1992). Therefore, either a CRB or an OIB

setting could be the expected tectonic setting. We compiled data for 22 basic rock samples (Table S12), which enabled us to test all four sets of diagrams for basic and ultrabasic magmas. In the major element based diagrams all samples plotted only in the CRB and OIB fields (Figs. S20 and S21; Table S20). The percent success values for Agrawal et al. (2004) diagrams were about 44 % and 56 %, respectively, for the CRB and OIB settings, whereas those for the Verma et al. (2006) diagrams these were about 48 % and 52 %, respectively (Table S20). The trace element based diagrams of Agrawal et al. (2008) indicated a CRB setting with percent success of about 64 %, whereas those of Verma & Agrawal (2011) indicated an OIB setting with the corresponding percent success of about 68 % (Figs. S22 and S23; Table S20). Thus, the diagrams indicate either a CRB or an OIB setting for these rocks. Unfortunately, no clear distinction between these two very similar tectonic settings was achieved from these diagram sets. The geological history and crustal thickness of the White Island might resolve this controversy (Behrendt et al. 1991, 1992; Cooper et al. 2007).

The continental rift and ocean island tectonic settings are very similar, which makes their discrimination a rather difficult task. The four sets of multidimensional discrimination diagrams (Agrawal et al. 2004, 2008; Verma et al. 2006; Verma & Agrawal 2011) available as geochemical discrimination diagrams provided mutually inconsistent results. A combination technique of multidimensional discrimination and petrogenetic processes yet to be proposed and practiced might eventually throw further light on this complex problem because the discrimination diagrams have certain limitations as discussed recently by Verma et al. (2015b) and Verma (2015b, 2015c).

#### *Test study 4: McMurdo area, Antarctica*

Drill core basic volcanic glass samples of Miocene age (15.9–18.4 Ma; Table S12; Nyland et al. 2013) were recovered from the McMurdo Sound area, Antarctica. The tectonic setting of the area was not reported by Nyland et al. (2013), but it may well be either a continental rift or an ocean island. The basic rock diagrams might help us to distinguish between them. Fairly complete geochemical data, including alteration information, for 24 glass samples were reported by Nyland et al. (2013). Complete data (Table S12) for 24 samples were thus available for three sets of diagrams (Agrawal et al. 2004; Verma et al. 2006; Verma & Agrawal 2011) and data for 20 (out of 24) samples were complete for the diagrams of Agrawal et al. (2008). The major element based diagram sets indicated an ocean island setting, with about 63 % or 64 % percent success (Figs. S24 and S25; Table S21). The immobile trace element based diagrams of Agrawal et al. (2008) showed percent values of 55 % for the CRB and 45 % for the OIB setting; so they did not provide a clear answer (Fig. S26; Table S21). The other immobile element based diagrams (Verma & Agrawal 2011), however, suggested an OIB setting for these glass samples, with percent success of about 72 % (Fig. S27; Table S21). Therefore, an OIB setting could be inferred for the McMurdo Sound area during the Miocene.

*Testing of the diagrams for “fresh” volcanic rocks from continental rift tectonic setting*

*Test study 5: Garrotxa, Spain*

Geochemical data for 16 samples of Quaternary basic and ultrabasic rocks from the NE Volcanic Province of Spain (Garrotxa area) were reported by Cebriá et al. (2000). The use of all four sets of diagrams was possible (Table S12). These diagrams consistently confirmed a continental rift setting for these samples, with percent success values of 60 % to 80 % (Figs. S28–S31; Table S22).

*Test study 6: Styrian basin, Austria*

Geochemical data for 39 (9 basic and 30 ultrabasic) Quaternary rock samples from this area (Table S12; Ali et al. 2013) clearly indicated a continental rift setting in all four sets of diagrams, with percent success of about 71 % to 80 % (Figs. S32–S35; Table S23).

*Test study 7: Cameroon Mountains, Cameroon*

Fourteen samples of basic rocks from the year 1999 and 2000 (recent) eruptions (Table S12; Suh et al. 2003) had complete data for three sets of diagrams, all of which were consistent with a continental rift setting, with percent success values of 56 % to 74 % (Figs. S36–S38; Table S24).

*Test study 8: Nosy Be Archipelago, Madagascar*

Melluso & Morra (2000) reported geochemical data for 27 samples of Miocene mafic alkaline rocks from the Nosy Be Island (Table S12). Three sets of diagrams could be applied, all of which indicated a continental rift setting, with percent success values of about 56 % to 73 % (Figs. S39–S41; Table S25).

*Test study 9: Tianheyong, Inner Mongolia, China*

Geochemical data for only eight samples of early Miocene were reported by Yang et al. (2009). These samples had complete data for three sets of diagrams (Table S12). The two sets based on major elements (Agrawal et al. 2004; Verma et al. 2006) indicated a continental rift setting, with percent success of about 73 % for both of them (Figs. S42 and S43; Table S26). However, the set based on immobile elements (Agrawal et al. 2008) suggested an ocean island setting for these samples (percent success of 75 %; Fig. S44; Table S26).

*Test study 10: Halaha volcanic field, Central Great Xing'an Range, China*

Fourteen samples of Quaternary basic rocks (Table S12; Ho et al. 2013) from the Halaha volcanic field, NE China, indicated a continental rift setting (Table S27). Both sets of the major element based diagrams showed higher percent success values of 67 % and 71 % than both sets of immobile element based diagrams (44 % and 49 % only; Figs. S45–S48; Table S27). Nevertheless, the expected CRB tectonic setting was confirmed from all diagram sets.

*Testing of the diagrams for “fresh” volcanic rocks from continental arc tectonic settings*

*Test study 11: Aniakchak ignimbrite, Alaska*

Geochemical data for 9 samples from about 3400 years old ignimbrite (Table S12; Dreher et al. 2005) from the Aniakchak caldera, Aleutian Peninsula, were used to test all multidimensional diagrams for acid rocks (Verma et al. 2012, 2013). Both sets based on log-ratios of major elements (Figs. S49 and S50) showed a continental arc setting, with percent probability values of 85 % and 56 % (Table S28). The two sets based on log-ratios of immobile elements also indicated the same tectonic setting with percent probability values of 70 % and 77 % (Figs. S51 and S52; Table S28). This inference seems to be consistent with the continental arc setting for this peninsular part of the Aleutian arc and involvement of crustal material in the genesis of the ignimbritic magma (Dreher et al. 2005).

We will not present more diagrams because the reader should have ascertained from our presentation so far that the diagrams serve the purpose of visualization only and are not really required for the interpretation. TecD and TecDIA provide all necessary information to understand the results of the multidimensional diagrams. Furthermore, for intermediate and acid rocks TecDIA provides probability estimates which cannot be obtained directly from the examination of the respective diagrams.

*Test study 12a–12c: Guatemala, Central America*

Nine samples of intermediate volcanic rocks from recent eruptions of the Fuego volcanic complex (Test study 12a; Table S12; Chesner & Rose Jr. 1984) allowed the evaluation of the major element based diagram set (Verma & Verma 2013), which indicated the expected continental arc setting for these samples, with the total percent probability value of 65 % (Table S29).

Geochemical data for 40 samples of lava from the Meseta volcano (Test study 12b; Table S12; Chesner & Halsore 1997) also allowed the application of only one set of major element based diagrams (Verma & Verma 2013), which confirmed the expected continental arc setting for these samples, with the total percent probability value of 72 % (Table S30).

The final Test study (12c) from this group was for Quaternary volcanic rocks from the Santiaguito volcanic complex (Table S12; Scott et al. 2013). Eighteen samples of intermediate rocks had complete data for two sets of diagrams, which showed a continental arc setting (total percent probability values of 74 % and 55 %; Table S31). Only five of these samples had complete data for the remaining set of diagrams, which also indicated a continental arc setting for these samples (Table S31). Additionally, 17 samples of acid rocks allowed the application of all four sets of diagrams (Table S32). One set of major element based diagrams indicated an island arc setting for these samples, whereas the other set a continental arc setting. One set of immobile element based diagrams did not provide a consistent answer, indicating, in fact, a transitional continental arc to collision

setting. The final set of diagrams also based on immobile elements, on the other hand, provided a consistent answer of a continental arc setting, with total percent probability of 77 % (Table S32). These inconsistencies seem to be a natural consequence of crustal involvement in the genesis of these magmas as suggested by the original authors (Scott et al. 2013).

#### *Test study 13: Huequi volcano, Chile*

Nine intermediate rock samples of historic activity from this volcanic dome complex in the Andean southern volcanic zone (Table S12, Watt et al. 2011) had complete data for two of the three sets of diagrams, which showed the expected continental arc setting with total percent probability values of about 70 % (Table S33).

#### *Test study 14: Nisyros Island, Dodecanese, Greece*

Only the major element based diagram set could be tested from Quaternary volcanic rocks of Nisyros Island, Greece (Table S12; Di Paola 1974). Sixteen samples of intermediate rocks indicated a continental arc setting but with a rather low percent probability value of 49 % or a continental arc to collision transitional setting, with the respective probability values of 49 % and 40 %, respectively (Table S34). The acid rocks (11 samples) were also consistent with a continental arc setting and showed much higher percent probability values of 71 % and 75 % (Table S35). These different inferences may be related to different petrogenetic processes for these two magma types.

#### *Testing of the diagrams from “fresh” volcanic rocks of island arc tectonic setting*

#### *Test study 15: Augustine Island*

One set of diagrams based on major elements in intermediate rocks was tested from the geochemical data for Pleistocene-Holocene volcanic rocks from this small island in the Aleutian arc (Table S12; Johnson et al. 1996). Twenty-one samples consistently plotted in the arc setting, with the island arc predominating over the continental arc (total percent probability of 59 % and 41 %, respectively; Table S36). Thus, the expected tectonic setting of an island arc seems to be confirmed.

#### *Test study 16a: Barren Island, Andaman-Nicobar Islands*

Data for 25 samples of Quaternary basic volcanic rocks from the Barren Island were compiled (Test study 16a; Table S12; Chandrasekharan et al. 2009; Streck et al. 2011). In the major element based diagrams these island arc samples showed percent success of about 73 % and 80 % for the Agrawal et al. (2004) and Verma et al. (2006) diagrams, respectively (Table S37). Only 11 samples had complete data for immobile element based diagrams of Agrawal et al. (2008), whereas 24 of them had complete data for Verma & Agrawal (2011) diagrams. Both sets also indicated an arc setting, with high percent success of 80 % (Table S37). Similarly, 21 samples from the Barren Island proved to be from

intermediate magma, which, in the major element based diagrams (Verma & Verma 2013) showed an island arc setting with total percent probability of 52 %, followed by about 42 % for the continental arc setting (Table S38). The two sets of immobile element based diagrams confirmed the island arc setting for intermediate rocks, with higher total percent probability of about 74 % (Table S38). Thus, the expected tectonic setting of an island arc seems to be confirmed.

#### *Test study 16b: Narcondam Island, Andaman-Nicobar Islands*

For the Narcondam Island, only 10 samples of intermediate and 8 of acid rocks were available (Test study 16b; Table S12; Pal et al. 2007; Streck et al. 2011). Although for intermediate rocks the major element based diagrams indicated an island arc setting, the total percent probability was very low (only about 41 %; Table S39). Eight of these samples with complete data for the two sets of immobile element based diagrams, however, confirmed the island arc setting with total percent probability values of 71 % and 58 % (Table S39). The major element based diagrams for acid rocks also confirmed the island arc setting with total percent probability of about 72 % (Table S40). However, one set of immobile trace element based diagrams indicated a continental arc (total percent probability of about 58 %) rather than an island arc (total percent probability of about 42 %; Table S40). The reasons for this discrepancy will have to be evaluated, but one of them is probably related to the data quality of trace elements (larger analytical errors for trace than for major elements).

#### *Testing of the diagrams for “fresh” volcanic rocks from mid-ocean ridge tectonic settings*

#### *Test study 17: Central Indian Ridge*

Yi et al. (2014) reported geochemical data for axial positions of the Indian Ridge (Table S12). Thirty-three samples proved to be of basic magma types, whereas 14 turned out to be intermediate rocks. The latter were not used for testing because the mid-ocean ridge setting is missing from the diagrams for intermediate rocks (Verma & Verma 2013). Therefore, the Supplementary file does not have the corresponding report table. Nevertheless, this setting can be included in the future versions of these diagrams. The basic rocks confirmed the mid-ocean ridge tectonic setting in all four sets of diagrams, with high percent success values of 65 % to 76 % (Table S41).

#### *Testing of the diagrams for “fresh” volcanic rocks from collision tectonic settings*

#### *Test study 18: Shirak area, NW Armenia*

The Pliocene-Pleistocene volcanic rocks of Armenia are considered a key component of the Arabia-Eurasia collision (Neill et al. 2013). Thirteen samples of intermediate rocks had complete data for two sets of diagrams; 9 of these samples could be used for the remaining set of diagrams (Table S12). All diagram sets consistently indicated a collision set-

ting for these samples; the corresponding percent probability values varied from a low 43 % to a considerably high 67 % (Table S42).

#### Evaluation of the diagrams for “hydrothermally altered” or “weathered” volcanic rocks from different tectonic settings

##### *Test study A1: Eaio Island, Maquesas Islands, French Polynesia*

Twenty-five (24 basic and 1 ultrabasic; Caroff et al. 1999; Table S13) hydrothermally altered samples from three drill holes in the Eaio Island were used to evaluate three of the four sets of diagrams, which affirmed an ocean island tectonic setting in all diagram sets (Table S43). In spite of the alteration indicated by high-temperature iddingsite and low-temperature zeolites, gypsum, calcite, and clay minerals (Caroff et al. 1999), most of the compiled samples plotted in the OIB field and showed high percent success values of 75 % to 78 % (Table S43).

##### *Test study A2: Koolau, Haleakala, and Kohala, Hawaiian Islands*

Moderately to highly altered rocks (exfoliated shell, corestone, rind, and shell samples) affected by spheroidal weathering from three volcanoes (Koolau, Haleakala, and Kohala) of the Hawaiian Islands, were sampled and analysed by Patino et al. (2003). A sample from a corestone-shell set was divided into three subsuites (corestone, exfoliated shell, andrind) with different degrees of alteration (Patino et al. 2003). The approximate ages of these samples as reported by Patino et al. (2003) were about 2–4 Ma for Koolau (Oahu Island), 0.35–0.4 Ma for Haleakala (Maui Island), and 0.35 Ma for Kohala (Hawaii). For 9 samples of basic and ultrabasic rocks, unfortunately, only major element based diagrams could be tested; complete data for none of the immobile element based diagrams were available. Both sets of major element based diagrams indicated a continental rift setting with 62 % and 71 % percent success; the ocean island setting showed the next setting with 36 % and 25 % (Table S44). Thus, although the expected ocean island setting was not inferred for these moderately to intensely weathered rocks, the inferred continental rift setting is very similar to the expected setting; both of them belong to the within-plate setting.

##### *Test study A3: Hainan Island, China*

The geochemistry of basaltic lavas from Hainan Island near the northern edge of the South China Sea (Miocene to Holocene; Table S13) was reported by Wang et al. (2012). The alteration was indicated by high loss on ignition (LOI) values (Wang et al. 2012). We selected 13 slightly to intensely altered basic and 10 intermediate rock samples for this evaluation. The basic rock samples had complete datasets for only the major element based diagrams; for immobile trace element diagrams only four samples had complete data, which were not considered (Table S13). Both major element based diagrams indicated a continental rift setting with percent success of about 69 % and 74 %

(Table S45). The 10 intermediate rock samples also had complete data for major elements only; for immobile elements only three samples had complete data. The major element based diagrams showed a within-plate (CR+OI) setting for them, with a high total percent probability of 83 % (Table S46). Thus, in spite of alteration, a consistent result of a continental rift or a within-plate setting was obtained from basic and intermediate rocks, respectively.

##### *Test study A4: Moyuta and Tecuamburro volcanoes, Guatemala*

Highly altered rocks (exfoliated shell, corestone, rind, and columnar joint block samples; see also Test study A2 above) affected by spheroidal weathering from two volcanoes (Moyuta and Tecuamburro) of Guatemala, were sampled and analysed by Patino et al. (2003). The ages of the samples from Moyuta were not reported by Patino et al. (2003), although an approximate age of Pliocene–Pleistocene was indicated for the Tecuamburro volcano. As for the earlier Test study), only the major element based diagrams for intermediate rocks could be tested from 7 samples. This diagram set indicated a continental arc setting with about 53 % total percent probability value (Table S47). Thus, the expected tectonic setting was inferred in spite of the intense spheroidal weathering that affected these rock samples.

##### *Test study A5: Sarapiquí Miocene arc, Costa Rica*

Gazel et al. (2005) reported geochemical data for rocks from the Sarapiquí Miocene (11.4–22.2 Ma) arc (or paleo-arc), northern Costa Rica (Table S13). Gazel et al. (2005) stated that pyroclasts in their samples were altered; additionally,  $H_2O^+$  contents in three of the four samples showed relatively high values (1.70–7.00 %). Ten samples of basic rocks (probably of ages 15–22 Ma; Gazel et al. 2005) had complete data for the two major element based diagram sets and one immobile element set and suggested an arc setting for them (Table S48). From the basic rock diagrams, the distinction between an island and a continental arc is at present not possible, because the continental arc setting was not represented in the databases used for proposing these diagrams (Agrawal et al. 2004, 2008; Verma et al. 2006; Verma & Agrawal 2011). However, 14 samples of intermediate rocks (probably of ages 11–15 Ma, somewhat younger than the basic rocks; Gazel et al. 2005) from this paleoarc had complete data for two sets of diagrams, which clearly confirmed an island arc setting, with percent probability values of 67 % for the major element based diagrams and 57 % for one set of immobile element based diagrams (Table S49). It is not clear if this Miocene arc represents an island or a continental arc setting. Nevertheless, because these two tectonic settings are very similar, this inference could be interpreted as a valid result. Finally, only four rock samples proved to be of acid type, which were not used for testing the respective diagrams.

##### *Test study A6: Taupo Volcanic Zone, New Zealand*

From the Rotokawa and Ngatamariki geothermal systems, Taupo Volcanic Zone, New Zealand, hydrothermally altered intermediate rocks were sampled from deep drill holes and

analysed for their major and trace elements by Browne et al. (1992). These authors did not report the tectonic setting of their geothermal area with temperatures above 300 °C. Practically no samples escaped the alteration indicated by altered pseudomorph (altered hypersthene, titanomagnetite to leucoxene, high LOI up to 6.2 %, and high volatile contents; Browne et al. 1992). The present-day tectonic setting seems to be an active rifting of an arc (Deering et al. 2011). Twenty-eight samples had complete data for the major element based diagrams, which indicated an island arc setting with a relatively low total percent probability value of about 44 %, followed by about 36 % for the continental arc setting (Table S50). The diagram set based on immobile major and trace elements could be tested from only five samples. It also indicated an island arc setting but with higher probability of about 63 % followed by 37 % for the continental arc (Table S50).

#### *Test study A7a: SE Indian and SW Pacific seafloor, Indian and Pacific Oceans*

Pyle et al. (1995) reported geochemical data from fresh as well as altered seafloor rocks (dredged and drilled) of different ages (0–4 and 15–23 Ma; Table S13). The presence of micaeuous alteration minerals, low CaO/Al<sub>2</sub>O<sub>3</sub> reflecting pervasive alteration, unusually high Rb contents, and contamination from seawater alteration were suggested by Pyle et al. (1995) as the symptoms of alteration for most samples. The authors used an intense leaching procedure before sample preparation for geochemical data acquisition. Complete major element data were available for 9 samples, of which 7 samples had complete immobile element data as well. Therefore, all four diagram sets could be tested from these data. The application showed a mid-ocean ridge setting from all diagrams, with a high percent success of about 72–80 % (Table S51).

#### *Test study A7b: central Indian Ridge, Indian Ocean*

Geochemical data for mafic and ultramafic rocks were reported for the central part of the Indian Ridge (Yi et al. 2014; Table S13). Most samples are characterized by moderate to intense alteration of primary minerals. In highly altered gabbroic rocks, clinopyroxene is replaced by amphibole and chlorite, plagioclase changed to aggregates of prehnite or cryptocrystalline secondary minerals, and altered veins of Fe-Ti oxide and minor chlorite are present (Yi et al. 2014). In other samples, olivine is altered to aggregates of serpentine, iron oxide, and iron hydroxide; most harzburgites are strongly serpentized (Yi et al. 2014). Twenty-eight samples with complete major element data indicated a mid-ocean ridge setting with 64 % and 55 % percent success values (Table S52). A lesser number of samples (17 and 20) had complete immobile element data for the respective diagrams. They also indicated a mid-ocean ridge setting for these diagrams with high success rates of about 70 % (Table S52).

#### *Test study A8: Aeolian Island, Italy*

Only 17 samples of hydrothermally altered (7 intermediate and 10 acid) rocks could be compiled from Del Moro et al.

(2011; Table S13) for this final Test study. The volcanic and subvolcanic rocks underwent alteration processes induced by acid-sulphate hydrothermal systems (Del Moro et al. 2011). According to these authors, some rocks showed argillic to silicic alteration containing abundant hydrous sulphate and hydroxyl-sulphate minerals, whereas other rocks underwent pyrometamorphic processes. Two sets of diagrams for intermediate rocks could be tested; in both sets all samples consistently plotted in the collision field and showed high total percent probability values of about 83 % and 84 % (Table S53). For acid rocks, all four sets of diagrams could be applied. The first set of major element based diagrams showed a collision setting but with a low total percent probability of 42 %, whereas the other set indicated a transitional arc to collision setting (Table S54). However, both sets of immobile element based diagrams were consistent with a collision setting for these samples (total percent probability values of about 82 % and 60 %; Table S54).

#### *Use of freely-available geochemical databases for tectonic discrimination*

Agrawal & Verma (2007) were the first to show that freely-available geochemical databases should not be indiscriminately used for tectonic discrimination. Here, we use the example of GEOROC-Mainz to confirm the difficulties in using compiled data without critically examining the original papers from which the data were compiled.

Tongan arc data were downloaded as an excel file on May 27, 2015. This file contains 222 rows of samples compiled from 29 references. However, only 151 samples have complete major element data compiled from 19 references. There may also be discrepancies regarding the information on age or alteration parameters and references listed but we will point out only the discrepancies between the database and the data presented in the corresponding literature references. One problem with the database is that it contains zero (0) concentration values for numerous elements; zero values are not possible because this means that either the element of interest was not measured or it was not determinable by the analytical technique used. Therefore, the zero values should simply be blank cells.

Haase et al. (2002) reported data for 27 samples from the arc setting (Havre, Monowai, Rauol, Vulcanolog, Brothers, and Clark) whereas the GEOROC database has only 5 samples. Similarly, Hergt and Woodhead (2007) reported data for 8 samples from Eua Island whereas the database has only 4 samples from this paper. Furthermore, these two papers (Haase et al. 2002; Hergt and Woodhead 2007) were already compiled and used by the proponents of the multidimensional diagrams; these data therefore should not be used for testing of diagrams. For the data from Pearce et al. (2007), the database shows one sample (s16-95-2) listed as of Tongan arc, but this sample with TiO<sub>2</sub> contents of 3.54 % and Nb of 74.07 ppm is listed in the original paper as an ocean island basalt. Furthermore, in this paper (Pearce et al. 2007), 16 samples listed as Tongan arc are not present in the database. Similar discrepancies are also observed between the database and the original work of Hawkins et al. (1977). The database

reports 5 samples which were not found in Hawkins et al. (1977); these authors did not report any new data rather than average values from earlier papers. Therefore, it is not clear from where these samples were compiled. Fallon et al. (2007) reported data for numerous samples from forearc, ridge, and backarc regions; however, the database contains data for 3 samples from the Melville ridge registered as from the Tongan arc. Thus, it will not be advisable to use the database without prior examination of the original references.

Even if we ignore all the above problems, for five major element-based diagram sets (two for basic and ultrabasic rocks, Tables S1 and S2; one for intermediate rocks, Table S5; and two for acid rocks, Tables S8 and S9), a total of 151 rock samples are available in this database. The database also indicates that in terms of the three main subdivisions for diagram sets, these samples are distributed as follows: 91 samples of basic and ultrabasic rocks (65 basalts, 22 tholeiites, and 4 more basalts listed as basalt/not given); 48 intermediate (9 andesite, 34 basaltic andesite, and 5 boninite); and 7 acid (4 dacite and 3 rhyolite); 5 rock type not given. This subdivision for the use of multidimensional discrimination diagrams would simply not match that obtained from the application of IgRoCS strictly following the IUGS recommendations. When major element data for 151 samples in this database are processed in IgRoCS, the following subdivision was obtained: 84 samples of basic (1 alkali basalt, 1 picrite, 1 potassio trachybasalt, and 81 subalkali basalt) and 2 of ultrabasic rocks (basanite); 52 intermediate (11 andesite, 37 basaltic andesite, and 4 boninite); and 13 acid (9 dacite and 4 rhyolite). Because of these discrepancies, the user will have to process the database in IgRoCS before using the multidimensional diagrams.

Further considerations of the Tongan arc datafile from the GEOROC-Mainz compilation are concerned with the number of samples with valid concentration values for the major-trace or trace element-based diagrams. For basic and ultrabasic rocks, out of 86 samples only 29 and 22 samples are available for the diagram sets of Agrawal et al. (2008; complete data required for La, Sm, Yb, Nb, and Th) and Verma & Agrawal (2011; complete data required for Nb, V, Y, Zr, and TiO<sub>2</sub>), respectively.

For the combined major and trace element-based diagram set for intermediate rocks, the required elements with complete data are TiO<sub>2</sub>, MgO, P<sub>2</sub>O<sub>5</sub>, Nb, Ni, V, Y, and Zr (Table S6). Out of 52 samples in the database only 22 samples had complete data for use of this diagram set (in fact, 5 more samples had a 0 value for Nb, which were not counted as valid samples). Similarly, for the trace element-based diagram set for intermediate rocks, 23 samples had complete data for the required elements (La, Ce, Sm, Yb, Nb, Th, Y, and Zr; Table S7). Finally, for the major-trace and trace element-based diagram sets for acid rocks (Tables S10 and S11), complete data were available for only 3 samples and 1 sample, respectively (4 out of 13 samples).

Because of all these difficulties, the multidimensional diagrams were not used for testing these Tongan data. We conclude that the freely-available databases should be used with caution.

#### *Additional explanation on the performance of multidimensional diagrams*

We finally mention the possible reasons for obtaining varying percent success values in different diagram sets. Occasionally, the total percent success values are much lower than the highest value of about 80 % for basic and ultrabasic rocks (Agrawal et al. 2004, 2008; Verma et al. 2006; Verma & Agrawal 2011). This highest percent success value could be even somewhat higher for probability-based counting in the diagram sets for intermediate and acid rocks (Verma et al. 2012, 2013; Verma & Verma 2013). When the total percent success values are relatively small (much less than 80 %), we must first resort to the by-chance probability values for a given diagram set. Because the total probabilities are divided into four tectonic settings in the final synthesis of a diagram set, the total by-chance percent probability for a given tectonic setting will be around 25 %. Therefore, this by-chance probability serves the purpose of better interpreting our inferences.

Although the statistical problems associated with the use of crude compositional data (e.g., Pearson 1897; Chayes 1960, 1971; Butler 1979) have been overcome by the log-ratio transformation technique in the new multidimensional diagrams (e.g., Aitchison 1984, 1986, 1999; Egozcue et al. 2003; Thomas & Aitchison 2005; Pawlowsky-Glahn & Egozcue 2006; Buccianti 2013; Verma 2015a), other problems still prevail. Some of them can be summarized as follows: (i) the data quality plays an important role, but the appropriate information is seldom available in the published geochemical literature (only indications are sometimes provided as overall percent errors and not for individual geochemical data); (ii) post-emplacement changes are relatively common in older terrains, which may move the samples from one tectonic setting to another although the multidimensional diagrams are shown to be relatively robust against small concentration changes of a few tens of percent; (iii) age data are seldom available for individual geochemically analysed samples, which renders the sample grouping difficult; (iv) even when age data are available, the corresponding uncertainty may span tens of millions of years, a period relatively large to have caused significant changes in the tectonic setting of a given area; and (v) the different types of magmas in a given region may have originated from different sources (mantle or crustal or both), which is not taken into account in the multidimensional diagrams but will also cause dispersion in such diagrams.

#### Conclusions

Satisfactory application of the new multidimensional diagrams has been demonstrated for 18 test studies of relatively fresh rocks and 8 application studies of hydrothermally altered or weathered rocks. In most cases studies, the expected tectonic setting was indicated by the respective applicable diagrams. The importance of petrogenetic processes and data quality is highlighted, especially, for cases where the expected tectonic setting was not inferred from the diagrams.

**Acknowledgements:** This work was partly supported by DGAPA-PAPIIT grant IN104813. M.A. Rivera-Gómez is grateful to Conacyt for her doctoral fellowship. We are grateful to the journal Editor handling our manuscript, three anonymous reviewers, and the managing editor of the journal, for numerous suggestions which helped us improve our presentation.

## References

- Agrawal S. & Verma S.P. 2007: Comment on “Tectonic classification of basalts with classification trees” by Pieter Vermeesch (2006). *Geochim Cosmochim Acta* 71, 3388–3390.
- Agrawal S., Guevara M. & Verma S.P. 2004: Discriminant analysis applied to establish major-element field boundaries for tectonic varieties of basic rocks. *Int. Geol. Rev.* 46, 575–594.
- Agrawal S., Guevara M. & Verma S.P. 2008: Tectonic discrimination of basic and ultrabasic rocks through log-transformed ratios of immobile trace elements. *Int. Geol. Rev.* 50, 1057–1079.
- Aitchison J. 1984: Statistical analysis of geochemical compositions. *Math. Geol.* 16, 531–564.
- Aitchison J. 1986: The statistical analysis of compositional data. *Chapman and Hall*, London, UK, 1–416.
- Aitchison J. 1999: Logratios and natural laws in compositional data analysis. *Math. Geol.* 31, 563–580.
- Ali S., Ntaflos T. & Upton B.G.J. 2013: Petrogenesis and mantle source characteristics of Quaternary alkaline mafic lavas in the western Carpathian-Pannonian Region, Styria, Austria. *Chem. Geol.* 337–338, 99–113.
- Armstrong-Altrin J.S. 2015: Evaluation of two multidimensional discrimination diagrams from beach and deep-sea sediments from the Gulf of Mexico and their application to Precambrian clastic sedimentary rocks. *Int. Geol. Rev.* 57, 1446–1461.
- Armstrong-Altrin J.S. & Verma S.P. 2005: Critical evaluation of six tectonic setting discrimination diagrams using geochemical data of Neogene sediments from known tectonic settings. *Sed. Geol.* 177, 115–129.
- Bailey J.C. 1981: Geochemical criteria for a refined tectonic discrimination of orogenic andesites. *Chem. Geol.* 32, 139–154.
- Behrendt J.C., LeMasurier W.E., Cooper A.K., Tessensohn F., Treuil A. & Damaske D. 1991: Geophysical studies of the West Antarctic Rift System. *Tectonics* 10, 1257–1273.
- Behrendt J.C., LeMasurier W.E. & Cooper A.K. 1992: The West Antarctic Rift System — A propagating rift captured by a mantle plume? In: Yoshida Y., Kaminuma K. & Shiraishi K. (Eds.): Recent Progress in Antarctic Earth Science. *Terra Science*, Tokyo, 315–322.
- Bora S. & Kumar S. 2015: Geochemistry of biotites and host granitoid plutons from the Proterozoic Mahakoshal Belt, central India tectonic zone: implication for nature and tectonic setting of magmatism. *Int. Geol. Rev.* 57, 1686–1706.
- Browne P.R.L., Graham I.J., Parker R.J. & Wood C.P. 1992: Subsurface andesite lavas and plutonic rocks in the Rotokawa and Ngatamariki geothermal systems, Taupo volcanic zone, New Zealand. *J. Volcanol. Geotherm. Res.* 51, 199–215.
- Buccianti A. 2013: Is compositional data analysis a way to see beyond the illusion? *Comput. Geosci.* 50, 165–173.
- Butler J.C. 1979: Trends in ternary petrologic variation diagrams – fact or fantasy? *Am. Mineral.* 64, 1115–1121.
- Butler J.C. & Woronow A. 1986: Discrimination among tectonic settings using trace element abundances of basalts. *J. Geophys. Res.* 91, 10289–10300.
- Cabanis B. & Lecolle M. 1989: Le diagramme La/10-Y/15-Nb/8: un outil pour la discrimination des séries volcaniques et la mise en évidence des processus de mélange et/ou de contamination crustale. *Compte Rendu Acad. Sci. Paris* 309, 2023–2029.
- Caroff M., Guillou H., Maliaux M., Maury R.C., Guille G. & Cotten J. 1999: Assimilation of ocean crust by hawaiitic and mugearitic magmas: an example from Eiao (Marquesas). *Lithos* 46, 235–258.
- Cebriá J.M., López-Ruiz J., Doblas M., Oyarzun R., Hertogen J. & Benito R. 2000: Geochemistry of the Quaternary alkali basalts of Garrotxa (NE volcanic province, Spain): a case of double enrichment of the mantle lithosphere. *J. Volcanol. Geotherm. Res.* 102, 217–235.
- Chandrasekharan D., Santo A.P., Capaccioni B., Vaselli O., Alam M.A., Manetti P. & Tassi F. 2009: Volcanological and petrological evolution of Barren Island (Andaman Sea, Indian Ocean). *J. Asian Earth Sci.* 35, 469–487.
- Chayes F. 1960: On correlation between variables of constant sum. *J. Geophys. Res.* 65, 4185–4193.
- Chayes F. 1971: Ratio correlation. A manual for students of petrology and geochemistry. *The University of Chicago Press*, Chicago and London, 1–99.
- Chesner C.A. & Halsor S.P. 1997: Geochemical trends of sequential lava flows from Meseta volcano, Guatemala. *J. Volcanol. Geotherm. Res.* 78, 221–237.
- Chesner C.A. & Rose Jr. W.I. 1984: Geochemistry and evolution of the Fuego volcanic complex, Guatemala. *J. Volcanol. Geotherm. Res.* 21, 25–44.
- Cooper A.F., Adam L.J., Coulter R.F., Eby G.N. & McIntosh W.C. 2007: Geology, geochronology and geochemistry of a basanitic volcano, White Island, Ross Sea, Antarctica. *J. Volcanol. Geotherm. Res.* 165, 189–216.
- Deering C.D., Bachmann O., Dufek J. & Gravley D.M. 2011: Rift-related transition from andesite to rhyolite volcanism in the Taupo Volcanic Zone (New Zealand) controlled by crystal-melt dynamics in mush zones with variable mineral assemblages. *J. Petrol.* 52, 2243–2263.
- Del Moro S., Renzulli A. & Tribaudino M. 2011: Pyrometamorphic processes at the magma-hydrothermal system interface of active volcanoes: evidence from buchite ejecta of Stromboli (Aeolian Islands, Italy). *J. Petrol.* 52, 541–564.
- Di Paola G.M. 1974: Volcanology and petrology of Nisyros Island (Dodecanese, Greece). *Bull. Volcanol.* 38, 944–987.
- Dreher S.T., Eichelberger J.C. & Larsen J.F. 2005: The petrology and geochemistry of the Aniakchak caldera-forming ignimbrite, Aleutian arc, Alaska. *J. Petrol.* 46, 1747–1768.
- Egozcue J.J., Pawlowsky-Glahn V., Mateu-Figueras G. & Barceló-Vidal C. 2003: Isometric logratio transformations for compositional data analysis. *Math. Geol.* 35, 279–300.
- Fallon T.J., Danyushevsky L.V., Crawford T.J., Maas R., Woodward J.D., Eggins S.M., Bloomer S.H., Wright D.J., Zlobin S.K. & Stacey A.R. 2007: Multiple mantle plume components involved in the petrogenesis of subduction-related lavas from the northern Lau basin: evidence from the geochemistry of arc and backarc submarine volcanoes. *Geochim. Geophys. Geosys.* 8, doi:10.1029/2007GC001619.
- Gazel E., Alvarado G.E., Obando J. & Alfaro A. 2005: Geología y evolución magmática del arco de Sarapiquí, Costa Rica. *Rev. Geol. Am. Cen.* 32, 13–31.
- Gorton M.P. & Schandl E.S. 2000: From continents to island arcs: a geochemical index of tectonic setting for arc-related and within-plate felsic to intermediate volcanic rocks. *Can. Mineral.* 38, 1065–1073.
- Haase K.M., Worthington T.J., Stoffers P., Garbe-Schönberg D. & Wright I.C. 2002: Mantle dynamics, element recycling, and magma genesis beneath the Kermadec arc-Havre trough. *Geochim. Geophys. Geosys.* 3, 1071, doi:10.1029/

- 2002GC00035.
- Hawkins J.W. Jr. 1977: Petrological and geochemical characteristics of marginal basin basalts island arcs. In: Talwani M. & Pitman W.C.III (Eds.): Deep Sea Trenches and Back-Arc Basins. *American Geophysical Union*, Washington D.C. 355–365.
- Hergt J.M. & Woodhead J.D. 2007: A critical evaluation of recent models for Lau-tonga arc-backarc basin magmatic evolution. *Chem. Geol.* 245, 9–44.
- Ho K.-S., Ge W.-C., Chen J.-C., You C.-F., Yang H.-J. & Zhang Y.-L. 2013: Late Cenozoic magmatic transitions in the central Great Xing'an Range, Northeast China: Geochemical and isotopic constraints on petrogenesis. *Chem. Geol.* 352, 1–18.
- Jackson M.C., Frey F.A., Garcia M.O. & Wilmoth R.A. 1999: Geology and geochemistry of basaltic lava flows and dikes from the Trans-Koolau tunnel, Oahu, Hawaii. *Bull. Volcanol.* 60, 381–401.
- Johnson K.E., Harmon R.S., Richardson J.M., Moorbath S. & Strong D. 1996: Isotope and trace element geochemistry of Augustine Volcano, Alaska: implications for magmatic evolution. *J. Petrol.* 37, 95–115.
- Kaur P., Chaudhri N. & Hofmann A.W. 2015: New evidence for two sharp replacement fronts during albitization of granitoids from northern Aravalli orogen, northwest India. *Int. Geol. Rev.* 57, 1660–1685.
- Le Bas M.J., Le Maitre R.W., Streckeisen A. & Zanettin B. 1986: A chemical classification of volcanic rocks based on the total alkali-silica diagram. *J. Petrol.* 27, 745–750.
- Le Bas M.J. & Streckeisen A.L. 1991: The IUGS systematics of igneous rocks. *J. Geol. Soc. London* 148, 825–833.
- Le Maitre R.W., Streckeisen A., Zanettin B., Le Bas M.J., Bonin B., Bateman P., Bellieni G., Dudek A., Schmid R., Sorensen H. & Woolley A.R. 2002: Igneous rocks. A classification and glossary of terms: recommendations of the International Union of Geological Sciences, Subcommission of the Systematics of Igneous Rocks, ed. 2nd. *Cambridge University Press*, Cambridge, 1–236.
- Marques L.S., Ulbrich M.N.C., Ruberti E. & Tassinari C.G. 1999: Petrology, geochemistry and Sr-Nd isotopes of the Trindade and Martin Vaz volcanic rocks (southern Atlantic Ocean). *J. Volcanol. Geotherm. Res.* 93, 191–216.
- Melluso L. & Morra V. 2000: Petrogenesis of Late Cenozoic mafic alkaline rocks of the Nosy Be archipelago (northern Madagascar): relationships with Comorean magmatism. *J. Volcanol. Geotherm. Res.* 96, 129–142.
- Meschede M. 1986: A method of discriminating between different types of mid-ocean ridge basalts and continental tholeiites with the Nb-Zr-Y diagram. *Chem. Geol.* 56, 207–218.
- Mullen E.D. 1983: MnO/TiO<sub>2</sub>/P<sub>2</sub>O<sub>5</sub>: a minor element discrimination for basaltic rocks of oceanic environments and its implications for petrogenesis. *Earth Planet. Sci. Lett.* 62, 53–62.
- Neill I., Meliksetian K., Allen M.B., Navarsardyan G. & Karapetyan S. 2013: Pliocene-Quaternary volcanic rocks of NW Armenia: Magmatism and lithospheric dynamics within an active orogenic plateau. *Lithos* 180–181, 200–215.
- Nyland R.E., Panter K.S., Rocchi S., Di Vincenzo G., Del Carlo P., Tiepolo M., Field B. & Gorsevski P. 2013: Volcanic activity and its link to glaciation cycles: Single-grain age and geochemistry of Early to Middle Miocene volcanic glass from ANDRILL AND-2A core, Antarctica. *J. Volcanol. Geotherm. Res.* 250, 106–128.
- Pal T., Mitra S.K., Sengupta S., Katari A., Bandopadhyay P.C. & Bhattacharya A.K. 2007: Dacite-andesites of Narcondam volcano in the Andaman Sea — an imprint of magma mixing in the inner arc of the Andaman-Java subduction system. *J. Volcanol. Geotherm. Res.* 168, 93–113.
- Pandarinath K. 2014a: Testing of the recently developed tectonomagmatic discrimination diagrams from hydrothermally altered igneous rocks of 7 geothermal fields. *Turk. J. Earth Sci.* 23, 412–426.
- Pandarinath K. 2014b: Tectonomagmatic origin of Precambrian rocks of Mexico and Argentina inferred from multi-dimensional discriminant-function based discrimination diagrams. *J. South. Am. Earth. Sci.* 56, 464–484.
- Patino L.C., Velbel M.A., Price J.R. & Wade J.A. 2003: Trace element mobility during spheroidal weathering of basalts and andesites in Hawaii and Guatemala. *Chem. Geol.* 202, 343–364.
- Pawlowsky-Glahn V. & Egozcue J.J. 2006: Compositional data and their analysis: an introduction. In: A. Buccianti, G. Mateu-Figueras & V. Pawlowsky-Glahn (Eds.), Compositional data analysis in the Geosciences: from theory to practice. *Geol. Soc. London Spec. Publ.*, London, 1–10.
- Pearce J.A. 1976: Statistical analysis of major element patterns in basalts. *J. Petrol.* 17, 15–43.
- Pearce J.A. 1982: Trace element characteristics of lavas from destructive plate boundaries. In: Thorpe R.S. (Ed.): *Andesites*. John Wiley & Sons, Chichester, 525–548.
- Pearce J.A. & Cann J.R. 1971: Ophiolite origin investigated by discriminant analysis using Ti, Zr and Y. *Earth Planet. Sci. Lett.* 12, 339–349.
- Pearce J.A. & Cann J.R. 1973: Tectonic setting of basic volcanic rocks determined using trace element analyses. *Earth Planet. Sci. Lett.* 19, 290–300.
- Pearce J.A. & Gale G.H. 1977: Identification of ore-deposition environment from trace-element geochemistry of associated igneous host rocks. *Geol. Soc. London Spec. Publ.* 7, 14–24.
- Pearce J.A. & Norry M.J. 1979: Petrogenetic implications of Ti, Zr, Y, and Nb variations in volcanic rocks. *Contrib. Mineral. Petrol.* 69, 33–47.
- Pearce T.H., Gorman B.E. & Birkett T.C. 1977: The relationship between major element chemistry and tectonic environment of basic and intermediate volcanic rocks. *Earth Planet. Sci. Lett.* 36, 121–132.
- Pearce J.A., Harris N.B.W. & Tindle A.G. 1984: Trace element discrimination diagrams for the tectonic interpretation of granitic rocks. *J. Petrol.* 25, 956–983.
- Pearce J.A., Kempton P.D. & Gill J.B. 2007: Hf-Nd evidence for the origin and distribution of mantle domains in the SW Pacific. *Earth Planet. Sci. Lett.* 260, 98–114.
- Pearson K. 1897: Mathematical contribution to the theory of evolution — on a form of spurious correlation which may arise when indices are used in the measurement of organs. *Proc. Royal Soc. London* 60, 489–502.
- Pyle D.G., Christie D.M., Mahoney J.J. & Duncan R.A. 1995: Geochemistry and geochronology of ancient southeast Indian and southwest Pacific seafloor. *J. Geophys. Res.* 100, 22261–22282.
- Rahman M.S. & Mondal M.E.A. 2015: Evolution of continental crust of the Aravalli craton, NW India, during the Neoarchean-Palaeoproterozoic: evidence from geochemistry of granitoids. *Int. Geol. Rev.* 57, 1510–1525.
- Rhodes J.M. 2012: Compositional diversity of Mauna Kea shield lavas recovered by the Hawaii Scientific Drilling Project: Inferences on source lithology, magma supply, and the role of multiple volcanoes. *Geochem. Geophys. Geosys.* 13, 2–28.
- Rhodes J.M. & Vollinger M.J. 2004: Composition of basaltic lavas sampled by phase-2 of the Hawaii scientific drilling project: Geochemical stratigraphy and magma types. *Geochem. Geophys. Geosys.* 5, 1–38.
- Scott J.A.J., Pyle D.M., Mather T.A. & Rose W.I. 2013: Geochemistry and evolution of the Santiago volcanic dome com-

- plex, Guatemala. *J. Volcanol. Geotherm. Res.* 252, 92–107.
- Sherrod D.R., Murai T. & Tagami T. 2007: New K-Ar ages for calculating end-of-shield extrusion rates at West Maui volcano, Hawaiian island chain. *Bull. Volcanol.* 69, 627–642.
- Shervais J.W. 1982: Ti-V plots and the petrogenesis of modern and ophiolitic lavas. *Earth Planet. Sci. Lett.* 59, 101–118.
- Srivastava R.K., Samal A.K. & Gautam G.C. 2015: Geochemical characteristics and petrogenesis of four Palaeoproterozoic mafic dike swarms and associated large igneous provinces from the eastern Dharwar craton, India. *Int. Geol. Rev.* 57, 1462–1484.
- Streck M.J., Ramos F., Gillam A., Haldar D. & Duncan R.A. 2011: The intra-oceanic Barren Island and Narcondam arc volcanoes, Andaman Sea: Implications for subduction inputs and crustal overprint of a depleted mantle source. In: Ray J., Sen G. & Ghosh B. (Eds.): Topics in Igneous Petrology. Springer Science+Business Media, 241–273.
- Suh C.E., Sparks R.S.J., Fitton J.G., Ayonghe S.N., Annen C., Nana R. & Luckman A. 2003: The 1999 and 2000 eruptions of Mount Cameroon: eruption behaviour and petrochemistry of lava. *Bull. Volcanol.* 65, 267–281.
- Thomas C.W. & Aitchison J. 2005: Compositional data analysis of geological variability and process: a case study. *Math. Geol.* 37, 753–772.
- Verma S.K. & Oliveira E.P. 2013: Application of multi-dimensional discrimination diagrams and probability calculations to Paleoproterozoic acid rocks from Brazilian cratons and provinces to infer tectonic settings. *J. South Am. Earth Sci.* 45, 117–146.
- Verma S.K. & Oliveira E.P. 2015: Tectonic setting of basic igneous and metagneous rocks of Borborema Province, Brazil using multi-dimensional geochemical discrimination diagrams. *J. South Am. Earth Sci.* 58, 309–317.
- Verma S.P. 2010: Statistical evaluation of bivariate, ternary and discriminant function tectonomagmatic discrimination diagrams. *Turk. J. Earth Sci.* 19, 185–238.
- Verma S.P. 2015a: Monte Carlo comparison of conventional ternary diagrams with new log-ratio bivariate diagrams and an example of tectonic discrimination. *Geochim. J.* 49, 393–412.
- Verma S.P. 2015b: Origin, evolution, and tectonic setting of the eastern part of the Mexican Volcanic Belt and comparison with the Central American Volcanic Arc from conventional multi-element normalized and new multidimensional discrimination diagrams and discordancy and significance tests. *Turk. J. Earth Sci.* 24, 111–164.
- Verma S.P. 2015c: Present state of knowledge and new geochemical constraints on the central part of the Mexican Volcanic Belt and comparison with the Central American Volcanic Arc in terms of near and far trench magmas. *Turk. J. Earth Sci.* 24, 399–460.
- Verma S.P. & Agrawal S. 2011: New tectonic discrimination diagrams for basic and ultrabasic volcanic rocks through log-transformed ratios of high field strength elements and implications for petrogenetic processes. *Rev. Mex. Cienc. Geol.* 28, 24–44.
- Verma S.P. & Armstrong-Altrin J.S. 2013: New multi-dimensional diagrams for tectonic discrimination of siliciclastic sediments and their application to Precambrian basins. *Chem. Geol.* 355, 117–133.
- Verma S.P. & Armstrong-Altrin J.S. 2016: Geochemical discrimination of siliciclastic sediments from active and passive margin settings. *Sediment. Geol.*, 332, 1–12.
- Verma S.P. & Rivera-Gómez M.A. 2013a: Computer programs for the classification and nomenclature of igneous rocks. *Episodes* 36, 115–124.
- Verma S.P. & Rivera-Gómez M.A. 2013b: New computer program TecD for tectonomagmatic discrimination from discriminant function diagrams for basic and ultrabasic magmas and its application to ancient rocks. *J. Iber. Geol.* 39, 167–179.
- Verma S.P. & Verma S.K. 2013: First 15 probability-based multidimensional discrimination diagrams for intermediate magmas and their robustness against post-emplacement compositional changes and petrogenetic processes. *Turk. J. Earth Sci.* 22, 931–995.
- Verma S.P., Torres-Alvarado I.S. & Sotelo-Rodríguez Z.T. 2002: SINCLAS: standard igneous norm and volcanic rock classification system. *Comput. Geosci.* 28, 711–715.
- Verma S.P., Guevara M. & Agrawal S. 2006: Discriminating four tectonic settings: five new geochemical diagrams for basic and ultrabasic volcanic rocks based on log-ratio transformation of major-element data. *J. Earth Syst. Sci.* 115, 485–528.
- Verma S.K., Pandarinath K. & Verma S.P. 2012: Statistical evaluation of tectonomagmatic discrimination diagrams for granitic rocks and proposal of new discriminant-function-based multidimensional diagrams for acid rocks. *Int. Geol. Rev.* 54, 325–347.
- Verma S.P., Pandarinath K., Verma S.K. & Agrawal S. 2013: Fifteen new discriminant-function-based multi-dimensional robust diagrams for acid rocks and their application to Precambrian rocks. *Lithos* 168–169, 113–123.
- Verma S.K., Oliveira E.P. & Verma S.P. 2015a: Plate tectonic settings for Precambrian basic rocks from Brazil by multi-dimensional tectonomagmatic discrimination diagrams and their limitations. *Int. Geol. Rev.* 57, 1566–1581.
- Verma S.P., Verma S.K. & Oliveira E.P. 2015b: Application of 55 multi-dimensional tectonomagmatic discrimination diagrams to Precambrian belts. *Int. Geol. Rev.* 57, 1365–1388.
- Verma S.P., Cruz-Huicochea R., Díaz-González L. & Verma S.K. 2015c: A new computer program TecDIA for multidimensional tectonic discrimination of intermediate and acid magmas and its application to the Bohemian Massif, Czech Republic. *J. Geosci.* 60, 203–218.
- Verma S.P., Díaz-González L. & Armstrong-Altrin J.S. 2016: Application of a new computer program for tectonic discrimination of Cambrian to Holocene clastic sediments. *Earth Sci. Inform.*, 10.1007/s12145-015-0244-0 published on-line, in press.
- Wang X.-C., Li Z.-X., Li X.-H., Li J., Liu Y., Long W.-G., Zhou J.-B. & Wang F. 2012: Temperature, pressure, and composition of the mantle source region of Late Cenozoic basalts in Hainan Island, SE Asia: a consequence of a young thermal mantle plume close to subduction zones? *J. Petrol.* 53, 177–233.
- Watt S.F.L., Pyle D.M. & Mather T.A. 2011: Geology, petrology and geochemistry of the dome complex of Huequi volcano, southern Chile. *Andean Geol.* 38, 335–348.
- Wood D.A. 1980: The application of a Th-Hf-Ta diagram to problems of tectonomagmatic classification and to establishing the nature of crustal contamination of basaltic lavas of the British Tertiary volcanic province. *Earth Planet. Sci. Lett.* 50, 11–30.
- Yang Z., Luo Z., Zhang H., Zhang Y., Huang F., Sun C. & Dai J. 2009: Petrogenesis and Geological Implications of the Tianheyong Cenozoic Basalts, Inner Mongolia China. *Earth Sci. Front.* 16, 90–106.
- Yi S.-B., Oh C.-W., Pak S.J., Kim J. & Moon J.-W. 2014: Geochemistry and petrogenesis of mafic-ultramafic rocks from the Central Indian Ridge, latitude 8°–17° S: denudation of mantle harzburgites and gabbroic rocks and compositional variation of basalts. *Int. Geol. Rev.* 56, 691–1719.

## Supplementary Material

The discriminant function DF1-DF2 equations were recently summarized by Verma et al. (2015b), which are reproduced here in Tables S1-S11 for an easy reference.

**Table S1.**

DF1-DF2 equations for the first set of five diagrams proposed by Agrawal et al. (2004) for basic and ultrabasic magmas.

Figure reference; figure type	Discrimination diagram	Discriminant function equations
Agrawal et al. (2004); adjusted major element concentrations	IAB-CRB-OIB- MORB	$\text{DF1}_{(\text{IAB-CRB-OIB-MORB})\text{m1}} = 0.258 \times (\text{SiO}_2)_{\text{adj}} + 2.395 \times (\text{TiO}_2)_{\text{adj}} + 0.106 \times (\text{Al}_2\text{O}_3)_{\text{adj}} + 1.019 \times (\text{Fe}_2\text{O}_3)_{\text{adj}} - 6.778 \times (\text{MnO})_{\text{adj}} + 0.405 \times (\text{MgO})_{\text{adj}} + 0.119 \times (\text{CaO})_{\text{adj}} + 0.071 \times (\text{Na}_2\text{O})_{\text{adj}} - 0.198 \times (\text{K}_2\text{O})_{\text{adj}} + 0.613 \times (\text{P}_2\text{O}_5)_{\text{adj}} - 24.065$ $\text{DF2}_{(\text{IAB-CRB-OIB-MORB})\text{m1}} = 0.730 \times (\text{SiO}_2)_{\text{adj}} + 1.119 \times (\text{TiO}_2)_{\text{adj}} + 0.156 \times (\text{Al}_2\text{O}_3)_{\text{adj}} + 1.332 \times (\text{Fe}_2\text{O}_3)_{\text{adj}} + 4.376 \times (\text{MnO})_{\text{adj}} + 0.493 \times (\text{MgO})_{\text{adj}} + 0.936 \times (\text{CaO})_{\text{adj}} + 0.882 \times (\text{Na}_2\text{O})_{\text{adj}} - 0.291 \times (\text{K}_2\text{O})_{\text{adj}} - 1.572 \times (\text{P}_2\text{O}_5)_{\text{adj}} - 59.472$
	IAB-CRB-OIB	$\text{DF1}_{(\text{IAB-CRB-OIB})\text{m1}} = 0.251 \times (\text{SiO}_2)_{\text{adj}} + 2.034 \times (\text{TiO}_2)_{\text{adj}} - 0.100 \times (\text{Al}_2\text{O}_3)_{\text{adj}} + 0.573 \times (\text{Fe}_2\text{O}_3)_{\text{adj}} + 0.032 \times (\text{FeO})_{\text{adj}} - 2.877 \times (\text{MnO})_{\text{adj}} + 0.260 \times (\text{MgO})_{\text{adj}} + 0.052 \times (\text{CaO})_{\text{adj}} + 0.322 \times (\text{Na}_2\text{O})_{\text{adj}} - 0.229 \times (\text{K}_2\text{O})_{\text{adj}} - 18.974$ $\text{DF2}_{(\text{IAB-CRB-OIB})\text{m1}} = 2.150 \times (\text{SiO}_2)_{\text{adj}} + 2.711 \times (\text{TiO}_2)_{\text{adj}} + 1.792 \times (\text{Al}_2\text{O}_3)_{\text{adj}} + 2.295 \times (\text{Fe}_2\text{O}_3)_{\text{adj}} + 1.484 \times (\text{FeO})_{\text{adj}} - 8.594 \times (\text{MnO})_{\text{adj}} + 1.896 \times (\text{MgO})_{\text{adj}} + 2.158 \times (\text{CaO})_{\text{adj}} + 1.201 \times (\text{Na}_2\text{O})_{\text{adj}} + 1.763 \times (\text{K}_2\text{O})_{\text{adj}} - 200.276$
	IAB-CRB-MORB	$\text{DF1}_{(\text{IAB-CRB-MORB})\text{m1}} = 0.435 \times (\text{SiO}_2)_{\text{adj}} - 1.392 \times (\text{TiO}_2)_{\text{adj}} + 0.183 \times (\text{Al}_2\text{O}_3)_{\text{adj}} + 0.148 \times (\text{FeO})_{\text{adj}} + 7.690 \times (\text{MnO})_{\text{adj}} + 0.021 \times (\text{MgO})_{\text{adj}} + 0.380 \times (\text{CaO})_{\text{adj}} + 0.036 \times (\text{Na}_2\text{O})_{\text{adj}} + 0.462 \times (\text{K}_2\text{O})_{\text{adj}} - 1.192 \times (\text{P}_2\text{O}_5)_{\text{adj}} - 29.435$ $\text{DF2}_{(\text{IAB-CRB-MORB})\text{m1}} = 0.601 \times (\text{SiO}_2)_{\text{adj}} - 0.335 \times (\text{TiO}_2)_{\text{adj}} + 1.332 \times (\text{Al}_2\text{O}_3)_{\text{adj}} + 1.449 \times (\text{FeO})_{\text{adj}} + 0.756 \times (\text{MnO})_{\text{adj}} + 0.893 \times (\text{MgO})_{\text{adj}} + 0.448 \times (\text{CaO})_{\text{adj}} + 0.525 \times (\text{Na}_2\text{O})_{\text{adj}} + 1.734 \times (\text{K}_2\text{O})_{\text{adj}} + 2.494 \times (\text{P}_2\text{O}_5)_{\text{adj}} - 78.236$
	IAB-OIB-MORB	$\text{DF1}_{(\text{IAB-OIB-MORB})\text{m1}} = 1.232 \times (\text{SiO}_2)_{\text{adj}} + 4.166 \times (\text{TiO}_2)_{\text{adj}} + 1.085 \times (\text{Al}_2\text{O}_3)_{\text{adj}} + 3.522 \times (\text{Fe}_2\text{O}_3)_{\text{adj}} + 0.500 \times (\text{FeO})_{\text{adj}} - 3.930 \times (\text{MnO})_{\text{adj}} + 1.334 \times (\text{MgO})_{\text{adj}} + 1.085 \times (\text{CaO})_{\text{adj}} + 0.416 \times (\text{Na}_2\text{O})_{\text{adj}} + 0.827 \times (\text{K}_2\text{O})_{\text{adj}} - 119.050$ $\text{DF2}_{(\text{IAB-OIB-MORB})\text{m1}} = 1.384 \times (\text{SiO}_2)_{\text{adj}} + 1.091 \times (\text{TiO}_2)_{\text{adj}} + 0.908 \times (\text{Al}_2\text{O}_3)_{\text{adj}} + 2.419 \times (\text{Fe}_2\text{O}_3)_{\text{adj}} + 0.886 \times (\text{FeO})_{\text{adj}} + 5.281 \times (\text{MnO})_{\text{adj}} + 1.269 \times (\text{MgO})_{\text{adj}} + 1.790 \times (\text{CaO})_{\text{adj}} + 2.572 \times (\text{Na}_2\text{O})_{\text{adj}} + 0.138 \times (\text{K}_2\text{O})_{\text{adj}} - 134.295$
	CRB-OIB-MORB	$\text{DF1}_{(\text{CRB-OIB-MORB})\text{m1}} = 0.310 \times (\text{SiO}_2)_{\text{adj}} + 1.936 \times (\text{TiO}_2)_{\text{adj}} + 0.341 \times (\text{Al}_2\text{O}_3)_{\text{adj}} + 0.760 \times (\text{Fe}_2\text{O}_3)_{\text{adj}} + 0.351 \times (\text{FeO})_{\text{adj}} - 11.315 \times (\text{MnO})_{\text{adj}} + 0.526 \times (\text{MgO})_{\text{adj}} + 0.084 \times (\text{CaO})_{\text{adj}} + 0.312 \times (\text{K}_2\text{O})_{\text{adj}} + 1.892 \times (\text{P}_2\text{O}_5)_{\text{adj}} - 32.909$ $\text{DF2}_{(\text{CRB-OIB-MORB})\text{m1}} = 0.703 \times (\text{SiO}_2)_{\text{adj}} + 2.454 \times (\text{TiO}_2)_{\text{adj}} + 0.233 \times (\text{Al}_2\text{O}_3)_{\text{adj}} + 1.943 \times (\text{Fe}_2\text{O}_3)_{\text{adj}} + 0.182 \times (\text{FeO})_{\text{adj}} - 2.421 \times (\text{MnO})_{\text{adj}} + 0.618 \times (\text{MgO})_{\text{adj}} + 0.712 \times (\text{CaO})_{\text{adj}} - 0.866 \times (\text{K}_2\text{O})_{\text{adj}} - 1.180 \times (\text{P}_2\text{O}_5)_{\text{adj}} - 56.455$

The tectonic fields are: IAB–island arc basic (or ultrabasic) rocks; CRB–continental rift basic (or ultrabasic) rocks; OIB–ocean island basic (or ultrabasic) rocks; and MORB–mid ocean ridge basic (or ultrabasic) rocks. The subscript <sub>adj</sub> refers to adjusted data from the SINCLAS (Verma et al. 2002) or IgRoCS computer program (Verma and Rivera-Gómez 2013a).

**Table S2.**

DF1-DF2 equations (approximate coefficients) for the second set of five diagrams proposed by Verma et al. (2006) for basic and ultrabasic magmas.

Figure reference; figure type	Discrimination diagram	Discriminant function equations
Verma et al. (2006); log-ratios of major elements	IAB-CRB-OIB- MORB	$\text{DF1}_{(\text{IAB-CRB-OIB-MORB})\text{m2}} = -4.676 \times \ln(\text{TiO}_2/\text{SiO}_2) + 2.533 \times \ln(\text{Al}_2\text{O}_3/\text{SiO}_2) - 0.388 \times \ln(\text{Fe}_2\text{O}_3/\text{SiO}_2) + 3.969 \times \ln(\text{FeO}/\text{SiO}_2) + 0.898 \times \ln(\text{MnO}/\text{SiO}_2) - 0.583 \times \ln(\text{MgO}/\text{SiO}_2) - 0.290 \times \ln(\text{CaO}/\text{SiO}_2) - 0.270 \times \ln(\text{Na}_2\text{O}/\text{SiO}_2) + 1.081 \times \ln(\text{K}_2\text{O}/\text{SiO}_2) + 0.184 \times \ln(\text{P}_2\text{O}_5/\text{SiO}_2) + 1.544$ $\text{DF2}_{(\text{IAB-CRB-OIB-MORB})\text{m2}} = 0.675 \times \ln(\text{TiO}_2/\text{SiO}_2) + 4.590 \times \ln(\text{Al}_2\text{O}_3/\text{SiO}_2) + 2.090 \times \ln(\text{Fe}_2\text{O}_3/\text{SiO}_2) + 0.851 \times \ln(\text{FeO}/\text{SiO}_2) - 0.433 \times \ln(\text{MnO}/\text{SiO}_2) + 1.483 \times \ln(\text{MgO}/\text{SiO}_2) - 2.363 \times \ln(\text{CaO}/\text{SiO}_2) - 1.656 \times \ln(\text{Na}_2\text{O}/\text{SiO}_2) - 0.676 \times \ln(\text{K}_2\text{O}/\text{SiO}_2) + 0.413 \times \ln(\text{P}_2\text{O}_5/\text{SiO}_2) + 13.164$
	IAB-CRB-OIB	$\text{DF1}_{(\text{IAB-CRB-OIB})\text{m2}} = 4.000 \times \ln(\text{TiO}_2/\text{SiO}_2) - 2.238 \times \ln(\text{Al}_2\text{O}_3/\text{SiO}_2) + 0.811 \times \ln(\text{Fe}_2\text{O}_3/\text{SiO}_2) - 2.586 \times \ln(\text{FeO}/\text{SiO}_2) - 1.243 \times \ln(\text{MnO}/\text{SiO}_2) + 0.587 \times \ln(\text{MgO}/\text{SiO}_2) - 0.315 \times \ln(\text{CaO}/\text{SiO}_2) + 0.432 \times \ln(\text{Na}_2\text{O}/\text{SiO}_2) - 1.026 \times \ln(\text{K}_2\text{O}/\text{SiO}_2) + 0.051 \times \ln(\text{P}_2\text{O}_5/\text{SiO}_2) - 0.572$ $\text{DF2}_{(\text{IAB-CRB-OIB})\text{m2}} = -1.370 \times \ln(\text{TiO}_2/\text{SiO}_2) + 3.010 \times \ln(\text{Al}_2\text{O}_3/\text{SiO}_2) + 0.324 \times \ln(\text{Fe}_2\text{O}_3/\text{SiO}_2) + 1.900 \times \ln(\text{FeO}/\text{SiO}_2) - 1.975 \times \ln(\text{MnO}/\text{SiO}_2) + 1.441 \times \ln(\text{MgO}/\text{SiO}_2) - 2.266 \times \ln(\text{CaO}/\text{SiO}_2) + 1.866 \times \ln(\text{Na}_2\text{O}/\text{SiO}_2) + 0.287 \times \ln(\text{K}_2\text{O}/\text{SiO}_2) + 0.814 \times \ln(\text{P}_2\text{O}_5/\text{SiO}_2) + 1.820$
	IAB-CRB-MORB	$\text{DF1}_{(\text{IAB-CRB-MORB})\text{m2}} = -1.574 \times \ln(\text{TiO}_2/\text{SiO}_2) + 6.150 \times \ln(\text{Al}_2\text{O}_3/\text{SiO}_2) + 1.554 \times \ln(\text{Fe}_2\text{O}_3/\text{SiO}_2) + 3.413 \times \ln(\text{FeO}/\text{SiO}_2) - 0.009 \times \ln(\text{MnO}/\text{SiO}_2) + 1.248 \times \ln(\text{MgO}/\text{SiO}_2) - 2.110 \times \ln(\text{CaO}/\text{SiO}_2) - 0.768 \times \ln(\text{Na}_2\text{O}/\text{SiO}_2) + 1.143 \times \ln(\text{K}_2\text{O}/\text{SiO}_2) + 0.352 \times \ln(\text{P}_2\text{O}_5/\text{SiO}_2) + 16.871$ $\text{DF2}_{(\text{IAB-CRB-MORB})\text{m2}} = 3.984 \times \ln(\text{TiO}_2/\text{SiO}_2) + 0.220 \times \ln(\text{Al}_2\text{O}_3/\text{SiO}_2) + 1.152 \times \ln(\text{Fe}_2\text{O}_3/\text{SiO}_2) - 2.204 \times \ln(\text{FeO}/\text{SiO}_2) - 1.623 \times \ln(\text{MnO}/\text{SiO}_2) + 1.429 \times \ln(\text{MgO}/\text{SiO}_2) - 1.252 \times \ln(\text{CaO}/\text{SiO}_2) + 0.358 \times \ln(\text{Na}_2\text{O}/\text{SiO}_2) - 0.641 \times \ln(\text{K}_2\text{O}/\text{SiO}_2) + 0.265 \times \ln(\text{P}_2\text{O}_5/\text{SiO}_2) + 5.051$
	IAB-OIB-MORB	$\text{DF1}_{(\text{IAB-OIB-MORB})\text{m2}} = 5.340 \times \ln(\text{TiO}_2/\text{SiO}_2) - 1.628 \times \ln(\text{Al}_2\text{O}_3/\text{SiO}_2) + 0.834 \times \ln(\text{Fe}_2\text{O}_3/\text{SiO}_2) - 4.736 \times \ln(\text{FeO}/\text{SiO}_2) - 0.125 \times \ln(\text{MnO}/\text{SiO}_2) + 0.645 \times \ln(\text{MgO}/\text{SiO}_2) + 1.515 \times \ln(\text{CaO}/\text{SiO}_2) - 0.815 \times \ln(\text{Na}_2\text{O}/\text{SiO}_2) - 0.889 \times \ln(\text{K}_2\text{O}/\text{SiO}_2) - 0.226 \times \ln(\text{P}_2\text{O}_5/\text{SiO}_2) + 5.776$ $\text{DF2}_{(\text{IAB-OIB-MORB})\text{m2}} = 1.180 \times \ln(\text{TiO}_2/\text{SiO}_2) + 5.511 \times \ln(\text{Al}_2\text{O}_3/\text{SiO}_2) + 2.774 \times \ln(\text{Fe}_2\text{O}_3/\text{SiO}_2) - 0.134 \times \ln(\text{FeO}/\text{SiO}_2) + 0.667 \times \ln(\text{MnO}/\text{SiO}_2) + 1.104 \times \ln(\text{MgO}/\text{SiO}_2) - 1.723 \times \ln(\text{CaO}/\text{SiO}_2) - 3.895 \times \ln(\text{Na}_2\text{O}/\text{SiO}_2) + 0.947 \times \ln(\text{K}_2\text{O}/\text{SiO}_2) - 0.108 \times \ln(\text{P}_2\text{O}_5/\text{SiO}_2) + 15.498$
	CRB-OIB-MORB	$\text{DF1}_{(\text{CRB-OIB-MORB})\text{m2}} = -0.518 \times \ln(\text{TiO}_2/\text{SiO}_2) + 4.989 \times \ln(\text{Al}_2\text{O}_3/\text{SiO}_2) + 2.220 \times \ln(\text{Fe}_2\text{O}_3/\text{SiO}_2) + 1.180 \times \ln(\text{FeO}/\text{SiO}_2) - 0.301 \times \ln(\text{MnO}/\text{SiO}_2) + 1.330 \times \ln(\text{MgO}/\text{SiO}_2) - 2.183 \times \ln(\text{CaO}/\text{SiO}_2) - 1.932 \times \ln(\text{Na}_2\text{O}/\text{SiO}_2) + 0.698 \times \ln(\text{K}_2\text{O}/\text{SiO}_2) + 0.900 \times \ln(\text{P}_2\text{O}_5/\text{SiO}_2) + 13.262$ $\text{DF2}_{(\text{CRB-OIB-MORB})\text{m2}} = 5.051 \times \ln(\text{TiO}_2/\text{SiO}_2) - 0.497 \times \ln(\text{Al}_2\text{O}_3/\text{SiO}_2) + 1.005 \times \ln(\text{Fe}_2\text{O}_3/\text{SiO}_2) - 3.385 \times \ln(\text{FeO}/\text{SiO}_2) + 0.553 \times \ln(\text{MnO}/\text{SiO}_2) + 0.292 \times \ln(\text{MgO}/\text{SiO}_2) + 0.401 \times \ln(\text{CaO}/\text{SiO}_2) - 2.864 \times \ln(\text{Na}_2\text{O}/\text{SiO}_2) - 0.219 \times \ln(\text{K}_2\text{O}/\text{SiO}_2) - 1.056 \times \ln(\text{P}_2\text{O}_5/\text{SiO}_2) + 2.888$

The tectonic fields are: IAB–island arc basic (or ultrabasic) rocks; CRB–continental rift basic (or ultrabasic) rocks; OIB–ocean island basic (or ultrabasic) rocks; and MORB–mid ocean ridge basic (or ultrabasic) rocks. The subscript <sup>adj</sup> refers to adjusted data from the SINCLAS (Verma et al. 2002) or IgRoCS computer program (Verma and Rivera-Gómez 2013a), but is eliminated from these equations.

**Table S3.**

DF1-DF2 equations for the set of five diagrams based on trace element ratios proposed by Agrawal et al. (2008) for basic and ultrabasic magmas.

Figure reference; figure type	Discrimination diagram	Discriminant function equations
Agrawal et al. (2008); log-ratios of immobile trace elements	IAB-CRB+OIB- MORB	$DF1_{(IAB-CRB+OIB-MORB)I} = 0.3518 \times \ln(\text{La/Th}) + 0.6013 \times \ln(\text{Sm/Th}) - 1.3450 \times \ln(\text{Yb/Th}) + 2.1056 \times \ln(\text{Nb/Th}) - 5.4763$ $DF2_{(IAB-CRB+OIB-MORB)I} = -0.3050 \times \ln(\text{La/Th}) - 1.1801 \times \ln(\text{Sm/Th}) + 1.6189 \times \ln(\text{Yb/Th}) + 1.2260 \times \ln(\text{Nb/Th}) - 0.9944$
	IAB-CRB-OIB	$DF1_{(IAB-CRB-OIB)I} = 0.5533 \times \ln(\text{La/Th}) + 0.2173 \times \ln(\text{Sm/Th}) - 0.0969 \times \ln(\text{Yb/Th}) + 2.0454 \times \ln(\text{Nb/Th}) - 5.6305$ $DF2_{(IAB-CRB-OIB)I} = -2.4498 \times \ln(\text{La/Th}) + 4.8562 \times \ln(\text{Sm/Th}) - 2.1240 \times \ln(\text{Yb/Th}) - 0.1567 \times \ln(\text{Nb/Th}) + 0.9400$
	IAB-CRB-MORB	$DF1_{(IAB-CRB-MORB)I} = 0.3305 \times \ln(\text{La/Th}) + 0.3484 \times \ln(\text{Sm/Th}) - 0.9562 \times \ln(\text{Yb/Th}) + 2.0777 \times \ln(\text{Nb/Th}) - 4.5628$ $DF2_{(IAB-CRB-MORB)I} = -0.1928 \times \ln(\text{La/Th}) - 1.1989 \times \ln(\text{Sm/Th}) + 1.7531 \times \ln(\text{Yb/Th}) + 0.6607 \times \ln(\text{Nb/Th}) - 0.4384$
	IAB-OIB-MORB	$DF1_{(IAB-OIB-MORB)I} = 1.7517 \times \ln(\text{Sm/Th}) - 1.9508 \times \ln(\text{Yb/Th}) + 1.9573 \times \ln(\text{Nb/Th}) - 5.0928$ $DF2_{(IAB-OIB-MORB)I} = -2.2412 \times \ln(\text{Sm/Th}) + 2.2060 \times \ln(\text{Yb/Th}) + 1.2481 \times \ln(\text{Nb/Th}) - 0.8243$
	CRB-OIB-MORB	$DF1_{(CRB-OIB-MORB)I} = -0.5558 \times \ln(\text{La/Th}) - 1.4260 \times \ln(\text{Sm/Th}) + 2.2935 \times \ln(\text{Yb/Th}) - 0.6890 \times \ln(\text{Nb/Th}) + 4.1422$ $DF2_{(CRB-OIB-MORB)I} = -0.9207 \times \ln(\text{La/Th}) + 3.6520 \times \ln(\text{Sm/Th}) - 1.9866 \times \ln(\text{Yb/Th}) + 1.0574 \times \ln(\text{Nb/Th}) - 4.4283$

The tectonic fields are: IAB–island arc basic (or ultrabasic) rocks; CRB–continental rift basic (or ultrabasic) rocks; OIB–ocean island basic (or ultrabasic) rocks; and MORB–mid ocean ridge basic (or ultrabasic) rocks.

**Table S4.**

DF1-DF2 equations for the set of five diagrams based on major and trace element ratios proposed by Verma and Agrawal (2011) for basic and ultrabasic magmas.

Figure reference; figure type	Discrimination diagram	Discriminant function equations
Verma and Agrawal (2011); log-ratios of immobile major and trace elements	IAB-CRB+OIB-MORB	$\text{DF1}_{(\text{IAB-CRB+OIB-MORB})2} = -0.6611 \times \ln(\text{Nb}/(\text{TiO}_2)_{\text{adj}}) + 2.2926 \times \ln(\text{V}/(\text{TiO}_2)_{\text{adj}}) + 1.6774 \times \ln(\text{Y}/(\text{TiO}_2)_{\text{adj}}) + 1.0916 \times \ln(\text{Zr}/(\text{TiO}_2)_{\text{adj}}) + 21.3603$ $\text{DF2}_{(\text{IAB-CRB+OIB-MORB})2} = 0.4702 \times \ln(\text{Nb}/(\text{TiO}_2)_{\text{adj}}) + 3.7649 \times \ln(\text{V}/(\text{TiO}_2)_{\text{adj}}) - 3.911 \times \ln(\text{Y}/(\text{TiO}_2)_{\text{adj}}) + 2.2697 \times \ln(\text{Zr}/(\text{TiO}_2)_{\text{adj}}) + 4.8487$
	IAB-CRB-OIB	$\text{DF1}_{(\text{IAB-CRB-OIB})2} = -0.6146 \times \ln(\text{Nb}/(\text{TiO}_2)_{\text{adj}}) + 2.3510 \times \ln(\text{V}/(\text{TiO}_2)_{\text{adj}}) + 1.6828 \times \ln(\text{Y}/(\text{TiO}_2)_{\text{adj}}) + 1.1911 \times \ln(\text{Zr}/(\text{TiO}_2)_{\text{adj}}) + 22.7253$ $\text{DF2}_{(\text{IAB-CRB-OIB})2} = 1.3765 \times \ln(\text{Nb}/(\text{TiO}_2)_{\text{adj}}) - 0.9452 \times \ln(\text{V}/(\text{TiO}_2)_{\text{adj}}) + 4.0461 \times \ln(\text{Y}/(\text{TiO}_2)_{\text{adj}}) - 2.0789 \times \ln(\text{Zr}/(\text{TiO}_2)_{\text{adj}}) + 22.2450$
	IAB-CRB-MORB	$\text{DF1}_{(\text{IAB-CRB-MORB})2} = -0.6624 \times \ln(\text{Nb}/(\text{TiO}_2)_{\text{adj}}) + 2.4498 \times \ln(\text{V}/(\text{TiO}_2)_{\text{adj}}) + 1.2867 \times \ln(\text{Y}/(\text{TiO}_2)_{\text{adj}}) + 1.0920 \times \ln(\text{Zr}/(\text{TiO}_2)_{\text{adj}}) + 18.7466$ $\text{DF2}_{(\text{IAB-CRB-MORB})2} = 0.4938 \cdot \ln(\text{Nb}/(\text{TiO}_2)_{\text{adj}}) + 3.4741 \cdot \ln(\text{V}/(\text{TiO}_2)_{\text{adj}}) - 3.8053 \cdot \ln(\text{Y}/(\text{TiO}_2)_{\text{adj}}) + 2.0070 \cdot \ln(\text{Zr}/(\text{TiO}_2)_{\text{adj}}) + 3.3163$
	IAB-OIB-MORB	$\text{DF1}_{(\text{IAB-OIB-MORB})2} = -0.2646 \times \ln(\text{Nb}/(\text{TiO}_2)_{\text{adj}}) + 2.0491 \times \ln(\text{V}/(\text{TiO}_2)_{\text{adj}}) + 3.4565 \times \ln(\text{Y}/(\text{TiO}_2)_{\text{adj}}) + 0.8573 \times \ln(\text{Zr}/(\text{TiO}_2)_{\text{adj}}) + 32.9472$ $\text{DF2}_{(\text{IAB-OIB-MORB})2} = 0.01874 \times \ln(\text{Nb}/(\text{TiO}_2)_{\text{adj}}) + 4.0937 \times \ln(\text{V}/(\text{TiO}_2)_{\text{adj}}) - 4.8550 \times \ln(\text{Y}/(\text{TiO}_2)_{\text{adj}}) + 2.9900 \times \ln(\text{Zr}/(\text{TiO}_2)_{\text{adj}}) + 0.1995$
	CRB-OIB-MORB	$\text{DF1}_{(\text{CRB-OIB-MORB})2} = -0.7829 \times \ln(\text{Nb}/(\text{TiO}_2)_{\text{adj}}) + 0.3379 \times \ln(\text{V}/(\text{TiO}_2)_{\text{adj}}) + 3.3239 \times \ln(\text{Y}/(\text{TiO}_2)_{\text{adj}}) - 0.51232 \times \ln(\text{Zr}/(\text{TiO}_2)_{\text{adj}}) + 16.0941$ $\text{DF2}_{(\text{CRB-OIB-MORB})2} = 1.7478 \times \ln(\text{Nb}/(\text{TiO}_2)_{\text{adj}}) - 0.0421 \times \ln(\text{V}/(\text{TiO}_2)_{\text{adj}}) + 3.5301 \times \ln(\text{Y}/(\text{TiO}_2)_{\text{adj}}) - 1.4503 \times \ln(\text{Zr}/(\text{TiO}_2)_{\text{adj}}) + 28.3592$

The tectonic fields are: IAB–island arc basic (or ultrabasic) rocks; CRB–continental rift basic (or ultrabasic) rocks; OIB–ocean island basic (or ultrabasic) rocks; and MORB–mid ocean ridge basic (or ultrabasic) rocks. The subscript <sub>adj</sub> refers to adjusted data from the SINCLAS (Verma et al. 2002) or IgRoCS computer program (Verma and Rivera-Gómez 2013a).

**Table S5.**

DF1-DF2 equations (approximate coefficients) for the set of five diagrams based on major element ratios proposed by Verma and Verma (2013) for intermediate magmas.

Figure reference; figure type	Discrimination diagram	Discriminant function equations
Verma and Verma (2013); log-ratios of major elements (mint)	IA+CA-CR+OI-Col	$\text{DF1}_{(\text{IA+CA-CR+OI-Col})_{\text{mint}}} = (-2.456 \times \ln(\text{TiO}_2/\text{SiO}_2)_{\text{adj}}) + (1.120 \times \ln(\text{Al}_2\text{O}_3/\text{SiO}_2)_{\text{adj}}) + (-2.225 \times \ln(\text{Fe}_2\text{O}_3/\text{SiO}_2)_{\text{adj}}) + (2.489 \times \ln(\text{FeO}/\text{SiO}_2)_{\text{adj}}) + (-0.212 \times \ln(\text{MnO}/\text{SiO}_2)_{\text{adj}}) + (-0.067 \times \ln(\text{MgO}/\text{SiO}_2)_{\text{adj}}) + (1.291 \times \ln(\text{CaO}/\text{SiO}_2)_{\text{adj}}) + (-0.284 \times \ln(\text{Na}_2\text{O}/\text{SiO}_2)_{\text{adj}}) + (-0.402 \times \ln(\text{K}_2\text{O}/\text{SiO}_2)_{\text{adj}}) + (0.031 \times \ln(\text{P}_2\text{O}_5/\text{SiO}_2)_{\text{adj}}) - 11.431$ $\text{DF2}_{(\text{IA+CA-CR+OI-Col})_{\text{mint}}} = (-0.578 \times \ln(\text{TiO}_2/\text{SiO}_2)_{\text{adj}}) + (-0.011 \times \ln(\text{Al}_2\text{O}_3/\text{SiO}_2)_{\text{adj}}) + (0.691 \times \ln(\text{Fe}_2\text{O}_3/\text{SiO}_2)_{\text{adj}}) + (-1.998 \times \ln(\text{FeO}/\text{SiO}_2)_{\text{adj}}) + (-1.720 \times \ln(\text{MnO}/\text{SiO}_2)_{\text{adj}}) + (0.305 \times \ln(\text{MgO}/\text{SiO}_2)_{\text{adj}}) + (0.816 \times \ln(\text{CaO}/\text{SiO}_2)_{\text{adj}}) + (-1.792 \times \ln(\text{Na}_2\text{O}/\text{SiO}_2)_{\text{adj}}) + (0.871 \times \ln(\text{K}_2\text{O}/\text{SiO}_2)_{\text{adj}}) + (0.335 \times \ln(\text{P}_2\text{O}_5/\text{SiO}_2)_{\text{adj}}) - 12.202$
	IA-CA-CR+OI	$\text{DF1}_{(\text{IA-CA-CR+OI})_{\text{mint}}} = (-2.519 \times \ln(\text{TiO}_2/\text{SiO}_2)_{\text{adj}}) + (0.542 \times \ln(\text{Al}_2\text{O}_3/\text{SiO}_2)_{\text{adj}}) + (-3.790 \times \ln(\text{Fe}_2\text{O}_3/\text{SiO}_2)_{\text{adj}}) + (3.846 \times \ln(\text{FeO}/\text{SiO}_2)_{\text{adj}}) + (-0.363 \times \ln(\text{MnO}/\text{SiO}_2)_{\text{adj}}) + (-0.177 \times \ln(\text{MgO}/\text{SiO}_2)_{\text{adj}}) + (1.426 \times \ln(\text{CaO}/\text{SiO}_2)_{\text{adj}}) + (0.112 \times \ln(\text{Na}_2\text{O}/\text{SiO}_2)_{\text{adj}}) + (-0.219 \times \ln(\text{K}_2\text{O}/\text{SiO}_2)_{\text{adj}}) + (-0.072 \times \ln(\text{P}_2\text{O}_5/\text{SiO}_2)_{\text{adj}}) - 14.315$ $\text{DF2}_{(\text{IA-CA-CR+OI})_{\text{mint}}} = (-1.049 \times \ln(\text{TiO}_2/\text{SiO}_2)_{\text{adj}}) + (3.440 \times \ln(\text{Al}_2\text{O}_3/\text{SiO}_2)_{\text{adj}}) + (-3.433 \times \ln(\text{Fe}_2\text{O}_3/\text{SiO}_2)_{\text{adj}}) + (4.807 \times \ln(\text{FeO}/\text{SiO}_2)_{\text{adj}}) + (-3.499 \times \ln(\text{MnO}/\text{SiO}_2)_{\text{adj}}) + (0.374 \times \ln(\text{MgO}/\text{SiO}_2)_{\text{adj}}) + (-2.148 \times \ln(\text{CaO}/\text{SiO}_2)_{\text{adj}}) + (3.002 \times \ln(\text{Na}_2\text{O}/\text{SiO}_2)_{\text{adj}}) + (-0.774 \times \ln(\text{K}_2\text{O}/\text{SiO}_2)_{\text{adj}}) + (1.062 \times \ln(\text{P}_2\text{O}_5/\text{SiO}_2)_{\text{adj}}) - 13.489$
	IA-CA-Col	$\text{DF1}_{(\text{IA-CA-Col})_{\text{mint}}} = (-0.887 \times \ln(\text{TiO}_2/\text{SiO}_2)_{\text{adj}}) + (-0.782 \times \ln(\text{Al}_2\text{O}_3/\text{SiO}_2)_{\text{adj}}) + (-2.432 \times \ln(\text{Fe}_2\text{O}_3/\text{SiO}_2)_{\text{adj}}) + (4.106 \times \ln(\text{FeO}/\text{SiO}_2)_{\text{adj}}) + (2.050 \times \ln(\text{MnO}/\text{SiO}_2)_{\text{adj}}) + (-0.387 \times \ln(\text{MgO}/\text{SiO}_2)_{\text{adj}}) + (-0.740 \times \ln(\text{CaO}/\text{SiO}_2)_{\text{adj}}) + (1.360 \times \ln(\text{Na}_2\text{O}/\text{SiO}_2)_{\text{adj}}) + (-0.816 \times \ln(\text{K}_2\text{O}/\text{SiO}_2)_{\text{adj}}) + (-0.468 \times \ln(\text{P}_2\text{O}_5/\text{SiO}_2)_{\text{adj}}) + 4.312$ $\text{DF2}_{(\text{IA-CA-Col})_{\text{mint}}} = (1.760 \times \ln(\text{TiO}_2/\text{SiO}_2)_{\text{adj}}) + (-4.329 \times \ln(\text{Al}_2\text{O}_3/\text{SiO}_2)_{\text{adj}}) + (2.601 \times \ln(\text{Fe}_2\text{O}_3/\text{SiO}_2)_{\text{adj}}) + (-4.961 \times \ln(\text{FeO}/\text{SiO}_2)_{\text{adj}}) + (2.897 \times \ln(\text{MnO}/\text{SiO}_2)_{\text{adj}}) + (-0.362 \times \ln(\text{MgO}/\text{SiO}_2)_{\text{adj}}) + (2.230 \times \ln(\text{CaO}/\text{SiO}_2)_{\text{adj}}) + (-2.967 \times \ln(\text{Na}_2\text{O}/\text{SiO}_2)_{\text{adj}}) + (0.790 \times \ln(\text{K}_2\text{O}/\text{SiO}_2)_{\text{adj}}) + (-1.326 \times \ln(\text{P}_2\text{O}_5/\text{SiO}_2)_{\text{adj}}) + 7.586$
	IA-CR+OI-Col	$\text{DF1}_{(\text{IA-CR+OI-Col})_{\text{mint}}} = (-2.436 \times \ln(\text{TiO}_2/\text{SiO}_2)_{\text{adj}}) + (1.539 \times \ln(\text{Al}_2\text{O}_3/\text{SiO}_2)_{\text{adj}}) + (-1.517 \times \ln(\text{Fe}_2\text{O}_3/\text{SiO}_2)_{\text{adj}}) + (1.456 \times \ln(\text{FeO}/\text{SiO}_2)_{\text{adj}}) + (0.496 \times \ln(\text{MnO}/\text{SiO}_2)_{\text{adj}}) + (-0.050 \times \ln(\text{MgO}/\text{SiO}_2)_{\text{adj}}) + (1.258 \times \ln(\text{CaO}/\text{SiO}_2)_{\text{adj}}) + (-0.827 \times \ln(\text{Na}_2\text{O}/\text{SiO}_2)_{\text{adj}}) + (-0.488 \times \ln(\text{K}_2\text{O}/\text{SiO}_2)_{\text{adj}}) + (0.112 \times \ln(\text{P}_2\text{O}_5/\text{SiO}_2)_{\text{adj}}) - 7.895$ $\text{DF2}_{(\text{IA-CR+OI-Col})_{\text{mint}}} = (-0.737 \times \ln(\text{TiO}_2/\text{SiO}_2)_{\text{adj}}) + (-0.0788 \times \ln(\text{Al}_2\text{O}_3/\text{SiO}_2)_{\text{adj}}) + (0.066 \times \ln(\text{Fe}_2\text{O}_3/\text{SiO}_2)_{\text{adj}}) + (-1.130 \times \ln(\text{FeO}/\text{SiO}_2)_{\text{adj}}) + (-2.131 \times \ln(\text{MnO}/\text{SiO}_2)_{\text{adj}}) + (0.246 \times \ln(\text{MgO}/\text{SiO}_2)_{\text{adj}}) + (0.682 \times \ln(\text{CaO}/\text{SiO}_2)_{\text{adj}}) + (-1.328 \times \ln(\text{Na}_2\text{O}/\text{SiO}_2)_{\text{adj}}) + (0.771 \times \ln(\text{K}_2\text{O}/\text{SiO}_2)_{\text{adj}}) + (0.296 \times \ln(\text{P}_2\text{O}_5/\text{SiO}_2)_{\text{adj}}) - 15.241$

---

CA-CR+OI-Col	$\text{DF1}_{(\text{CA-CR+OI-Col})_{\text{mint}}} = (-2.322 \times \ln(\text{TiO}_2/\text{SiO}_2)_{\text{adj}}) + (1.971 \times \ln(\text{Al}_2\text{O}_3/\text{SiO}_2)_{\text{adj}}) + (-0.537 \times \ln(\text{Fe}_2\text{O}_3/\text{SiO}_2)_{\text{adj}}) + (0.431 \times \ln(\text{FeO}/\text{SiO}_2)_{\text{adj}}) + (-1.139 \times \ln(\text{MnO}/\text{SiO}_2)_{\text{adj}}) + (0.528 \times \ln(\text{MgO}/\text{SiO}_2)_{\text{adj}}) + (0.988 \times \ln(\text{CaO}/\text{SiO}_2)_{\text{adj}}) + (-0.894 \times \ln(\text{Na}_2\text{O}/\text{SiO}_2)_{\text{adj}}) + (0.161 \times \ln(\text{K}_2\text{O}/\text{SiO}_2)_{\text{adj}}) + (0.078 \times \ln(\text{P}_2\text{O}_5/\text{SiO}_2)_{\text{adj}}) - 12.350$
	$\text{DF2}_{(\text{CA-CR+OI-Col})_{\text{mint}}} = (-0.407 \times \ln(\text{TiO}_2/\text{SiO}_2)_{\text{adj}}) + (2.606 \times \ln(\text{Al}_2\text{O}_3/\text{SiO}_2)_{\text{adj}}) + (0.161 \times \ln(\text{Fe}_2\text{O}_3/\text{SiO}_2)_{\text{adj}}) + (1.346 \times \ln(\text{FeO}/\text{SiO}_2)_{\text{adj}}) + (0.446 \times \ln(\text{MnO}/\text{SiO}_2)_{\text{adj}}) + (-0.260 \times \ln(\text{MgO}/\text{SiO}_2)_{\text{adj}}) + (-0.465 \times \ln(\text{CaO}/\text{SiO}_2)_{\text{adj}}) + (0.921 \times \ln(\text{Na}_2\text{O}/\text{SiO}_2)_{\text{adj}}) + (-1.277 \times \ln(\text{K}_2\text{O}/\text{SiO}_2)_{\text{adj}}) + (-0.143 \times \ln(\text{P}_2\text{O}_5/\text{SiO}_2)_{\text{adj}}) + 3.501$

---

The tectonic settings are: IA=island arc; CA=continental arc; CR=continental rift; OI=ocean island; and Col=collision. The subscript <sub>adj</sub> refers to adjusted data from the SINCLAS (Verma et al. 2002) or IgRoCS computer program (Verma and Rivera-Gómez 2013a).

**Table S6.**

DF1-DF2 equations (approximate coefficients) for the set of five diagrams based on immobile major and trace element ratios proposed by Verma and Verma (2013) for intermediate magmas.

Figure reference; figure type	Discrimination diagram	Discriminant function equations
Verma and Verma (2013); log-ratios of immobile major and trace elements (mtint)	IA+CA-CR+OI-Col	$\text{DF1}_{(\text{IA+CA-CR+OI-Col})_{\text{mtint}}} = (1.023 \times \ln(\text{MgO}/\text{TiO}_2)_{\text{adj}}) + (0.631 \times \ln(\text{P}_2\text{O}_5/\text{TiO}_2)_{\text{adj}}) + (-0.939 \times \ln(\text{Nb}/\text{TiO}_2)_{\text{adj}}) + (-0.415 \times \ln(\text{Ni}/\text{TiO}_2)_{\text{adj}}) + (1.677 \times \ln(\text{V}/\text{TiO}_2)_{\text{adj}}) + (0.454 \times \ln(\text{Y}/\text{TiO}_2)_{\text{adj}}) + (0.583 \times \ln(\text{Zr}/\text{TiO}_2)_{\text{adj}}) + 1.901$ $\text{DF2}_{(\text{IA+CA-CR+OI-Col})_{\text{mtint}}} = (0.249 \times \ln(\text{MgO}/\text{TiO}_2)_{\text{adj}}) + (-0.477 \ln(\text{P}_2\text{O}_5/\text{TiO}_2)_{\text{adj}}) + (-0.336 \times \ln(\text{Nb}/\text{TiO}_2)_{\text{adj}}) + (-0.131 \times \ln(\text{Ni}/\text{TiO}_2)_{\text{adj}}) + (-1.712 \times \ln(\text{V}/\text{TiO}_2)_{\text{adj}}) + (0.214 \times \ln(\text{Y}/\text{TiO}_2)_{\text{adj}}) + (-2.008 \times \ln(\text{Zr}/\text{TiO}_2)_{\text{adj}}) - 18.638$
	IA-CA-CR+OI	$\text{DF1}_{(\text{IA-CA-CR+OI})_{\text{mtint}}} = (0.875 \times \ln(\text{MgO}/\text{TiO}_2)_{\text{adj}}) + (0.428 \times \ln(\text{P}_2\text{O}_5/\text{TiO}_2)_{\text{adj}}) + (-0.686 \times \ln(\text{Nb}/\text{TiO}_2)_{\text{adj}}) + (-0.372 \times \ln(\text{Ni}/\text{TiO}_2)_{\text{adj}}) + (1.924 \times \ln(\text{V}/\text{TiO}_2)_{\text{adj}}) + (0.835 \times \ln(\text{Y}/\text{TiO}_2)_{\text{adj}}) + (0.843 \times \ln(\text{Zr}/\text{TiO}_2)_{\text{adj}}) + 8.228$ $\text{DF2}_{(\text{IA-CA-CR+OI})_{\text{mtint}}} = (-1.172 \times \ln(\text{MgO}/\text{TiO}_2)_{\text{adj}}) + (-2.651 \times \ln(\text{P}_2\text{O}_5/\text{TiO}_2)_{\text{adj}}) + (0.176 \times \ln(\text{Nb}/\text{TiO}_2)_{\text{adj}}) + (0.118 \times \ln(\text{Ni}/\text{TiO}_2)_{\text{adj}}) + (-0.185 \times \ln(\text{V}/\text{TiO}_2)_{\text{adj}}) + (1.921 \times \ln(\text{Y}/\text{TiO}_2)_{\text{adj}}) + (0.387 \times \ln(\text{Zr}/\text{TiO}_2)_{\text{adj}}) + 12.452$
	IA-CA-Col	$\text{DF1}_{(\text{IA-CA-Col})_{\text{mtint}}} = (-0.801 \times \ln(\text{MgO}/\text{TiO}_2)_{\text{adj}}) + (0.125 \times \ln(\text{P}_2\text{O}_5/\text{TiO}_2)_{\text{adj}}) + (0.908 \times \ln(\text{Nb}/\text{TiO}_2)_{\text{adj}}) + (0.320 \times \ln(\text{Ni}/\text{TiO}_2)_{\text{adj}}) + (-0.368 \times \ln(\text{V}/\text{TiO}_2)_{\text{adj}}) + (-0.641 \times \ln(\text{Y}/\text{TiO}_2)_{\text{adj}}) + (0.723 \times \ln(\text{Zr}/\text{TiO}_2)_{\text{adj}}) + 8.109$ $\text{DF2}_{(\text{IA-CA-Col})_{\text{mtint}}} = (1.317 \times \ln(\text{MgO}/\text{TiO}_2)_{\text{adj}}) + (2.200 \times \ln(\text{P}_2\text{O}_5/\text{TiO}_2)_{\text{adj}}) + (-0.124 \times \ln(\text{Nb}/\text{TiO}_2)_{\text{adj}}) + (-0.134 \times \ln(\text{Ni}/\text{TiO}_2)_{\text{adj}}) + (-0.872 \times \ln(\text{V}/\text{TiO}_2)_{\text{adj}}) + (-1.783 \times \ln(\text{Y}/\text{TiO}_2)_{\text{adj}}) + (-1.365 \times \ln(\text{Zr}/\text{TiO}_2)_{\text{adj}}) - 20.630$
	IA-CA-CR+OI	$\text{DF1}_{(\text{IA-CA-CR+OI})_{\text{mtint}}} = (-0.856 \times \ln(\text{MgO}/\text{TiO}_2)_{\text{adj}}) + (-0.301 \times \ln(\text{P}_2\text{O}_5/\text{TiO}_2)_{\text{adj}}) + (0.862 \times \ln(\text{Nb}/\text{TiO}_2)_{\text{adj}}) + (0.385 \times \ln(\text{Ni}/\text{TiO}_2)_{\text{adj}}) + (-1.583 \times \ln(\text{V}/\text{TiO}_2)_{\text{adj}}) + (-0.757 \times \ln(\text{Y}/\text{TiO}_2)_{\text{adj}}) + (-0.692 \times \ln(\text{Zr}/\text{TiO}_2)_{\text{adj}}) - 4.469$ $\text{DF2}_{(\text{IA-CA-CR+OI})_{\text{mtint}}} = (0.215 \times \ln(\text{MgO}/\text{TiO}_2)_{\text{adj}}) + (-0.504 \times \ln(\text{P}_2\text{O}_5/\text{TiO}_2)_{\text{adj}}) + (-0.323 \times \ln(\text{Nb}/\text{TiO}_2)_{\text{adj}}) + (-0.122 \times \ln(\text{Ni}/\text{TiO}_2)_{\text{adj}}) + (-1.710 \times \ln(\text{V}/\text{TiO}_2)_{\text{adj}}) + (0.426 \times \ln(\text{Y}/\text{TiO}_2)_{\text{adj}}) + (-1.981 \times \ln(\text{Zr}/\text{TiO}_2)_{\text{adj}}) - 17.041$
	CA-CR+OI-Col	$\text{DF1}_{(\text{CA-CR+OI-Col})_{\text{mtint}}} = (-1.256 \times \ln(\text{MgO}/\text{TiO}_2)_{\text{adj}}) + (-1.082 \times \ln(\text{P}_2\text{O}_5/\text{TiO}_2)_{\text{adj}}) + (1.438 \times \ln(\text{Nb}/\text{TiO}_2)_{\text{adj}}) + (0.545 \times \ln(\text{Ni}/\text{TiO}_2)_{\text{adj}}) + (-1.620 \times \ln(\text{V}/\text{TiO}_2)_{\text{adj}}) + (0.337 \times \ln(\text{Y}/\text{TiO}_2)_{\text{adj}}) + (-0.714 \times \ln(\text{Zr}/\text{TiO}_2)_{\text{adj}}) + 5.752$ $\text{DF2}_{(\text{CA-CR+OI-Col})_{\text{mtint}}} = (-0.0240 \times \ln(\text{MgO}/\text{TiO}_2)_{\text{adj}}) + (-0.054 \times \ln(\text{P}_2\text{O}_5/\text{TiO}_2)_{\text{adj}}) + (-0.861 \times \ln(\text{Nb}/\text{TiO}_2)_{\text{adj}}) + (-0.174 \times \ln(\text{Ni}/\text{TiO}_2)_{\text{adj}}) + (-1.641 \times \ln(\text{V}/\text{TiO}_2)_{\text{adj}}) + (0.069 \times \ln(\text{Y}/\text{TiO}_2)_{\text{adj}}) + (-1.772 \times \ln(\text{Zr}/\text{TiO}_2)_{\text{adj}}) - 21.028$

The tectonic settings are: IA=island arc; CA=continental arc; CR=continental rift; OI=ocean island; and Col=collision. The subscript <sub>adj</sub> refers to adjusted data from the SINCLAS (Verma et al. 2002) or IgRoCS computer program (Verma and Rivera-Gómez 2013a).

**Table S7.**

DF1-DF2 equations (approximate coefficients) for the set of five diagrams based on immobile trace element ratios proposed by Verma and Verma (2013) for intermediate magmas.

Figure reference; figure type	Discrimination diagram	Discriminant function equations
Verma and Verma (2013); log-ratios of immobile trace elements (tint)	IA+CA-CR+OI-Col	$\text{DF1}_{(\text{IA}+\text{CA}-\text{CR}+\text{OI}-\text{Col})_{\text{tint}}} = (-0.167 \times \ln(\text{La/Yb}) + (-1.254 \times \ln(\text{Ce/Yb}) + (1.295 \times \ln(\text{Sm/Yb}) + (1.332 \times \ln(\text{Nb/Yb}) + (0.270 \times \ln(\text{Th/Yb}) + (1.929 \times \ln(\text{Y/Yb}) + (0.181 \times \ln(\text{Zr/Yb}) - 3.816$ $\text{DF2}_{(\text{IA}+\text{CA}-\text{CR}+\text{OI}-\text{Col})_{\text{tint}}} = (-0.243 \times \ln(\text{La/Yb}) + (1.727 \times \ln(\text{Ce/Yb}) + (0.490 \times \ln(\text{Sm/Yb}) + (-1.276 \times \ln(\text{Nb/Yb}) + (0.960 \times \ln(\text{Th/Yb}) + (0.851 \times \ln(\text{Y/Yb}) + (-0.489 \times \ln(\text{Zr/Yb}) - 3.306$
	IA-CA-CR+OI	$\text{DF1}_{(\text{IA}-\text{CA}-\text{CR}+\text{OI})_{\text{tint}}} = (0.018 \times \ln(\text{La/Yb}) + (-1.269 \times \ln(\text{Ce/Yb}) + (1.741 \times \ln(\text{Sm/Yb}) + (1.324 \times \ln(\text{Nb/Yb}) + (0.029 \times \ln(\text{Th/Yb}) + (1.581 \times \ln(\text{Y/Yb}) + (0.172 \times \ln(\text{Zr/Yb}) - 3.385$ $\text{DF2}_{(\text{IA}-\text{CA}-\text{CR}+\text{OI})_{\text{tint}}} = (-2.100 \times \ln(\text{La/Yb}) + (-2.044 \times \ln(\text{Ce/Yb}) + (-0.412 \times \ln(\text{Sm/Yb}) + (1.022 \times \ln(\text{Nb/Yb}) + (1.244 \times \ln(\text{Th/Yb}) + (1.877 \times \ln(\text{Y/Yb}) + (1.070 \times \ln(\text{Zr/Yb}) - 0.292$
	IA-CA-Col	$\text{DF1}_{(\text{IA}-\text{CA}-\text{Col})_{\text{tint}}} = (0.093 \times \ln(\text{La/Yb}) + (0.752 \times \ln(\text{Ce/Yb}) + (0.930 \times \ln(\text{Sm/Yb}) + (0.124 \times \ln(\text{Nb/Yb}) + (0.348 \times \ln(\text{Th/Yb}) + (1.473 \times \ln(\text{Y/Yb}) + (-0.034 \times \ln(\text{Zr/Yb}) - 5.801$ $\text{DF2}_{(\text{IA}-\text{CA}-\text{CR}+\text{OI})_{\text{tint}}} = (-2.038 \times \ln(\text{La/Yb}) + (-0.073 \times \ln(\text{Ce/Yb}) + (-1.360 \times \ln(\text{Sm/Yb}) + (-0.078 \times \ln(\text{Nb/Yb}) + (1.825 \times \ln(\text{Th/Yb}) + (2.774 \times \ln(\text{Y/Yb}) + (0.444 \times \ln(\text{Zr/Yb}) - 3.684$
	IA-CR+OI-Col	$\text{DF1}_{(\text{IA}-\text{CR}+\text{OI}-\text{Col})_{\text{tint}}} = (0.721 \times \ln(\text{La/Yb}) + (-1.352 \times \ln(\text{Ce/Yb}) + (1.379 \times \ln(\text{Sm/Yb}) + (1.164 \times \ln(\text{Nb/Yb}) + (-0.042 \times \ln(\text{Th/Yb}) + (1.558 \times \ln(\text{Y/Yb}) + (-0.164 \times \ln(\text{Zr/Yb}) - 2.934$ $\text{DF2}_{(\text{IA}-\text{CR}+\text{OI}-\text{Col})_{\text{tint}}} = (0.238 \times \ln(\text{La/Yb}) + (-2.035 \times \ln(\text{Ce/Yb}) + (-0.250 \times \ln(\text{Sm/Yb}) + (1.347 \times \ln(\text{Nb/Yb}) + (-0.761 \times \ln(\text{Th/Yb}) + (-0.787 \times \ln(\text{Y/Yb}) + (0.377 \times \ln(\text{Zr/Yb}) + 4.155$
	CA-CR+OI-Col	$\text{DF1}_{(\text{CA}-\text{CR}+\text{OI}-\text{Col})_{\text{tint}}} = (-0.977 \times \ln(\text{La/Yb}) + (-1.389 \times \ln(\text{Ce/Yb}) + (1.366 \times \ln(\text{Sm/Yb}) + (1.900 \times \ln(\text{Nb/Yb}) + (0.569 \times \ln(\text{Th/Yb}) + (1.658 \times \ln(\text{Y/Yb}) + (-0.305 \times \ln(\text{Zr/Yb}) - 0.877$ $\text{DF2}_{(\text{CA}-\text{CR}+\text{OI}-\text{Col})_{\text{tint}}} = (-0.0870 \times \ln(\text{La/Yb}) + (1.164 \times \ln(\text{Ce/Yb}) + (0.364 \times \ln(\text{Sm/Yb}) + (-0.901 \times \ln(\text{Nb/Yb}) + (1.126 \times \ln(\text{Th/Yb}) + (1.191 \times \ln(\text{Y/Yb}) + (-0.400 \times \ln(\text{Zr/Yb}) - 3.915$

The tectonic settings are: IA=island arc; CA=continental arc; CR=continental rift; OI=ocean island; and Col=collision.

**Table S8.**

DF1-DF2 equations (approximate coefficients) for the set of five diagrams based on major element ratios proposed by Verma et al. (2012) for acid magmas.

Figure reference; figure type	Discrimination diagram	Discriminant function equations
Verma et al. (2012); log-ratios of major elements (m3)	IA+CA-CR-Col	$\text{DF1}_{(\text{IA+CA-CR-Col})_{\text{m3}}} = (0.361 \times \ln(\text{TiO}_2/\text{SiO}_2)_{\text{adj}}) + (0.957 \times \ln(\text{Al}_2\text{O}_3/\text{SiO}_2)_{\text{adj}}) + (-2.092 \times \ln(\text{Fe}_2\text{O}_3/\text{SiO}_2)_{\text{adj}}) + (0.934 \times \ln(\text{FeO}/\text{SiO}_2)_{\text{adj}}) + (0.427 \times \ln(\text{MnO}/\text{SiO}_2)_{\text{adj}}) + (0.187 \times \ln(\text{MgO}/\text{SiO}_2)_{\text{adj}}) + (0.456 \times \ln(\text{CaO}/\text{SiO}_2)_{\text{adj}}) + (0.561 \times \ln(\text{Na}_2\text{O}/\text{SiO}_2)_{\text{adj}}) + (-1.652 \times \ln(\text{K}_2\text{O}/\text{SiO}_2)_{\text{adj}}) + (-0.156 \times \ln(\text{P}_2\text{O}_5/\text{SiO}_2)_{\text{adj}}) - 1.583$ $\text{DF2}_{(\text{IA+CA-CR-Col})_{\text{m3}}} = (0.472 \times \ln(\text{TiO}_2/\text{SiO}_2)_{\text{adj}}) + (-0.955 \times \ln(\text{Al}_2\text{O}_3/\text{SiO}_2)_{\text{adj}}) + (0.110 \times \ln(\text{Fe}_2\text{O}_3/\text{SiO}_2)_{\text{adj}}) + (0.699 \times \ln(\text{FeO}/\text{SiO}_2)_{\text{adj}}) + (0.740 \times \ln(\text{MnO}/\text{SiO}_2)_{\text{adj}}) + (-0.028 \times \ln(\text{MgO}/\text{SiO}_2)_{\text{adj}}) + (-0.245 \times \ln(\text{CaO}/\text{SiO}_2)_{\text{adj}}) + (0.232 \times \ln(\text{Na}_2\text{O}/\text{SiO}_2)_{\text{adj}}) + (0.174 \times \ln(\text{K}_2\text{O}/\text{SiO}_2)_{\text{adj}}) + (-0.354 \times \ln(\text{P}_2\text{O}_5/\text{SiO}_2)_{\text{adj}}) + 6.691$
	IA-CA-CR	$\text{F1}_{(\text{IA-CA-CR})_{\text{m3}}} = (-0.479 \times \ln(\text{TiO}_2/\text{SiO}_2)_{\text{adj}}) + (-0.087 \times \ln(\text{Al}_2\text{O}_3/\text{SiO}_2)_{\text{adj}}) + (2.743 \times \ln(\text{Fe}_2\text{O}_3/\text{SiO}_2)_{\text{adj}}) + (-1.066 \times \ln(\text{FeO}/\text{SiO}_2)_{\text{adj}}) + (-0.139 \times \ln(\text{MnO}/\text{SiO}_2)_{\text{adj}}) + (-0.191 \times \ln(\text{MgO}/\text{SiO}_2)_{\text{adj}}) + (-0.852 \times \ln(\text{CaO}/\text{SiO}_2)_{\text{adj}}) + (-0.714 \times \ln(\text{Na}_2\text{O}/\text{SiO}_2)_{\text{adj}}) + (1.717 \times \ln(\text{K}_2\text{O}/\text{SiO}_2)_{\text{adj}}) + (0.339 \times \ln(\text{P}_2\text{O}_5/\text{SiO}_2)_{\text{adj}}) + 6.257$ $\text{DF2}_{(\text{IA-CA-CR})_{\text{m3}}} = (-0.320 \times \ln(\text{TiO}_2/\text{SiO}_2)_{\text{adj}}) + (-1.758 \times \ln(\text{Al}_2\text{O}_3/\text{SiO}_2)_{\text{adj}}) + (-3.205 \times \ln(\text{Fe}_2\text{O}_3/\text{SiO}_2)_{\text{adj}}) + (1.121 \times \ln(\text{FeO}/\text{SiO}_2)_{\text{adj}}) + (0.217 \times \ln(\text{MnO}/\text{SiO}_2)_{\text{adj}}) + (-0.074 \times \ln(\text{MgO}/\text{SiO}_2)_{\text{adj}}) + (1.250 \times \ln(\text{CaO}/\text{SiO}_2)_{\text{adj}}) + (1.314 \times \ln(\text{Na}_2\text{O}/\text{SiO}_2)_{\text{adj}}) + (1.662 \times \ln(\text{K}_2\text{O}/\text{SiO}_2)_{\text{adj}}) + (0.019 \times \ln(\text{P}_2\text{O}_5/\text{SiO}_2)_{\text{adj}}) + 0.998$
	IA-CA-Col	$\text{DF1}_{(\text{IA-CA-Col})_{\text{m3}}} = (-0.362 \times \ln(\text{TiO}_2/\text{SiO}_2)_{\text{adj}}) + (-0.034 \times \ln(\text{Al}_2\text{O}_3/\text{SiO}_2)_{\text{adj}}) + (0.520 \times \ln(\text{Fe}_2\text{O}_3/\text{SiO}_2)_{\text{adj}}) + (-0.498 \times \ln(\text{FeO}/\text{SiO}_2)_{\text{adj}}) + (-0.722 \times \ln(\text{MnO}/\text{SiO}_2)_{\text{adj}}) + (-0.123 \times \ln(\text{MgO}/\text{SiO}_2)_{\text{adj}}) + (-0.139 \times \ln(\text{CaO}/\text{SiO}_2)_{\text{adj}}) + (-0.817 \times \ln(\text{Na}_2\text{O}/\text{SiO}_2)_{\text{adj}}) + (1.507 \times \ln(\text{K}_2\text{O}/\text{SiO}_2)_{\text{adj}}) + (0.268 \times \ln(\text{P}_2\text{O}_5/\text{SiO}_2)_{\text{adj}}) - 3.083$ $\text{DF2}_{(\text{IA-CA-Col})_{\text{m3}}} = (-0.142 \times \ln(\text{TiO}_2/\text{SiO}_2)_{\text{adj}}) + (1.984 \times \ln(\text{Al}_2\text{O}_3/\text{SiO}_2)_{\text{adj}}) + (1.747 \times \ln(\text{Fe}_2\text{O}_3/\text{SiO}_2)_{\text{adj}}) + (-0.735 \times \ln(\text{FeO}/\text{SiO}_2)_{\text{adj}}) + (-1.226 \times \ln(\text{MnO}/\text{SiO}_2)_{\text{adj}}) + (0.062 \times \ln(\text{MgO}/\text{SiO}_2)_{\text{adj}}) + (-1.152 \times \ln(\text{CaO}/\text{SiO}_2)_{\text{adj}}) + (-3.189 \times \ln(\text{Na}_2\text{O}/\text{SiO}_2)_{\text{adj}}) + (-2.339 \times \ln(\text{K}_2\text{O}/\text{SiO}_2)_{\text{adj}}) + (0.495 \times \ln(\text{P}_2\text{O}_5/\text{SiO}_2)_{\text{adj}}) - 18.190$
	IA-CR-Col	$\text{DF1}_{(\text{IA-CR-Col})_{\text{m3}}} = (0.023 \times \ln(\text{TiO}_2/\text{SiO}_2)_{\text{adj}}) + (1.288 \times \ln(\text{Al}_2\text{O}_3/\text{SiO}_2)_{\text{adj}}) + (-2.641 \times \ln(\text{Fe}_2\text{O}_3/\text{SiO}_2)_{\text{adj}}) + (2.949 \times \ln(\text{FeO}/\text{SiO}_2)_{\text{adj}}) + (0.197 \times \ln(\text{MnO}/\text{SiO}_2)_{\text{adj}}) + (0.067 \times \ln(\text{MgO}/\text{SiO}_2)_{\text{adj}}) + (0.062 \times \ln(\text{CaO}/\text{SiO}_2)_{\text{adj}}) + (0.622 \times \ln(\text{Na}_2\text{O}/\text{SiO}_2)_{\text{adj}}) + (-2.058 \times \ln(\text{K}_2\text{O}/\text{SiO}_2)_{\text{adj}}) + (-0.075 \times \ln(\text{P}_2\text{O}_5/\text{SiO}_2)_{\text{adj}}) - 2.179$

---


$$\begin{aligned} \text{DF2}_{(\text{IA-CR-Col})\text{m}^3} = & (0.279 \times \ln(\text{TiO}_2/\text{SiO}_2)_{\text{adj}}) + (-1.054 \times \ln(\text{Al}_2\text{O}_3/\text{SiO}_2)_{\text{adj}}) + \\ & (0.827 \times \ln(\text{Fe}_2\text{O}_3/\text{SiO}_2)_{\text{adj}}) + (0.303 \times \ln(\text{FeO}/\text{SiO}_2)_{\text{adj}}) + (0.408 \times \ln(\text{MnO}/\text{SiO}_2)_{\text{adj}}) + \\ & (-0.090 \times \ln(\text{MgO}/\text{SiO}_2)_{\text{adj}}) + (-0.326 \times \ln(\text{CaO}/\text{SiO}_2)_{\text{adj}}) + (0.152 \times \ln(\text{Na}_2\text{O}/\text{SiO}_2)_{\text{adj}}) + \\ & (0.670 \ln(\text{K}_2\text{O}/\text{SiO}_2)_{\text{adj}}) + (-0.226 \times \ln(\text{P}_2\text{O}_5/\text{SiO}_2)_{\text{adj}}) + 6.517 \end{aligned}$$


---

CA-CR-Col	$\text{DF1}_{(\text{CA-CR-Col})\text{m}^3} = (0.064 \times \ln(\text{TiO}_2/\text{SiO}_2)_{\text{adj}}) + (-1.794 \times \ln(\text{Al}_2\text{O}_3/\text{SiO}_2)_{\text{adj}}) +$ $(0.526 \times \ln(\text{Fe}_2\text{O}_3/\text{SiO}_2)_{\text{adj}}) + (0.638 \times \ln(\text{FeO}/\text{SiO}_2)_{\text{adj}}) + (0.341 \times \ln(\text{MnO}/\text{SiO}_2)_{\text{adj}}) +$ $(-0.072 \times \ln(\text{MgO}/\text{SiO}_2)_{\text{adj}}) + (-0.326 \times \ln(\text{CaO}/\text{SiO}_2)_{\text{adj}}) + (0.106 \times \ln(\text{Na}_2\text{O}/\text{SiO}_2)_{\text{adj}}) +$ $(1.810 \times \ln(\text{K}_2\text{O}/\text{SiO}_2)_{\text{adj}}) + (-0.034 \times \ln(\text{P}_2\text{O}_5/\text{SiO}_2)_{\text{adj}}) + 8.262$
	$\text{DF2}_{(\text{CA-CR-Col})\text{m}^3} = (0.876 \times \ln(\text{TiO}_2/\text{SiO}_2)_{\text{adj}}) + (0.802 \times \ln(\text{Al}_2\text{O}_3/\text{SiO}_2)_{\text{adj}}) +$ $(0.247 \times \ln(\text{Fe}_2\text{O}_3/\text{SiO}_2)_{\text{adj}}) + (-0.880 \times \ln(\text{FeO}/\text{SiO}_2)_{\text{adj}}) + (0.754 \times \ln(\text{MnO}/\text{SiO}_2)_{\text{adj}}) +$ $(-0.001 \times \ln(\text{MgO}/\text{SiO}_2)_{\text{adj}}) + (-0.062 \times \ln(\text{CaO}/\text{SiO}_2)_{\text{adj}}) + (-0.205 \times \ln(\text{Na}_2\text{O}/\text{SiO}_2)_{\text{adj}}) +$ $(-3.309 \times \ln(\text{K}_2\text{O}/\text{SiO}_2)_{\text{adj}}) + (-0.353 \times \ln(\text{P}_2\text{O}_5/\text{SiO}_2)_{\text{adj}}) - 3.896$

---

The tectonic settings are: IA=island arc; CA=continental arc; CR=continental rift; and Col=collision. The subscript <sub>adj</sub> refers to adjusted data from the SINCLAS (Verma et al. 2002) or IgRoCS computer program (Verma and Rivera-Gómez 2013a).

**Table S9.**

DF1-DF2 equations (approximate coefficients) for the set of five diagrams based on major element ratios proposed by Verma et al. (2013) for acid magmas.

Figure reference; figure type	Discrimination diagram	Discriminant function equations
Verma et al. (2013); log-ratios of major elements (macid)	IA+CA-CR+OI-Col	$\text{DF1}_{(\text{IA+CA-CR+OI-Col})_{\text{macid}}} = (0.051 \times \ln(\text{TiO}_2/\text{SiO}_2)_{\text{adj}}) + (0.226 \times \ln(\text{Al}_2\text{O}_3/\text{SiO}_2)_{\text{adj}}) + (-1.769 \times \ln(\text{Fe}_2\text{O}_3/\text{SiO}_2)_{\text{adj}}) + (1.831 \times \ln(\text{FeO}/\text{SiO}_2)_{\text{adj}}) + (-0.0652 \times \ln(\text{MnO}/\text{SiO}_2)_{\text{adj}}) + (0.134 \times \ln(\text{MgO}/\text{SiO}_2)_{\text{adj}}) + (0.225 \times \ln(\text{CaO}/\text{SiO}_2)_{\text{adj}}) + (0.742 \times \ln(\text{Na}_2\text{O}/\text{SiO}_2)_{\text{adj}}) + (-1.781 \times \ln(\text{K}_2\text{O}/\text{SiO}_2)_{\text{adj}}) + (0.146 \times \ln(\text{P}_2\text{O}_5/\text{SiO}_2)_{\text{adj}}) - 2.115$ $\text{DF2}_{(\text{IA+CA-CR+OI-Col})_{\text{macid}}} = (1.091 \times \ln(\text{TiO}_2/\text{SiO}_2)_{\text{adj}}) + (-1.648 \times \ln(\text{Al}_2\text{O}_3/\text{SiO}_2)_{\text{adj}}) + (-1.189 \times \ln(\text{Fe}_2\text{O}_3/\text{SiO}_2)_{\text{adj}}) + (1.030 \times \ln(\text{FeO}/\text{SiO}_2)_{\text{adj}}) + (0.823 \times \ln(\text{MnO}/\text{SiO}_2)_{\text{adj}}) + (0.026 \times \ln(\text{MgO}/\text{SiO}_2)_{\text{adj}}) + (0.023 \times \ln(\text{CaO}/\text{SiO}_2)_{\text{adj}}) + (0.212 \times \ln(\text{Na}_2\text{O}/\text{SiO}_2)_{\text{adj}}) + (0.085 \times \ln(\text{K}_2\text{O}/\text{SiO}_2)_{\text{adj}}) + (-0.854 \times \ln(\text{P}_2\text{O}_5/\text{SiO}_2)_{\text{adj}}) + 2.543$
IA-CA-CR+OI		$\text{DF1}_{(\text{IA-CA-CR+OI})_{\text{macid}}} = (0.130 \times \ln(\text{TiO}_2/\text{SiO}_2)_{\text{adj}}) + (0.623 \times \ln(\text{Fe}_2\text{O}_3/\text{SiO}_2)_{\text{adj}}) + (-0.761 \times \ln(\text{FeO}/\text{SiO}_2)_{\text{adj}}) + (-0.083 \times \ln(\text{MnO}/\text{SiO}_2)_{\text{adj}}) + (-0.147 \times \ln(\text{MgO}/\text{SiO}_2)_{\text{adj}}) + (-0.239 \times \ln(\text{CaO}/\text{SiO}_2)_{\text{adj}}) + (-0.520 \times \ln(\text{Na}_2\text{O}/\text{SiO}_2)_{\text{adj}}) + (2.038 \times \ln(\text{K}_2\text{O}/\text{SiO}_2)_{\text{adj}}) + (-0.164 \times \ln(\text{P}_2\text{O}_5/\text{SiO}_2)_{\text{adj}}) + 2.650$ $\text{DF2}_{(\text{IA-CA-CR+OI})_{\text{macid}}} = (-0.045 \times \ln(\text{TiO}_2/\text{SiO}_2)_{\text{adj}}) + (5.102 \times \ln(\text{Fe}_2\text{O}_3/\text{SiO}_2)_{\text{adj}}) + (-5.151 \times \ln(\text{FeO}/\text{SiO}_2)_{\text{adj}}) + (1.160 \times \ln(\text{MnO}/\text{SiO}_2)_{\text{adj}}) + (-0.253 \times \ln(\text{MgO}/\text{SiO}_2)_{\text{adj}}) + (-0.451 \times \ln(\text{CaO}/\text{SiO}_2)_{\text{adj}}) + (-2.448 \times \ln(\text{Na}_2\text{O}/\text{SiO}_2)_{\text{adj}}) + (-1.405 \times \ln(\text{K}_2\text{O}/\text{SiO}_2)_{\text{adj}}) + (0.002 \times \ln(\text{P}_2\text{O}_5/\text{SiO}_2)_{\text{adj}}) - 2.979$
IA-CA-Col		$\text{DF1}_{(\text{IA-CA-Col})_{\text{macid}}} = (-0.489 \times \ln(\text{TiO}_2/\text{SiO}_2)_{\text{adj}}) + (2.271 \times \ln(\text{Al}_2\text{O}_3/\text{SiO}_2)_{\text{adj}}) + (0.619 \times \ln(\text{Fe}_2\text{O}_3/\text{SiO}_2)_{\text{adj}}) + (-1.238 \times \ln(\text{FeO}/\text{SiO}_2)_{\text{adj}}) + (-0.912 \times \ln(\text{MnO}/\text{SiO}_2)_{\text{adj}}) + (0.156 \times \ln(\text{MgO}/\text{SiO}_2)_{\text{adj}}) + (-1.231 \times \ln(\text{Na}_2\text{O}/\text{SiO}_2)_{\text{adj}}) + (1.154 \times \ln(\text{K}_2\text{O}/\text{SiO}_2)_{\text{adj}}) + (0.409 \times \ln(\text{P}_2\text{O}_5/\text{SiO}_2)_{\text{adj}}) - 3.220$ $\text{DF2}_{(\text{IA-CA-Col})_{\text{macid}}} = (0.681 \times \ln(\text{TiO}_2/\text{SiO}_2)_{\text{adj}}) + (2.244 \times \ln(\text{Al}_2\text{O}_3/\text{SiO}_2)_{\text{adj}}) + (-3.899 \times \ln(\text{Fe}_2\text{O}_3/\text{SiO}_2)_{\text{adj}}) + (3.691 \times \ln(\text{FeO}/\text{SiO}_2)_{\text{adj}}) + (-0.374 \times \ln(\text{MnO}/\text{SiO}_2)_{\text{adj}}) + (0.255 \times \ln(\text{MgO}/\text{SiO}_2)_{\text{adj}}) + (3.036 \times \ln(\text{Na}_2\text{O}/\text{SiO}_2)_{\text{adj}}) + (1.163 \times \ln(\text{K}_2\text{O}/\text{SiO}_2)_{\text{adj}}) + (-0.226 \times \ln(\text{P}_2\text{O}_5/\text{SiO}_2)_{\text{adj}}) + 12.688$
IA-CR+OI-Col		$\text{DF1}_{(\text{IA-CR+OI-Col})_{\text{macid}}} = (-0.144 \times \ln(\text{TiO}_2/\text{SiO}_2)_{\text{adj}}) + (-0.743 \times \ln(\text{Al}_2\text{O}_3/\text{SiO}_2)_{\text{adj}}) + (-0.443 \times \ln(\text{MnO}/\text{SiO}_2)_{\text{adj}}) + (0.075 \times \ln(\text{CaO}/\text{SiO}_2)_{\text{adj}}) + (0.383 \times \ln(\text{Na}_2\text{O}/\text{SiO}_2)_{\text{adj}}) + (2.577 \times \ln(\text{K}_2\text{O}/\text{SiO}_2)_{\text{adj}}) + (-0.024 \times \ln(\text{P}_2\text{O}_5/\text{SiO}_2)_{\text{adj}}) + 4.290$ $\text{DF2}_{(\text{IA-CR+OI-Col})_{\text{macid}}} = (-0.873 \times \ln(\text{TiO}_2/\text{SiO}_2)_{\text{adj}}) + (1.545 \times \ln(\text{Al}_2\text{O}_3/\text{SiO}_2)_{\text{adj}}) + (-0.753 \times \ln(\text{MnO}/\text{SiO}_2)_{\text{adj}}) + (0.023 \times \ln(\text{CaO}/\text{SiO}_2)_{\text{adj}}) + (0.150 \times \ln(\text{Na}_2\text{O}/\text{SiO}_2)_{\text{adj}}) + (-0.320 \times \ln(\text{K}_2\text{O}/\text{SiO}_2)_{\text{adj}}) + (0.751 \times \ln(\text{P}_2\text{O}_5/\text{SiO}_2)_{\text{adj}}) - 2.595$
CA-CR+OI-Col		$\text{DF1}_{(\text{CA-CR+OI-Col})_{\text{macid}}} = (-0.022 \times \ln(\text{TiO}_2/\text{SiO}_2)_{\text{adj}}) + (1.065 \times \ln(\text{Al}_2\text{O}_3/\text{SiO}_2)_{\text{adj}}) + (-1.651 \times \ln(\text{Fe}_2\text{O}_3/\text{SiO}_2)_{\text{adj}}) + (1.889 \times \ln(\text{FeO}/\text{SiO}_2)_{\text{adj}}) + (-0.296 \times \ln(\text{MnO}/\text{SiO}_2)_{\text{adj}}) + (0.119 \times \ln(\text{MgO}/\text{SiO}_2)_{\text{adj}}) + (0.650 \times \ln(\text{Na}_2\text{O}/\text{SiO}_2)_{\text{adj}}) + (-2.431 \times \ln(\text{K}_2\text{O}/\text{SiO}_2)_{\text{adj}}) + (0.212 \times \ln(\text{P}_2\text{O}_5/\text{SiO}_2)_{\text{adj}}) - 4.332$

---


$$\text{DF2}_{(\text{CA-CR+OI-Col})_{\text{macid}}} = (-1.084 \times \ln(\text{TiO}_2/\text{SiO}_2)_{\text{adj}}) + (1.626 \times \ln(\text{Al}_2\text{O}_3/\text{SiO}_2)_{\text{adj}}) + (0.992 \times \ln(\text{Fe}_2\text{O}_3/\text{SiO}_2)_{\text{adj}}) + \\ (-0.798 \times \ln(\text{FeO}/\text{SiO}_2)_{\text{adj}}) + (-0.779 \times \ln(\text{MnO}/\text{SiO}_2)_{\text{adj}}) + (-0.018 \times \ln(\text{MgO}/\text{SiO}_2)_{\text{adj}}) + (-0.223 \times \ln(\text{Na}_2\text{O}/\text{SiO}_2)_{\text{adj}}) + \\ (0.651 \times \ln(\text{K}_2\text{O}/\text{SiO}_2)_{\text{adj}}) + (0.726 \times \ln(\text{P}_2\text{O}_5/\text{SiO}_2)_{\text{adj}}) - 0.916$$


---

The tectonic settings are: IA=island arc; CA=continental arc; CR=continental rift; OI=ocean island; and Col=collision. The subscript <sub>adj</sub> refers to adjusted data from the SINCLAS (Verma et al. 2002) or IgRoCS computer program (Verma and Rivera-Gómez 2013a).

**Table S10.**

DF1-DF2 equations (approximate coefficients) for the set of five diagrams based on immobile major and trace element ratios proposed by Verma et al. (2013) for acid magmas.

Figure reference; figure type	Discrimination diagram	Discriminant function equations
Verma et al. (2013); log-ratios of immobile major and trace elements (mtacid)	IA+CA-CR+OI-Col	$\text{DF1}_{(\text{IA+CA-CR+OI-Col})_{\text{mtacid}}} = (-0.091 \times \ln(\text{MgO}/\text{TiO}_2)_{\text{adj}}) + (-0.228 \times \ln(\text{P}_2\text{O}_5/\text{TiO}_2)_{\text{adj}}) + (0.729 \times \ln(\text{Nb}/\text{TiO}_2)_{\text{adj}}) + (-0.237 \times \ln(\text{Y}/\text{TiO}_2)_{\text{adj}}) + (0.577 \times \ln(\text{Zr}/\text{TiO}_2)_{\text{adj}}) + 4.704$ $\text{DF2}_{(\text{IA+CA-CR+OI-Col})_{\text{mtacid}}} = (-0.268 \times \ln(\text{MgO}/\text{TiO}_2)_{\text{adj}}) + (-1.253 \times \ln(\text{P}_2\text{O}_5/\text{TiO}_2)_{\text{adj}}) + (-0.476 \times \ln(\text{Nb}/\text{TiO}_2)_{\text{adj}}) + (0.209 \times \ln(\text{Y}/\text{TiO}_2)_{\text{adj}}) + (-0.082 \times \ln(\text{Zr}/\text{TiO}_2)_{\text{adj}}) - 3.709$
	IA-CA-CR+OI	$\text{DF1}_{(\text{IA-CA-CR+OI})_{\text{mtacid}}} = (-0.018 \times \ln(\text{MgO}/\text{TiO}_2)_{\text{adj}}) + (-0.025 \times \ln(\text{P}_2\text{O}_5/\text{TiO}_2)_{\text{adj}}) + (1.060 \times \ln(\text{Nb}/\text{TiO}_2)_{\text{adj}}) + (-0.530 \times \ln(\text{Y}/\text{TiO}_2)_{\text{adj}}) + (0.301 \times \ln(\text{Zr}/\text{TiO}_2)_{\text{adj}}) + 4.701$ $\text{DF2}_{(\text{IA-CA-CR+OI})_{\text{mtacid}}} = (-0.197 \times \ln(\text{MgO}/\text{TiO}_2)_{\text{adj}}) + (0.118 \times \ln(\text{P}_2\text{O}_5/\text{TiO}_2)_{\text{adj}}) + (-0.724 \times \ln(\text{Nb}/\text{TiO}_2)_{\text{adj}}) + (1.099 \times \ln(\text{Y}/\text{TiO}_2)_{\text{adj}}) + (0.742 \times \ln(\text{Zr}/\text{TiO}_2)_{\text{adj}}) + 3.702$
	IA-CA-Col	$\text{DF1}_{(\text{IA-CA-Col})_{\text{mtacid}}} = (0.248 \times \ln(\text{P}_2\text{O}_5/\text{TiO}_2)_{\text{adj}}) + (1.183 \times \ln(\text{Nb}/\text{TiO}_2)_{\text{adj}}) + (-0.861 \times \ln(\text{Y}/\text{TiO}_2)_{\text{adj}}) + (0.136 \times \ln(\text{Zr}/\text{TiO}_2)_{\text{adj}}) + 3.988$ $\text{DF2}_{(\text{IA-CA-Col})_{\text{mtacid}}} = (1.129 \times \ln(\text{P}_2\text{O}_5/\text{TiO}_2)_{\text{adj}}) + (-0.382 \times \ln(\text{Nb}/\text{TiO}_2)_{\text{adj}}) + (1.126 \times \ln(\text{Y}/\text{TiO}_2)_{\text{adj}}) + (0.682 \times \ln(\text{Zr}/\text{TiO}_2)_{\text{adj}}) + 7.274$
	IA-CR+OI-Col	$\text{DF1}_{(\text{IA-CR+OI-Col})_{\text{mtacid}}} = (0.095 \times \ln(\text{MgO}/\text{TiO}_2)_{\text{adj}}) + (-0.079 \times \ln(\text{P}_2\text{O}_5/\text{TiO}_2)_{\text{adj}}) + (1.104 \times \ln(\text{Nb}/\text{TiO}_2)_{\text{adj}}) + (-0.900 \times \ln(\text{Y}/\text{TiO}_2)_{\text{adj}}) + (0.333 \times \ln(\text{Zr}/\text{TiO}_2)_{\text{adj}}) + 2.771$ $\text{DF2}_{(\text{IA-CR+OI-Col})_{\text{mtacid}}} = (-0.298 \times \ln(\text{MgO}/\text{TiO}_2)_{\text{adj}}) + (-0.998 \times \ln(\text{P}_2\text{O}_5/\text{TiO}_2)_{\text{adj}}) + (-0.279 \times \ln(\text{Nb}/\text{TiO}_2)_{\text{adj}}) + (0.339 \times \ln(\text{Y}/\text{TiO}_2)_{\text{adj}}) + (0.171 \times \ln(\text{Zr}/\text{TiO}_2)_{\text{adj}}) - 0.805$
	CA-CR+OI-Col	$\text{DF1}_{(\text{CA-CR+OI-Col})_{\text{mtacid}}} = (-0.081 \times \ln(\text{MgO}/\text{TiO}_2)_{\text{adj}}) + (-0.432 \times \ln(\text{P}_2\text{O}_5/\text{TiO}_2)_{\text{adj}}) + (0.444 \times \ln(\text{Nb}/\text{TiO}_2)_{\text{adj}}) + (-0.131 \times \ln(\text{Y}/\text{TiO}_2)_{\text{adj}}) + (0.824 \times \ln(\text{Zr}/\text{TiO}_2)_{\text{adj}}) + 3.726$

---


$$\text{DF2}_{(\text{CA-CR-Col})_{\text{mtacid}}} = (-0.341 \times \ln(\text{MgO}/\text{TiO}_2)_{\text{adj}}) + (-1.110 \times \ln(\text{P}_2\text{O}_5/\text{TiO}_2)_{\text{adj}}) + \\ (-0.754 \times \ln(\text{Nb}/\text{TiO}_2)_{\text{adj}}) + (0.271 \times \ln(\text{Y}/\text{TiO}_2)_{\text{adj}}) + \\ (-0.377 \times \ln(\text{Zr}/\text{TiO}_2)_{\text{adj}}) - 5.425$$


---

The tectonic settings are: IA–island arc; CA–continental arc; CR–continental rift; OI–ocean island; and Col–collision. The subscript <sub>adj</sub> refers to adjusted data from the SINCLAS (Verma et al. 2002) or IgRoCS computer program (Verma and Rivera-Gómez 2013a).

**Table S11.**

DF1-DF2 equations (approximate coefficients) for the set of five diagrams based on immobile trace element ratios proposed by Verma et al. (2013) for acid magmas.

Figure reference; figure type	Discrimination diagram	Discriminant function equations
Verma et al. (2013); log-ratios of immobile trace elements (tacid)	IA+CA-CR+OI-Col	$\text{DF1}_{(\text{IA}+\text{CA}-\text{CR}+\text{OI}-\text{Col})_{\text{tacid}}} = (-4.994 \times \ln(\text{La/Yb})) + (7.810 \times \ln(\text{Ce/Yb})) + (-4.329 \times \ln(\text{Sm/Yb})) + (0.822 \times \ln(\text{Nb/Yb})) + (0.063 \times \ln(\text{Th/Yb})) + (0.644 \times \ln(\text{Y/Yb})) + (-0.567 \times \ln(\text{Zr/Yb})) - 9.497$ $\text{DF2}_{(\text{IA}+\text{CA}-\text{CR}+\text{OI}-\text{Col})_{\text{tacid}}} = (2.325 \times \ln(\text{La/Yb})) + (-3.620 \times \ln(\text{Ce/Yb})) + (2.621 \times \ln(\text{Sm/Yb})) + (0.250 \times \ln(\text{Nb/Yb})) + (0.843 \times \ln(\text{Th/Yb})) + (-1.139 \times \ln(\text{Y/Yb})) + (-1.269 \times \ln(\text{Zr/Yb})) + 10.251$
	IA-CA-CR+OI	$\text{DF1}_{(\text{IA}-\text{CA}-\text{CR}+\text{OI})_{\text{tacid}}} = (-5.209 \times \ln(\text{La/Yb})) + (6.616 \times \ln(\text{Ce/Yb})) + (-3.632 \times \ln(\text{Sm/Yb})) + (1.692 \times \ln(\text{Nb/Yb})) + (0.334 \times \ln(\text{Th/Yb})) + (1.558 \times \ln(\text{Y/Yb})) + (-0.488 \times \ln(\text{Zr/Yb})) - 9.614$ $\text{DF2}_{(\text{IA}-\text{CA}-\text{CR}+\text{OI})_{\text{tacid}}} = (-3.72 \times \ln(\text{La/Yb})) + (4.792 \times \ln(\text{Ce/Yb})) + (-2.678 \times \ln(\text{Sm/Yb})) + (0.158 \times \ln(\text{Nb/Yb})) + (-0.499 \times \ln(\text{Th/Yb})) + (1.035 \times \ln(\text{Y/Yb})) + (-0.342 \times \ln(\text{Zr/Yb})) - 4.934$
	IA-CA-Col	$\text{DF1}_{(\text{IA}-\text{CA}-\text{Col})_{\text{tacid}}} = (-0.047 \times \ln(\text{La/Yb})) + (1.076 \times \ln(\text{Ce/Yb})) + (-0.963 \times \ln(\text{Sm/Yb})) + (0.840 \times \ln(\text{Nb/Yb})) + (0.594 \times \ln(\text{Th/Yb})) + (-0.878 \times \ln(\text{Zr/Yb})) - 0.731$ $\text{DF2}_{(\text{IA}-\text{CA}-\text{Col})_{\text{tacid}}} = (-4.067 \times \ln(\text{La/Yb})) + (4.736 \times \ln(\text{Ce/Yb})) + (-0.077 \times \ln(\text{Sm/Yb})) + (-0.225 \times \ln(\text{Nb/Yb})) + (0.774 \times \ln(\text{Th/Yb})) + (-2.495 \times \ln(\text{Zr/Yb})) + 5.099$
	IA-CR+OI-Col	$\text{DF1}_{(\text{IA}-\text{CR}+\text{OI}-\text{Col})_{\text{tacid}}} = (0.259 \times \ln(\text{La/Yb})) + (1.047 \times \ln(\text{Ce/Yb})) + (-1.004 \times \ln(\text{Sm/Yb})) + (0.898 \times \ln(\text{Nb/Yb})) + (0.542 \times \ln(\text{Th/Yb})) + (0.089 \times \ln(\text{Y/Yb})) + (-0.620 \times \ln(\text{Zr/Yb})) - 2.914$ $\text{DF2}_{(\text{IA}-\text{CR}+\text{OI}-\text{Col})_{\text{tacid}}} = (-5.356 \times \ln(\text{La/Yb})) + (8.414 \times \ln(\text{Ce/Yb})) + (-5.369 \times \ln(\text{Sm/Yb})) + (0.483 \times \ln(\text{Nb/Yb})) + (-0.411 \times \ln(\text{Th/Yb})) + (1.119 \times \ln(\text{Y/Yb})) + (0.373 \times \ln(\text{Zr/Yb})) - 13.950$
	CA-CR+OI-Col	$\text{DF1}_{(\text{CA}-\text{CR}+\text{OI}-\text{Col})_{\text{tacid}}} = (-5.409 \times \ln(\text{La/Yb})) + (8.436 \times \ln(\text{Ce/Yb})) + (-4.783 \times \ln(\text{Sm/Yb})) + (0.776 \times \ln(\text{Nb/Yb})) + (-0.079 \times \ln(\text{Th/Yb})) + (0.636 \times \ln(\text{Y/Yb})) + (-0.263 \times \ln(\text{Zr/Yb})) - 11.340$ $\text{DF2}_{(\text{CA}-\text{CR}+\text{OI}-\text{Col})_{\text{tacid}}} = (1.683 \times \ln(\text{La/Yb})) + (-1.730 \times \ln(\text{Ce/Yb})) + (0.516 \times \ln(\text{Sm/Yb})) + (0.838 \times \ln(\text{Nb/Yb})) + (1.037 \times \ln(\text{Th/Yb})) + (-0.984 \times \ln(\text{Y/Yb})) + (-1.414 \times \ln(\text{Zr/Yb})) + 6.088$

The tectonic settings are: IA=island arc; CA=continental arc; CR=continental rift; OI=ocean island; and Col=collision.

**Table S12**

Synthesis of the compilation of “fresh” rock samples used in the present study for testing of discrimination diagrams (18 test studies).

Test study		Approximate location		Number of Samples* <i>(Figure no; Table no. for results)</i>			Age and rock type		Inferred Tectonic setting	Reference
Region	Sub-region	Long. (°)	Lat. (°)	B + U m1/m2, t1, t2	I m, mt, t	A m, mt, t	Age (Ma)	Author rock type		
<b>Expected tectonic setting: Ocean Island</b>										
1. Hawaiian Islands (Pacific Ocean)	1a. Mauna Kea	-155.5	19.8	303+3, 0, 303+3 <i>(Figs. I, S2, S3; Table I)</i>	---	---	0.1-0.4	submarine basaltic lava	OIB	Rhodes and Vollinger (2004), Rhodes (2012)
	1b. Mauna Loa	-155.6	19.5	43+2, 0, 43+2 <i>(Figs. S4-S6; Table S14)</i>	---	---	0.1-0.4	submarine basaltic lava	OIB	Rhodes and Vollinger (2004)
	1c. Maui	-156.6	20.9	10, 0, 10 <i>(Figs. S7- S9; Table S15)</i>	---	---	1.9-2.1	basaltic lava	OIB	Sherrod et al. (2007)
	1d. Oahu	-157.9	21.5	9, 4, 9 <i>(Figs. S10- S12; Table S16)</i>	15, 15, 3 <i>(Figs. S13- S14; Table S17)</i>	---	2.9-3.9	basaltic lava and dike rocks	OIB; OI	Jackson et al. (1999)
2. Trindade Island (southern Atlantic Ocean)	2. Trindade	-29.3	-20.5	2+12, 2+11, 0 <i>(Figs. S15- S17; Table S18)</i>	24, 0, 13 <i>(Figs. S18- S19; Table S19)</i>	---	<0.27-3.6	different types of alkalic rocks	OIB; CR+OI	Marques et al.(1999)
<b>Expected tectonic setting: Ocean Island or Continental rift</b>										
3. Antarctica (Ross Sea)	3. White Island	168.0	-78.0	22, 22, 22 <i>(Figs. S20- S23; Table S20)</i>	---	---	0.17-7.65	Alkali rocks	CRB; OIB	Cooper et al. (2007)
4. Antarctica	4. McMurdo Sound	166.9	-77.8	24, 20, 20 <i>(Figs. S24- S27; Table S21)</i>	---	---	15.9-18.4	drill core glasses	OIB	Nyland et al. (2013)
<b>Expected tectonic setting: Continental rift</b>										
5. Spain	5. Garrotxa, NE Volcanic province	2.5	42	8+8, 8+7, 8+7 <i>(Figs. S28- S31; Table S22)</i>	---	---	0.7-0.0115	alkaline rocks	CRB	Cebriá et al. (2000)
6. Austria	6. Styrian basin	14.4	47.5	9+30, 9+30, 9+30 <i>(Figs. S32- S35; Table S18)</i>	---	---	Quaternary	Styrian basin lavas	CRB	Ali et al. (2013)
7. Cameroon	7. Mount Cameroon	9.2	4.2	14, 0, 14 <i>(Figs. S36- S38; Table S18)</i>	---	---	Eruptions of years 1999 and 2000	Lava flow	CRB	Suh et al. (2003)

<b>8.</b> Madagascar	<b>8.</b> Nosy Be Archipelago	48.3	-13.3	27, 0, 27 ( <i>Figs. S39- S41; Table S25</i> )	---	---	7-10	Mafic alkaline rocks	CRB	Melluso and Morra (2000)
<b>9.</b> Inner Mongolia, China	<b>9.</b> Tianheyong	114.0	41.0	8, 8, 0 ( <i>Figs. S42- S44; Table S26</i> )	---	---	21.7±1.7	basanites	CRB; OIB	Yang et al. (2009)
<b>10.</b> China (north-east)	<b>10.</b> Halaha volcanic field, Central Great Xing'an Range	120.5	47.5	14, 14, 14 ( <i>Figs. S45- S48; Table S27</i> )	---	---	0.17-2.04	basalt	CRB	Ho et al. (2013)
Expected tectonic setting: <b>Continental arc</b>										
<b>11.</b> Aleutian arc, Alaska	<b>11.</b> Aniakchak ignimbrite	-158.1	56.9	---	---	9, 9, 9 ( <i>Figs. S49- S52; Table S28</i> )	0.0034	rhyodacitic to andesitic ignimbrite	CA	Dreher et al. (2005)
	12a. Fuego volcanic complex	-90.9	14.5	---	9, 0, 0 ( <i>Table S29</i> )	---	Recent eruptions	lava	CA	Chesner and Rose Jr. (1984)
<b>12.</b> Guatemala	12b. Meseta Volcano	-90.7	14.6	---	40, 0, 0 ( <i>Table S30</i> )	---	Quaternary	lava	CA	Chesner and Halsor (1997)
	12c. Santiaguito volcanic dome complex	-91.6	14.8	---	18, 5, 18 ( <i>Table S31</i> )	17, 17, 17 ( <i>Table S32</i> )	0.000112	lava	CA; IA or CA-Col	Scott et al.(2013)
<b>13.</b> Chile	<b>13.</b> Huequi volcano dome complex	-72.6	-42.5	---	9, 9, 0 ( <i>Table S33</i> )	---	0.000123	lava	CA	Watt et al. (2011)
<b>14.</b> Greece	<b>14.</b> Nisyros Island, Dodecanese	27	36.6	---	16, 0, 0 ( <i>Table S34</i> )	11, 0, 0 ( <i>Table S35</i> )	Quaternary	volcanic rocks	CA	Di Paola (1974)
Expected tectonic setting: <b>Island arc</b>										
<b>15.</b> Aleutian arc	<b>15.</b> Augustine Island	-153.4	59.36	---	21, 0, 0 ( <i>Table S36</i> )	---	6.0	volcanic rocks	IA	Johnson et al. (1996)
<b>16.</b> Andaman-Nicobar Islands	16a. Barren Island	93.85	12.29	25, 11, 24 ( <i>Table S37</i> )	21, 21, 9 ( <i>Table S38</i> )	---	Quaternary	volcanic rocks	Arc	Chandrasekharan et al. (2009); Streck et al. (2011)
	16b. Narcondam Island	94.28	13.43	---	10, 8, 8 ( <i>Table S39</i> )	8, 0, 0 ( <i>Table S40</i> )	Quaternary	volcanic rocks	IA	Pal et al. (2007); Streck et al. (2011)
Expected tectonic setting: <b>Mid-ocean ridge</b>										
<b>17.</b> Indian Ocean	<b>17.</b> Indian Ridge (central)	66	-14	33, 32, 33 ( <i>Table S41</i> )	[14, 14, 14] (---)	---	Quaternary	basaltic rocks	MORB	Yi et al. (2014)

---

Expected tectonic setting: Collision

---

18. Armenia	18. Shirak area	43.9	40.9	---	13, 9, 13 <i>(Table S42)</i>	---	2.5-4.6	volcanic rocks	Col	Neill et al. (2013)
-------------	-----------------	------	------	-----	---------------------------------	-----	---------	----------------	-----	---------------------

---

**B**=basic rock; **U**=ultrabasic rocks : m1=first set of major element based diagrams (Agrawal et al. 2004); m2=second set of major element based diagrams (Verma et al. 2006); t1=first set of trace element based diagrams (Agrawal et al. 2008); t2=second set of trace element based diagrams (Verma and Agrawal 2011); **I**=set of intermediate rocks based diagrams (Verma and Verma 2013); **A**=set of acid rocks based diagrams (Verma et al. 2012; Verma et al. 2013); m= major elements mt=(immobile) major and trace elements; t=(immobile) trace elements, for each set respectively; --- no sample; note less than five (an arbitrarily set lower number) samples are not considered for evaluation. Inferred tectonic setting: Arc=island or continental arc; CRB=continental rift for basic rocks; OIB=ocean island for basic rocks; MORB=mid-ocean ridge for basic rocks, IA=Island Arc, CA=Continental Arc, CR=continental rift; OI=ocean island; CR+OI-within-plate; Col=Collision.

**Table S13**

Synthesis of the compilation of hydrothermally altered rock samples used in the present study for testing of discrimination diagrams (8 application studies).

Test study		Approximate location		Number of Samples* (Table no. for results)			Age and rock type		Inferred Tectonic setting	Reference
Region	Sub-region	Long. (°)	Lat. (°)	B + U m1/ m2, t1, t2	I m, mt, t	A m, mt, t	Age (Ma)	Author rock type		
Expected tectonic setting: <b>Ocean Island</b>										
<b>A1.</b> Marquesas Islands	A1. Eao Island	-140.67	-7.98	24+1, 0, 24+1 (Table S43)	---	---	4.95-5.52	hydrothermally altered rocks	OIB	Caroff et al. (1999)
<b>A2.</b> Hawaiian Islands	A2. Haleakala, Koolau, and Kohala volcanoes	-156	20	4+5, 0, 0 (Table S44)	---	---	0.35-4	spheroidal weathering	CRB	Patino et al. (2003)
Expected tectonic setting: <b>Ocean Island or continental rift</b>										
<b>A3.</b> Hainan Island, China	A3. Hainan Island	109.5	19.8	13, 4, 4 (Table S45)	10, 3, 3 (Table S46)	---	13-Holocene	slightly to intensely altered	CRB; WP	Wang et al. (2012)
Expected tectonic setting: <b>Continental arc</b>										
<b>A4.</b> Guatemala	A4. Moyuta and Tecuamburro volcanoes	-90.43	14.16	---	7, 0, 0 (Table S47)	---	probably Pliocene-Pleistocene	spheroidal weathering	CA	Patino et al. (2003)
Expected tectonic setting: <b>Island or continental arc</b>										
<b>A5.</b> Costa Rica	A5. Sarapiqui Miocene arc	-84.23	10.77	10, 3, 10 (Table S48)	14, 14, 3 (Table S49)	4, 4, 1	11.4-22.2	altered rocks	Arc; IA	Gazel et al. (2005)
<b>A6.</b> New Zealand	A6. Taupo Volcanic Zone	176.18	-38.65	---	28, 5, 0 (Table S50)	---	> 0.33	drill hole hydrothermally altered rocks	IA	Browne et al. (1992)
Expected tectonic setting: <b>Mid-ocean ridge</b>										
<b>A7.</b> Indian and Pacific Oceans	A7a. SE Indian and SW Pacific seafloor	110 to 160	-40 to -60	9, 7, 9 (Table S51)	---	---	0-4 and 15-23	altered and fresh rocks	MORB	Pyle et al. (1995)
	A7b. central Indian Ridge	66	-8 to -17	26+2, 17, 20 (Table S52)	[4, 3, 3]	---	Quaternary	altered and fresh rocks	MORB	Yi et al. (2014)
Expected tectonic setting: <b>collision</b>										
<b>A8.</b> Italy	A8. Stromboli volcano, Aeolian Island	14.92	38.49	---	7, 3, 7 (Table S53)	10, 10, 10 (Table S54)	Quaternary	buchite ejecta	Col	Del Moro et al. (2011)

For more explanation, see footnote of Table S12.

**Table S14.**

Testing of multidimensional diagrams from Quaternary (0.1-0.4 Ma) basic and ultrabasic rocks of Mauna Loa, Hawaii (Rhodes and Vollinger, 2004; Test study 1b).

Figure reference; figure type	Discrimination diagram	Total no. of samples (%)	Predicted tectonic affinity and number of discriminated samples (%)				
			IAB	CRB+OIB	CRB	OIB	MORB
Agrawal et al. (2004); adjusted major element concentrations	IAB-CRB-OIB-MORB	45 (100)	0 (0)	---	2 (4.5)	38 (84.4)	5 (11.1)
	IAB-CRB-OIB	45 (100)	0 (0)	---	1 (2.2)	44 (97.8)	---
	IAB-CRB-MORB	45 (100)	0 (0)	---	23 (51.1)	---	22 (48.9)
	IAB-OIB-MORB	45 (100)	0 (0)	---	---	45 (100)	0 (0)
	CRB-OIB-MORB	45 (100)	---	---	0 (0)	44 (97.8)	1 (2.2)
<b>Test study 1b. Synthesis of all five diagrams of Agrawal et al. (2004)</b>		<b>225 (100)</b>	<b>0 (0)</b>	---	<b>26 (11.6)</b>	<b>171 (76.0)</b>	<b>28 (12.4)</b>
Verma et al. (2006); log-ratios of major elements	IAB-CRB-OIB-MORB	45 (100)	0 (0)	---	0 (0)	37 (82.2)	8 (17.8)
	IAB-CRB-OIB	45 (100)	0 (0)	---	0 (0)	45 (100)	---
	IAB-CRB-MORB	45 (100)	0 (0)	---	1 (2.2)	---	44 (97.8)
	IAB-OIB-MORB	45 (100)	0 (0)	---	---	45 (100)	0 (0)
	CRB-OIB-MORB	45 (100)	---	---	0 (0)	45 (100)	0 (0)
<b>Test study 1b. Synthesis of all five diagrams of Verma et al. (2006)</b>		<b>225 (100)</b>	<b>0 (0)</b>	---	<b>1 (0.4)</b>	<b>172 (76.4)</b>	<b>52 (23.1)</b>
Verma and Agrawal (2011); log-ratios of immobile major and trace elements	IAB-CRB+OIB-MORB	45 (100)	0 (0)	45 (100)	---	---	0 (0)
	IAB-CRB-OIB	45 (100)	0 (0)	---	0 (0)	45 (100)	---
	IAB-CRB-MORB	45 (100)	0 (0)	---	45 (100)	---	0 (0)
	IAB-OIB-MORB	45 (100)	0 (0)	---	---	45 (100)	0 (0)
	CRB-OIB-MORB	45 (100)	---	---	0 (0)	45 (100)	0 (0)
<b>Test study 1b. Synthesis of all five diagrams of Verma and Agrawal (2011)</b>		<b>225 (100)</b>	<b>0 (0)</b>	<b>45 (---)</b>	<b>56 (24.9)</b>	<b>169 (75.1)</b>	<b>0(0)</b>

IAB=island (or continental) arc basic rock; CRB=continental rift basic rock; OIB=ocean island basic rock; MORB=mid-ocean ridge basic rock; CRB+OIB=combined continental rift and ocean island, i.e., within-plate (WP) basic rocks; IA, CR, OI, and MOR will be the corresponding tectonic settings; --- means no samples; the numbers within the parentheses refer to the percent values for the corresponding number of samples; note, for the calculations of percent synthesis values, the samples plotting in the combined CR+OI field (CRB+OIB column) are proportionately distributed between the CR and OI settings.

**Table S15.**

Testing of multidimensional diagrams from Quaternary (1.9–2.1 Ma) basic and ultrabasic rocks of the Maui Island, Hawaii (Sherrod et al. 2007; Test study 1c).

Figure reference; figure type	Discrimination diagram	Total no. of samples (%)	Predicted tectonic affinity and number of discriminated samples (%)				
			IAB	CRB+OIB	CRB	OIB	MORB
Agrawal et al. (2004); adjusted major element concentrations	IAB-CRB-OIB-MORB	10 (100)	0 (0)	---	0 (0)	10 (100)	0 (0)
	IAB-CRB-OIB	10 (100)	0 (0)	---	0 (0)	10 (100)	---
	IAB-CRB-MORB	10 (100)	0 (0)	---	9 (90)	---	1 (10)
	IAB-OIB-MORB	10 (100)	0 (0)	---	---	10 (100)	0 (0)
	CRB-OIB-MORB	10 (100)	---	---	0 (0)	10 (100)	0 (0)
<b>Test study 1c. Synthesis of all five diagrams of Agrawal et al. (2004)</b>		<b>50 (100)</b>	<b>0 (0)</b>	<b>---</b>	<b>9 (18)</b>	<b>40 (80)</b>	<b>1 (2)</b>
Verma et al. (2006); log-ratios of major elements	IAB-CRB-OIB-MORB	10 (100)	0 (0)	---	0 (0)	9 (90)	1 (10)
	IAB-CRB-OIB	10 (100)	0 (0)	---	0 (0)	10 (100)	---
	IAB-CRB-MORB	10 (100)	0 (0)	---	3 (30)	---	7 (70)
	IAB-OIB-MORB	10 (100)	0 (0)	---	---	10 (100)	0 (0)
	CRB-OIB-MORB	10 (100)	---	---	0 (0)	10 (100)	0 (0)
<b>Test study 1c. Synthesis of all five diagrams of Verma et al. (2006)</b>		<b>50 (100)</b>	<b>0 (0)</b>	<b>---</b>	<b>3 (6)</b>	<b>39 (78)</b>	<b>8 (16)</b>
Verma and Agrawal (2011); log-ratios of immobile major and trace elements	IAB-CRB+OIB-MORB	10 (100)	0 (0)	9 (90)	---	---	1 (10)
	IAB-CRB-OIB	10 (100)	0 (0)	---	3 (30)	7 (70)	---
	IAB-CRB-MORB	10 (100)	0 (0)	---	9 (90)	---	1 (10)
	IAB-OIB-MORB	10 (100)	0 (0)	---	---	9 (90)	1 (10)
	CRB-OIB-MORB	10 (100)	---	---	0 (0)	9 (90)	1 (10)
<b>Test study 1c. Synthesis of all five diagrams of Verma and Agrawal (2011)</b>		<b>50 (100)</b>	<b>0 (0)</b>	<b>9 (---)</b>	<b>15 (30)</b>	<b>31 (62)</b>	<b>4(8)</b>

For the explanation of abbreviations, see footnote of Table 1 or S14.

**Table S16.**

Testing of multidimensional diagrams from Quaternary (2.9–3.9 Ma) basic and ultrabasic rocks of the Oahu Island, Hawaii (Jackson et al. 1999; Test study 1d).

Figure reference; figure type	Discrimination diagram	Total no. of samples (%)	Predicted tectonic affinity and number of discriminated samples (%)				
			IAB	CRB+OI B	CRB	OIB	MORB
Agrawal et al. (2004); adjusted major element concentrations	IAB-CRB-OIB-MORB	9 (100)	0 (0)	---	0 (0)	8 (88.9)	1 (11.1)
	IAB-CRB-OIB	9 (100)	0 (0)	---	0 (0)	9 (100)	---
	IAB-CRB-MORB	9 (100)	0 (0)	---	1 (11.1)	---	8 (88.9)
	IAB-OIB-MORB	9 (100)	0 (0)	---	---	9 (100)	0 (0)
	CRB-OIB-MORB	9 (100)	---	---	0 (0)	9 (100)	0 (0)
<i>Test study 1d. Synthesis of all five diagrams of Agrawal et al. (2004)</i>		<b>45 (100)</b>	<b>0 (0)</b>	---	<b>1 (2)</b>	<b>35 (78)</b>	<b>9 (20)</b>
Verma et al. (2006); log-ratios of major elements	IAB-CRB-OIB-MORB	9 (100)	0 (0)	---	0 (0)	6 (66.7)	3 (33.3)
	IAB-CRB-OIB	9 (100)	0 (0)	---	0 (0)	9 (100)	---
	IAB-CRB-MORB	9 (100)	0 (0)	---	0 (0)	---	9 (100)
	IAB-OIB-MORB	9 (100)	0 (0)	---	---	8 (88.9)	1 (11.1)
	CRB-OIB-MORB	9 (100)	---	---	0 (0)	7 (77.8)	2 (22.2)
<i>Test study 1d. Synthesis of all five diagrams of Verma et al. (2006)</i>		<b>45 (100)</b>	<b>0 (0)</b>	---	<b>0 (0)</b>	<b>30 (67)</b>	<b>15 (33)</b>
Verma and Agrawal (2011); log-ratios of immobile major and trace elements	IAB-CRB+OIB-MORB	9 (100)	0 (0)	9 (100)	---	---	0 (0)
	IAB-CRB-OIB	9 (100)	0 (0)	---	0 (0)	9 (100)	---
	IAB-CRB-MORB	9 (100)	0 (0)	---	9 (100)	---	0 (0)
	IAB-OIB-MORB	9 (100)	0 (0)	---	---	9 (100)	0 (0)
	CRB-OIB-MORB	9 (100)	---	---	0 (0)	9 (100)	0 (0)
<i>Test study 1d. Synthesis of all five diagrams of Verma and Agrawal (2011)</i>		<b>45 (100)</b>	<b>0 (0)</b>	<b>9 (---)</b>	<b>11 (24)</b>	<b>34 (76)</b>	<b>0 (0)</b>

For the explanation of abbreviations, see footnote of Table 1 or S14.

**Table S17.**

Testing of multidimensional diagrams from Quaternary (2.9–3.9 Ma) intermediate rocks of the Oahu Island, Hawaii (Jackson et al. 1999; Test study 1d).

Magma type, Figure name; Figure number	Figure type	Total number of samples	Number of discriminated samples					
			Arc			Within-plate CR+OI [ $\bar{x} \pm s$ ] [ $p_{CR+OI}$ ] $\Theta$	Collision Col [ $\bar{x} \pm s$ ] [ $p_{Col}$ ] $\Theta$	
			IA+CA [ $\bar{x} \pm s$ ] ( $p_{IA+CA}$ ) $\Theta$	IA [ $\bar{x} \pm s$ ] [ $p_{IA}$ ] $\Theta$	CA [ $\bar{x} \pm s$ ] [ $p_{CA}$ ] $\Theta$			
Intermediate; Verma and Verma (2013); log-ratios of all major elements;	IA+CA-CR+OI-Col	15	0 (0)	---	---	15 [0.777±0.087] (0.6282-0.9942)	0 (0)	
	IA-CA-CR+OI	15	---	0 (0)	0 (0)	15 [0.763±0.092] (0.6015-0.9929)	---	
	IA-CA-Col	15	---	[0.7525±0.0444] (0.6727-0.8286)	0 (0)	---	0 (0)	
	IA-CR+OI-Col	15	---	0 (0)	---	15 [0.796±0.085] (0.6617-0.9961)	0 (0)	
	CA-CR+OI-Col	15	---	---	0 (0)	15 [0.780±0.084] (0.6548-0.9940)	0 (0)	
<i>Test study 1d.</i> <i>Diagrams based</i> <i>on log-ratios of</i> <i>major elements</i>		{Σn} {Σprob} [%prob]	75	{0} {0} [0%]	{15} {11.2869} [19%]	{0} {0} [0%]	{60} {46.7383} [81%]	{0} {0} [0%]
Intermediate; Verma and Verma (2013); log-ratios of immobile major and trace elements	IA+CA-CR+OI-Col	15	0 (0)	---	---	15 [0.99334±0.00382] (0.9852-0.9985)	0 (0)	
	IA-CA-CR+OI	15	---	0 (0)	0 (0)	15 [0.9925±0.0050] (0.9811-0.9993)	---	
	IA-CA-Col	15	---	0 (0)	[0.568±0.055] (0.5048- 0.6604)	---	1 (0.6189)	
	IA-CR+OI-Col	15	---	0 (0)	---	15 [0.99229±0.00366] (0.9848-0.9976)	0 (0)	
	CA-CR+OI-Col	15	---	---	0 (0)	15 [0.9764±0.0167] (0.9365-0.9973)	0 (0)	
<i>Test study 1d.</i> <i>Diagrams based</i> <i>on log-ratios of</i> <i>selected immobile</i> <i>major and trace</i> <i>elements</i>		{Σn} {Σprob} [%prob]	75	{0} {0} [0%]	{0} {0} [0%]	{14} {7.9546} [12%]	{60} {59.3177} [87%]	{1} {0.6189} [1%]

IA—island arc; CA—continental arc; IA+CA—combined island and continental arcs, i.e., arc setting; CR—continental rift; OI—ocean island; CR+OI—combined continental rift and ocean island, i.e., within-plate (WP) setting; Col—collision;  $\Theta$  the probability values for samples from a given locality are represented by ( $p_{IA+CA}$ ) — probability for the combined island and continental arc setting in the first diagram; [ $p_{IA}$ ] — probability for the island arc setting in the diagrams; [ $p_{CA}$ ] — probability for the continental arc setting in the diagrams; [ $p_{CR+OI}$ ] — probability for the combined continental rift and ocean island setting in all diagrams; [ $p_{Col}$ ] — probability for the collision setting in the diagrams;  $\bar{x} \pm s$  – mean  $\pm$  1SD (standard deviation) of the probability estimates for all samples discriminated in a given tectonic setting; these are reported in []; the final row gives a synthesis of results as {Σn} {Σprob} [%prob], where {Σn} is the total number of samples or data points plotting in all five diagrams is reported in the column of total number of samples, whereas the sum of samples plotting in a given tectonic field is reported in the respective tectonic field column; {Σprob} is the sum of probability values for all samples plotting in a given tectonic field is reported in the respective tectonic field column; and [%prob] is the total probability of a given tectonic setting expressed in percent after assigning the probability of IA + CA to IA and CA (using weighing factors explained in Verma and Verma 2013).

**Table S18.**

Testing of multidimensional diagrams from Quaternary (<0.27–3.6 Ma) basic and ultrabasic rocks of Trindade Island, southern Atlantic Ocean (Marques et al. 1999; Test study 2).

Figure reference; figure type	Discrimination diagram	Total no. of samples (%)	Predicted tectonic affinity and number of discriminated samples (%)				
			IAB	CRB+OIB	CRB	OIB	MORB
Agrawal et al. (2004); adjusted major element concentrations	IAB-CRB-OIB-MORB	14 (100)	0 (0)	---	1 (7.1)	12 (85.8)	1 (7.1)
	IAB-CRB-OIB	14 (100)	0 (0)	---	2 (14.3)	12 (85.7)	---
	IAB-CRB-MORB	14 (100)	0 (0)	---	14 (100)	---	0 (0)
	IAB-OIB-MORB	14 (100)	0 (0)	---	---	13 (92.9)	1 (7.1)
<i>Test study 2. Synthesis of all five diagrams of Agrawal et al. (2004)</i>	CRB-OIB-MORB	14 (100)	---	---	2 (14.3)	12 (85.7)	0 (0)
	<i>Test study 2. Synthesis of all five diagrams of Agrawal et al. (2004)</i>		<b>70 (100)</b>	<b>0 (0)</b>	<b>---</b>	<b>19 (27)</b>	<b>49 (70)</b>
							<b>2 (3)</b>
Verma et al. (2006); log-ratios of major elements	IAB-CRB-OIB-MORB	14 (100)	0 (0)	---	1 (7.1)	12 (85.8)	1 (7.1)
	IAB-CRB-OIB	14 (100)	0 (0)	---	2 (14.3)	12 (85.7)	---
	IAB-CRB-MORB	14 (100)	0 (0)	---	13 (92.9)	---	1 (7.1)
	IAB-OIB-MORB	14 (100)	0 (0)	---	---	13 (92.9)	1 (7.1)
<i>Test study 2. Synthesis of all five diagrams of Verma et al. (2006)</i>	CRB-OIB-MORB	14 (100)	---	---	1 (7.1)	12 (85.8)	1 (7.1)
	<i>Test study 2. Synthesis of all five diagrams of Verma et al. (2006)</i>		<b>70 (100)</b>	<b>0 (0)</b>	<b>---</b>	<b>17 (24)</b>	<b>49 (70)</b>
							<b>4 (6)</b>
Agrawal et al. (2008); log-ratios of immobile trace elements	IAB-CRB+OIB-MORB	13 (100)	0 (0)	13 (100)	---	---	0 (0)
	IAB-CRB-OIB	13 (100)	0 (0)	---	6 (46.2)	7 (53.8)	---
	IAB-CRB-MORB	13 (100)	0 (0)	---	13 (100)	---	0 (0)
	IAB-OIB-MORB	13 (100)	0 (0)	---	---	13 (100)	0 (0)
<i>Test study 2. Synthesis of all five diagrams of Agrawal et al. (2008)</i>	CRB-OIB-MORB	13 (100)	---	---	1 (7.7)	12 (92.3)	0 (0)
	<i>Test study 2. Synthesis of all five diagrams of Agrawal et al. (2008)</i>		<b>65 (100)</b>	<b>0 (0)</b>	<b>13 (---)</b>	<b>25 (38)</b>	<b>40 (62)</b>
							<b>0 (0)</b>

For the explanation of abbreviations, see footnote of Table 1 or S14.

**Table S19.**

Testing of multidimensional diagrams from Quaternary (<0.27-3.6 Ma) intermediate rocks of the Trindade Island (Marques et al. 1999; Test study 2).

Magma type, Figure name	Figure type	Total number of samples	Number of discriminated samples					
			Arc			Within-plate CR+OI [ $\bar{x} \pm s$ ] [ $p_{CR+OI}$ ] $\Theta$	Collision [ $\bar{x} \pm s$ ] [ $p_{Col}$ ] $\Theta$	
			IA+CA [ $\bar{x} \pm s$ ] [ $p_{IA+CA}$ ] $\Theta$	IA [ $\bar{x} \pm s$ ] [ $p_{IA}$ ] $\Theta$	CA [ $\bar{x} \pm s$ ] [ $p_{CA}$ ] $\Theta$			
Intermediate; Verma and Verma (2013); log-ratios of all major elements	IA+CA-CR+OI-Col	24	1 (0.4915)	---	---	23 [0.863±0.177] (0.4372-0.9981)	0 (0)	
	IA-CA-CR+OI	24	---	1 (0.4582)	2 [0.4920±0.0240] (0.4750, 0.5089)	21 [0.887±0.151] (0.4579-0.9941)	---	
	IA-CA-Col	24	---	1 (0.4845)	15 [0.718±0.095] (0.5470-0.8654)	---	8 [0.605±0.152] (0.4006-0.7849)	
	IA-CR+OI-Col	24	---	1 (0.5906)	---	19 [0.920±0.063] (0.7475-0.9980)	4 [0.4938±0.0346] (0.4482-0.5291)	
	CA-CR+OI-Col	24	---	---	1 (0.4758)	19 [0.807±0.121] (0.5207-0.9909)	4 [0.484±0.046] (0.4387-0.5428)	
<i>Test study 2. Diagrams based on log-ratios of major elements</i>	{Σn} {Σprob} [%prob]	120	{I} {0.4915} [---]	{3} {1.5333} [1.7%]	{18} {12.2347} [13.4%]	{82} {71.2933} [75.6%]	{16} {8.7540} [9.3%]	
Intermediate; Verma and Verma (2013); log-ratios of immobile trace elements	IA+CA-CR+OI-Col	13	0 (0)	---	---	13 [0.9811±0.0109] (0.9560-0.9946)	0 (0)	
	IA-CA-CR+OI	13	---	0 (0)	0 (0)	13 [0.99727±0.00412] (0.9857-0.9997)	---	
	IA-CA-Col	13	---	0 (0)	0 (0)	---	13 [0.9776±0.0238] (0.9199-0.9966)	
	IA-CR+OI-Col	13	---	0 (0)	---	13 [0.9678±0.0147] (0.9365-0.9875)	0 (0)	
	CA-CR+OI-Col	13	---	---	0 (0)	13 [0.9266±0.0329] (0.8669-0.9706)	0 (0)	
<i>Test study 2. Diagrams based on log-ratios of immobile trace elements</i>	{Σn} {Σprob} [%prob]	65	{0} {0} [ 0%]	{0} {0} [ 0%]	{0} {0} [ 0%]	{52} {50.3470} [80%]	{13} {12.7086} [20%]	

For the explanation of abbreviations, see footnote of Table S17.

**Table S20.**

Testing of multidimensional diagrams from Neogene-Quaternary (0.17-7.65Ma; Pliocene-Pleistocene) basic rocks from White Island, Ross Sea, Antarctica (Cooper et al. 2007; Test study 3).

Figure reference; figure type	Discrimination diagram	Total no. of samples (%)	Predicted tectonic affinity and number of discriminated samples (%)				
			IAB	CRB+OIB	CRB	OIB	MORB
Agrawal et al. (2004); adjusted major element concentrations	IAB-CRB-OIB-MORB	22 (100)	0 (0)	---	4 (18.2)	18 (81.8)	0 (0)
	IAB-CRB-OIB	22 (100)	0 (0)	---	14 (63.6)	8 (36.4)	---
	IAB-CRB-MORB	22 (100)	0 (0)	---	22 (100)	---	0 (0)
	IAB-OIB-MORB	22 (100)	0 (0)	---	---	22 (100)	0 (0)
	CRB-OIB-MORB	22 (100)	---	---	9 (40.9)	13 (59.1)	0 (0)
<i>Test study 3. Synthesis of all five diagrams of Agrawal et al. (2004)</i>		<b>110 (100)</b>	<b>0 (0)</b>	<b>---</b>	<b>49 (44.5)</b>	<b>61 (55.5)</b>	<b>0 (0)</b>
Verma et al. (2006); log-ratios of major elements	IAB-CRB-OIB-MORB	22 (100)	0 (0)	---	8 (36.4)	14 (63.6)	0 (0)
	IAB-CRB-OIB	22 (100)	0 (0)	---	12 (54.5)	10 (45.5)	---
	IAB-CRB-MORB	22 (100)	0 (0)	---	22 (100)	---	0 (0)
	IAB-OIB-MORB	22 (100)	0 (0)	---	---	22 (100)	0 (0)
	CRB-OIB-MORB	22 (100)	---	---	11 (50)	11 (50)	0 (0)
<i>Test study 3. Synthesis of all five diagrams of Verma et al. (2006)</i>		<b>110 (100)</b>	<b>0 (0)</b>	<b>---</b>	<b>53 (48.2)</b>	<b>57 (51.8)</b>	<b>0 (0)</b>
Agrawal et al. (2008); log-ratios of immobile trace elements	IAB-CRB+OIB-MORB	22 (100)	0 (0)	22 (100)	---	---	0 (0)
	IAB-CRB-OIB	22 (100)	0 (0)	---	21 (95.5)	1 (4.5)	---
	IAB-CRB-MORB	22 (100)	0 (0)	---	22 (100)	---	0 (0)
	IAB-OIB-MORB	22 (100)	0 (0)	---	---	22 (100)	0 (0)
	CRB-OIB-MORB	22 (100)	---	---	14 (63.6)	8 (36.4)	0 (0)
<i>Test study 3. Synthesis of all five diagrams of Agrawal et al. (2008)</i>		<b>110 (100)</b>	<b>0 (0)</b>	<b>22 (---)</b>	<b>71 (64.5)</b>	<b>39 (35.5)</b>	<b>0 (0)</b>
Verma and Agrawal (2011); log-ratios of immobile major and trace elements	IAB-CRB+OIB-MORB	22 (100)	0 (0)	22 (100)	---	---	0 (0)
	IAB-CRB-OIB	22 (100)	0 (0)	---	3 (13.6)	19 (86.4)	---
	IAB-CRB-MORB	22 (100)	0 (0)	---	22 (100)	---	0 (0)
	IAB-OIB-MORB	22 (100)	0 (0)	---	---	22 (100)	0 (0)
	CRB-OIB-MORB	22 (100)	---	---	3 (13.6)	19 (86.4)	0 (0)
<i>Test study 3. Synthesis of all five diagrams of Verma and Agrawal (2011)</i>		<b>110 (100)</b>	<b>0 (0)</b>	<b>22 (---)</b>	<b>35 (31.8)</b>	<b>75 (68.2)</b>	<b>0(0)</b>

For the explanation of abbreviations, see footnote of Table 1 or S14.

**Table S21.**

Testing of multidimensional diagrams from Miocene (15.91-18.41 Ma) drill core basic volcanic glass samples of the McMurdo Sound area, Antarctica (Nyland et al. 2013; Test study 4).

Figure reference; figure type	Discrimination diagram	Total no. of samples (%)	Predicted tectonic affinity and number of discriminated samples (%)				
			IAB	CRB+OIB	CRB	OIB	MORB
Agrawal et al. (2004); adjusted major element concentrations	IAB-CRB-OIB-MORB	24 (100)	0 (0)	---	6 (25)	18 (75)	0 (0)
	IAB-CRB-OIB	24 (100)	0 (0)	---	6 (25)	18 (75)	---
	IAB-CRB-MORB	24 (100)	0 (0)	---	24 (100)	---	0 (0)
	IAB-OIB-MORB	24 (100)	0 (0)	---	---	24 (100)	0 (0)
	CRB-OIB-MORB	24 (100)	---	---	8 (33.3)	16 (66.7)	0 (0)
<i>Test study 4. Synthesis of all five diagrams of Agrawal et al. (2004)</i>		<b>120 (100)</b>	<b>0 (0)</b>	<b>---</b>	<b>44 (36.7)</b>	<b>76 (63.3)</b>	<b>0 (0)</b>
Verma et al. (2006); log-ratios of major elements	IAB-CRB-OIB-MORB	24 (100)	0 (0)	---	6 (25)	18 (75)	0 (0)
	IAB-CRB-OIB	24 (100)	0 (0)	---	6 (25)	18 (75)	---
	IAB-CRB-MORB	24 (100)	0 (0)	---	24 (100)	---	0 (0)
	IAB-OIB-MORB	24 (100)	0 (0)	---	---	24 (100)	0 (0)
	CRB-OIB-MORB	24 (100)	---	---	7 (29.2)	17 (70.8)	0 (0)
<i>Test study 4. Synthesis of all five diagrams of Verma et al. (2006)</i>		<b>120 (100)</b>	<b>0 (0)</b>	<b>---</b>	<b>43 (35.8)</b>	<b>77 (64.2)</b>	<b>0 (0)</b>
Agrawal et al. (2008); log-ratios of immobile trace elements	IAB-CRB+OIB-MORB	20 (100)	0 (0)	20 (100)	---	---	0 (0)
	IAB-CRB-OIB	20 (100)	0 (0)	---	14 (70)	6 (30)	---
	IAB-CRB-MORB	20 (100)	0 (0)	---	20 (100)	---	0 (0)
	IAB-OIB-MORB	20 (100)	0 (0)	---	---	20 (100)	0 (0)
	CRB-OIB-MORB	20 (100)	---	---	10 (50)	10 (50)	0 (0)
<i>Test study 4. Synthesis of all five diagrams of Agrawal et al. (2008)</i>		<b>100 (100)</b>	<b>0 (0)</b>	<b>20 (---)</b>	<b>55 (55)</b>	<b>45 (45)</b>	<b>0 (0)</b>
Verma and Agrawal (2011); log-ratios of immobile major and trace elements	IAB-CRB+OIB-MORB	20 (100)	0 (0)	20 (100)	---	---	0 (0)
	IAB-CRB-OIB	20 (100)	0 (0)	---	1 (5)	19 (95)	---
	IAB-CRB-MORB	20 (100)	0 (0)	---	20 (100)	---	0 (0)
	IAB-OIB-MORB	20 (100)	0 (0)	---	---	20 (100)	0 (0)
	CRB-OIB-MORB	20 (100)	---	---	1 (5)	19 (95)	0 (0)
<i>Test study 4. Synthesis of all five diagrams of Verma and Agrawal (2011)</i>		<b>100 (100)</b>	<b>0 (0)</b>	<b>20 (---)</b>	<b>28 (28.0)</b>	<b>72 (72.0)</b>	<b>0(0)</b>

For the explanation of abbreviations, see footnote of Table 1 or S14.

**Table S22.**

Testing of multidimensional diagrams from Quaternary (0.70-0.0115 Ma) basic rocks of Garrotxa, NE Volcanic province, Spain (Cebriá et al. 2000; Test study 5).

Figure reference; figure type	Discrimination diagram	Total no. of samples (%)	Predicted tectonic affinity and number of discriminated samples (%)				
			IAB	CRB+OIB	CRB	OIB	MORB
Agrawal et al. (2004); adjusted major element concentrations	IAB-CRB-OIB-MORB	16 (100)	0 (0)	---	14 (88)	2 (12)	0 (0)
	IAB-CRB-OIB	16 (100)	0 (0)	---	16 (100)	0 (0)	---
	IAB-CRB-MORB	16 (100)	0 (0)	---	16 (100)	---	0 (0)
	IAB-OIB-MORB	16 (100)	1 (6)	---	---	10 (63)	5 (31)
	CRB-OIB-MORB	16 (100)	---	---	16 (100)	0 (0)	0 (0)
<i>Test study 5. Synthesis of all five diagrams of Agrawal et al. (2004)</i>		<b>80 (100)</b>	<b>1 (1)</b>	<b>---</b>	<b>62 (78)</b>	<b>12 (15)</b>	<b>5 (6)</b>
Verma et al. (2006); log-ratios of major elements	IAB-CRB-OIB-MORB	16 (100)	0 (0)	---	16 (100)	0 (0)	0 (0)
	IAB-CRB-OIB	16 (100)	0 (0)	---	16 (100)	0 (0)	---
	IAB-CRB-MORB	16 (100)	0 (0)	---	16 (100)	---	0 (0)
	IAB-OIB-MORB	16 (100)	0 (0)	---	---	15 (93.8)	1 (6.2)
	CRB-OIB-MORB	16 (100)	---	---	16 (100)	0 (0)	0 (0)
<i>Test study 5. Synthesis of all five diagrams of Verma et al. (2006)</i>		<b>80 (100)</b>	<b>0 (0)</b>	<b>---</b>	<b>64 (80)</b>	<b>15 (19)</b>	<b>1 (1)</b>
Agrawal et al. (2008); log-ratios of immobile trace elements	IAB-CRB+OIB-MORB	15 (100)	0 (0)	15 (100)	---	---	0 (0)
	IAB-CRB-OIB	15 (100)	0 (0)	---	14 (93.3)	1 (6.7)	---
	IAB-CRB-MORB	15 (100)	0 (0)	---	15 (100)	---	0 (0)
	IAB-OIB-MORB	15 (100)	0 (0)	---	---	15 (100)	0 (0)
	CRB-OIB-MORB	15 (100)	---	---	7 (46.7)	8 (53.3)	0 (0)
<i>Test study 5. Synthesis of all five diagrams of Agrawal et al. (2008)</i>		<b>75 (100)</b>	<b>0 (0)</b>	<b>15 (---)</b>	<b>45 (60)</b>	<b>30 (40)</b>	<b>0 (0)</b>
Verma and Agrawal (2011); log-ratios of immobile major and trace elements	IAB-CRB+OIB-MORB	15 (100)	0 (0)	15 (100)	---	---	0 (0)
	IAB-CRB-OIB	15 (100)	0 (0)	---	8 (53.3)	7 (46.7)	---
	IAB-CRB-MORB	15 (100)	0 (0)	---	15 (100)	---	0 (0)
	IAB-OIB-MORB	15 (100)	0 (0)	---	---	15 (100)	0 (0)
	CRB-OIB-MORB	15 (100)	---	---	14 (93.3)	1 (6.7)	0 (0)
<i>Test study 5. Synthesis of all five diagrams of Verma and Agrawal (2011)</i>		<b>75 (100)</b>	<b>0 (0)</b>	<b>15 (---)</b>	<b>46 (61)</b>	<b>29 (397)</b>	<b>0 (0)</b>

For the explanation of abbreviations, see footnote of Table 1 or S14.

**Table S23.**

Testing of multidimensional diagrams from Quaternary (1.9-2.4 Ma) basic rocks from the Styrian basin, Austria (Ali et al. 2013; Test study 6).

Figure reference; figure type	Discrimination diagram	Total no. of samples (%)	Predicted tectonic affinity and number of discriminated samples (%)				
			IAB	CRB+OIB	CRB	OIB	MORB
Agrawal et al. (2004); adjusted major element concentrations	IAB-CRB-OIB-MORB	39 (100)	18 (46.2)	---	21 (53.8)	0 (0)	0 (0)
	IAB-CRB-OIB	39 (100)	0 (0)	---	39 (100)	0 (0)	---
	IAB-CRB-MORB	39 (100)	0 (0)	---	39 (100)	---	0 (0)
	IAB-OIB-MORB	39 (100)	0 (0)	---	---	1 (2.6)	38 (97.4)
	CRB-OIB-MORB	39 (100)	---	---	39 (100)	0 (0)	0 (0)
<i>Test study 6. Synthesis of all five diagrams of Agrawal et al. (2004)</i>		<b>195 (100)</b>	<b>18 (9.2)</b>	<b>---</b>	<b>138 (70.8)</b>	<b>1 (0.5)</b>	<b>38 (19.5)</b>
Verma et al. (2006); log-ratios of major elements	IAB-CRB-OIB-MORB	39 (100)	0 (0)	---	39 (100)	0 (0)	0 (0)
	IAB-CRB-OIB	39 (100)	0 (0)	---	39 (100)	0 (0)	---
	IAB-CRB-MORB	39 (100)	0 (0)	---	39 (100)	---	0 (0)
	IAB-OIB-MORB	39 (100)	0 (0)	---	---	15 (38.5)	24 (61.5)
	CRB-OIB-MORB	39 (100)	---	---	39 (100)	0 (0)	0 (0)
<i>Test study 6. Synthesis of all five diagrams of Verma et al. (2006)</i>		<b>195 (100)</b>	<b>0 (0)</b>	<b>---</b>	<b>156 (80)</b>	<b>15 (7.7)</b>	<b>24 (12.3)</b>
Agrawal et al. (2008); log-ratios of immobile trace elements	IAB-CRB+OIB-MORB	39 (100)	0 (0)	39 (100)	---	---	0 (0)
	IAB-CRB-OIB	39 (100)	0 (0)	---	39 (100)	0 (0)	---
	IAB-CRB-MORB	39 (100)	0 (0)	---	39 (100)	---	0 (0)
	IAB-OIB-MORB	39 (100)	0 (0)	---	---	39 (100)	0 (0)
	CRB-OIB-MORB	39 (100)	---	---	39 (100)	0 (0)	0 (0)
<i>Test study 6. Synthesis of all five diagrams of Agrawal et al. (2008)</i>		<b>195 (100)</b>	<b>0 (0)</b>	<b>39 (---)</b>	<b>146 (74.9)</b>	<b>49 (25.1)</b>	<b>0 (0)</b>
Verma and Agrawal (2011); log-ratios of immobile major and trace elements	IAB-CRB+OIB-MORB	39 (100)	0 (0)	39 (100)	---	---	0 (0)
	IAB-CRB-OIB	39 (100)	0 (0)	---	39 (100)	0 (0)	---
	IAB-CRB-MORB	39 (100)	0 (0)	---	39 (100)	---	0 (0)
	IAB-OIB-MORB	39 (100)	0 (0)	---	---	19 (48.7)	20 (51.3)
	CRB-OIB-MORB	39 (100)	---	---	39 (100)	0 (0)	0 (0)
<i>Test study 6. Synthesis of all five diagrams of Verma and Agrawal (2011)</i>		<b>195 (100)</b>	<b>0 (0)</b>	<b>39 (---)</b>	<b>151 (77.4)</b>	<b>24 (12.3)</b>	<b>20 (10.3)</b>

For the explanation of abbreviations, see footnote of Table 1 or S14.

**Table S24.**

Testing of multidimensional diagrams from Recent (years 1999 and 2000 eruptions) basic rocks of the Mount Cameroon, Cameroon (Suh et al. 2003; Test study 7).

Figure reference; figure type	Discrimination diagram	Total no. of samples (%)	Predicted tectonic affinity and number of discriminated samples (%)				
			IAB	CRB+OIB	CRB	OIB	MORB
Agrawal et al. (2004); adjusted major element concentrations	IAB-CRB-OIB-MORB	14 (100)	0 (0)	---	7 (50)	7 (50)	0 (0)
	IAB-CRB-OIB	14 (100)	0 (0)	---	12 (86)	2 (14)	---
	IAB-CRB-MORB	14 (100)	0 (0)	---	14 (100)	---	0 (0)
	IAB-OIB-MORB	14 (100)	0 (0)	---	---	14 (100)	0 (0)
	CRB-OIB-MORB	14 (100)	---	---	8 (57)	6 (43)	0 (0)
<b>Test study 7. Synthesis of all five diagrams of Agrawal et al. (2004)</b>		<b>70 (100)</b>	<b>0 (0)</b>	<b>---</b>	<b>41 (59)</b>	<b>29 (41)</b>	<b>0 (0)</b>
Verma et al. (2006); log-ratios of major elements	IAB-CRB-OIB-MORB	14 (100)	0 (0)	---	5 (36)	9 (64)	0 (0)
	IAB-CRB-OIB	14 (100)	0 (0)	---	8 (57)	6 (43)	---
	IAB-CRB-MORB	14 (100)	0 (0)	---	14 (100)	---	0 (0)
	IAB-OIB-MORB	14 (100)	0 (0)	---	---	14 (100)	0 (0)
	CRB-OIB-MORB	14 (100)	---	---	12 (86)	2 (14)	0 (0)
<b>Test study 7. Synthesis of all five diagrams of Verma et al. (2006)</b>		<b>70 (100)</b>	<b>0 (0)</b>	<b>---</b>	<b>39 (56)</b>	<b>31 (44)</b>	<b>0 (0)</b>
Verma and Agrawal (2011); log-ratios of immobile major and trace elements	IAB-CRB+OIB-MORB	14 (100)	0 (0)	14 (100)	---	---	0 (0)
	IAB-CRB-OIB	14 (100)	0 (0)	---	14 (100)	0 (0)	---
	IAB-CRB-MORB	14 (100)	0 (0)	---	14 (100)	---	0 (0)
	IAB-OIB-MORB	14 (100)	0 (0)	---	---	14 (100)	0 (0)
	CRB-OIB-MORB	14 (100)	---	---	14 (100)	0 (0)	0 (0)
<b>Test study 7. Synthesis of all five diagrams of Verma and Agrawal (2011)</b>		<b>70 (100)</b>	<b>0 (0)</b>	<b>14 (---)</b>	<b>52 (74)</b>	<b>18 (26)</b>	<b>0 (0)</b>

For the explanation of abbreviations, see footnote of Table 1 or S14.

**Table S25.**

Testing of multidimensional diagrams from Miocene (7-10 Ma) basic rocks of the Nosy Be Archipelago, Madagascar (Melluso and Morra, 2000; Test study 8).

Figure reference; figure type	Discrimination diagram	Total no. of samples (%)	Predicted tectonic affinity and number of discriminated samples (%)				
			IAB	CRB+OIB	CRB	OIB	MORB
Agrawal et al. (2004); adjusted major element concentrations	IAB-CRB-OIB-MORB	27 (100)	0 (0)	---	3 (11)	23 (85)	1 (4)
	IAB-CRB-OIB	27 (100)	0 (0)	---	26 (96)	1 (4)	---
	IAB-CRB-MORB	27 (100)	0 (0)	---	27 (100)	---	0 (0)
	IAB-OIB-MORB	27 (100)	0 (0)	---	---	16 (59)	11 (41)
	CRB-OIB-MORB	27 (100)	---	---	20 (74)	7 (26)	0 (0)
<i>Test study 8. Synthesis of all five diagrams of Agrawal et al. (2004)</i>		<b>135 (100)</b>	<b>0 (0)</b>	---	<b>76 (56.3)</b>	<b>47 (34.8)</b>	<b>12 (8.9)</b>
Verma et al. (2006); log-ratios of major elements	IAB-CRB-OIB-MORB	27 (100)	0 (0)	---	11 (41)	15 (56)	1 (4)
	IAB-CRB-OIB	27 (100)	0 (0)	---	22 (82)	5 (18)	---
	IAB-CRB-MORB	27 (100)	0 (0)	---	26 (96)	---	1 (4)
	IAB-OIB-MORB	27 (100)	0 (0)	---	---	17 (63)	10 (37)
	CRB-OIB-MORB	27 (100)	---	---	25 (92)	1 (4)	1 (4)
<i>Test study 8. Synthesis of all five diagrams of Verma et al. (2006)</i>		<b>135 (100)</b>	<b>0 (0)</b>	---	<b>84 (62.2)</b>	<b>38 (28.1)</b>	<b>13 (9.6)</b>
Verma and Agrawal (2011); log-ratios of immobile major and trace elements	IAB-CRB+OIB-MORB	27 (100)	0 (0)	27 (100)	---	---	0 (0)
	IAB-CRB-OIB	27 (100)	0 (0)	---	26 (96)	1 (4)	---
	IAB-CRB-MORB	27 (100)	0 (0)	---	27 (100)	---	0 (0)
	IAB-OIB-MORB	27 (100)	0 (0)	---	---	27 (100)	0 (0)
	CRB-OIB-MORB	27 (100)	---	---	26 (96)	1 (4)	0 (0)
<i>Test study 8. Synthesis of all five diagrams of Verma and Agrawal (2011)</i>		<b>135 (100)</b>	<b>0 (0)</b>	<b>27 (---)</b>	<b>99 (73.3)</b>	<b>36 (26.7)</b>	<b>0(0)</b>

For the explanation of abbreviations, see footnote of Table 1 or S14.

**Table S26.**

Testing of multidimensional diagrams from Miocene (21.7 Ma) basic rocks of the Tianheyong region, Mongolia China (Yang et al. 2009; Test study 9).

Figure reference; figure type	Discrimination diagram	Total no. of samples (%)	Predicted tectonic affinity and number of discriminated samples (%)				
			IAB	CRB+OIB	CRB	OIB	MORB
Agrawal et al. (2004); adjusted major element concentrations	IAB-CRB-OIB-MORB	8 (100)	0 (0)	---	7 (88)	1 (12)	0 (0)
	IAB-CRB-OIB	8 (100)	0 (0)	---	7 (88)	1 (12)	---
	IAB-CRB-MORB	8 (100)	0 (0)	---	8 (100)	---	0 (0)
	IAB-OIB-MORB	8 (100)	0 (0)	---	---	6 (75)	2 (25)
	CRB-OIB-MORB	8 (100)	---	---	7 (88)	1 (12)	0 (0)
<i>Test study 9 Synthesis of all five diagrams of Agrawal et al. (2004)</i>		<b>40 (100)</b>	<b>0 (0)</b>	<b>---</b>	<b>29 (73)</b>	<b>9 (22)</b>	<b>2 (5)</b>
Verma et al. (2006); log-ratios of major elements	IAB-CRB-OIB-MORB	8 (100)	0 (0)	---	7 (87.5)	1 (12.5)	0 (0)
	IAB-CRB-OIB	8 (100)	0 (0)	---	7 (87.5)	1 (12.5)	---
	IAB-CRB-MORB	8 (100)	0 (0)	---	8 (100)	---	0 (0)
	IAB-OIB-MORB	8 (100)	2 (25)	---	---	6 (75)	0 (0)
	CRB-OIB-MORB	8 (100)	---	---	7 (87.5)	1 (12.5)	0 (0)
<i>Test study 9. Synthesis of all five diagrams of Verma et al. (2006)</i>		<b>40 (100)</b>	<b>2 (5)</b>	<b>---</b>	<b>29 (73)</b>	<b>9 (22)</b>	<b>0 (0)</b>
Agrawal et al. (2008); log-ratios of immobile trace elements	IAB-CRB+OIB-MORB	8 (100)	0 (0)	8 (100)	---	---	0 (0)
	IAB-CRB-OIB	8 (100)	0 (0)	---	0 (0)	8 (100)	---
	IAB-CRB-MORB	8 (100)	0 (0)	---	8 (100)	---	0 (0)
	IAB-OIB-MORB	8 (100)	0 (0)	---	---	8 (100)	0 (0)
	CRB-OIB-MORB	8 (100)	---	---	0 (0)	8 (100)	0 (0)
<i>Test study 9. Synthesis of all five diagrams of Agrawal et al. (2008)</i>		<b>40 (100)</b>	<b>0 (0)</b>	<b>8 (---)</b>	<b>10 (25)</b>	<b>30 (75)</b>	<b>0 (0)</b>

For the explanation of abbreviations, see footnote of Table 1 or S14.

**Table S27.**

Testing of multidimensional diagrams from Quaternary (0.17–2.04 Ma) basic rocks of the Halaha volcanic field, Central Great Xing'an Range, NE China (Ho et al. 2013; Test study 10).

Figure reference; figure type	Discrimination diagram	Total no. of samples (%)	Predicted tectonic affinity and number of discriminated samples (%)				
			IAB	CRB+OIB	CRB	OIB	MORB
Agrawal et al. (2004); adjusted major element concentrations	IAB-CRB-OIB-MORB	14 (100)	0 (0)	---	11 (79)	3 (21)	0 (0)
	IAB-CRB-OIB	14 (100)	0 (0)	---	12 (86)	2 (14)	---
	IAB-CRB-MORB	14 (100)	0 (0)	---	12 (86)	---	2 (14)
	IAB-OIB-MORB	14 (100)	0 (0)	---	---	8 (57)	6 (43)
	CRB-OIB-MORB	14 (100)	---	---	12 (86)	2 (14)	0 (0)
<i>Test study 10. Synthesis of all five diagrams of Agrawal et al. (2004)</i>		<b>70 (100)</b>	<b>0 (0)</b>	<b>---</b>	<b>47 (67)</b>	<b>15 (22)</b>	<b>8 (11)</b>
Verma et al. (2006); log-ratios of major elements	IAB-CRB-OIB-MORB	14 (100)	0 (0)	---	11 (79)	3 (21)	0 (0)
	IAB-CRB-OIB	14 (100)	0 (0)	---	12 (86)	2 (14)	---
	IAB-CRB-MORB	14 (100)	0 (0)	---	14 (100)	---	0 (0)
	IAB-OIB-MORB	14 (100)	0 (0)	---	---	3 (21)	11 (79)
	CRB-OIB-MORB	14 (100)	---	---	13 (93)	1 (7)	0 (0)
<i>Test study 10. Synthesis of all five diagrams of Verma et al. (2006)</i>		<b>70 (100)</b>	<b>0 (0)</b>	<b>---</b>	<b>50 (71)</b>	<b>9 (13)</b>	<b>11 (16)</b>
Agrawal et al. (2008); log-ratios of immobile trace elements	IAB-CRB+OIB-MORB	14 (100)	5 (36)	9 (64)	---	---	0 (0)
	IAB-CRB-OIB	14 (100)	5 (36)	---	6 (43)	3 (21)	---
	IAB-CRB-MORB	14 (100)	5 (36)	---	9 (64)	---	0 (0)
	IAB-OIB-MORB	14 (100)	5 (36)	---	---	9 (64)	0 (0)
	CRB-OIB-MORB	14 (100)	---	---	10 (71)	4 (29)	0 (0)
<i>Test study 10. Synthesis of all five diagrams of Agrawal et al. (2008)</i>		<b>70 (100)</b>	<b>20 (28)</b>	<b>9 (---)</b>	<b>30 (44)</b>	<b>20 (28)</b>	<b>0 (0)</b>
Verma and Agrawal (2011); log-ratios of immobile major and trace elements	IAB-CRB+OIB-MORB	14 (100)	0 (0)	9 (64)	---	---	5 (36)
	IAB-CRB-OIB	14 (100)	5 (36)	---	9 (64)	0 (0)	---
	IAB-CRB-MORB	14 (100)	0 (0)	---	9 (64)	---	5 (36)
	IAB-OIB-MORB	14 (100)	0 (0)	---	---	9 (64)	5 (36)
	CRB-OIB-MORB	14 (100)	---	---	9 (64)	0 (0)	5 (36)
<i>Test study 10. Synthesis of all five diagrams of Verma and Agrawal (2011)</i>		<b>70 (100)</b>	<b>5 (7)</b>	<b>9 (---)</b>	<b>34 (49)</b>	<b>11 (16)</b>	<b>20(28)</b>

For the explanation of abbreviations, see footnote of Table 1 or S14.

**Table S28.**

Testing of multidimensional diagrams from Holocene (0.0034 Ma) acid rocks of the Aniakchak area, Aleutian arc, Alaska (Dreher et al. 2005; Test study 11).

Magma type, Figure name	Figure type	Total number of samples	Number of discriminated samples				
			IA+CA [ $\bar{x} \pm s$ ] [ $p_{IA+CA}$ Θ]	Arc IA [ $\bar{x} \pm s$ ] [ $p_{IA}$ Θ]	CA [ $\bar{x} \pm s$ ] [ $p_{CA}$ Θ]	Within-plate CR+OI [ $\bar{x} \pm s$ ] [ $p_{CR+OI}$ Θ]	Collision Col [ $\bar{x} \pm s$ ] [ $p_{Col}$ Θ]
Acid; Verma et al. (2012); log-ratios of all major elements	IA+CA-CR-Col	9	9 [0.820±0.071] (0.6983-0.9389)	---	---	0 (0)	0 (0)
	IA-CA-CR	9	---	0 (0)	9 [0.707±0.078] (0.6024-0.8055)	0 (0)	---
	IA-CA-Col	9	---	0 (0)	[0.8195±0.0384] (0.7657-0.8627)	---	0 (0)
	IA-CR-Col	9	---	1 (0.8659)	---	8 [0.486±0.091] (0.3894-0.6456)	0 (0)
	CA-CR-Col	9	---	---	[0.8965±0.0422] (0.8143-0.9415)	0 (0)	0 (0)
<b>Test study 11.</b>							
Diagrams based on log-ratios of major elements	{Σn} {Σprob} [%prob]	45	{9} {7.3795} [---]	{1} {0.8659} [4%]	{27} {21.8069} [85%]	{8} {3.8874} [11%]	{0} {0} [0%]
	IA+CA-CR+OI-Col	9	4 [0.663±0.116] (0.5457-0.8222)	---	---	5 [0.5279±0.0443] (0.4685-0.5723)	0 (0)
	IA-CA-CR+OI	9	---	0 (0)	6 [0.559±0.137] (0.4338-0.8235)	[0.4849±0.0263] (0.4594-0.5119)	---
	IA-CA-Col	9	---	0 (0)	9 [0.727±0.061] (0.6606-0.8411)	---	0 (0)
	IA-CR+OI-Col	9	---	0 (0)	---	9 [0.688±0.086] (0.5396-0.7986)	0 (0)
Acid; Verma et al. (2013); log-ratios of all major elements	CA-CR+OI-Col	9	---	---	5 [0.646±0.134] (0.4946-0.8445)	4 [0.5220±0.0361] (0.4772-0.5573)	0 (0)
<b>Test study 11.</b>							
{Σn} {Σprob} [%prob]	45	{4} {2.6500} [---]	{0} {0} [0%]	{20} {13.1225} [56%]	{21} {12.3711} [44%]	{0} {0} [0%]	
IA+CA-CR+OI-Col	9	7 [0.521±0.081] (0.3854-0.6072)	---	---	2 [0.4290±0.0095] (0.4223, 0.4357)	0 (0)	
IA-CA-CR+OI	9	---	0 (0)	6 [0.600±0.060] (0.5051-0.6492)	3 [0.4812±0.0336] (0.4424-0.5019)	---	
Acid; Verma et al. (2013); log-ratios of immobile major and trace elements	IA-CA-Col	9	---	0 (0)	[0.5618±0.0443] (0.4666-0.5951)	7 [0.44745±0.00361] (0.4449, 0.4500)	2
	IA-CR+OI-Col	9	---	0 (0)	---	6 [0.497±0.066] (0.3766-0.5547)	3 [0.3694±0.0222] (0.3553-0.3950)
	CA-CR+OI-Col	9	---	---	9 [0.592±0.113] (0.4338-0.7193)	0 (0)	0 (0)
<b>Test study 2a.</b>							
Diagrams based on log-ratios of immobile major and trace elements	{Σn} {Σprob} [%prob]	45	{7} {3.6470} [---]	{0} {0} [0%]	{22} {12.8589} [70%]	{11} {5.2815} [22%]	{5} {2.0031} [8%]
	IA+CA-CR+OI-Col	9	9 [0.8546±0.0157] (0.8199-0.8689)	---	---	0 (0)	0 (0)
	IA-CA-CR+OI	9	---	0 (0)	9 [0.7986±0.0247] (0.7740-0.8427)	0 (0)	---
	IA-CA-Col	9	---	0 (0)	9 [0.7761±0.0208]	---	0 (0)

				(0.7487-0.8141)		
<b>IA-CR+OI- Col</b>	9	---	9 [0.764±0.071] (0.5921- 0.8310)	---	0 (0)	0 (0)
<b>CA-CR+OI- Col</b>	9	---	---	9 [0.9612±0.0087] (0.9412-0.9699)	0 (0)	0 (0)
<b><i>Test study 11.</i></b>						
<b><i>Diagrams based on log- ratios of immobile trace elements</i></b>						
{Σn} {Σprob}	45	{9} {7.6911}	{9} {6.8736}	{27} {22.8229}	{0} {0}	{0} {0}
[%prob]		[--]	[23%]	[77%]	[ 0%]	[ 0%]

For the explanation of abbreviations, see footnote of Table S17.

**Table S29.**

Testing of multidimensional diagrams from recent intermediate rocks of the Fuego volcanic complex, Guatemala (Chesner and Rose Jr., 1984; Test study 12a).

Magma type, Figure name; Figure number	Figure type	Total number of samples	Number of discriminated samples					
			Arc			Within-plate CR+OI [ $\bar{x} \pm s$ ] [ $p_{CR+OI}$ ] $\Theta$	Collision Col [ $\bar{x} \pm s$ ] [ $p_{Col}$ ] $\Theta$	
			IA+CA [ $\bar{x} \pm s$ ] ( $p_{IA+CA}$ ) $\Theta$	IA [ $\bar{x} \pm s$ ] [ $p_{IA}$ ] $\Theta$	CA [ $\bar{x} \pm s$ ] [ $p_{CA}$ ] $\Theta$			
Intermediate; Verma and Verma (2013); log-ratios of all major elements;	<b>IA+CA-CR+OI- Col</b>	9	8 [0.790±0.213] (0.4815-0.9661)	---	---	0 (0)	1 (0.9977)	
	<b>IA-CA-CR+OI</b>	9	---	0 (0)	9 [0.759±0.127] (0.5884-0.9997)	0 (0)	---	
	<b>IA-CA-Col</b>	9	---	0 (0)	8 [0.687±0.123] (0.5353-0.8289)	---	1 (0.9739)	
	<b>IA-CR+OI-Col</b>	9	---	5 [0.891±0.075] (0.7653- 0.9493)	---	0 (0)	4 [0.706±0.201] (0.5665-1.0000)	
	<b>CA-CR+OI-Col</b>	9	---	---	6 [0.873±0.111] (0.6702-0.9621)	0 (0)	3 [0.587±0.164] (0.4865-0.7758)	
<i>Test study 12a. Diagrams based on log-ratios of major elements</i>	{Σn} {Σprob} [%prob]	45	{8} {6.3219} [--]	{5} {4.4546} [16%]	{23} {17.5595} [65%]	{0} {0} [0%]	{9} {6.5585} [19%]	

For the explanation of abbreviations, see footnote of Table S17.

**Table S30.**

Testing of multidimensional diagrams from Quaternary intermediate rocks of the Meseta volcano, Guatemala (Chesner and Halsor, 1997; Test study 12b).

Magma type, Figure name; Figure number	Figure type	Total number of sample s	Number of discriminated samples				
			Arc			Within-plate CR+OI [ $\bar{x} \pm s$ ] [ $p_{CR+OI}$ ] $\Theta$	Collision Col [ $\bar{x} \pm s$ ] [ $p_{Col}$ ] $\Theta$
			IA+CA [ $\bar{x} \pm s$ ] ( $p_{IA+CA}$ ) $\Theta$	IA [ $\bar{x} \pm s$ ] [ $p_{IA}$ ] $\Theta$	CA [ $\bar{x} \pm s$ ] [ $p_{CA}$ ] $\Theta$		
Intermediate; Verma and Verma (2013); log-ratios of all major elements;	<b>IA+CA-CR+OI-Col</b>	40	40 [0.9617±0.0285] (0.8814-0.9815)	---	---	0 (0)	0 (0)
	<b>IA-CA-CR+OI</b>	40	---	0 (0)	40 [0.746±0.053] (0.6385-0.8271)	0 (0)	---
	<b>IA-CA-Col</b>	40	---	0 (0)	40 [0.769±0.046] (0.6789-0.8360)	---	0 (0)
	<b>IA-CR+OI-Col</b>	40	---	[0.9577±0.028 7] (0.8800- 0.9809)	---	0 (0)	0 (0)
	<b>CA-CR+OI-Col</b>	40	---	---	40 [0.9484±0.0426] (0.8093-0.9789)	0 (0)	0 (0)
<i>Test study 12b. Diagrams based on log-ratios of major elements</i>	{Σn} {Σprob} [%prob]	200	{40} {38.4681} [--]	{40} {38.3098} [28.0%]	{120} {98.5657} [72.0%]	{0} {0} [0%]	{0} {0} [0%]

For the explanation of abbreviations, see footnote of Table S17.

**Table S31.**

Testing of multidimensional diagrams from Holocene (0.000112) intermediate rocks of the Santiaguito complex, Guatemala (Scott et al. 2013; Test study 12c).

Magma type, Figure name	Figure type	Total number of samples	Number of discriminated samples					
			Arc			Within-plate CR+OI [ $\bar{x} \pm s$ ] [ $p_{CR+OI}$ ] $\Theta$	Collision Col [ $\bar{x} \pm s$ ] [ $p_{Col}$ ] $\Theta$	
			IA+CA [ $\bar{x} \pm s$ ] ( $p_{IA+CA}$ ) $\Theta$	IA [ $\bar{x} \pm s$ ] [ $p_{IA}$ ] $\Theta$	CA [ $\bar{x} \pm s$ ] [ $p_{CA}$ ] $\Theta$			
Intermediate; Verma and Verma (2013); log-ratios of all major elements	IA+CA-CR+OI- Col	18	18 [ $0.808 \pm 0.067$ ] (0.7547-0.9500)	---	---	0 (0)	0 (0)	
	IA-CA-CR+OI	18	---	0 (0)	[ $0.7359 \pm 0.0255$ ] (0.7112-0.8137)	0 (0)	---	
	IA-CA-Col	18	---	0 (0)	18 [ $0.687 \pm 0.048$ ] (0.6501-0.8012)	---	0 (0)	
	IA-CR+OI-Col	18	---	[ $0.7203 \pm 0.0995$ ] (0.6322-0.9160)	---	0 (0)	0 (0)	
	CA-CR+OI-Col	18	---	---	18 [ $0.669 \pm 0.139$ ] (0.5705-0.9348)	0 (0)	0 (0)	
<i>Test study 12c. Diagrams based on log-ratios of major elements</i>		{ $\Sigma n$ } { $\Sigma prob$ } [%prob]	90	{18} {14.5494} [--]	{18} {12.9660} [26%]	{54} {37.6497} [74%]	{0} {0} [0%]	{0} {0} [0%]
Intermediate; Verma and Verma (2013); log-ratios of immobile major and trace elements	IA+CA-CR+OI- Col	5	5 [ $0.811 \pm 0.151$ ] (0.5541-0.9444)	---	---	0 (0)	0 (0)	
	IA-CA-CR+OI	5	---	1 (0.5617)	4 [ $0.594 \pm 0.068$ ] (0.5056-0.6694)	0 (0)	---	
	IA-CA-Col	5	---	1 (0.5530)	3 [ $0.5540 \pm 0.0275$ ] (0.5290-0.5834)	---	1 (0.3917)	
	IA-CR+OI-Col	5	---	5 [ $0.774 \pm 0.134$ ] (0.5579-0.9210)	---	0 (0)	0 (0)	
	CA-CR+OI-Col	5	---	---	5 [ $0.938 \pm 0.094$ ] (0.7699-0.9894)	0 (0)	0 (0)	
<i>Test study 12c. Diagrams based on log-ratios of immobile major and trace elements</i>		{ $\Sigma n$ } { $\Sigma prob$ } [%prob]	25	{5} {4.0545} [--]	{7} {4.9838} [36%]	{12} {8.7249} [62%]	{0} {0} [0%]	{1} {0.3917} [2%]
Intermediate; Verma and Verma (2013); log-ratios of immobile trace elements	IA+CA-CR+OI- Col	18	18 [ $0.696 \pm 0.093$ ] (0.5167-0.8366)	---	---	0 (0)	0 (0)	
	IA-CA-CR+OI	18	---	16 [ $0.448 \pm 0.071$ ] (0.3488-0.6806)	2 [ $0.4897 \pm 0.0062$ ] (0.4853, 0.4941)	0 (0)	---	
	IA-CA-Col	18	---	1 (0.6796)	17 [ $0.5055 \pm 0.0434$ ] (0.4633-0.6348)	---	0 (0)	
	IA-CR+OI-Col	18	---	18 [ $0.707 \pm 0.081$ ] (0.5452-0.8419)	---	0 (0)	0 (0)	
	CA-CR+OI-Col	18	---	---	18 [ $0.866 \pm 0.050$ ] (0.7749-0.9509)	0 (0)	0 (0)	
<i>Test study 12c. Diagrams based on log-ratios of immobile trace elements</i>		{ $\Sigma n$ } { $\Sigma prob$ } [%prob]	90	{18} {12.5319} [--]	{35} {20.5673} [45%]	{37} {25.1544} [55%]	{0} {0} [0%]	{0} {0} [0%]

For the explanation of abbreviations, see footnote of Table S17.

**Table S32.**

Testing of multidimensional diagrams from Holocene (0.000112) acid rocks of the Santiaguito complex, Guatemala (Scott et al. 2013; Test study 12c).

Magma type, Figure name	Figure type	Total number of samples	Number of discriminated samples				Within- plate CR+OI [ $\bar{x} \pm s$ ] [ $p_{CR+OI}$ ] $\Theta$	Collision [ $\bar{x} \pm s$ ] [ $p_{Col}$ ] $\Theta$	Col
			Arc IA+CA [ $\bar{x} \pm s$ ] ( $p_{IA+CA}$ ) $\Theta$	IA [ $\bar{x} \pm s$ ] [ $p_{IA}$ ] $\Theta$	CA [ $\bar{x} \pm s$ ] [ $p_{CA}$ ] $\Theta$				
Acid; Verma et al. (2012); All major elements	IA+CA- CR+OI-Col	17	17 [0.98126±0.00418] (0.9694-0.9859)	---	---	---	0 (0)	0 (0)	
	IA-CA- CR+OI	17	---	15 [0.598±0.049] (0.5207- 0.6870)	2 [0.590±0.088] (0.5280, 0.6528)	0 (0)	---	---	
	IA-CA-Col	17	---	16 [0.5990±0.0392] (0.5188-0.6715)	1 (0.5823)	---	---	0 (0)	
	IA-CR+OI- Col	17	---	17 [0.99699±0.00180] (0.9905-0.9983)	---	---	0 (0)	0 (0)	
	CA- CR+OI-Col	17	---	---	[0.99280±0.00210] (0.9863-0.9954)	0 (0)	0 (0)	0 (0)	
<i>Test study 12c.</i>									
<i>Diagrams based on log-ratios of major elements</i>		{Σn} {Σprob} [%prob]	85	{17} {16.6813} [--]	{48} {35.4968} [66%]	{20} {18.6406} [34%]	{0} {0} [0%]	{0} {0} [0%]	
Acid; Verma et al. (2013); All major elements	IA+CA- CR+OI-Col	17	17 [0.9743±0.0087] (0.9476-0.9834)	---	---	---	0 (0)	0 (0)	
	IA-CA- CR+OI	17	---	0 (0)	17 [0.7076±0.0204] (0.6708-0.7499)	0 (0)	---	---	
	IA-CA-Col	17	---	0 (0)	17 [0.8405±0.0216] (0.7991-0.8747)	---	---	0 (0)	
	IA-CR+OI- Col	17	---	17 [0.9331±0.0274] (0.8395-0.9611)	---	---	0 (0)	0 (0)	
	CA- CR+OI-Col	17	---	---	17 [0.9881±0.0051] (0.9714-0.9930)	0 (0)	0 (0)	0 (0)	
<i>Test study 12c.</i>									
<i>Diagrams based on log-ratios of major elements</i>		{Σn} {Σprob} [%prob]	85	{17} {16.5629} [--]	{17} {15.8622} [27%]	{51} {43.1143} [73%]	{0} {0} [0%]	{0} {0} [0%]	
Acid; Verma et al. (2013); log-ratios of immobile major and trace elements	IA+CA- CR+OI-Col	17	6 [0.561±0.059] (0.5014-0.6376)	---	---	---	0 (0)	11 [0.592±0.079] (0.4825-0.7154)	
	IA-CA- CR+OI	17	---	0 (0)	17 [0.6567±0.0428] (0.5394-0.7047)	0 (0)	---	---	
	IA-CA-Col	17	---	0 (0)	10 [0.4634±0.0370] (0.4031-0.5147)	---	7 [0.484±0.065] (0.4161-0.6002)		
	IA-CR+OI- Col	17	---	0 (0)	---	0 (0)	17 [0.690±0.077] (0.5354-0.7923)		
	CA- CR+OI-Col	17	---	---	10 [0.581±0.072] (0.4793-0.6976)	0 (0)	7 [0.554±0.051] (0.4896-0.6350)		
<i>Test study 12c.</i>									
<i>Diagrams based on log-ratios of immobile major and trace elements</i>		{Σn} {Σprob} [%prob]	85	{6} {3.3668} [--]	{0} {0} [0%]	{37} {21.6074} [49%]	{0} {0} [0%]	{42} {25.5029} [51%]	
Acid; Verma et al. (2013); log-ratios of immobile trace elements	IA+CA- CR+OI-Col	17	17 [0.9236±0.0161] (0.8822-0.9449)	---	---	---	0 (0)	0 (0)	
	IA-CA- CR+OI	17	---	0 (0)	17 [0.7405±0.0323] (0.6760-0.7861)	0 (0)	---	---	
	IA-CA-Col	17	---	0 (0)	17 [0.7617±0.0398] (0.6809-0.8356)	---	0 (0)	0 (0)	
	IA-CR+OI- Col	17	---	16 [0.765±0.079] (0.5939- 0.8973)	---	1 (0.4833)	0 (0)	0 (0)	
	CA- CR+OI-Col	17	---	---	17 [0.9705±0.0091] (0.9438-0.9827)	0 (0)	0 (0)	0 (0)	
<i>Test study 12c.</i>									
<i>Diagrams based on log-ratios of immobile trace elements</i>		{Σn} {Σprob} [%prob]	85	{17} {15.7007} [--]	{16} {12.2378} [22%]	{51} {42.0368} [77%]	{1} {0.4833} [1%]	{0} {0} [0%]	

For the explanation of abbreviations, see footnote of Table S17.

**Table S33.**

Testing of multidimensional diagrams from Holocene (0.000123) intermediate rocks of the Huequi volcano dome complex, Chile (Watt et al. 2011; Test study 13).

Magma type, Figure name	Figure type	Total number of samples	Number of discriminated samples					
			Arc IA+CA [ $\bar{x} \pm s$ ] [ $p_{IA+CA}$ ] $\Theta$	Arc IA [ $\bar{x} \pm s$ ] [ $p_{IA}$ ] $\Theta$	Arc CA [ $\bar{x} \pm s$ ] [ $p_{CA}$ ] $\Theta$	Within-plate CR+OI [ $\bar{x} \pm s$ ] [ $p_{CR+OI}$ ] $\Theta$	Collision $\bar{x} \pm s$ ] [ $p_{Col}$ ] $\Theta$	
Intermediate; Verma and Verma (2013); log-ratios of all major elements	IA+CA-CR+OI- Col	9	9 [0.916±0.074] (0.8015-0.9949)	---	---	0 (0)	0 (0)	
	IA-CA-CR+OI	9	---	1 (0.4993)	8 [0.784±0.165] (0.5574-0.9109)	0 (0)	---	
	IA-CA-Col	9	---	1 (0.5290)	8 [0.756±0.157] (0.5492-0.8786)	---	0 (0)	
	IA-CR+OI-Col	9	---	9 [0.841±0.154] (0.5868-0.9970)	---	0 (0)	0 (0)	
	CA-CR+OI-Col	9	---	---	9 [0.942±0.050] (0.8244-0.9877)	0 (0)	0 (0)	
<i>Test study 13.</i> <i>Diagrams based on log-ratios of major elements</i>		{Σn} {Σprob} [%prob]	45	{9} {8.2423} [--]	{11} {8.5945} [29%]	{25} {20.7899} [71%]	{0} {0} [ 0%]	{0} {0} [ 0%]
Intermediate; Verma and Verma (2013); log-ratios of immobile major and trace elements	IA+CA-CR+OI- Col	9	8 [0.805±0.115] (0.6487-0.9461)	---	---	0 (0)	1 (0.4591)	
	IA-CA-CR+OI	9	---	0 (0)	9 [0.588±0.054] (0.5038-0.7054)	0 (0)	---	
	IA-CA-Col	9	---	0 (0)	8 [0.534±0.095] (0.4085-0.7079)	---	1 (0.4950)	
	IA-CR+OI-Col	9	---	9 [0.737±0.150] (0.4447-0.9169)	---	0 (0)	0 (0)	
	CA-CR+OI-Col	9	---	---	9 [0.859±0.150] (0.5257-0.9832)	0 (0)	0 (0)	
<i>Test study 13.</i> <i>Diagrams based on log-ratios of immobile major and trace elements</i>		{Σn} {Σprob} [%prob]	45	{8} {6.4395} [--]	{9} {6.6365} [27%]	{26} {17.2963} [70%]	{0} {0} [ 0%]	{2} {0.9540} [ 3%]

For the explanation of abbreviations, see footnote of Table S17.

**Table S34.**

Testing of multidimensional diagrams from Quaternary intermediate rocks of the Nisyros Island, Greece (Di Paola, 1974; Test study 14).

Magma type, Figure name; Figure number	Figure type	Total number of samples	Number of discriminated samples				
			Arc			Within-plate CR+OI [ $\bar{x} \pm s$ ] [ $p_{CR+OI}$ ] $\Theta$	Collision Col [ $\bar{x} \pm s$ ] [ $p_{Col}$ ] $\Theta$
			IA+CA [ $\bar{x} \pm s$ ] ( $p_{IA+CA}$ ) $\Theta$	IA [ $\bar{x} \pm s$ ] [ $p_{IA}$ ] $\Theta$	CA [ $\bar{x} \pm s$ ] [ $p_{CA}$ ] $\Theta$		
Intermediate; Verma and Verma (2013); log-ratios of all major elements;	<b>IA+CA-CR+OI-Col</b>	16	7 [0.665±0.124] (0.4966-0.8626)	---	---	1 (0.6186)	8 [0.691±0.128] (0.5344-0.9240)
	<b>IA-CA-CR+OI</b>	16	---	0 (0)	15 [0.761±0.134] (0.4753-0.9752)	1 (0.8251)	---
	<b>IA-CA-Col</b>	16	---	0 (0)	9 [0.598±0.092] (0.5049-0.7717)	---	7 [0.734±0.130] (0.5420-0.8802)
	<b>IA-CR+OI-Col</b>	16	---	5 [0.592±0.152] (0.3940-0.7994)	---	1 (0.6185)	10 [0.804±0.088] (0.6912-0.9615)
<i>Test study 14.</i> <i>Diagrams based on log-ratios of major elements</i>	<b>CA-CR+OI-Col</b>	16	---	---	9 [0.652±0.102] (0.5109-0.8295)	1 (0.6005)	6 [0.569±0.084] (0.4270-0.6388)
	<b>{Σn} {Σprob} [%prob]</b>	80	{7} {4.6517} [---]	{5} {2.9598} [6%]	{33} {22.6620} [49%]	{4} {2.6627} [5%]	{31} {22.1191} [40%]

For the explanation of abbreviations, see footnote of Table S17.

**Table S35.**

Testing of multidimensional diagrams from Quaternary acid rocks of the Nisyros Island, Greece (Di Paola, 1974; Test study 14).

Magma type, Figure name	Figure type	Total number of samples	Number of discriminated samples				
			Arc IA+CA [ $\bar{x} \pm s$ ] [ $p_{IA+CA}$ Θ]	IA [ $\bar{x} \pm s$ ] [ $p_{IA}$ Θ]	CA [ $\bar{x} \pm s$ ] [ $p_{CA}$ Θ]	Within-plate CR+OI [ $\bar{x} \pm s$ ] [ $p_{CR+OI}$ Θ]	Collision Col [ $\bar{x} \pm s$ ] [ $p_{Col}$ Θ]
Acid; Verma <i>et al.</i> (2012); All major elements	IA+CA-CR+OI-Col	11	10 [0.731±0.160] (0.5079-0.9313)	---	---	0 (0)	1 (0.9648)
	IA-CA-CR+OI	11	---	0 (0)	11 [0.768±0.087] (0.6230-0.8683)	0 (0)	---
	IA-CA-Col	11	---	0 (0)	10 [0.7312±0.0446] (0.6385-0.8120)	---	1 (0.9690)
	IA-CR+OI-Col	11	---	7 [0.719±0.154] (0.4796-0.8826)	---	0 (0)	4 [0.640±0.253] (0.4241-0.9568)
	CA-CR+OI-Col	11	---	---	10 [0.712±0.162] (0.4600-0.9350)	0 (0)	1 (0.9236)
<i>Test study 14. Diagrams based on log-ratios of major elements</i>		55	{10} {7.3070} [--]	{7} {5.0311} [16%]	{31} {22.8785} [71%]	{0} {0} [0%]	{7} {5.4192} [13%]
Acid; Verma <i>et al.</i> (2013); All major elements	IA+CA-CR+OI-Col	11	9 [0.670±0.175] (0.3665-0.8633)	---	---	0 (0)	2 [0.552±0.262] (0.3673, 0.7376)
	IA-CA-CR+OI	11	---	0 (0)	10 [0.828±0.149] (0.4918-0.9373)	1 (0.9423)	---
	IA-CA-Col	11	---	0 (0)	10 [0.857±0.097] (0.6108-0.9346)	---	1 (0.9793)
	IA-CR+OI-Col	11	---	0 (0)	---	8 [0.5273±0.0419] (0.4764-0.6122)	3 [0.565±0.117] (0.4813-0.6979)
	CA-CR+OI-Col	11	---	---	9 [0.688±0.177] (0.3912-0.8875)	1 (0.3659)	1 (0.7049)
<i>Test study 14. Diagrams based on log-ratios of major elements</i>		55	{9} {6.0315} [--]	{0} {0} [0%]	{29} {23.0522} [75%]	{10} {5.5269} [14%]	{7} {4.4827} [11%]

For the explanation of abbreviations, see footnote of Table S17.

**Table S36.**

Testing of multidimensional diagrams from Pleistocene-Holocene intermediate rocks from the Augustine volcano, Alaska (Johnson et al. 1996; Test study 15).

Magma type, Figure name; Figure number	Figure type	Total number of samples	Number of discriminated samples				
			Arc IA+CA [ $\bar{x} \pm s$ ] ( $p_{IA+CA}$ ) $\Theta$	IA [ $\bar{x} \pm s$ ] [ $p_{IA}$ ] $\Theta$	CA [ $\bar{x} \pm s$ ] [ $p_{CA}$ ] $\Theta$	Within-plate CR+OI [ $\bar{x} \pm s$ ] ( $p_{CR+OI}$ ) $\Theta$	Collision Col [ $\bar{x} \pm s$ ] ( $p_{Col}$ ) $\Theta$
IA+CA-CR+OI- Col	IA+CA-CR+OI- Col	21	21 [0.905±0.054] (0.7810-0.9814)	---	---	0 (0)	0 (0)
Intermediate; Verma and Verma (2013); log- ratios of all major elements;	IA-CA-CR+OI	21	---	14 [0.5543±0.0344] (0.4999-0.6192)	7 [0.608±0.095] (0.4996-0.7092)	0 (0)	---
	IA-CA-Col	21	---	17 [0.585±0.059] (0.4988-0.7272)	4 [0.6371±0.0328] (0.6041-0.6730)	---	0 (0)
	IA-CR+OI-Col	21	---	21 [0.865±0.076] (0.6997-0.9733)	---	0 (0)	0 (0)
	CA-CR+OI-Col	21	---	---	21 [0.850±0.084] (0.6518-0.9607)	0 (0)	0 (0)
<i>Test study 15.</i> <i>Diagrams based on log- ratios of major elements</i>	{Σn} {Σprob} [%prob]	105	{21} {19.0011} [--]	{52} {35.8767} [59.3%]	{32} {24.6512} [40.7%]	{0} {0} [0%]	{0} {0} [0%]

For the explanation of abbreviations, see footnote of Table S17.

**Table S37.**

Testing of multidimensional diagrams from Quaternary basic rocks of the Barren Island, Andaman-Nicobar Islands (Chandrasekharam et al. 2009; Streck et al. 2011; Test study 16a).

Figure reference; figure type	Discrimination diagram	Total no. of samples (%)	Predicted tectonic affinity and number of discriminated samples (%)				
			IAB	CRB+OIB	CRB	OIB	MORB
Agrawal et al. (2004); adjusted major element concentrations	IAB-CRB-OIB-MORB	25 (100)	22 (88)	---	0 (0)	0 (0)	3 (12)
	IAB-CRB-OIB	25 (100)	25 (100)	---	0 (0)	0 (0)	---
	IAB-CRB-MORB	25 (100)	22 (88)	---	0 (0)	---	3 (12)
	IAB-OIB-MORB	25 (100)	22 (88)	---	---	0 (0)	3 (12)
	CRB-OIB-MORB	25 (100)	---	---	0 (0)	0 (0)	25 (100)
<i>Test study 16a. Synthesis of all five diagrams of Agrawal et al. (2004)</i>		<b>125 (100)</b>	<b>91 (72.8)</b>	---	<b>0 (0)</b>	<b>0 (0)</b>	<b>34 (27.2)</b>
Verma et al. (2006); log-ratios of major elements	IAB-CRB-OIB-MORB	25 (100)	25 (100)	---	0 (0)	0 (0)	0 (0)
	IAB-CRB-OIB	25 (100)	25 (100)	---	0 (0)	0 (0)	---
	IAB-CRB-MORB	25 (100)	25 (100)	---	0 (0)	---	0 (0)
	IAB-OIB-MORB	25 (100)	25 (100)	---	---	0 (0)	0 (0)
	CRB-OIB-MORB	25 (100)	---	---	0 (0)	0 (0)	25 (100)
<i>Test study 16a. Synthesis of all five diagrams of Verma et al. (2006)</i>		<b>125 (100)</b>	<b>100 (80.0)</b>	---	<b>0 (0)</b>	<b>0 (0)</b>	<b>25 (20.0)</b>
Agrawal et al. (2008); log-ratios of immobile trace elements	IAB-CRB+OIB-MORB	11 (100)	11 (100)	0 (0)	---	---	0 (0)
	IAB-CRB-OIB	11 (100)	11 (100)	---	0 (0)	0 (0)	---
	IAB-CRB-MORB	11 (100)	11 (100)	---	0 (0)	---	0 (0)
	IAB-OIB-MORB	11 (100)	11 (100)	---	---	0 (0)	0 (0)
	CRB-OIB-MORB	11 (100)	---	---	0 (0)	0 (0)	11 (100)
<i>Test study 16a. Synthesis of all five diagrams of Agrawal et al. (2008)</i>		<b>55 (100)</b>	<b>44 (80)</b>	<b>0 (---)</b>	<b>0 (0)</b>	<b>0 (0)</b>	<b>11 (20)</b>
Verma and Agrawal (2011); log-ratios of immobile major and trace elements	IAB-CRB+OIB-MORB	24 (100)	24 (100)	0 (0)	---	---	0 (0)
	IAB-CRB-OIB	24 (100)	24 (100)	---	0 (0)	0 (0)	---
	IAB-CRB-MORB	24 (100)	24 (100)	---	0 (0)	---	0 (0)
	IAB-OIB-MORB	24 (100)	24 (100)	---	---	0 (0)	0 (0)
	CRB-OIB-MORB	24 (100)	---	---	0 (0)	0 (0)	24 (100)
<i>Test study 16a. Synthesis of all five diagrams of Verma and Agrawal (2011)</i>		<b>120 (100)</b>	<b>96 (80.0)</b>	<b>0 (---)</b>	<b>0 (0)</b>	<b>0 (0)</b>	<b>24 (20.0)</b>

For the explanation of abbreviations, see footnote of Table 1 or S14.

**Table S38.**

Testing of multidimensional diagrams from Quaternary, intermediate rocks of the Barren Island, Andaman-Nicobar Islands (Chandrasekharam et al. 2009; Streck et al. 2011; Test study 16a).

Magma type, Figure name	Figure type	Total number of samples	Number of discriminated samples				
			IA+CA [ $\bar{X} \pm S$ ] [ $p_{IA+CA}$ ] $\Theta$	Arc IA [ $\bar{X} \pm S$ ] [ $p_{IA}$ ] $\Theta$	CA [ $\bar{X} \pm S$ ] [ $p_{CA}$ ] $\Theta$	Within-plate CR+OI [ $\bar{X} \pm S$ ] [ $p_{CR+OI}$ ] $\Theta$	Collision Col [ $\bar{X} \pm S$ ] [ $p_{Col}$ ] $\Theta$
Intermediate; Verma and Verma (2013); log-ratios of all major elements	IA+CA-CR+OI- Col	21	19 [0.887±0.117] (0.6356-0.9931)	---	---	1 (0.6605)	1 (0.9189)
	IA-CA-CR+OI	21	---	9 [0.5177±0.0379] (0.4805-0.5932)	11 [0.582±0.149] (0.4730-0.9993)	1 (0.3955)	---
	IA-CA-Col	21	---	16 [0.624±0.053] (0.5341-0.7284)	4 [0.5503±0.0405] (0.5185-0.6097)	---	1 (0.9569)
	IA-CR+OI-Col	21	---	19 [0.874±0.136] (0.5863-0.9952)	---	1 (0.6915)	1 (0.9974)
	CA-CR+OI- Col	21	---	---	20 [0.830±0.168] (0.5349-0.9945)	1 (0.7049)	0 (0)
<i>Test study 16a. Diagrams based on log-ratios of major elements</i>	{Σn} {Σprob} [%prob]	105	{19} {16.8541} [--]	{44} {31.2416} [51.6%]	{35} {25.2019} [41.6%]	{4} {2.4524} [3.1%]	{3} {2.8732} [3.7%]
Intermediate; Verma and Verma (2013); log-ratios of immobile major and trace elements	IA+CA-CR+OI- Col	21	21 [0.9967±0.0051] (0.9754-0.9994)	---	---	0 (0)	0 (0)
	IA-CA-CR+OI	21	---	21 [0.890±0.047] (0.7355-0.9299)	0 (0)	0 (0)	---
	IA-CA-Col	21	---	21 [0.899±0.050] (0.7278-0.9407)	0 (0)	---	0 (0)
	IA-CR+OI-Col	21	---	21 [0.9964±0.0060] (0.9710-0.9993)	---	0 (0)	0 (0)
	CA-CR+OI- Col	21	---	---	21 [0.99959±0.00133] (0.9938-1.0000)	0 (0)	0 (0)
<i>Test study 16a. Diagrams based on log-ratios of immobile major and trace elements</i>	{Σn} {Σprob} [%prob]	105	{21} {20.9317} [--]	{63} {58.5025} [73.6%]	{21} {20.9913} [26.4%]	{0} {0} [0%]	{0} {0} [0%]
Intermediate; Verma and Verma (2013); log-ratios of immobile trace elements	IA+CA-CR+OI- Col	9	9 [0.99417±0.00303] (0.9900-0.9994)	---	---	0 (0)	0 (0)
	IA-CA-CR+OI	9	---	9 [0.9069±0.0156] (0.8855-0.9375)	0 (0)	0 (0)	---
	IA-CA-Col	9	---	9 [0.9257±0.0084] (0.9123-0.9404)	0 (0)	---	0 (0)
	IA-CR+OI-Col	9	---	9 [0.99632±0.00191] (0.9935-0.9996)	---	0 (0)	0 (0)
	CA-CR+OI- Col	9	---	---	9 [0.99555±0.00229] (0.9926-0.9996)	0 (0)	0 (0)
<i>Test study 16a. Diagrams based on log-ratios of immobile trace elements</i>	{Σn} {Σprob} [%prob]	45	{9} {8.9475} [--]	{27} {25.4600} [74%]	{9} {8.9599} {26%}	{0} {0} [0%]	{0} {0} [0%]

For the explanation of abbreviations, see footnote of Table S17.

**Table S39.**

Testing of multidimensional diagrams from Quaternary, intermediate rocks of the Narcondam Island, Andaman-Nicobar Islands (Pal et al. 2009; Streck et al. 2011; Test study 16b).

Magma type, Figure name	Figure type	Total number of samples	Number of discriminated samples					
			Arc			Within- plate CR+OI [ $\bar{x} \pm s$ ] [ $p_{CR+OI}$ ] $\Theta$	Collision $\bar{x} \pm s$ ] [ $p_{Col}$ ] $\Theta$	Col [ $\bar{x} \pm s$ ] [ $p_{Col}$ ] $\Theta$
			IA+CA [ $\bar{x} \pm s$ ] ( $p_{IA+CA}$ ) $\Theta$	IA [ $\bar{x} \pm s$ ] [ $p_{IA}$ ] $\Theta$	CA [ $\bar{x} \pm s$ ] [ $p_{CA}$ ] $\Theta$			
Intermediate; Verma and Verma (2013); log-ratios of all major elements	IA+CA-CR+OI-Col	10	6 [0.720±0.138] (0.5329-0.8831)	---	---	0 (0)	4 [0.562±0.048] (0.5158-0.6223)	---
	IA-CA-CR+OI	10	---	5 [0.604±0.062] (0.5460-0.7093)	5 [0.552±0.049] (0.5031-0.6120)	0 (0)	---	---
	IA-CA-Col	10	---	6 [0.468±0.049] (0.4100-0.5427)	1 (0.3967)	---	3 [0.400±0.073] (0.3448-0.4822)	---
	IA-CR+OI-Col	10	---	6 [0.683±0.172] (0.4999-0.8629)	---	0 (0)	4 [0.645±0.066] (0.5571-0.7172)	---
	CA-CR+OI-Col	10	---	---	6 [0.709±0.164] (0.5194-0.8923)	0 (0)	4 [0.6253±0.0443] (0.5828-0.6696)	---
<b>Test study 16b.</b> <i>Diagrams based on log-ratios of major elements</i>		{Σn} {Σprob} [%prob]	50	{16} {4.3201} [--]	{17} {9.9209} [41%]	{12} {7.4106} [31%]	{0} {0} [0%]	{15} {8.5253} [28%]
Intermediate; Verma and Verma (2013); log-ratios of immobile major and trace elements	IA+CA-CR+OI-Col	8	8 [0.924±0.079] (0.7846-0.9952)	---	---	0 (0)	0 (0)	0 (0)
	IA-CA-CR+OI	8	---	8 [0.765±0.131] (0.5716-0.9087)	0 (0)	0 (0)	---	---
	IA-CA-Col	8	---	8 [0.743±0.144] (0.5235-0.8941)	0 (0)	---	0 (0)	0 (0)
	IA-CR+OI-Col	8	---	8 [0.916±0.092] (0.7515-0.9947)	---	0 (0)	0 (0)	0 (0)
	CA-CR+OI-Col	8	---	---	8 [0.9737±0.0279] (0.9302-0.9992)	0 (0)	0 (0)	0 (0)
<b>Test study 16b.</b> <i>Diagrams based on log-ratios of immobile major and trace elements</i>		{Σn} {Σprob} [%prob]	40	{8} {7.3902} [--]	{24} {19.3889} [71%]	{8} {7.7897} [29%]	{0} {0} [0%]	{0} {0} [0%]
Intermediate; Verma and Verma (2013); log-ratios of immobile trace elements	IA+CA-CR+OI-Col	8	4 [0.696±0.165] (0.5416-0.9013)	---	---	0 (0)	4 [0.574±0.060] (0.4999-0.6445)	---
	IA-CA-CR+OI	8	---	7 [0.659±0.086] (0.5372-0.8031)	1 (0.5999)	0 (0)	---	---
	IA-CA-Col	8	---	7 [0.607±0.123] (0.4888-0.8443)	0 (0)	---	1 (0.4605)	---
	IA-CR+OI-Col	8	---	6 [0.621±0.149] (0.5272-0.9209)	---	0 (0)	2 [0.565±0.049] (0.5311, 0.5998)	---
	CA-CR+OI-Col	8	---	---	4 [0.746±0.135] (0.6299-0.8934)	0 (0)	4 [0.6164±0.0431] (0.5543-0.6539)	---
<b>Test study 16b.</b> <i>Diagrams based on log-ratios of immobile trace elements</i>		{Σn} {Σprob} [%prob]	40	{4} {2.7834} [--]	{20} {12.5912} [58%]	{5} {3.5821} [17%]	{0} {0} [0%]	{11} {6.3540} [25%]

For the explanation of abbreviations, see footnote of Table S17.

**Table S40.**

Testing of multidimensional diagrams from Quaternary acid rocks of Narcondam Island, Andaman-Nicobar Islands (Pal et al. 2009; Streck et al. 2011; Test study 16b).

Magma type, Figure name	Figure type	Total number of samples	Number of discriminated samples				Within-plate CR+OI [ $\bar{x} \pm s$ ] [ $p_{CR+OI}$ ] $\Theta$	Collision Col [ $\bar{x} \pm s$ ] [ $p_{Col}$ ] $\Theta$		
			Arc							
			IA+CA [ $\bar{x} \pm s$ ] ( $p_{IA+CA}$ ) $\Theta$	IA [ $\bar{x} \pm s$ ] [ $p_{IA}$ ] $\Theta$	CA [ $\bar{x} \pm s$ ] [ $p_{CA}$ ] $\Theta$					
Acid; Verma <i>et al.</i> (2012); All major elements	IA+CA-CR+OI-Col	8	8 [0.9733±0.0082] (0.9547-0.9820)	---	---	0 (0)	0 (0)			
	IA-CA-CR+OI	8	---	8 [0.797±0.054] (0.6775-0.8414)	0 (0)	0 (0)	---			
	IA-CA-Col	8	---	8 [0.807±0.054] (0.7031-0.8526)	0 (0)	---	0 (0)			
	IA-CR+OI-Col	8	8	[0.99434±0.0039 7] (0.9848-0.9969)	---	0 (0)	0 (0)			
	CA-CR+OI-Col	8	---	---	8 [0.9945±0.0027] (0.9881-0.9964)	0 (0)	0 (0)			
	<i>Test study 16b.</i> <i>Diagrams based on log-ratios of major elements</i>	{Σn} {Σprob} [%prob]	40	{8} {7.7865} [---]	{24} {20.7847} [72%]	{8} {7.9560} [28%]	{0} {0} [0 %]	{0} {0} [0 %]		
Acid; Verma <i>et al.</i> (2013); All major elements	IA+CA-CR+OI-Col	8	8 [0.9688±0.0125] (0.9420-0.9794)	---	---	0 (0)	0 (0)			
	IA-CA-CR+OI	8	---	4 [0.5586±0.0319] (0.5271-0.6014)	4 [0.5522±0.0308] (0.5157-0.5796)	0 (0)	---			
	IA-CA-Col	8	---	1 (0.5576)	7 [0.596±0.046] (0.5480-0.6586)	---	0 (0)			
	IA-CR+OI-Col	8	---	8 [0.9582±0.0273] (0.8975-0.9768)	---	0 (0)	0 (0)			
	CA-CR+OI-Col	8	---	---	8 [0.9858±0.0073] (0.9695-0.9913)	0 (0)	0 (0)			
	<i>Test study 16b.</i> <i>Diagrams based on log-ratios of major elements</i>	{Σn} {Σprob} [%prob]	40	{8} {7.7506} [---]	{13} {10.4580} [42%]	{19} {14.2693} [58%]	{0} {0} [0 %]	{0} {0} [0 %]		

For the explanation of abbreviations, see footnote of Table S17.

**Table S41.**

Testing of multidimensional diagrams from recent basic rocks from the Indian Ridge (Yi et al. 2014; Test study 17).

Figure reference; figure type	Discrimination diagram	Total no. of samples (%)	Predicted tectonic affinity and number of discriminated samples (%)				
			IAB	CRB+OIB	CRB	OIB	MORB
Agrawal et al. (2004); adjusted major element concentrations	IAB-CRB-OIB-MORB	33 (100)	2 (6)	---	0 (0)	0 (0)	31 (94)
	IAB-CRB-OIB	33 (100)	29 (88)	---	1 (3)	3 (9)	---
	IAB-CRB-MORB	33 (100)	2 (6)	---	0 (0)	---	31 (94)
	IAB-OIB-MORB	33 (100)	2 (6)	---	---	0 (0)	31 (94)
	CRB-OIB-MORB	33 (100)	---	---	0 (0)	0 (0)	33 (100)
<i>Test study 17. Synthesis of all five diagrams of Agrawal et al. (2004)</i>		<b>165 (100)</b>	<b>35 (21.2)</b>	---	<b>1 (0.6)</b>	<b>3 (1.8)</b>	<b>126 (76.4)</b>
Verma et al. (2006); log-ratios of major elements	IAB-CRB-OIB-MORB	33 (100)	1 (3)	---	1 (3)	0 (0)	31 (94)
	IAB-CRB-OIB	33 (100)	2 (6)	---	5 (15)	26 (79)	---
	IAB-CRB-MORB	33 (100)	1 (3)	---	1 (3)	---	31 (94)
	IAB-OIB-MORB	33 (100)	1 (3)	---	---	0 (0)	32 (97)
	CRB-OIB-MORB	33 (100)	---	---	2 (6)	0 (0)	31 (94)
<i>Test study 17. Synthesis of all five diagrams of Verma et al. (2006)</i>		<b>165 (100)</b>	<b>5 (3.0)</b>	---	<b>9 (5.4)</b>	<b>26 (15.8)</b>	<b>125 (75.8)</b>
Agrawal et al. (2008); log-ratios of immobile trace elements	IAB-CRB+OIB-MORB	32 (100)	6 (19)	1 (3)	---	---	25 (78)
	IAB-CRB-OIB	32 (100)	7 (22)	---	11 (34)	14 (44)	---
	IAB-CRB-MORB	32 (100)	7 (22)	---	2 (6)	---	23 (72)
	IAB-OIB-MORB	32 (100)	6 (19)	---	---	0 (0)	26 (81)
	CRB-OIB-MORB	32 (100)	---	---	2 (6)	0 (0)	30 (94)
<i>Test study 17. Synthesis of all five diagrams of Agrawal et al. (2008)</i>		<b>160 (100)</b>	<b>26 (16.2)</b>	<b>1 (---)</b>	<b>16 (10.0)</b>	<b>14 (8.8)</b>	<b>104 (65.0)</b>
Verma and Agrawal (2011); log-ratios of immobile major and trace elements	IAB-CRB+OIB-MORB	33 (100)	0 (0)	2 (6)	---	---	31 (94)
	IAB-CRB-OIB	33 (100)	31 (94)	---	2 (6)	0 (0)	---
	IAB-CRB-MORB	33 (100)	0 (0)	---	2 (6)	---	31 (94)
	IAB-OIB-MORB	33 (100)	0 (0)	---	---	2 (6)	31 (94)
	CRB-OIB-MORB	33 (100)	---	---	2 (6)	0 (0)	31 (94)
<i>Test study 17. Synthesis of all five diagrams of Verma and Agrawal (2011)</i>		<b>165 (100)</b>	<b>31 (18.8)</b>	<b>2 (---)</b>	<b>8 (4.8)</b>	<b>2 (1.2)</b>	<b>124 (75.2)</b>

For the explanation of abbreviations, see footnote of Table 1 or S14.

**Table S42.**

Testing of multidimensional diagrams from late Miocene-Pleistocene (2.5-4.6 Ma) intermediate rocks of Shirak, Armenia (Neill et al. 2013; Test study 18).

Magma type, Figure name	Figure type	Total number of samples	Number of discriminated samples					
			IA+CA [ $\bar{x} \pm S$ ] [ $p_{IA+CA}$ Θ]	Arc IA [ $\bar{x} \pm S$ ] [ $p_{IA}$ Θ]	CA [ $\bar{x} \pm S$ ] [ $p_{CA}$ Θ]	Within-plate CR+OI [ $\bar{x} \pm S$ ] [ $p_{CR+OI}$ ] Θ	Collision [ $\bar{x} \pm S$ ] [ $p_{Col}$ ] Θ	
Intermediate; Verma and Verma (2013); log-ratios of all major elements	IA+CA-CR+OI-Col	13	0 (0)	---	---	5 [0.591±0.188] (0.4557-0.9061)	8 [0.763±0.180] (0.4610-0.9284)	
	IA-CA-CR+OI	13	---	0 (0)	7 [0.755±0.096] (0.5592-0.8473)	6 [0.649±0.156] (0.4796-0.8637)	---	
	IA-CA-Col	13	---	0 (0)	5 [0.584±0.077] (0.4621-0.6596)	---	8 [0.736±0.098] (0.5234-0.8480)	
	IA-CR+OI-Col	13	---	0 (0)	---	5 [0.635±0.182] (0.4899-0.9308)	8 [0.826±0.169] (0.5453-0.9688)	
	CA-CR+OI-Col	13	---	---	3 [0.491±0.053] (0.4517-0.5514)	3 [0.560±0.210] (0.4118-0.7999)	7 [0.692±0.193] (0.3740-0.8926)	
<i>Test study 18.</i> <i>Diagrams based on log-ratios of major elements</i>		{Σn} {Σprob} [%prob]	65	{0} {0} [ 0% ]	{0} {0} [ 0% ]	{15} {9.6749} [22%]	{19} {11.7012} [26%]	{31} {23.4464} [52%]
Intermediate; Verma and Verma (2013); log-ratios of immobile major and trace elements	IA+CA-CR+OI-Col	9	0 (0)	---	---	2 [0.794±0.112] (0.7143, 0.8728)	7 [0.807±0.167] (0.4841-0.9685)	
	IA-CA-CR+OI	9	---	0 (0)	4 [0.665±0.117] (0.5211-0.7604)	5 [0.714±0.154] (0.5674-0.9279)	---	
	IA-CA-Col	9	---	0 (0)	0 (0)	---	9 [0.774±0.142] (0.6140-0.9513)	
	IA-CR+OI-Col	9	---	0 (0)	---	3 [0.694±0.199] (0.4774-0.8693)	6 [0.856±0.104] (0.6676-0.9684)	
	CA-CR+OI-Col	9	---	---	0 (0)	2 [0.797±0.128] (0.7065, 0.8873)	7 [0.821±0.158] (0.5205-0.9807)	
<i>Test study 18.</i> <i>Diagrams based on log-ratios of immobile major and trace elements</i>		{Σn} {Σprob} [%prob]	45	{0} {0} [ 0% ]	{0} {0} [ 0% ]	{4} {2.6600} [8%]	{12} {8.8313} [25%]	{29} {23.5052} [67%]
Intermediate; Verma and Verma (2013); log-ratios of immobile trace elements	IA+CA-CR+OI-Col	13	2 [0.4754±0.0419] (0.4458, 0.5050)	---	---	5 [0.573±0.077] (0.4476-0.6392)	6 [0.659±0.158] (0.3935-0.8547)	
	IA-CA-CR+OI	13	---	0 (0)	6 [0.564±0.114] (0.4729-0.7587)	7 [0.634±0.134] (0.4218-0.8101)	---	
	IA-CA-Col	13	---	0 (0)	6 [0.647±0.143] (0.4507-0.7845)	---	7 [0.800±0.177] (0.5330-0.9522)	
	IA-CR+OI-Col	13	---	0 (0)	---	7 [0.616±0.068] (0.5380-0.7369)	6 [0.669±0.136] (0.4518-0.8473)	
	CA-CR+OI-Col	13	---	---	5 [0.586±0.125] (0.3928-0.7132)	2 [0.466±0.071] (0.4158, 0.5158)	6 [0.677±0.167] (0.3677-0.8346)	
<i>Test study 18.</i> <i>Diagrams based on log-ratios of immobile trace elements</i>		{Σn} {Σprob} [%prob]	65	{2} {0.9509} [---]	{0} {0} [ 0% ]	{17} {10.1969} [27%]	{21} {12.5533} [30%]	{25} {17.6317} [43%]

For the explanation of abbreviations, see footnote of Table S17.

**Table S43.**

Testing of multidimensional diagrams from late Miocene (4.95–5.52 Ma) drill hole basic and ultrabasic rocks of the Eiao Island, French Polynesia (Caroff et al. 1999; Test study A1).

Figure reference; figure type	Discrimination diagram	Total no. of samples (%)	Predicted tectonic affinity and number of discriminated samples (%)				
			IAB	CRB+OIB	CRB	OIB	MORB
Agrawal et al. (2004); adjusted major element concentrations	IAB-CRB-OIB-MORB	25 (100)	0 (0)	---	1 (4)	24 (96)	0 (0)
	IAB-CRB-OIB	25 (100)	0 (0)	---	1 (4)	24 (96)	---
	IAB-CRB-MORB	25 (100)	0 (0)	---	24 (96)	---	1 (4)
	IAB-OIB-MORB	25 (100)	0 (0)	---	---	25 (100)	0 (0)
	CRB-OIB-MORB	25 (100)	---	---	1 (4)	24 (96)	0 (0)
<i>Test study A1. Synthesis of all five diagrams of Agrawal et al. (2004)</i>		<b>125 (100)</b>	<b>0 (0)</b>	<b>---</b>	<b>27 (21.6)</b>	<b>97 (77.6)</b>	<b>1 (0.8)</b>
Verma et al. (2006); log-ratios of major elements	IAB-CRB-OIB-MORB	25 (100)	0 (0)	---	2 (8)	23 (92)	0 (0)
	IAB-CRB-OIB	25 (100)	0 (0)	---	0 (0)	25 (100)	---
	IAB-CRB-MORB	25 (100)	0 (0)	---	24 (96)	---	1 (4)
	IAB-OIB-MORB	25 (100)	0 (0)	---	---	25 (100)	0 (0)
	CRB-OIB-MORB	25 (100)	---	---	0 (0)	25 (100)	0 (0)
<i>Test study A1. Synthesis of all five diagrams of Verma et al. (2006)</i>		<b>125 (100)</b>	<b>0 (0)</b>	<b>---</b>	<b>26 (20.8)</b>	<b>98 (78.4)</b>	<b>1 (0.8)</b>
Verma and Agrawal (2011); log-ratios of immobile major and trace elements	IAB-CRB+OIB-MORB	25 (100)	0 (0)	25 (100)	---	---	0 (0)
	IAB-CRB-OIB	25 (100)	0 (0)	---	0 (0)	25 (100)	---
	IAB-CRB-MORB	25 (100)	0 (0)	---	25 (100)	---	0 (0)
	IAB-OIB-MORB	25 (100)	0 (0)	---	---	25 (100)	0 (0)
	CRB-OIB-MORB	25 (100)	---	---	0 (0)	25 (100)	0 (0)
<i>Test study A1. Synthesis of all five diagrams of Verma and Agrawal (2011)</i>		<b>125 (100)</b>	<b>0 (0)</b>	<b>25 (---)</b>	<b>31 (24.8)</b>	<b>94 (75.2)</b>	<b>0(0)</b>

For the explanation of abbreviations, see footnote of Table 1 or S14.

**Table S44.**

Testing of multidimensional diagrams from Pliocene-Pleistocene (0.35-4 Ma) altered basic and ultrabasic rocks of Koolau, Haleakala, and Kohala volcanoes, Hawaiian Islands (Patino et al. 2003; Test study A2).

Figure reference; figure type	Discrimination diagram	Total no. of samples (%)	Predicted tectonic affinity and number of discriminated samples (%)				
			IAB	CRB+OIB	CRB	OIB	MORB
Agrawal <i>et al.</i> (2004); adjusted major element concentrations	IAB-CRB-OIB-MORB	9 (100)	0 (0)	---	9 (100)	0 (0)	0 (0)
	IAB-CRB-OIB	9 (100)	1 (11)	---	7 (78)	1 (11)	---
	IAB-CRB-MORB	9 (100)	0 (0)	---	9 (100)	---	0 (0)
	IAB-OIB-MORB	9 (100)	1 (11)	---	---	8 (89)	0 (0)
	CRB-OIB-MORB	9 (100)	---	---	7 (77.8)	2 (22)	0 (0)
<i>Test study A2. Synthesis of all five diagrams of Agrawal <i>et al.</i> (2004)</i>		<b>45 (100)</b>	<b>2 (4)</b>	---	<b>32 (71)</b>	<b>11 (25)</b>	<b>0 (0)</b>
Verma <i>et al.</i> (2006); log-ratios of major elements	IAB-CRB-OIB-MORB	9 (100)	0 (0)	---	9 (100)	0 (0)	0 (0)
	IAB-CRB-OIB	9 (100)	0 (0)	---	5 (55.6)	4 (44.4)	---
	IAB-CRB-MORB	9 (100)	0 (0)	---	9 (100)	---	0 (0)
	IAB-OIB-MORB	9 (100)	1 (11)	---	---	8 (88.9)	0 (0)
	CRB-OIB-MORB	9 (100)	---	---	5 (55.6)	4 (44.4)	0 (0)
<i>Test study A2. Synthesis of all five diagrams of Verma <i>et al.</i> (2006)</i>		<b>45 (100)</b>	<b>1 (2)</b>	---	<b>28 (62)</b>	<b>16 (36)</b>	<b>0 (0)</b>

For the explanation of abbreviations, see footnote of Table 1 or S14.

**Table S45.**

Testing of multidimensional diagrams from late Miocene to Holocene slightly to intensely altered basic rocks of the Hainan Island, China (Wang et al. 2012; Test study A3).

Figure reference; figure type	Discrimination diagram	Total no. of samples (%)	Predicted tectonic affinity and number of discriminated samples (%)				
			IAB	CRB+OIB	CRB	OIB	MORB
Agrawal et al. (2004); adjusted major element concentrations	IAB-CRB-OIB-MORB	13 (100)	0 (0)	---	11 (84.6)	1 (7.7)	1 (7.7)
	IAB-CRB-OIB	13 (100)	0 (0)	---	13 (100)	0 (0)	---
	IAB-CRB-MORB	13 (100)	0 (0)	---	10 (76.9)	---	3 (23.1)
	IAB-OIB-MORB	13 (100)	0 (0)	---	---	10 (76.9)	3 (23.1)
<i>Test study A3. Synthesis of all five diagrams of Agrawal et al. (2004)</i>	CRB-OIB-MORB	13 (100)	---	---	11 (84.6)	1 (7.7)	1 (7.7)
		<b>65 (100)</b>	<b>0 (0)</b>	<b>---</b>	<b>45 (69.2)</b>	<b>12 (18.5)</b>	<b>8 (12.3)</b>
Verma et al. (2006); log-ratios of major elements	IAB-CRB-OIB-MORB	13 (100)	0 (0)	---	11 (84.6)	2 (15.4)	0 (0)
	IAB-CRB-OIB	13 (100)	0 (0)	---	12 (92.3)	1 (7.7)	---
	IAB-CRB-MORB	13 (100)	0 (0)	---	13 (100)	---	0 (0)
	IAB-OIB-MORB	13 (100)	0 (0)	---	---	9 (69.2)	4 (30.8)
	CRB-OIB-MORB	13 (100)	---	---	12 (92.3)	1 (7.7)	0 (0)
<i>Test study A3. Synthesis of all five diagrams of Verma et al. (2006)</i>		<b>65 (100)</b>	<b>0 (0)</b>	<b>---</b>	<b>48 (73.8)</b>	<b>13 (20)</b>	<b>4 (6.2)</b>

For the explanation of abbreviations, see footnote of Table 1 or S14.

**Table S46.**

Testing of multidimensional diagrams from late Miocene to Holocene slightly to intensely altered intermediate rocks of the Hainan Island, China (Wang et al. 2012; Test study A3).

Magma type, Figure name	Figure type	Total number of samples	Number of discriminated samples				
			Arc			Within-plate	Collision
			IA+CA [ $\bar{x} \pm s$ ] [ $p_{IA+CA}$ ] $\Theta$	IA [ $\bar{x} \pm s$ ] [ $p_{IA}$ ] $\Theta$	CA [ $\bar{x} \pm s$ ] [ $p_{CA}$ ] $\Theta$	CR+OI [ $\bar{x} \pm s$ ] [ $p_{CR+OI}$ ] $\Theta$	$\bar{x} \pm s$ ] [ $p_{Col}$ ] $\Theta$
	IA+CA-CR+OI-Col	10	0 (0)	---	---	10 [0.760±0.114] (0.6118-0.9400)	0 (0)
Intermediate; Verma and Verma (2013); log-ratios of all major elements	IA-CA-CR+OI	10	---	0 (0)	0 (0)	10 [0.649±0.132] (0.4636-0.8260)	---
	IA-CA-Col	10	---	4 [0.702±0.135] (0.5975-0.8870)	6 [0.584±0.077] (0.5009-0.7102)	---	0 (0)
	IA-CR+OI-Col	10	---	0 (0)	---	10 [0.843±0.083] (0.7229-0.9457)	0 (0)
	CA-CR+OI-Col	10	---	---	0 (0)	10 [0.729±0.158] (0.5172-0.9227)	0 (0)
<i>Test study A3. Diagrams based on log-ratios of major elements</i>	<i>{Σn} {Σprob} [%prob]</i>	<i>50</i>	<i>{0} {0} [0%]</i>	<i>{4} {2.8068} [8%]</i>	<i>{6} {3.5068} [9%]</i>	<i>{40} {29.8050} [83%]</i>	<i>{0} {0} [0%]</i>

For the explanation of abbreviations, see footnote of Table S17.

**Table S47.**

Testing of multidimensional diagrams from intermediate altered rocks of Moyuta and Tecuamburro volcanoes, Guatemala (Patino et al. 2003; Test study A4)

Magma type, Figure name	Figure type	Total number of samples	Number of discriminated samples					
			Arc			Within-plate		
			IA+CA [ $\bar{X} \pm S$ ] ( $p_{IA+CA}$ ) $\Theta$	IA [ $\bar{X} \pm S$ ] [ $p_{IA}$ ] $\Theta$	CA [ $\bar{X} \pm S$ ] ( $p_{CA}$ ) $\Theta$	CR+OI [ $\bar{X} \pm S$ ] ( $p_{CR+OI}$ ) $\Theta$	[ $\bar{X} \pm S$ ] [ $p_{Col}$ ] $\Theta$	
Intermediate; Verma and Verma (2013); log-ratios of all major elements	IA+CA-CR+OI- Col	7	4 [0.773±0.166] (0.5740-0.9469)	---	---	0 (0)	3 [0.6097±0.0334] (0.5726-0.6373)	
	IA-CA-CR+OI	7	---	1 (0.5005)	6 [0.645±0.129] (0.4962-0.7923)	0 (0)	---	---
	IA-CA-Col	7	---	2 [0.508±0.050] (0.4719, 0.5431)	5 [0.5223±0.0428] (0.4780-0.5900)	---	0 (0)	0 (0)
	IA-CR+OI-Col	7	---	4 [0.736±0.220] (0.5173-0.9342)	---	0 (0)	3 [0.807±0.073] (0.7236-0.8532)	
	CA-CR+OI-Col	7	---	---	5 [0.707±0.161] (0.5430-0.8958)	0 (0)	2 [0.51602±0.00324] (0.5137, 0.5183)	
<b>Test study A4.</b> <i>Diagrams based on log-ratios of major elements</i>	{ $\Sigma n$ } { $\Sigma prob$ } [%prob]	35	{4} {3.0921} [--]	{7} {4.4586} [24%]	{16} {10.0142} [53%]	{0} {0} [ 0%]	{8} {5.2829} [23%]	

For the explanation of abbreviations, see footnote of Table S17.

**Table S48.**

Testing of multidimensional diagrams from basic rocks from the Sarapiqui Miocene (11.4-22.2 Ma) arc, Costa Rica (Gazel et al. 2005; Test study A5).

Figure reference; figure type	Discrimination diagram	Total no. of samples (%)	Predicted tectonic affinity and number of discriminated samples (%)				
			IAB	CRB+OIB	CRB	OIB	MORB
Agrawal et al. (2004); adjusted major element concentrations	IAB-CRB-OIB-MORB	10 (100)	6 (60)	---	1 (10)	0 (0)	3 (30)
	IAB-CRB-OIB	10 (100)	6 (60)	---	1 (10)	3 (30)	---
	IAB-CRB-MORB	10 (100)	7 (70)	---	1 (10)	---	2 (20)
	IAB-OIB-MORB	10 (100)	6 (60)	---	---	1 (10)	3 (30)
	CRB-OIB-MORB	10 (100)	---	---	1 (10)	0 (0)	9 (90)
<i>Test study A5. Synthesis of all five diagrams of Agrawal et al. (2004)</i>		<b>50 (100)</b>	<b>25 (50)</b>	---	<b>4 (8)</b>	<b>4 (8)</b>	<b>17 (34)</b>
Verma et al. (2006); log-ratios of major elements	IAB-CRB-OIB-MORB	10 (100)	6 (60)	---	4 (40)	0 (0)	0 (0)
	IAB-CRB-OIB	10 (100)	7 (70)	---	1 (10)	2 (20)	---
	IAB-CRB-MORB	10 (100)	7 (70)	---	3 (30)	---	0 (0)
	IAB-OIB-MORB	10 (100)	6 (60)	---	---	4 (40)	0 (0)
	CRB-OIB-MORB	10 (100)	---	---	7 (70)	3 (30)	0 (0)
<i>Test study A5. Synthesis of all five diagrams of Verma et al. (2006)</i>		<b>50 (100)</b>	<b>26 (52)</b>	---	<b>15 (30)</b>	<b>9 (18)</b>	<b>0 (0)</b>
Verma and Agrawal (2011); log-ratios of immobile major and trace elements	IAB-CRB+OIB-MORB	10 (100)	6 (60)	1 (10)	---	---	3 (30)
	IAB-CRB-OIB	10 (100)	6 (60)	---	3 (30)	1 (10)	---
	IAB-CRB-MORB	10 (100)	6 (60)	---	2 (20)	---	2 (20)
	IAB-OIB-MORB	10 (100)	6 (60)	---	---	1 (10)	3 (30)
	CRB-OIB-MORB	10 (100)	---	---	1 (10)	1 (10)	8 (80)
<i>Test study A5. Synthesis of all five diagrams of Verma and Agrawal (2011)</i>		<b>50 (100)</b>	<b>24 (48)</b>	<b>1 (---)</b>	<b>7 (14)</b>	<b>3 (6)</b>	<b>16(32)</b>

For the explanation of abbreviations, see footnote of Table 1 or S14.

**Table S49.**

Testing of multidimensional diagrams from Miocene (11.4-22.2 Ma) basic rocks from the Sarapiqui paleoarc, Costa Rica (Gazel et al. 2005; Test study A5).

Magma type, Figure name; Figure number	Figure type	Total number of samples	Number of discriminated samples				
			Arc			Within-plate CR+OI [ $\bar{x} \pm s$ ] [ $p_{CR+OI}$ ] $\Theta$	Collision Col [ $\bar{x} \pm s$ ] [ $p_{Col}$ ] $\Theta$
			IA+CA [ $\bar{x} \pm s$ ] ( $p_{IA+CA}$ ) $\Theta$	IA [ $\bar{x} \pm s$ ] [ $p_{IA}$ ] $\Theta$	CA [ $\bar{x} \pm s$ ] [ $p_{CA}$ ] $\Theta$		
Intermediate; Verma and Verma (2013); log-ratios of all major elements;	IA+CA-CR+OI- Col	14	12 [0.889±0.080] (0.6909-0.9840)	---	---	0 (0)	2 [0.5734±0.0115] (0.5653, 0.5816)
	IA-CA-CR+OI	14	---	[0.745±0.132] (0.4222- 0.9030)	[0.565±0.074] (0.5126, 0.6176)	0 (0)	---
	IA-CA-Col	14	---	[0.773±0.118] (0.5209- 0.9481)	[0.613±0.068] (0.5652, 0.6613)	---	1 (0.3978)
	IA-CR+OI-Col	14	---	[0.903±0.126] (0.5191- 0.9932)	---	0 (0)	1 (0.5340)
	CA-CR+OI-Col	14	---	---	[0.775±0.142] (0.4974- 0.9492)	0 (0)	2 [0.580±0.076] (0.5267, 0.6339)
<i>Test study A5.</i> <i>Diagrams based on log-ratios of major elements</i>	{Σn} {Σprob} [%prob]	70	{12} {10.6683} [--]	{36} {29.1787} [67%]	{16} {11.6534} [27%]	{0} {0} [0%]	{6} {3.2393} [6%]
Intermediate; Verma and Verma (2013); log-ratios of immobile major and trace elements	IA+CA-CR+OI- Col	14	12 [0.874±0.182] (0.5066-0.9943)	---	---	0 (0)	2 [0.724±0.064] (0.6785, 0.7687)
	IA-CA-CR+OI	14	---	[0.670±0.057] (0.5495- 0.7442)	[0.489±0.054] (0.4263- 0.5208)	0 (0)	---
	IA-CA-Col	14	---	[0.641±0.060] (0.5366- 0.7109)	[0.529±0.049] (0.4947, 0.5636)	---	3 [0.624±0.169] (0.4331-0.7548)
	IA-CR+OI-Col	14	---	[0.889±0.145] (0.5928- 0.9917)	---	0 (0)	2 [0.669±0.065] (0.6225, 0.7150)
	CA-CR+OI-Col	14	---	---	[0.922±0.145] (0.5481- 0.9993)	1 (0.6499)	2 [0.592±0.160] (0.4793, 0.7050)
<i>Test study A5.</i> <i>Diagrams based on log-ratios of selected immobile major and trace elements</i>	{Σn} {Σprob} [%prob]	70	{12} {10.4894} [--]	{32} {23.7991} [57%]	{16} {12.6613} [31%]	{1} {0.6499} [1%]	{9} {5.8397} [11%]

For the explanation of abbreviations, see footnote of Table S17.

**Table S50.**

Testing of multidimensional diagrams from Quaternary (> 0.33 Ma) intermediate rocks of geothermal fields of the Taupo Volcanic Zone, New Zealand (Browne et al. 1992; Test study A6).

Magma type, Figure name	Figure type	Total number of samples	Number of discriminated samples					
			Arc			Within-plate	CR+OI	Collision
			IA+CA [ $\bar{X} \pm S$ ] [ $p_{IA+CA}$ ] $\Theta$	IA [ $\bar{X} \pm S$ ] [ $p_{IA}$ ] $\Theta$	CA [ $\bar{X} \pm S$ ] [ $p_{CA}$ ] $\Theta$	[ $\bar{X} \pm S$ ] [ $p_{CR+OI}$ ] $\Theta$	[ $\bar{X} \pm S$ ] [ $p_{Col}$ ] $\Theta$	
Intermediate; Verma and Verma (2013); log-ratios of all major elements	IA+CA-CR+OI- Col	28	22 [0.708±0.171] (0.5043-0.9941)	---	---	0 (0)	6 [0.693±0.171] (0.5458-0.9988)	
	IA-CA-CR+OI	28	---	18 [0.717±0.180] (0.5042-0.9814)	10 [0.655±0.177] (0.4044-0.8706)	0 (0)	---	
	IA-CA-Col	28	---	10 [0.716±0.251] (0.3534-0.9779)	9 [0.578±0.158] (0.3477-0.7784)	---	9 [0.591±0.180] (0.4102-0.9984)	
	IA-CR+OI-Col	28	---	19 [0.765±0.178] (0.5048-0.9942)	---	0 (0)	9 [0.685±0.158] (0.5308-0.9926)	
	CA-CR+OI-Col	28	---	---	22 [0.759±0.136] (0.5419-0.9985)	0 (0)	6 [0.671±0.215] (0.3729-0.9776)	
<i>Test study A6.</i> <i>Diagrams based on log-ratios of major elements</i>		{Σn} {Σprob} [%prob]	140	{22} {15.5813} [--]	{47} {34.6054} [43.9%]	{41} {28.4448} [36.1%]	{0} {0} [0%]	{30} {19.6639} [20.0%]
Intermediate; Verma and Verma (2013); log-ratios of immobile major and trace elements	IA+CA-CR+OI- Col	5	5 [0.936±0.061] (0.8286-0.9766)	---	---	0 (0)	0 (0)	
	IA-CA-CR+OI	5	---	4 [0.753±0.099] (0.6176-0.8295)	1 (0.6733)	0 (0)	---	
	IA-CA-Col	5	---	4 [0.747±0.095] (0.6134-0.8247)	1 (0.6179)	---	0 (0)	
	IA-CR+OI-Col	5	---	5 [0.919±0.073] (0.7884-0.9607)	---	0 (0)	0 (0)	
	CA-CR+OI-Col	5	---	---	5 [0.9744±0.0379] (0.9072-0.9988)	0 (0)	0 (0)	
<i>Test study A6.</i> <i>Diagrams based on log-ratios of immobile major and trace elements</i>		{Σn} {Σprob} [%prob]	25	{5} {4.6808} [--]	{13} {10.5968} [63%]	{7} {6.1633} [37%]	{0} {0} [0%]	{0} {0} [0%]

For the explanation of abbreviations, see footnote of Table S17.

**Table S51.**

Testing of multidimensional diagrams from Neogene-Quaternary (0-4 and 15-23 Ma) basic rocks from SW Indian and SW Pacific seafloor, Indian and Pacific Oceans (Pyle et al. 1995; Test study A7a).

Figure reference; figure type	Discrimination diagram	Total no. of samples (%)	Predicted tectonic affinity and number of discriminated samples (%)				
			IAB	CRB+OIB	CRB	OIB	MORB
Agrawal et al. (2004); adjusted major element concentrations	IAB-CRB-OIB-MORB	9 (100)	0 (0)	---	0 (0)	0 (0)	9 (100)
	IAB-CRB-OIB	9 (100)	2 (22)	---	3 (33)	4 (45)	---
	IAB-CRB-MORB	9 (100)	0 (0)	---	0 (0)	---	9 (100)
	IAB-OIB-MORB	9 (100)	0 (0)	---	---	0 (0)	9 (100)
	CRB-OIB-MORB	9 (100)	---	---	0 (0)	0 (0)	9 (100)
<i>Test study A7a. Synthesis of all five diagrams of Agrawal et al. (2004)</i>		<b>45 (100)</b>	<b>2 (4.4)</b>	---	<b>3 (6.7)</b>	<b>4 (8.9)</b>	<b>36 (80)</b>
Verma et al. (2006); log-ratios of major elements	IAB-CRB-OIB-MORB	9 (100)	0 (0)	---	0 (0)	0 (0)	9 (100)
	IAB-CRB-OIB	9 (100)	0 (0)	---	2 (22)	7 (78)	---
	IAB-CRB-MORB	9 (100)	0 (0)	---	0 (0)	---	9 (100)
	IAB-OIB-MORB	9 (100)	0 (0)	---	---	0 (0)	9 (100)
	CRB-OIB-MORB	9 (100)	---	---	0 (0)	0 (0)	9 (100)
<i>Test study A7a. Synthesis of all five diagrams of Verma et al. (2006)</i>		<b>45 (100)</b>	<b>0 (0)</b>	---	<b>2 (4.4)</b>	<b>7 (15.6)</b>	<b>36 (80)</b>
Agrawal et al. (2008); log-ratios of immobile trace elements	IAB-CRB+OIB-MORB	7 (100)	0 (0)	0 (0)	---	---	7 (100)
	IAB-CRB-OIB	7 (100)	0 (0)	---	2 (29)	5 (71)	---
	IAB-CRB-MORB	7 (100)	0 (0)	---	0 (0)	---	7 (100)
	IAB-OIB-MORB	7 (100)	0 (0)	---	---	0 (0)	7 (100)
	CRB-OIB-MORB	7 (100)	---	---	0 (0)	0 (0)	7 (100)
<i>Test study A7a. Synthesis of all five diagrams of Agrawal et al. (2008)</i>		<b>35 (100)</b>	<b>0 (0)</b>	<b>0 (---)</b>	<b>2 (5.7)</b>	<b>5 (14.3)</b>	<b>28 (80)</b>
Verma and Agrawal (2011); log-ratios of immobile major and trace elements	IAB-CRB+OIB-MORB	7 (100)	0 (0)	1 (14)	---	---	6 (86)
	IAB-CRB-OIB	7 (100)	5 (71)	---	2 (29)	0 (0)	---
	IAB-CRB-MORB	7 (100)	0 (0)	---	1 (14)	---	6 (86)
	IAB-OIB-MORB	7 (100)	0 (0)	---	---	0 (0)	7 (100)
	CRB-OIB-MORB	7 (100)	---	---	1 (14)	0 (0)	6 (86)
<i>Test study A7a. Synthesis of all five diagrams of Verma and Agrawal (2011)</i>		<b>35 (100)</b>	<b>5 (14)</b>	<b>1 (---)</b>	<b>5 (14)</b>	<b>0 (0)</b>	<b>25 (72)</b>

For the explanation of abbreviations, see footnote of Table 1 or S14.

**Table S52.**

Testing of multidimensional diagrams from Quaternary basic rocks from Central Indian Ridge, Indian Ocean (Yi et al. 2014; Test study A7b).

Figure reference; figure type	Discrimination diagram	Total no. of samples (%)	Predicted tectonic affinity and number of discriminated samples (%)				
			IAB	CRB+OIB	CRB	OIB	MORB
Agrawal et al. (2004); adjusted major element concentrations	IAB-CRB-OIB-MORB	28 (100)	2 (7)	---	2 (7)	2 (7)	22 (79)
	IAB-CRB-OIB	28 (100)	17 (61)	---	6 (21)	5 (18)	---
	IAB-CRB-MORB	28 (100)	2 (7)	---	4 (14)	---	22 (79)
	IAB-OIB-MORB	28 (100)	2 (7)	---	---	4 (14)	22 (79)
	CRB-OIB-MORB	28 (100)	---	---	0 (0)	4 (14)	24 (86)
<i>Test study A7b. Synthesis of all five diagrams of Agrawal et al. (2004)</i>		<b>140 (100)</b>	<b>23 (16.4)</b>	<b>---</b>	<b>12 (8.6)</b>	<b>15 (10.7)</b>	<b>90 (64.3)</b>
Verma et al. (2006); log-ratios of major elements	IAB-CRB-OIB-MORB	28 (100)	10 (36)	---	0 (0)	1 (3)	17 (61)
	IAB-CRB-OIB	28 (100)	10 (36)	---	2 (7)	16 (57)	---
	IAB-CRB-MORB	28 (100)	9 (32)	---	0 (0)	---	19 (68)
	IAB-OIB-MORB	28 (100)	10 (36)	---	---	1 (3)	17 (61)
	CRB-OIB-MORB	28 (100)	---	---	3 (11)	1 (3)	24 (86)
<i>Test study A7b. Synthesis of all five diagrams of Verma et al. (2006)</i>		<b>140 (100)</b>	<b>39 (27.9)</b>	<b>---</b>	<b>5 (3.6)</b>	<b>19 (13.6)</b>	<b>77 (55.0)</b>
Agrawal et al. (2008); log-ratios of immobile trace elements	IAB-CRB+OIB-MORB	17 (100)	3 (18)	0 (0)	---	---	14 (82)
	IAB-CRB-OIB	17 (100)	3 (18)	---	5 (29)	9 (53)	---
	IAB-CRB-MORB	17 (100)	3 (18)	---	0 (0)	---	14 (82)
	IAB-OIB-MORB	17 (100)	3 (18)	---	---	0 (0)	14 (82)
	CRB-OIB-MORB	17 (100)	---	---	0 (0)	0 (0)	17 (100)
<i>Test study A7b. Synthesis of all five diagrams of Agrawal et al. (2008)</i>		<b>85 (100)</b>	<b>12 (14.1)</b>	<b>0 (---)</b>	<b>5 (5.9)</b>	<b>9 (10.6)</b>	<b>59 (69.4)</b>
Verma and Agrawal (2011); log-ratios of immobile major and trace elements	IAB-CRB+OIB-MORB	20 (100)	3 (15)	0 (0)	---	---	17 (85)
	IAB-CRB-OIB	20 (100)	19 (95)	---	1 (5)	0 (0)	---
	IAB-CRB-MORB	20 (100)	3 (15)	---	0 (0)	---	17 (85)
	IAB-OIB-MORB	20 (100)	3 (15)	---	---	0 (0)	17 (85)
	CRB-OIB-MORB	20 (100)	---	---	0 (0)	1 (5)	19 (95)
<i>Test study A7b. Synthesis of all five diagrams of Verma and Agrawal (2011)</i>		<b>100 (100)</b>	<b>28 (28.0)</b>	<b>0 (---)</b>	<b>1 (1.0)</b>	<b>1 (1.0)</b>	<b>70 (70.0)</b>

For the explanation of abbreviations, see footnote of Table 1 or S14.

**Table S53.**

Testing of multidimensional diagrams from Quaternary intermediate rocks from the Aeolian Island, Italy (Del Moro et al. 2011; Test study A8).

Magma type, Figure name	Figure type	Total number of samples	Number of discriminated samples				
			Arc			Within-plate CR+OI [ $\bar{x} \pm S$ ] [ $p_{CR+OI}$ ] $\Theta$	Collision Col [ $\bar{x} \pm S$ ] [ $p_{Col}$ ] $\Theta$
			IA+CA [ $\bar{x} \pm S$ ] ( $p_{IA+CA}$ ) $\Theta$	IA [ $\bar{x} \pm S$ ] [ $p_{IA}$ ] $\Theta$	CA [ $\bar{x} \pm S$ ] [ $p_{CA}$ ] $\Theta$		
	IA+CA-CR+OI-Col	7	0 (0)	---	---	0 (0)	7 [0.99996±0.00004] (0.9999-1.0000)
Intermediate; Verma and Verma (2013); log-ratios of all major elements	IA-CA-CR+OI	7	---	0 (0)	6 [0.812±0.197] (0.5043-0.9999)	1 (0.4546)	---
	IA-CA-Col	7	---	0 (0)	0 (0)	---	7 [0.99868±0.00204] (0.9948-1.0000)
	IA-CR+OI-Col	7	---	0 (0)	---	0 (0)	7 [0.99993±0.00014] (0.9996-1.0000)
	CA-CR+OI-Col	7	---	---	0 (0)	0 (0)	7 [0.9722±0.0280] (0.9321-0.9994)
<b>Test study A8.</b>							
<b>Diagrams based on log-ratios of major elements</b>		{Σn} {Σprob} [%prob]	35	{0} {0} [ 0%]	{0} {0} [ 0%]	{6} {4.8713} [15%]	{1} {0.4546} [1%]
	IA+CA-CR+OI-Col	7	0 (0)	---	---	0 (0)	7 [0.939±0.071] (0.7932-0.9970)
Intermediate; Verma and Verma (2013); log-ratios of immobile trace elements	IA-CA-CR+OI	7	---	0 (0)	4 [0.660±0.120] (0.4889- 0.7676)	3 [0.868±0.197] (0.6398- 0.9823)	---
	IA-CA-Col	7	---	0 (0)	0 (0)	---	7 [0.9719±0.0256] (0.9309-0.9926)
	IA-CR+OI-Col	7	---	0 (0)	---	0 (0)	7 [0.913±0.108] (0.6929-0.9952)
	CA-CR+OI-Col	7	---	---	0 (0)	0 (0)	7 [0.922±0.109] (0.6869-0.9948)
<b>Test study A8.</b>							
<b>Diagrams based on log-ratios of immobile trace elements</b>		{Σn} {Σprob} [%prob]	35	{0} {0} [ 0%]	{0} {0} [ 0%]	{4} {2.6402} [9%]	{3} {2.6030} [8%]

For the explanation of abbreviations, see footnote of Table S17.

**Table S54.**

Testing of multidimensional diagrams from Quaternary acid rocks from the Aeolian Island, Italy (Del Moro et al. 2011; Test study A8).

Magma type, Figure name	Figure type	Total number of samples	Number of discriminated samples					
			Arc			Within-plate		
			IA+CA [ $\bar{x} \pm s$ ] ( $p_{IA+CA}$ ) $\Theta$	IA [ $\bar{x} \pm s$ ] ( $p_{IA}$ ) $\Theta$	CA [ $\bar{x} \pm s$ ] ( $p_{CA}$ ) $\Theta$	CR+OI [ $\bar{x} \pm s$ ] ( $p_{CR+OI}$ ) $\Theta$	Collision [ $\bar{x} \pm s$ ] [ $p_{Col}$ ] $\Theta$	Col
Acid; Verma et al. (2012); All major elements	IA+CA-CR+OI-Col	10	4 [0.793±0.201] (0.5185-0.9877)	---	---	1 (0.5346)	5 [0.736±0.231] (0.5020-0.9704)	
	IA-CA-CR+OI	10	---	6 [0.773±0.181] (0.5775-0.9982)	1 (0.5718)	3 [0.688±0.235] (0.4576-0.9270)	---	
	IA-CA-Col	10	---	3 [0.790±0.205] (0.5876-0.9983)	1 (0.8847)	---	6 [0.902±0.153] (0.5963-0.9987)	
	IA-CR+OI-Col	10	---	2 [0.713±0.240] (0.5437, 0.8831)	---	1 (0.7291)	7 [0.951±0.047] (0.8596-0.9889)	
	CA-CR+OI-Col	10	---	---	[0.9703±0.0410] (0.8924-1.0000)	1 (0.6449)	2 [0.697±0.291] (0.4917, 0.9025)	
<i>Test study A8. Diagrams based on log-ratios of major elements</i>		{Σn} {Σprob} [%prob]	50	{4} {3.1709} [--]	{11} {8.4333} [24%]	{9} {8.2488} [24%]	{6} {3.9731} [10%]	{20} {17.1507} [42%]
Acid; Verma et al. (2013); All major elements	IA+CA-CR+OI-Col	10	4 [0.795±0.215] (0.5030-0.9983)	---	---	1 (0.5617)	5 [0.819±0.140] (0.6095-0.9645)	
	IA-CA-CR+OI	10	---	5 [0.904±0.204] (0.5392-1.0000)	0 (0)	5 [0.802±0.096] (0.7246-0.9310)	---	
	IA-CA-Col	10	---	4 [0.9991±0.0011] (0.9980-1.0000)	1 (0.8844)	---	5 [0.99939±0.00033] (0.9990-0.9997)	
	IA-CR+OI-Col	10	---	5 [0.940±0.082] (0.8403-1.0000)	---	1 (0.6177)	4 [0.834±0.095] (0.7233-0.9536)	
	CA-CR+OI-Col	10	---	---	4 [0.822±0.167] (0.6768-0.9997)	[2] [0.5634±0.0240] (0.5465, 0.5804)	4 [0.763±0.145] (0.6131-0.9453)	
<i>Test study A8. Diagrams based on log-ratios of major elements</i>		{Σn} {Σprob} [%prob]	50	{4} {3.1790} [--]	{14} {13.2117} [37%]	{5} {4.1727} [12%]	{9} {6.3171} [14%]	{18} {15.4767} [37%]
Acid; Verma et al. (2013); log-ratios of immobile major and trace elements	IA+CA-CR+OI-Col	10	0 (0)	---	---	1 (0.4611)	9 [0.766±0.119] (0.5796-0.9446)	
	IA-CA-CR+OI	10	---	0 (0)	[5] [0.5284±0.0195] (0.5037-0.5492)	5 [0.577±0.085] (0.5132-0.7105)	---	
	IA-CA-Col	10	---	0 (0)	0 (0)	0 (0)	---	10 [0.748±0.122] (0.5632-0.9144)
	IA-CR+OI-Col	10	---	0 (0)	---	0 (0)	10 [0.781±0.119] (0.5388-0.9439)	
	CA-CR+OI-Col	10	---	---	0 (0)	0 (0)	10 [0.685±0.163] (0.3833-0.9117)	
<i>Test study A8. Diagrams based on log-ratios of immobile major and trace elements</i>		{Σn} {Σprob} [%prob]	50	{0} {0} [0%]	{0} {0} [0%]	{5} {2.6418} [8%]	{6} {3.3471} [10%]	{39} {29.0341} [82%]
Acid; Verma et al. (2013); log-ratios of immobile trace elements	IA+CA-CR+OI-Col	10	0 (0)	---	---	4 [0.773±0.195] (0.5366-0.9645)	6 [0.764±0.138] (0.5160-0.9392)	
	IA-CA-CR+OI	10	---	0 (0)	6 [0.821±0.163] (0.6021-0.9999)	4 [0.907±0.105] (0.7764-0.9998)	---	
	IA-CA-Col	10	---	0 (0)	1 (0.6838)	---	9 [0.812±0.084] (0.6754-0.9554)	
	IA-CR+OI-Col	10	---	0 (0)	---	3 [0.755±0.213] (0.5764-0.9905)	7 [0.855±0.169] (0.5299-1.0000)	
	CA-CR+OI-Col	10	---	---	0 (0)	2 [0.834±0.157] (0.7222, 0.9448)	8 [0.758±0.154] (0.4944-0.9651)	
<i>Test study A8. Diagrams based on log-ratios of immobile trace elements</i>		{Σn} {Σprob} [%prob]	50	{0} {0} [0%]	{0} {0} [0%]	{7} {5.6121} [14%]	{13} {10.6515} [26%]	{30} {23.9439} [60%]

For the explanation of abbreviations, see footnote of Table S17.

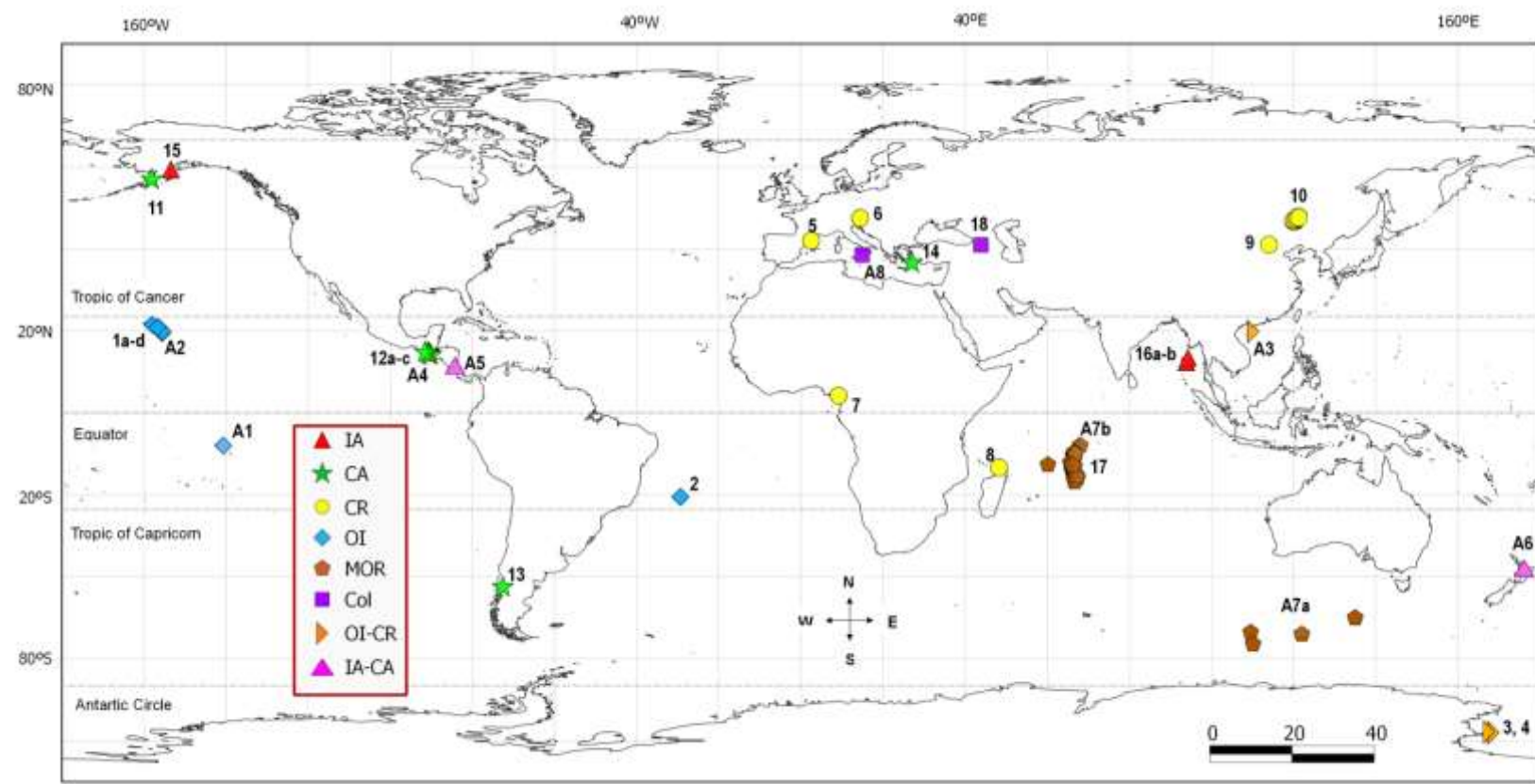


**Fig. S1.** Schematic locations of the 18 test (numbers 1 to 18) and 8 (numbers A1 to A8) application studies.

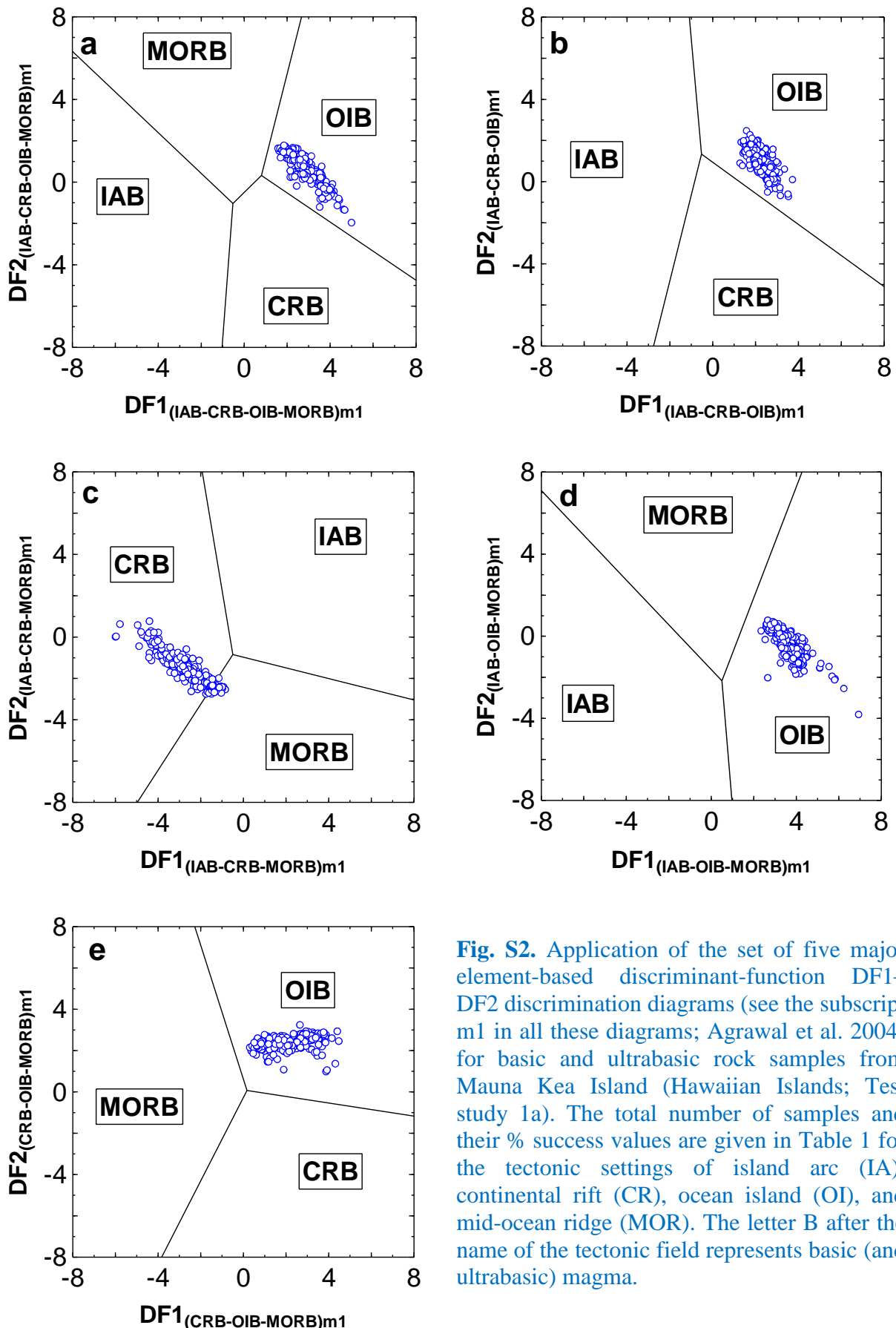


**Fig. S2.** Application of the set of five major element-based discriminant-function DF1–DF2 discrimination diagrams (see the subscript m1 in all these diagrams; Agrawal et al. 2004) for basic and ultrabasic rock samples from Mauna Kea Island (Hawaiian Islands; Test study 1a). The total number of samples and their % success values are given in Table 1 for the tectonic settings of island arc (IA), continental rift (CR), ocean island (OI), and mid-ocean ridge (MOR). The letter B after the name of the tectonic field represents basic (and ultrabasic) magma.

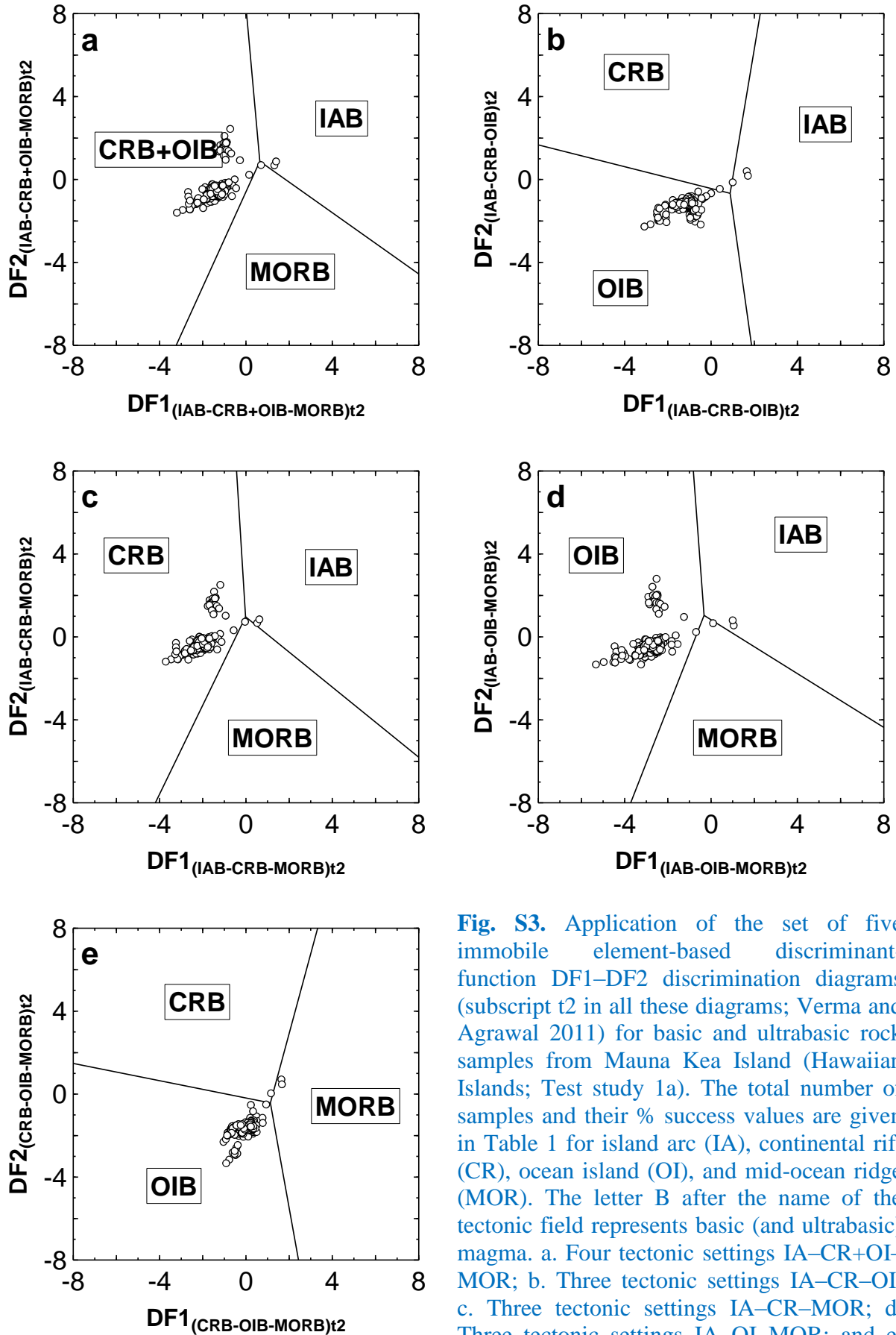


**Fig. S3.** Application of the set of five immobile element-based discriminant-function DF1–DF2 discrimination diagrams (subscript t2 in all these diagrams; Verma and Agrawal 2011) for basic and ultrabasic rock samples from Mauna Kea Island (Hawaiian Islands; Test study 1a). The total number of samples and their % success values are given in Table 1 for island arc (IA), continental rift (CR), ocean island (OI), and mid-ocean ridge (MOR). The letter B after the name of the tectonic field represents basic (and ultrabasic) magma. a. Four tectonic settings IA–CR+OI–MOR; b. Three tectonic settings IA–CR–OI; c. Three tectonic settings IA–CR–MOR; d. Three tectonic settings IA–OI–MOR; and e. Three tectonic settings CR–OI–MOR.

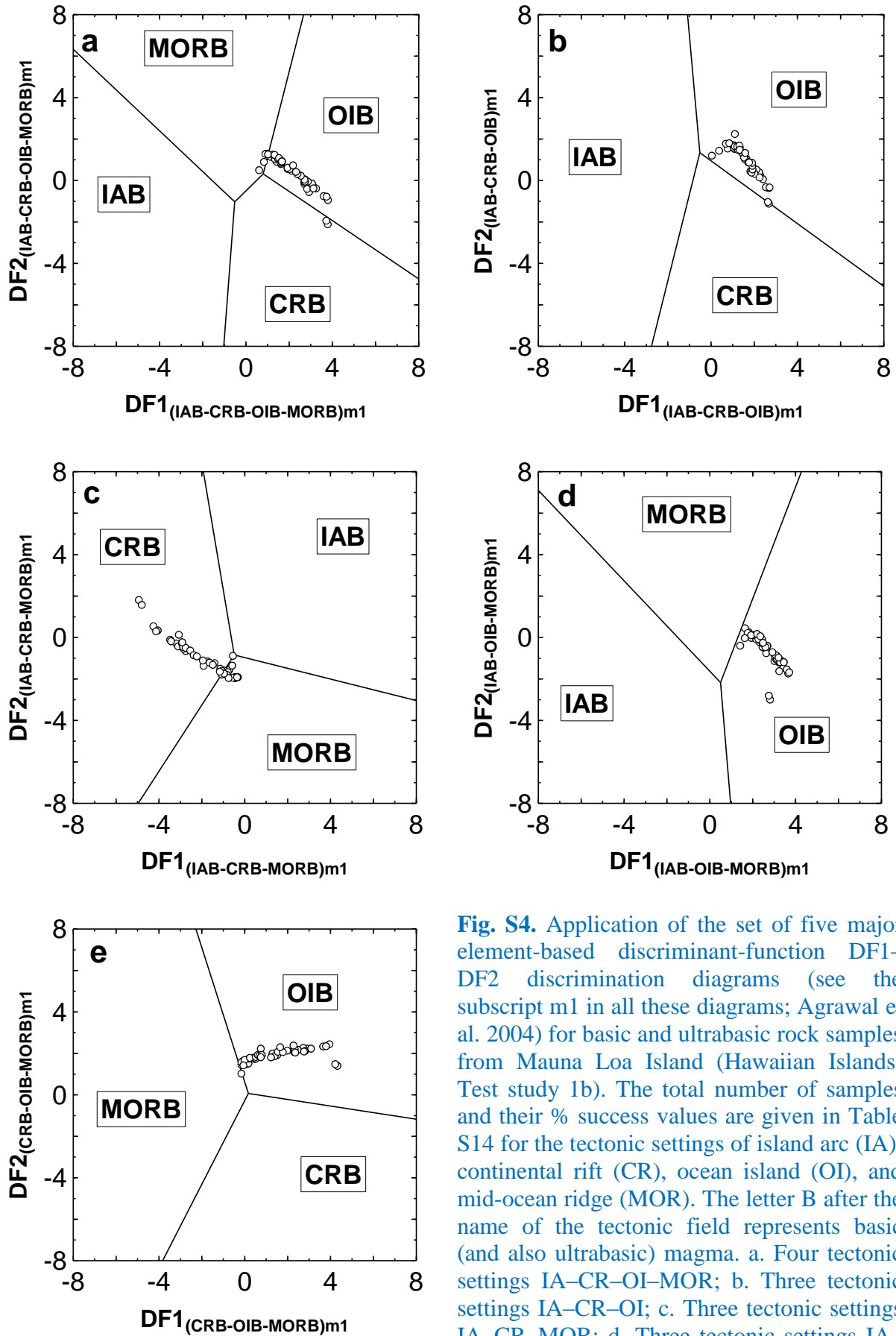


**Fig. S4.** Application of the set of five major element-based discriminant-function  $DF1-DF2$  discrimination diagrams (see the subscript m1 in all these diagrams; Agrawal et al. 2004) for basic and ultrabasic rock samples from Mauna Loa Island (Hawaiian Islands; Test study 1b). The total number of samples and their % success values are given in Table S14 for the tectonic settings of island arc (IA), continental rift (CR), ocean island (OI), and mid-ocean ridge (MOR). The letter B after the name of the tectonic field represents basic (and also ultrabasic) magma. a. Four tectonic settings IA–CR–OI–MOR; b. Three tectonic settings IA–CR–OI; c. Three tectonic settings IA–CR–MOR; d. Three tectonic settings IA–OI–MOR; and e. Three tectonic settings CR–OI–MOR.

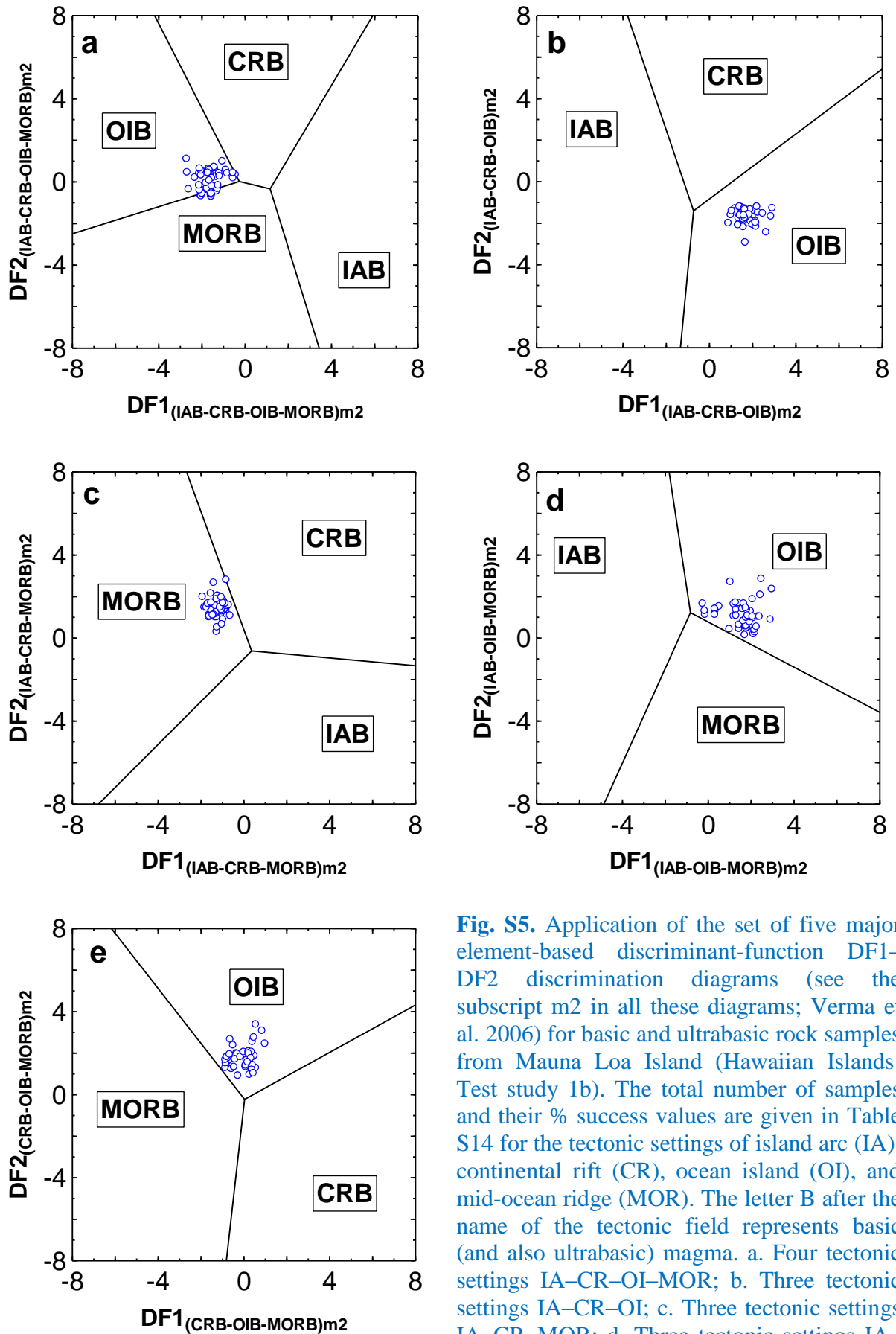


**Fig. S5.** Application of the set of five major element-based discriminant-function  $DF1-DF2$  discrimination diagrams (see the subscript m2 in all these diagrams; Verma et al. 2006) for basic and ultrabasic rock samples from Mauna Loa Island (Hawaiian Islands; Test study 1b). The total number of samples and their % success values are given in Table S14 for the tectonic settings of island arc (IA), continental rift (CR), ocean island (OI), and mid-ocean ridge (MOR). The letter B after the name of the tectonic field represents basic (and also ultrabasic) magma. a. Four tectonic settings IA-CR-OI-MOR; b. Three tectonic settings IA-CR-OI; c. Three tectonic settings IA-CR-MOR; d. Three tectonic settings IA-OI-MOR; and e. Three tectonic settings CR-OI-MOR.

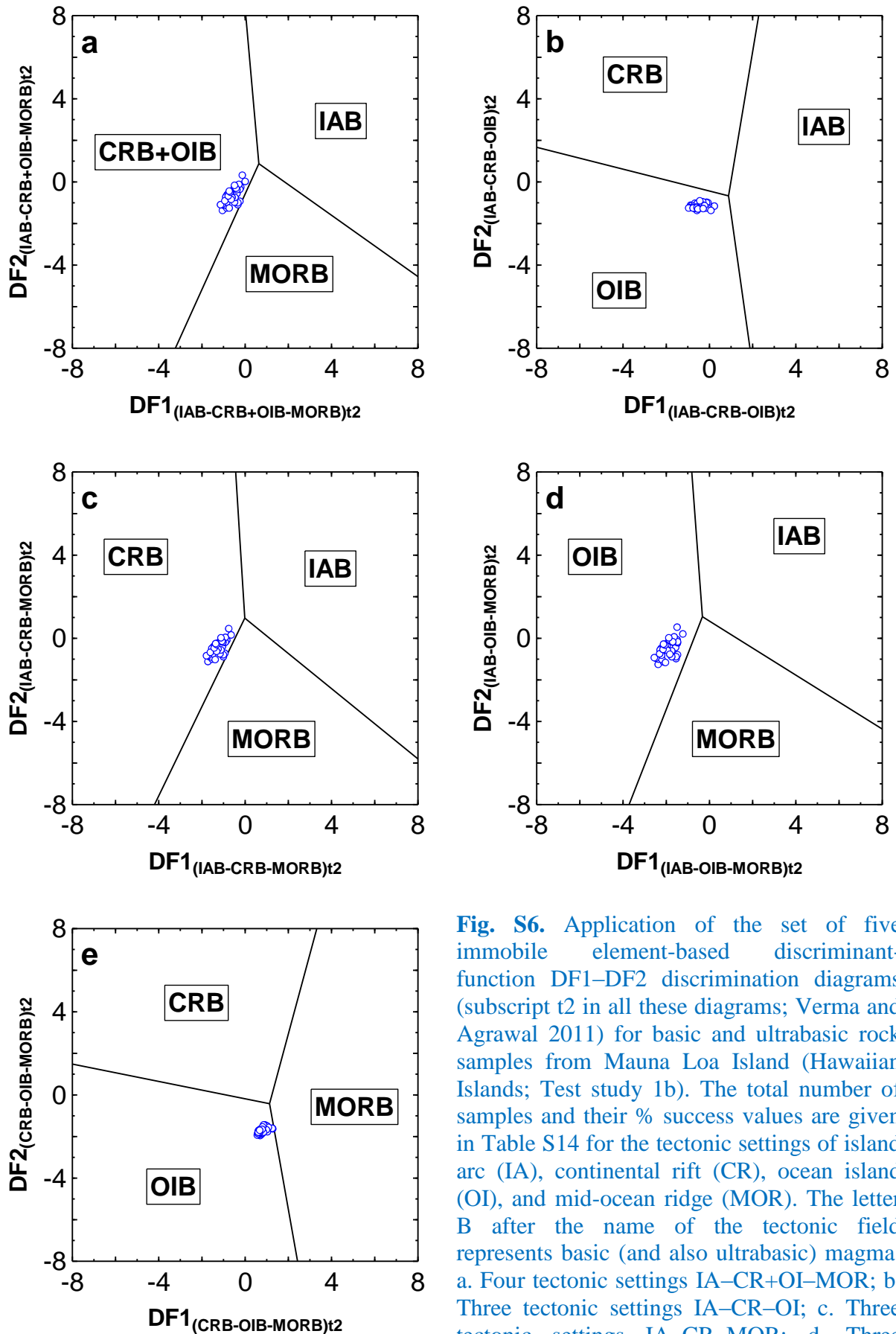


**Fig. S6.** Application of the set of five immobile element-based discriminant-function DF1–DF2 discrimination diagrams (subscript t2 in all these diagrams; Verma and Agrawal 2011) for basic and ultrabasic rock samples from Mauna Loa Island (Hawaiian Islands; Test study 1b). The total number of samples and their % success values are given in Table S14 for the tectonic settings of island arc (IA), continental rift (CR), ocean island (OI), and mid-ocean ridge (MOR). The letter B after the name of the tectonic field represents basic (and also ultrabasic) magma.

a. Four tectonic settings IA–CR+OI–MOR; b. Three tectonic settings IA–CR–OI; c. Three tectonic settings IA–CR–MOR; d. Three tectonic settings IA–OI–MOR; and e. Three tectonic settings CR–OI–MOR.

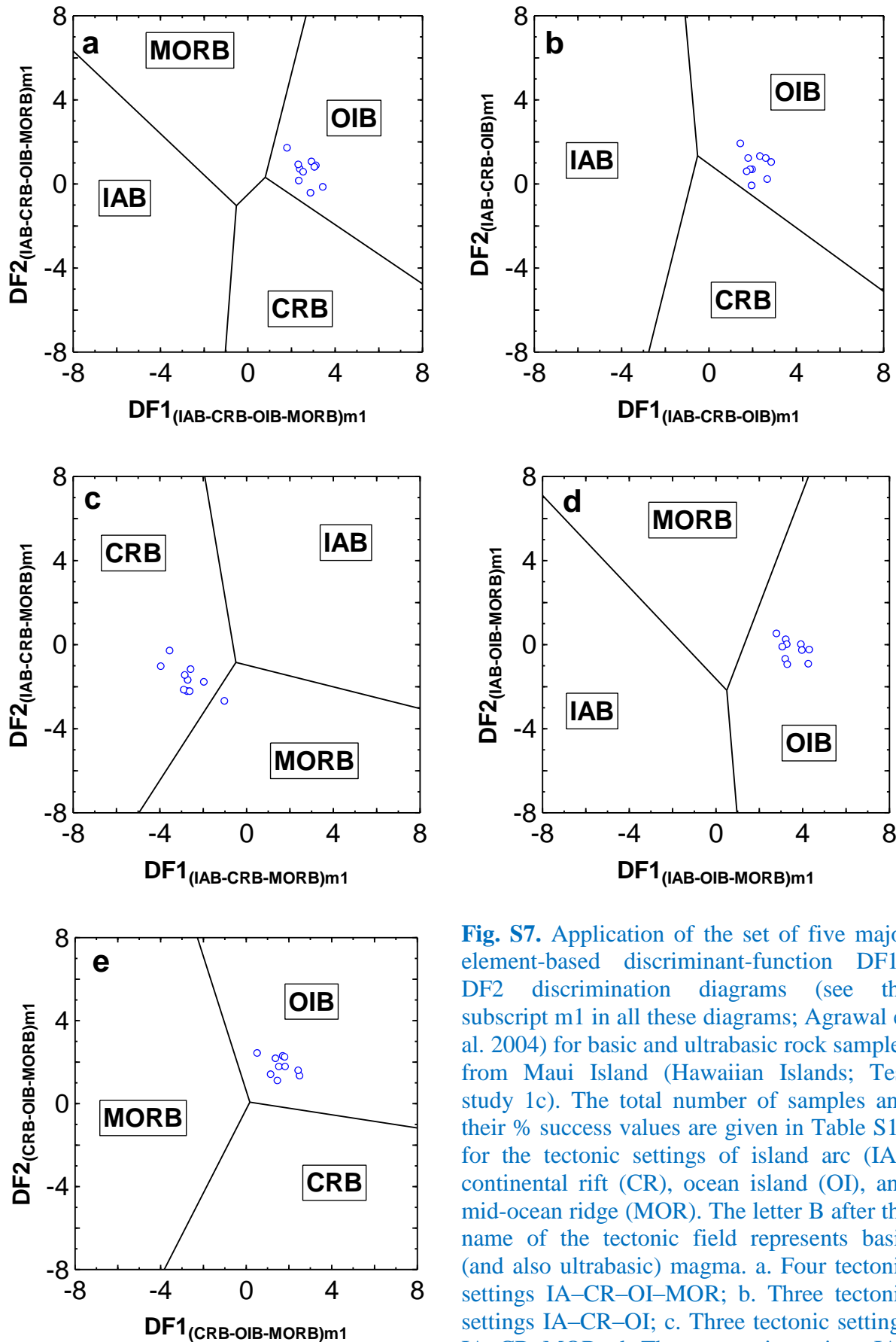


**Fig. S7.** Application of the set of five major element-based discriminant-function  $DF_1$ – $DF_2$  discrimination diagrams (see the subscript m1 in all these diagrams; Agrawal et al. 2004) for basic and ultrabasic rock samples from Maui Island (Hawaiian Islands; Test study 1c). The total number of samples and their % success values are given in Table S15 for the tectonic settings of island arc (IA), continental rift (CR), ocean island (OI), and mid-ocean ridge (MOR). The letter B after the name of the tectonic field represents basic (and also ultrabasic) magma. a. Four tectonic settings IA–CR–OI–MOR; b. Three tectonic settings IA–CR–OI; c. Three tectonic settings IA–CR–MOR; d. Three tectonic settings IA–OI–MOR; and e. Three tectonic settings CR–OI–MOR.

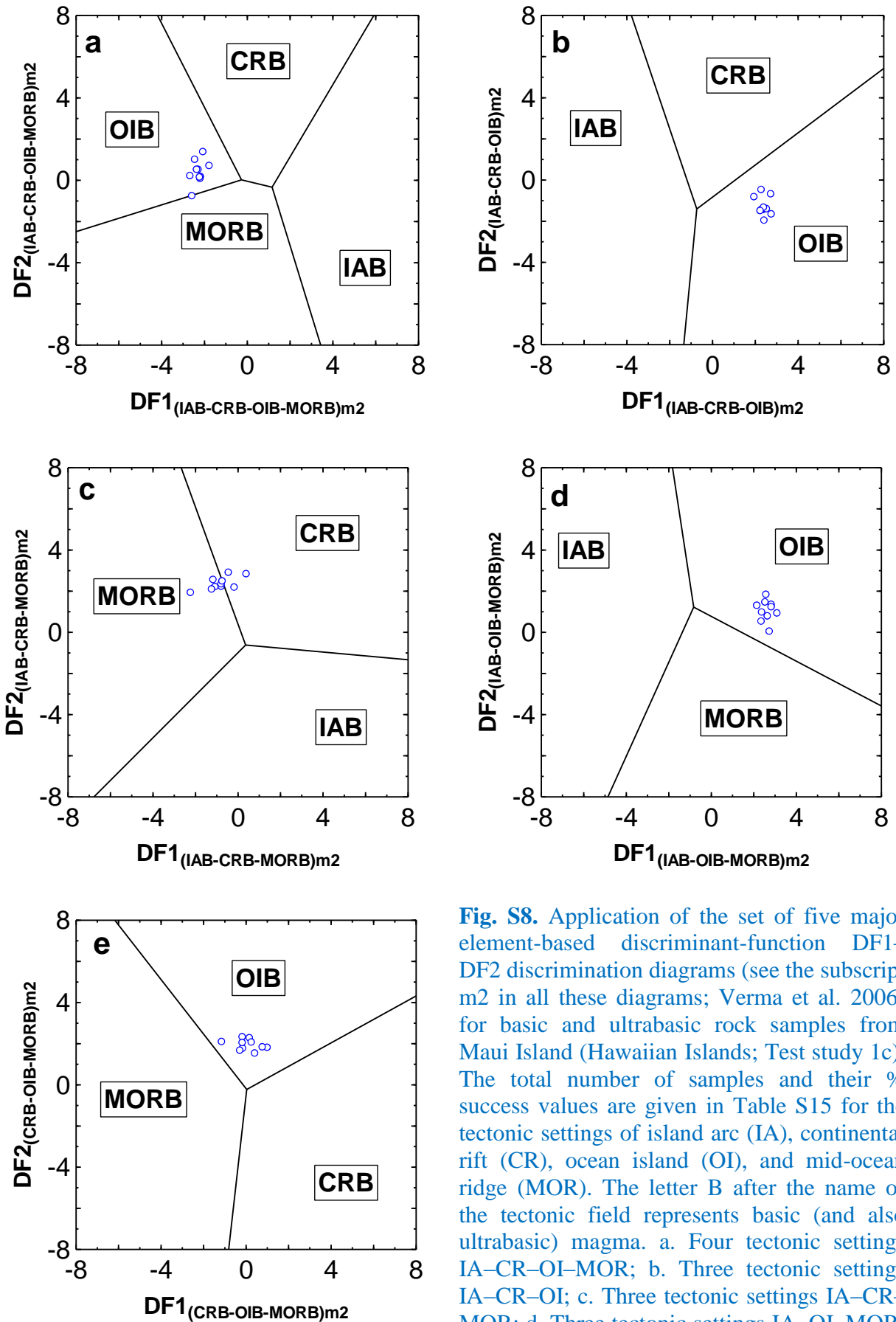


**Fig. S8.** Application of the set of five major element-based discriminant-function  $DF_1$ – $DF_2$  discrimination diagrams (see the subscript m2 in all these diagrams; Verma et al. 2006) for basic and ultrabasic rock samples from Maui Island (Hawaiian Islands; Test study 1c). The total number of samples and their % success values are given in Table S15 for the tectonic settings of island arc (IA), continental rift (CR), ocean island (OI), and mid-ocean ridge (MOR). The letter B after the name of the tectonic field represents basic (and also ultrabasic) magma. a. Four tectonic settings IA–CR–OI–MOR; b. Three tectonic settings IA–CR–OI; c. Three tectonic settings IA–CR–MOR; d. Three tectonic settings IA–OI–MOR; and e. Three tectonic settings CR–OI–MOR.

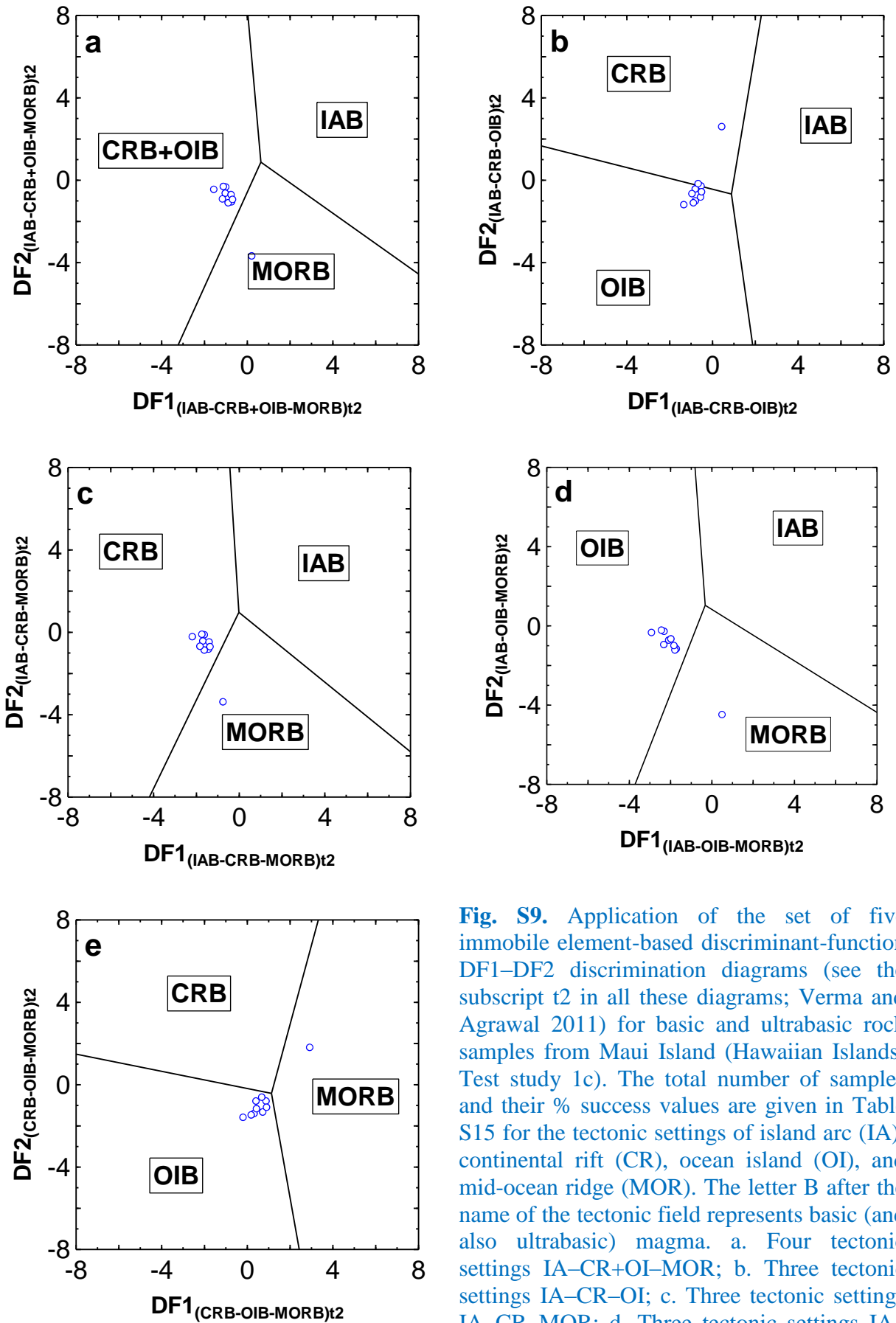


**Fig. S9.** Application of the set of five immobile element-based discriminant-function DF1-DF2 discrimination diagrams (see the subscript t2 in all these diagrams; Verma and Agrawal 2011) for basic and ultrabasic rock samples from Maui Island (Hawaiian Islands; Test study 1c). The total number of samples and their % success values are given in Table S15 for the tectonic settings of island arc (IA), continental rift (CR), ocean island (OI), and mid-ocean ridge (MOR). The letter B after the name of the tectonic field represents basic (and also ultrabasic) magma. a. Four tectonic settings IA-CR+OI-MOR; b. Three tectonic settings IA-CR-OI; c. Three tectonic settings IA-CR-MOR; d. Three tectonic settings IA-OI-MOR; and e. Three tectonic settings CR-OI-MOR.

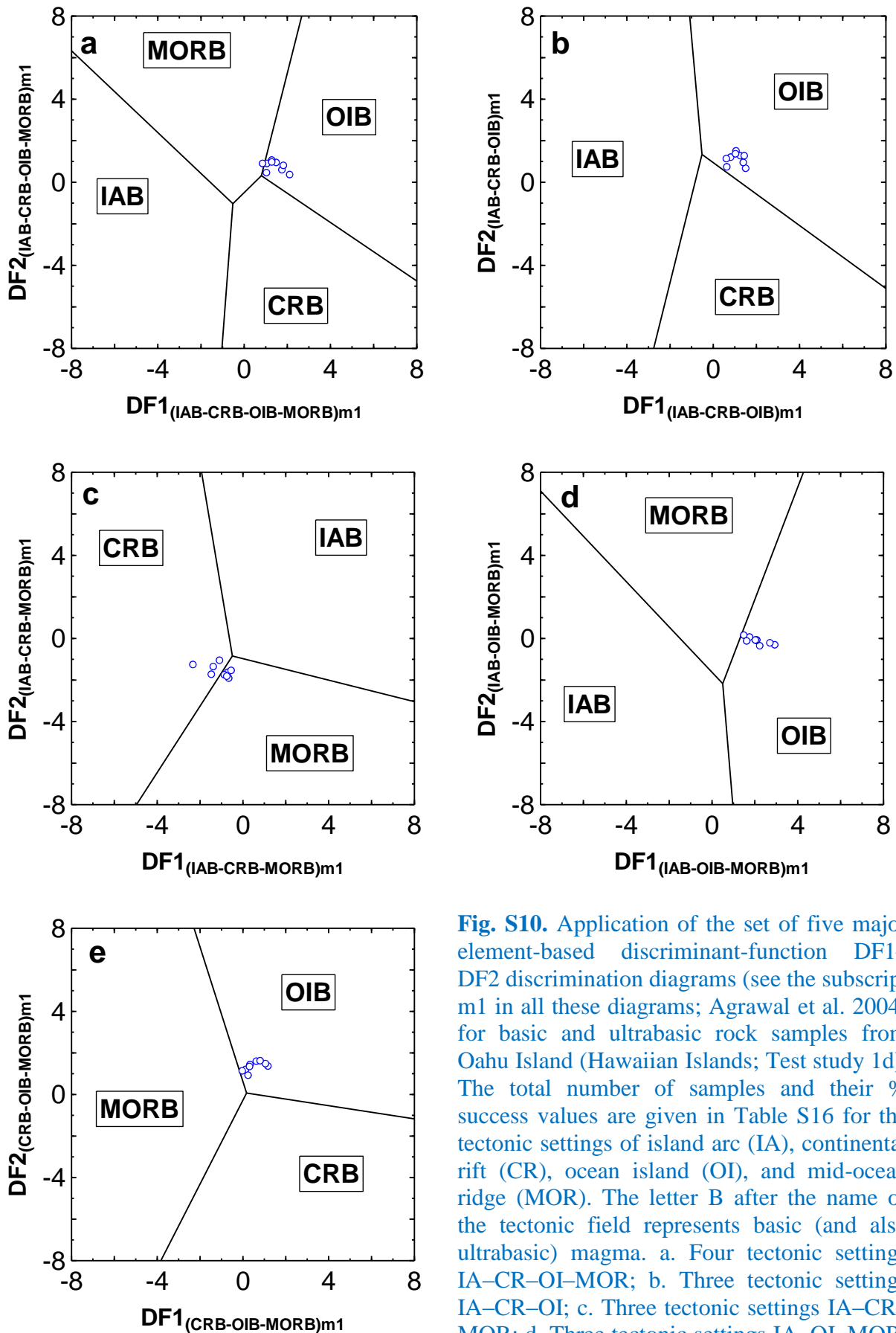


**Fig. S10.** Application of the set of five major element-based discriminant-function  $DF1-DF2$  discrimination diagrams (see the subscript m1 in all these diagrams; Agrawal et al. 2004) for basic and ultrabasic rock samples from Oahu Island (Hawaiian Islands; Test study 1d). The total number of samples and their % success values are given in Table S16 for the tectonic settings of island arc (IA), continental rift (CR), ocean island (OI), and mid-ocean ridge (MOR). The letter B after the name of the tectonic field represents basic (and also ultrabasic) magma. a. Four tectonic settings IA-CR-OI-MOR; b. Three tectonic settings IA-CR-OI; c. Three tectonic settings IA-CR-MOR; d. Three tectonic settings IA-OI-MOR; and e. Three tectonic settings CR-OI-MOR.

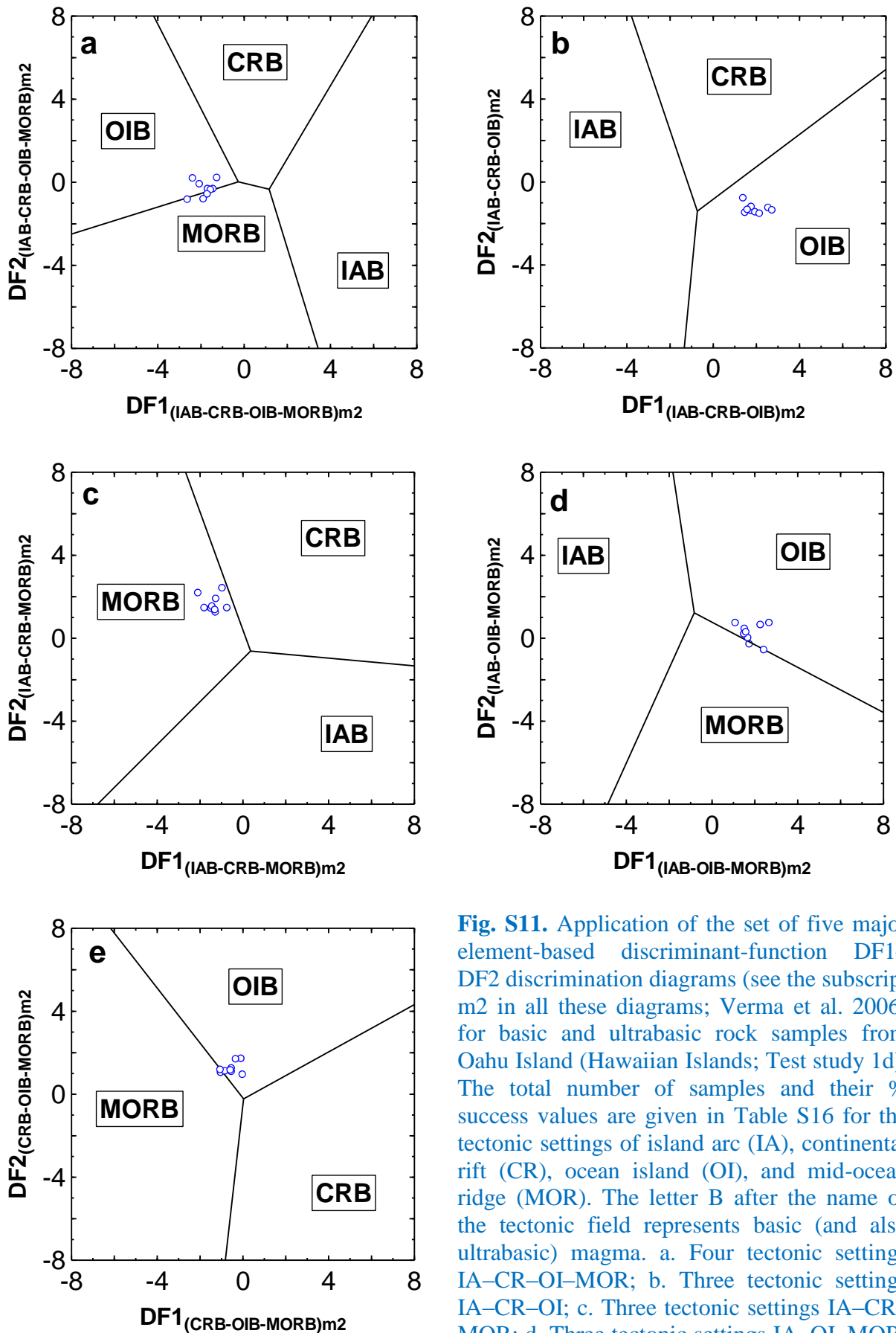


**Fig. S11.** Application of the set of five major element-based discriminant-function DF1–DF2 discrimination diagrams (see the subscript m2 in all these diagrams; Verma et al. 2006) for basic and ultrabasic rock samples from Oahu Island (Hawaiian Islands; Test study 1d). The total number of samples and their % success values are given in Table S16 for the tectonic settings of island arc (IA), continental rift (CR), ocean island (OI), and mid-ocean ridge (MOR). The letter B after the name of the tectonic field represents basic (and also ultrabasic) magma. a. Four tectonic settings IA–CR–OI–MOR; b. Three tectonic settings IA–CR–OI; c. Three tectonic settings IA–CR–MORB; d. Three tectonic settings IA–OI–MOR; and e. Three tectonic settings CR–OI–MOR.

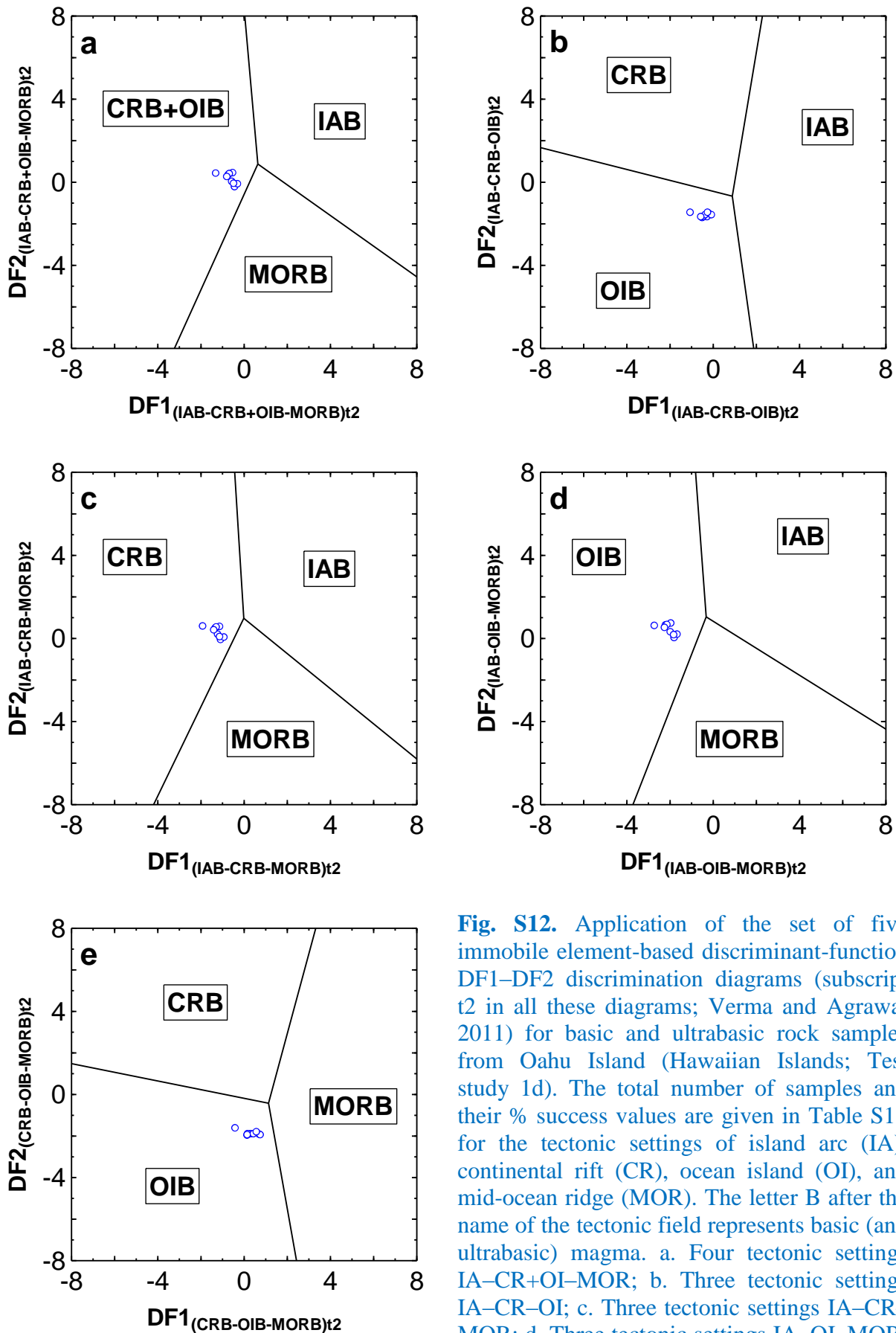


**Fig. S12.** Application of the set of five immobile element-based discriminant-function DF1-DF2 discrimination diagrams (subscript t2 in all these diagrams; Verma and Agrawal 2011) for basic and ultrabasic rock samples from Oahu Island (Hawaiian Islands; Test study 1d). The total number of samples and their % success values are given in Table S16 for the tectonic settings of island arc (IA), continental rift (CR), ocean island (OI), and mid-ocean ridge (MOR). The letter B after the name of the tectonic field represents basic (and ultrabasic) magma. a. Four tectonic settings IA-CR+OI-MOR; b. Three tectonic settings IA-CR-OI; c. Three tectonic settings IA-CR-MOR; d. Three tectonic settings IA-OI-MOR; and e. Three tectonic settings CR-OI-MOR.

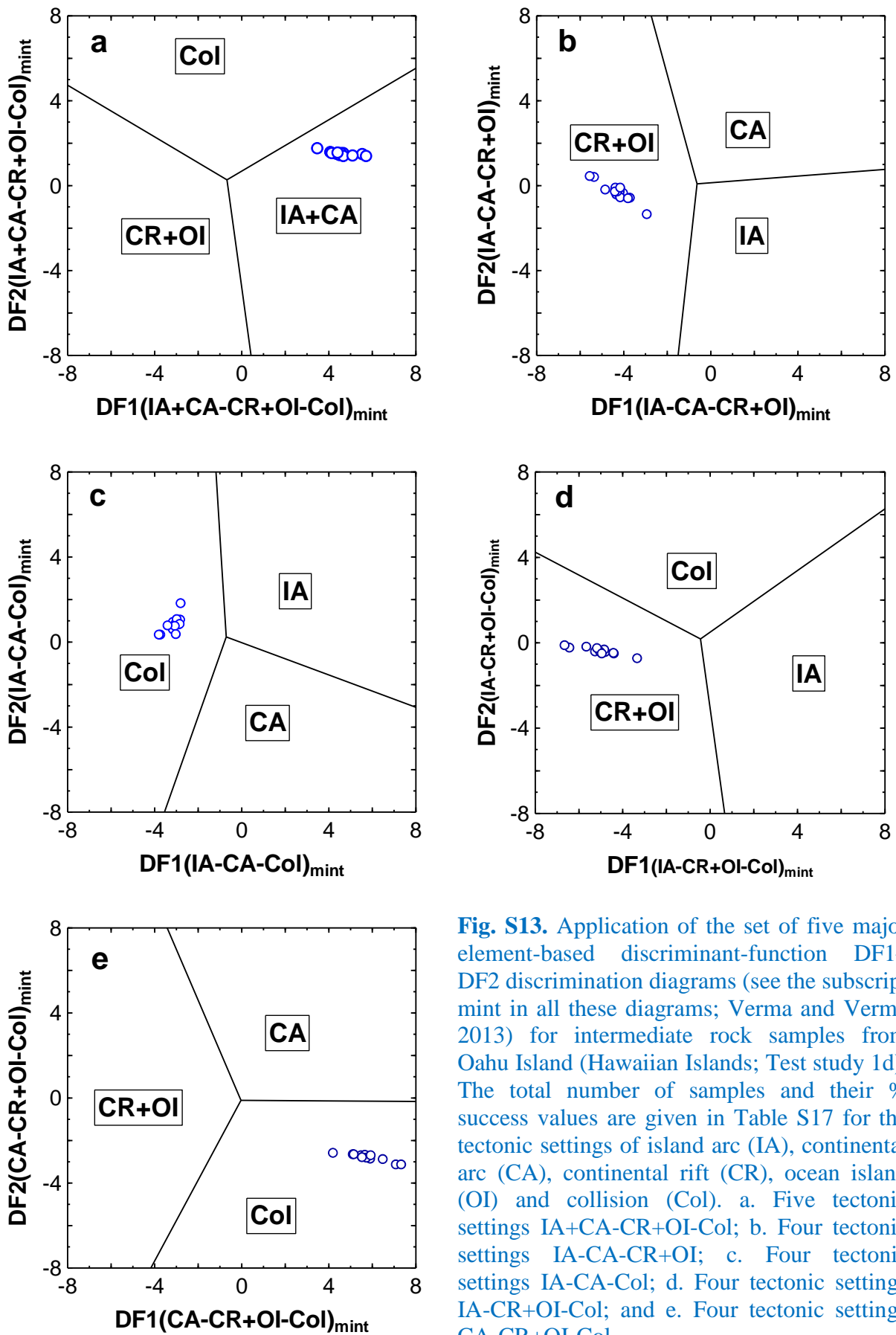


**Fig. S13.** Application of the set of five major element-based discriminant-function DF1–DF2 discrimination diagrams (see the subscript mint in all these diagrams; Verma and Verma 2013) for intermediate rock samples from Oahu Island (Hawaiian Islands; Test study 1d). The total number of samples and their % success values are given in Table S17 for the tectonic settings of island arc (IA), continental arc (CA), continental rift (CR), ocean island (OI) and collision (Col). a. Five tectonic settings IA+CA-CR+OI-Col; b. Four tectonic settings IA-CA-CR+OI; c. Four tectonic settings IA-CA-Col; d. Four tectonic settings IA-CR+OI-Col; and e. Four tectonic settings CA-CR+OI-Col.

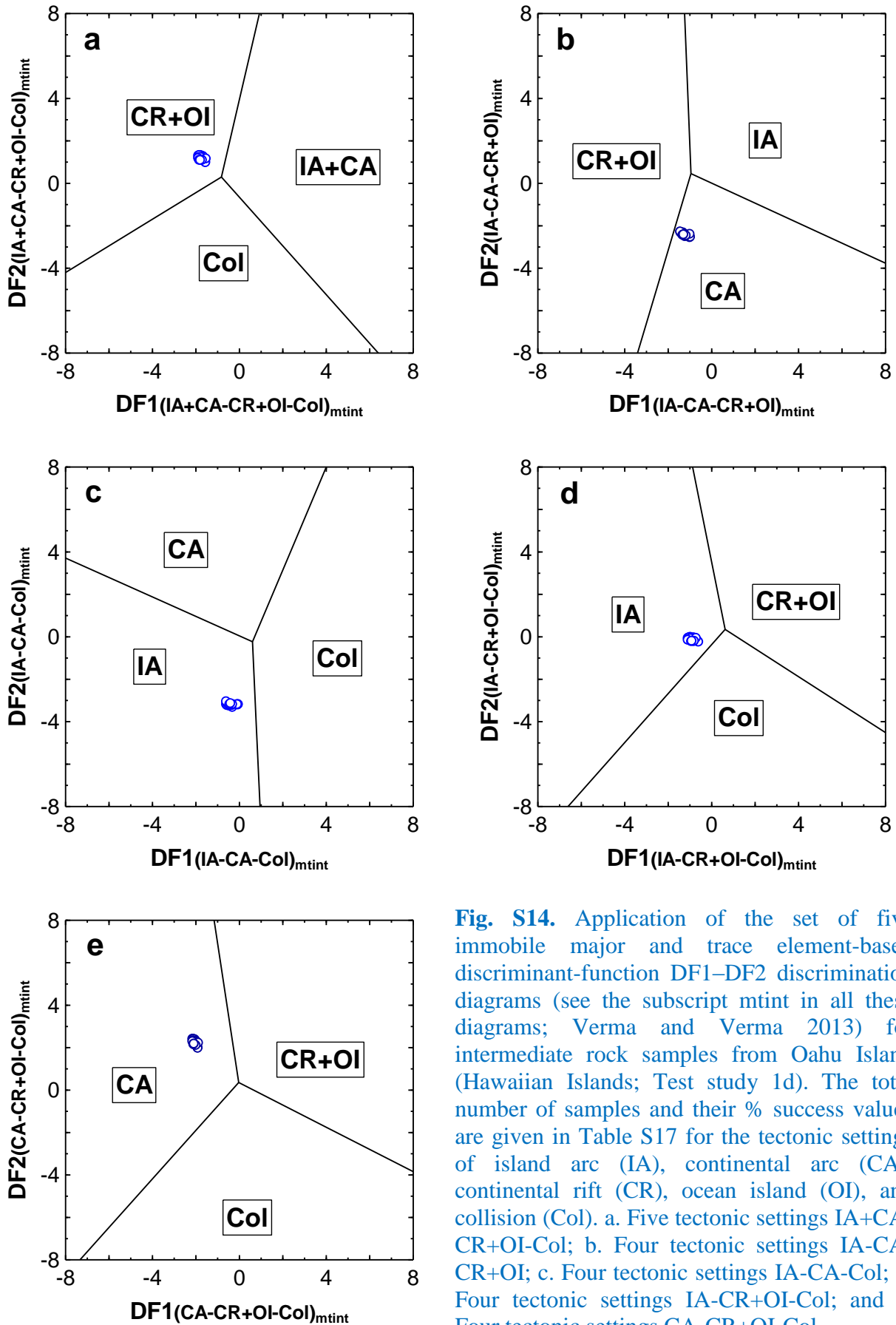


**Fig. S14.** Application of the set of five immobile major and trace element-based discriminant-function DF1–DF2 discrimination diagrams (see the subscript mtint in all these diagrams; Verma and Verma 2013) for intermediate rock samples from Oahu Island (Hawaiian Islands; Test study 1d). The total number of samples and their % success values are given in Table S17 for the tectonic settings of island arc (IA), continental arc (CA), continental rift (CR), ocean island (OI), and collision (Col). a. Five tectonic settings IA+CA-CR+OI-Col; b. Four tectonic settings IA-CA-CR+OI; c. Four tectonic settings IA-CA-Col; d. Four tectonic settings IA-CR+OI-Col; and e. Four tectonic settings CA-CR+OI-Col.

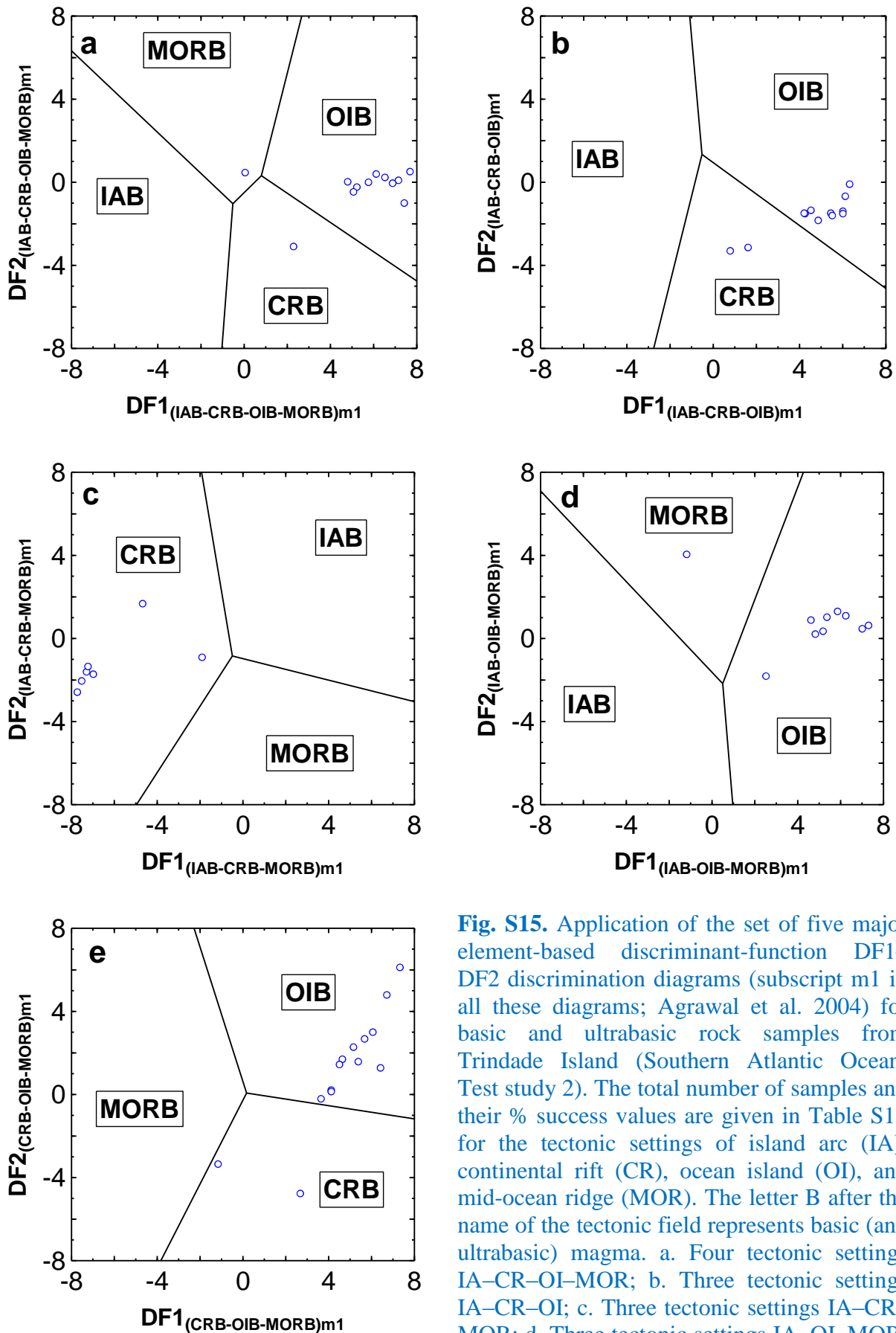


**Fig. S15.** Application of the set of five major element-based discriminant-function DF1–DF2 discrimination diagrams (subscript m1 in all these diagrams; Agrawal et al. 2004) for basic and ultrabasic rock samples from Trindade Island (Southern Atlantic Ocean; Test study 2). The total number of samples and their % success values are given in Table S18 for the tectonic settings of island arc (IA), continental rift (CR), ocean island (OI), and mid-ocean ridge (MOR). The letter B after the name of the tectonic field represents basic (and ultrabasic) magma. a. Four tectonic settings IA–CR–OI–MOR; b. Three tectonic settings IA–CR–OI; c. Three tectonic settings IA–CR–MOR; d. Three tectonic settings IA–OI–MOR; and e. Three tectonic settings CR–OI–MOR.

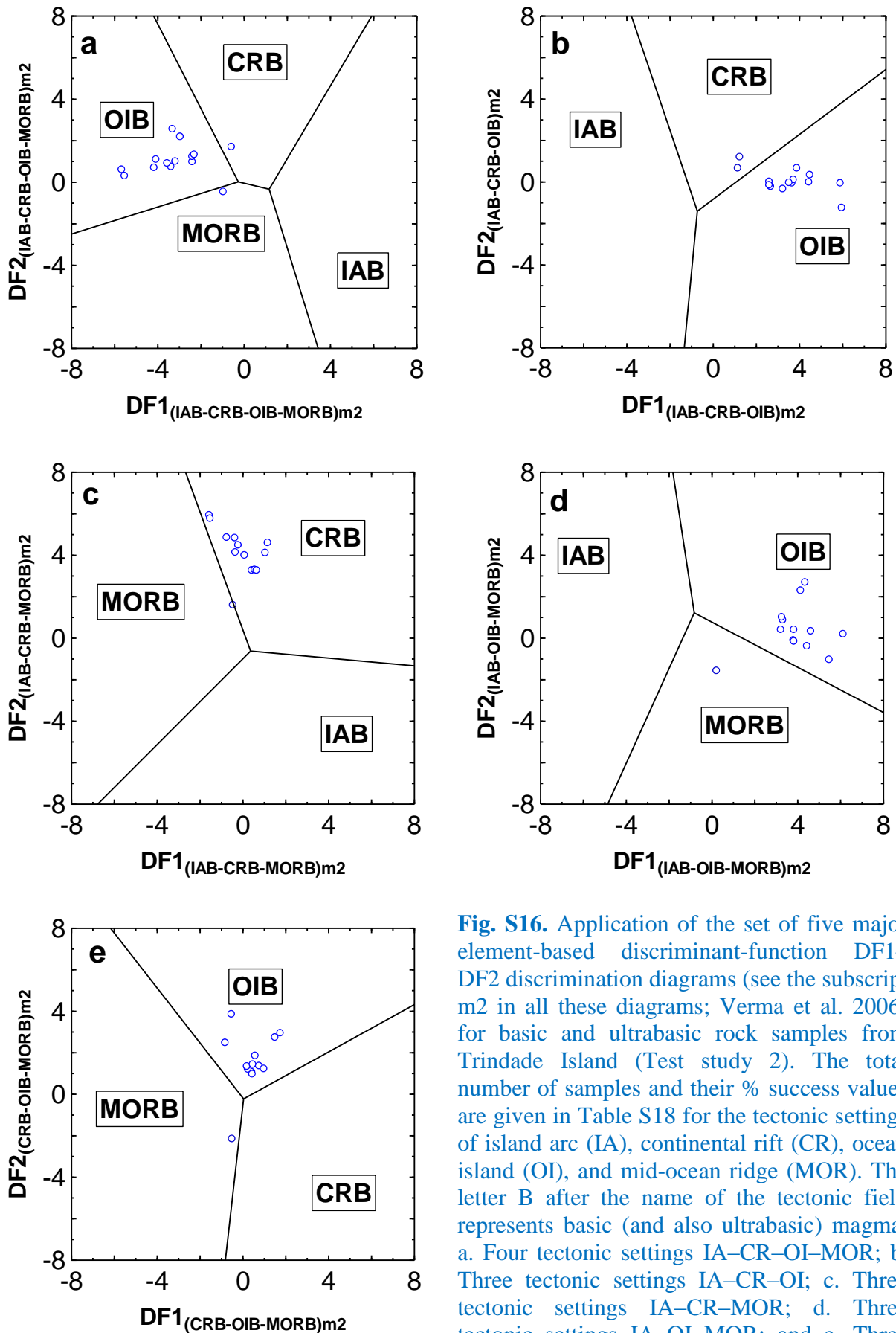


**Fig. S16.** Application of the set of five major element-based discriminant-function DF1–DF2 discrimination diagrams (see the subscript m2 in all these diagrams; Verma et al. 2006) for basic and ultrabasic rock samples from Trindade Island (Test study 2). The total number of samples and their % success values are given in Table S18 for the tectonic settings of island arc (IA), continental rift (CR), ocean island (OI), and mid-ocean ridge (MOR). The letter B after the name of the tectonic field represents basic (and also ultrabasic) magma. a. Four tectonic settings IA–CR–OI–MOR; b. Three tectonic settings IA–CR–OI; c. Three tectonic settings IA–CR–MOR; d. Three tectonic settings IA–OI–MOR; and e. Three tectonic settings CR–OI–MOR.

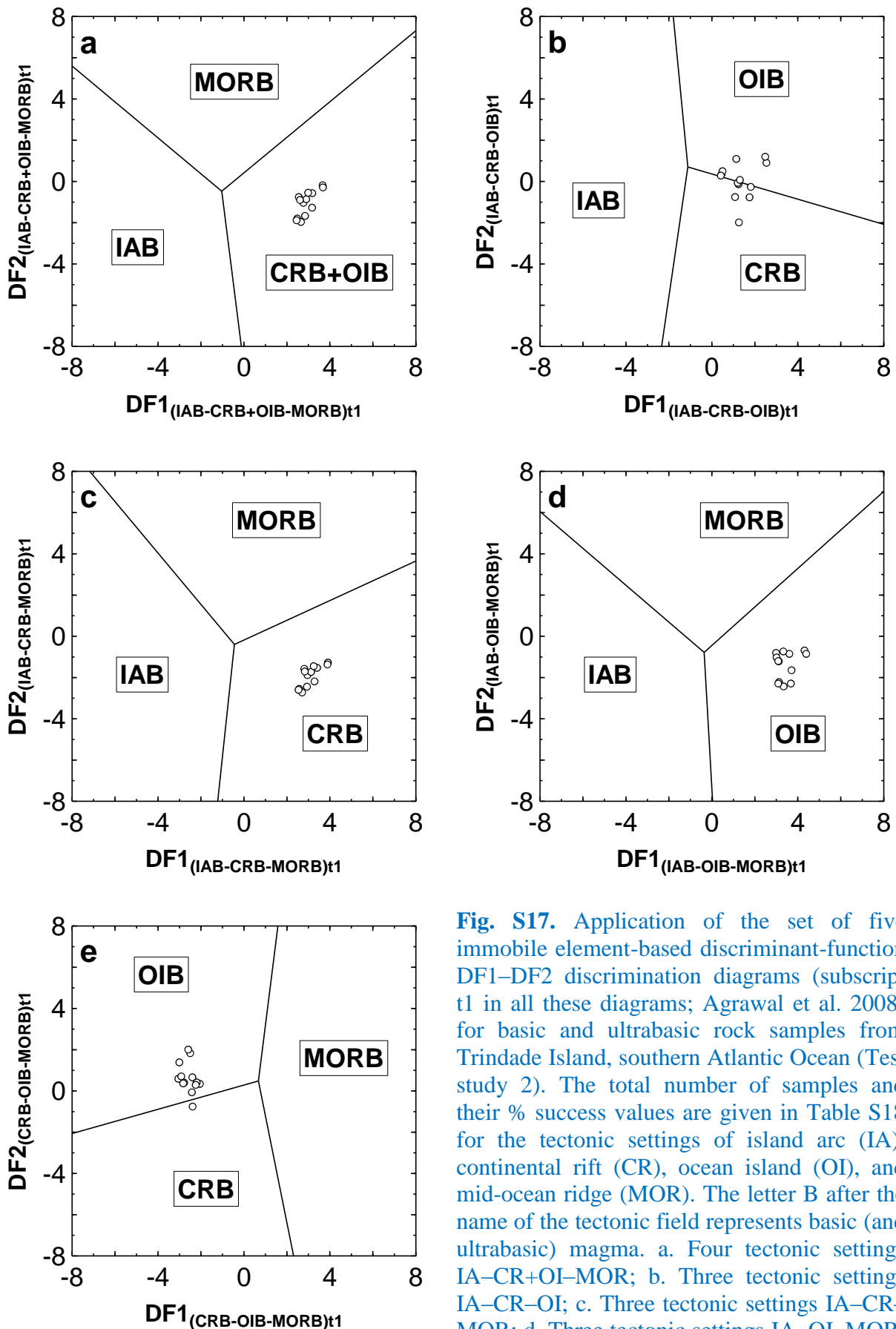


**Fig. S17.** Application of the set of five immobile element-based discriminant-function DF1-DF2 discrimination diagrams (subscript t1 in all these diagrams; Agrawal et al. 2008) for basic and ultrabasic rock samples from Trindade Island, southern Atlantic Ocean (Test study 2). The total number of samples and their % success values are given in Table S18 for the tectonic settings of island arc (IA), continental rift (CR), ocean island (OI), and mid-ocean ridge (MOR). The letter B after the name of the tectonic field represents basic (and ultrabasic) magma. a. Four tectonic settings IA-CR+OI-MOR; b. Three tectonic settings IA-CR-OI; c. Three tectonic settings IA-CR-MOR; d. Three tectonic settings IA-OI-MOR; and e. Three tectonic settings CR-OI-MOR.

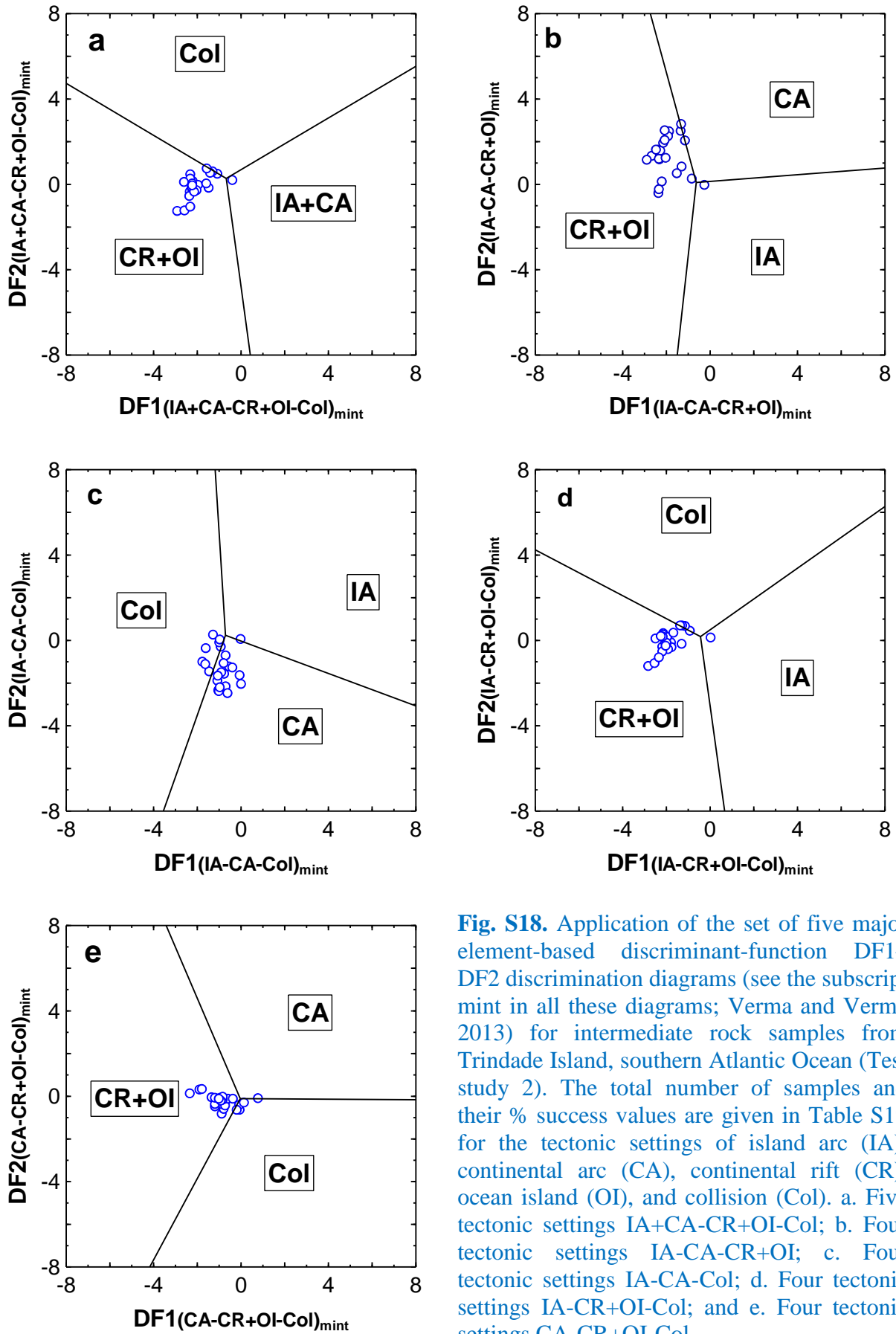


**Fig. S18.** Application of the set of five major element-based discriminant-function DF1–DF2 discrimination diagrams (see the subscript mint in all these diagrams; Verma and Verma 2013) for intermediate rock samples from Trindade Island, southern Atlantic Ocean (Test study 2). The total number of samples and their % success values are given in Table S19 for the tectonic settings of island arc (IA), continental arc (CA), continental rift (CR), ocean island (OI), and collision (Col). a. Five tectonic settings IA+CA-CR+OI-Col; b. Four tectonic settings IA-CA-CR+OI; c. Four tectonic settings IA-CA-Col; d. Four tectonic settings IA-CR+OI-Col; and e. Four tectonic settings CA-CR+OI-Col.

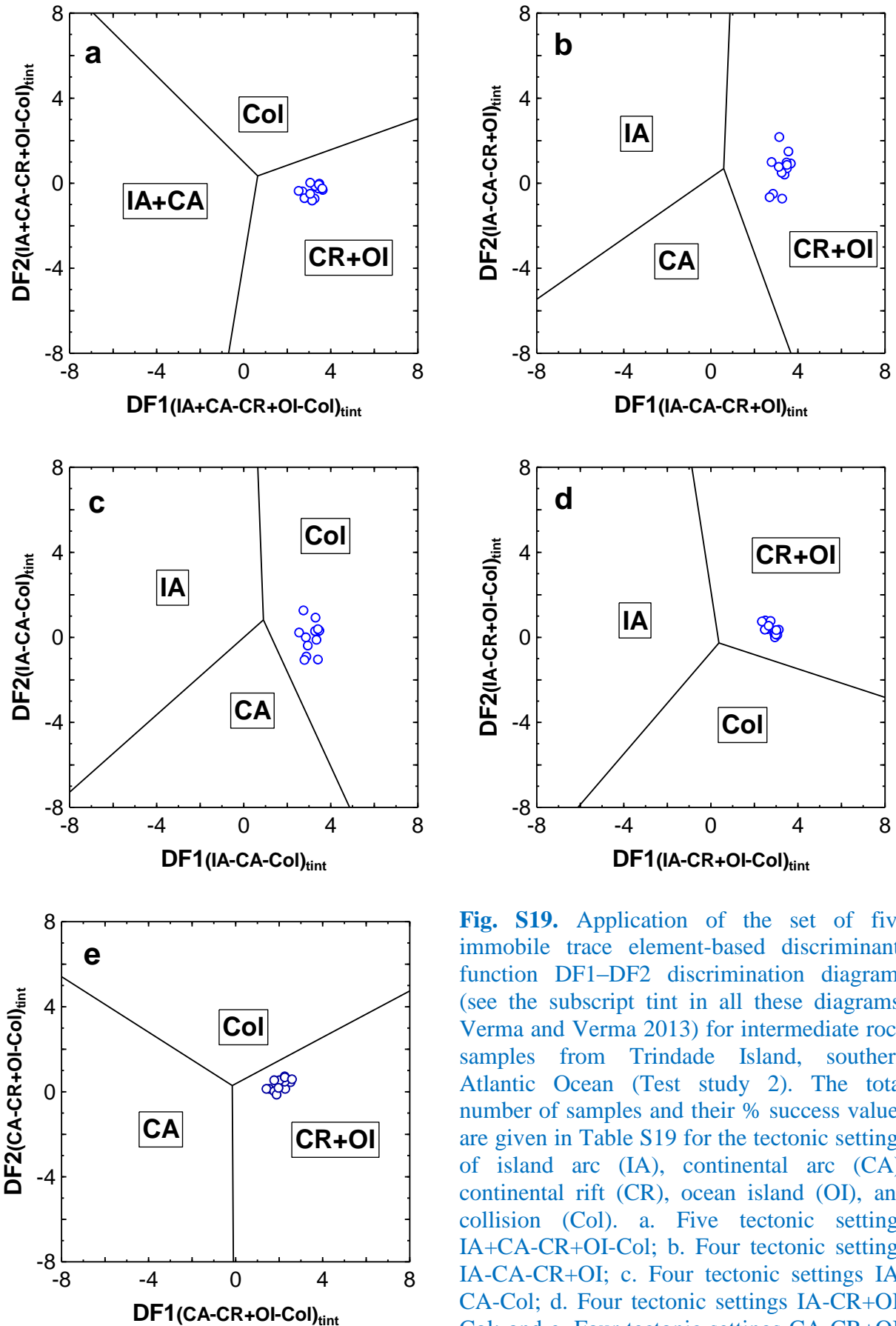


**Fig. S19.** Application of the set of five immobile trace element-based discriminant-function DF1–DF2 discrimination diagrams (see the subscript tint in all these diagrams; Verma and Verma 2013) for intermediate rock samples from Trindade Island, southern Atlantic Ocean (Test study 2). The total number of samples and their % success values are given in Table S19 for the tectonic settings of island arc (IA), continental arc (CA), continental rift (CR), ocean island (OI), and collision (Col).

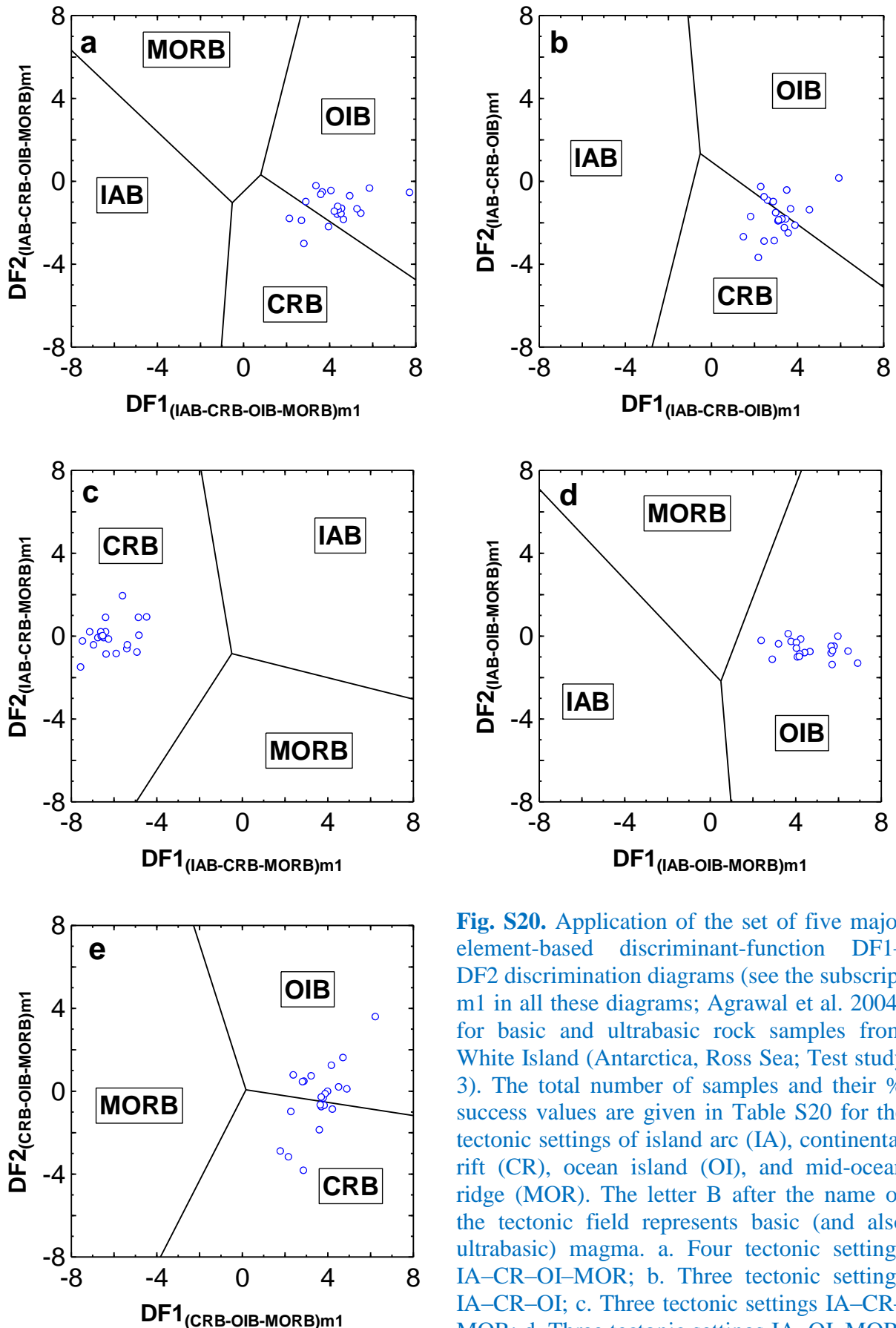


**Fig. S20.** Application of the set of five major element-based discriminant-function  $DF1-DF2$  discrimination diagrams (see the subscript m1 in all these diagrams; Agrawal et al. 2004) for basic and ultrabasic rock samples from White Island (Antarctica, Ross Sea; Test study 3). The total number of samples and their % success values are given in Table S20 for the tectonic settings of island arc (IA), continental rift (CR), ocean island (OI), and mid-ocean ridge (MOR). The letter B after the name of the tectonic field represents basic (and also ultrabasic) magma. a. Four tectonic settings IA–CR–OI–MOR; b. Three tectonic settings IA–CR–OI; c. Three tectonic settings IA–CR–MOR; d. Three tectonic settings IA–OI–MOR; and e. Three tectonic settings CR–OI–MOR.

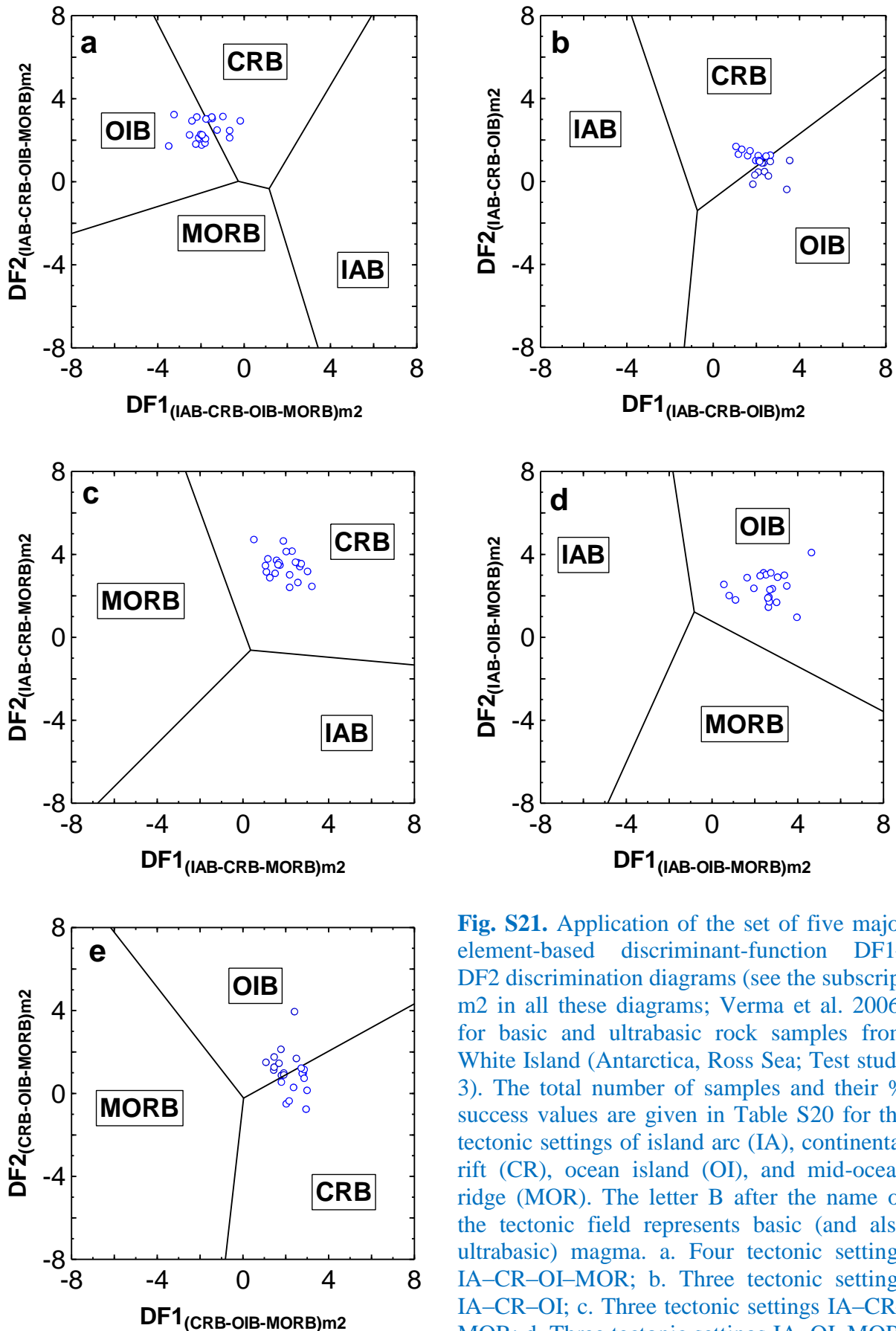


**Fig. S21.** Application of the set of five major element-based discriminant-function DF1–DF2 discrimination diagrams (see the subscript m2 in all these diagrams; Verma et al. 2006) for basic and ultrabasic rock samples from White Island (Antarctica, Ross Sea; Test study 3). The total number of samples and their % success values are given in Table S20 for the tectonic settings of island arc (IA), continental rift (CR), ocean island (OI), and mid-ocean ridge (MOR). The letter B after the name of the tectonic field represents basic (and also ultrabasic) magma. a. Four tectonic settings IA–CR–OI–MOR; b. Three tectonic settings IA–CR–OI; c. Three tectonic settings IA–CR–MORB; d. Three tectonic settings IA–OI–MORB; and e. Three tectonic settings CR–OI–MORB.

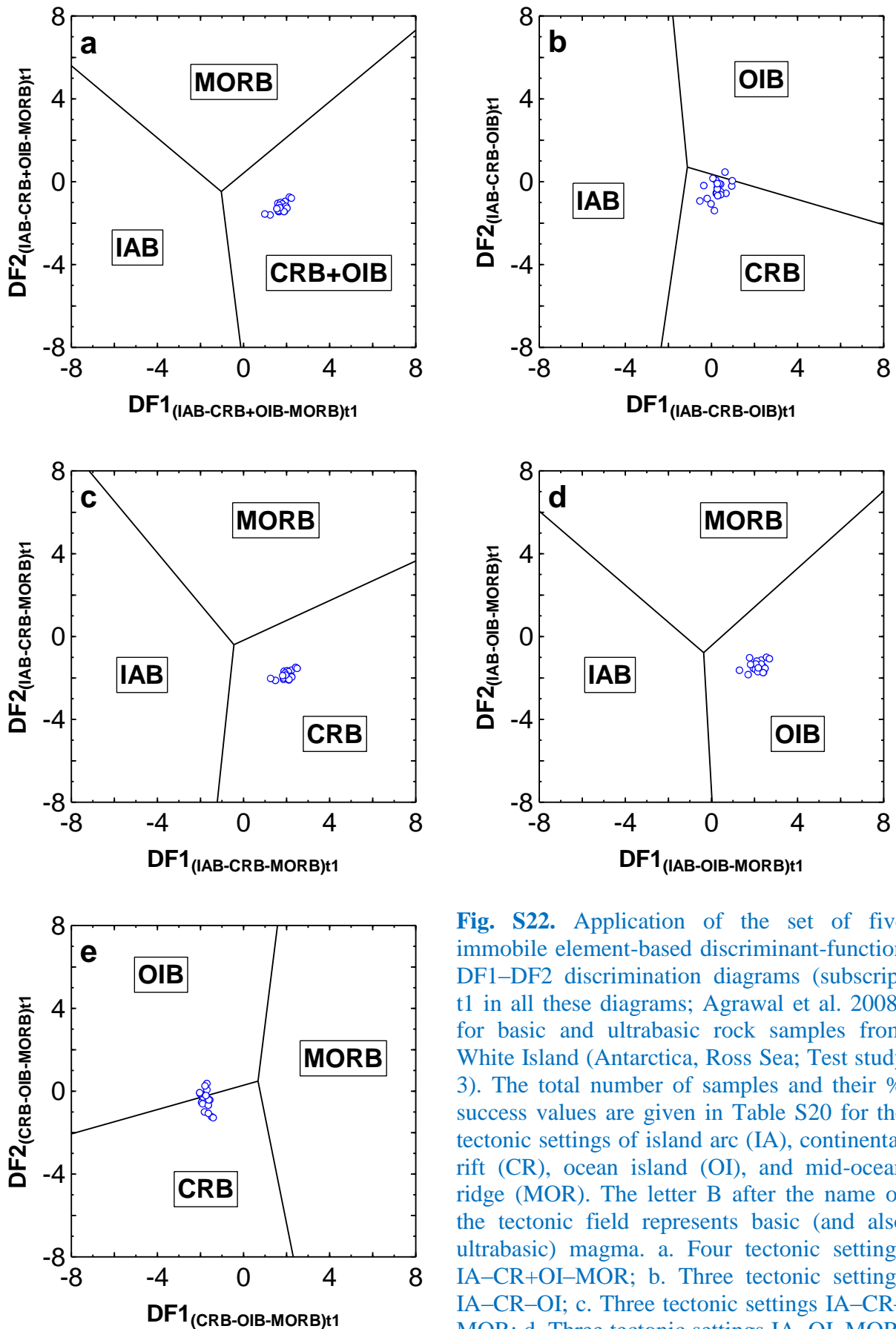


**Fig. S22.** Application of the set of five immobile element-based discriminant-function DF1-DF2 discrimination diagrams (subscript t1 in all these diagrams; Agrawal et al. 2008) for basic and ultrabasic rock samples from White Island (Antarctica, Ross Sea; Test study 3). The total number of samples and their % success values are given in Table S20 for the tectonic settings of island arc (IA), continental rift (CR), ocean island (OI), and mid-ocean ridge (MOR). The letter B after the name of the tectonic field represents basic (and also ultrabasic) magma. a. Four tectonic settings IA-CR+OI-MOR; b. Three tectonic settings IA-CR-OI; c. Three tectonic settings IA-CR-MOR; d. Three tectonic settings IA-OI-MOR; and e. Three tectonic settings CR-OI-MOR.

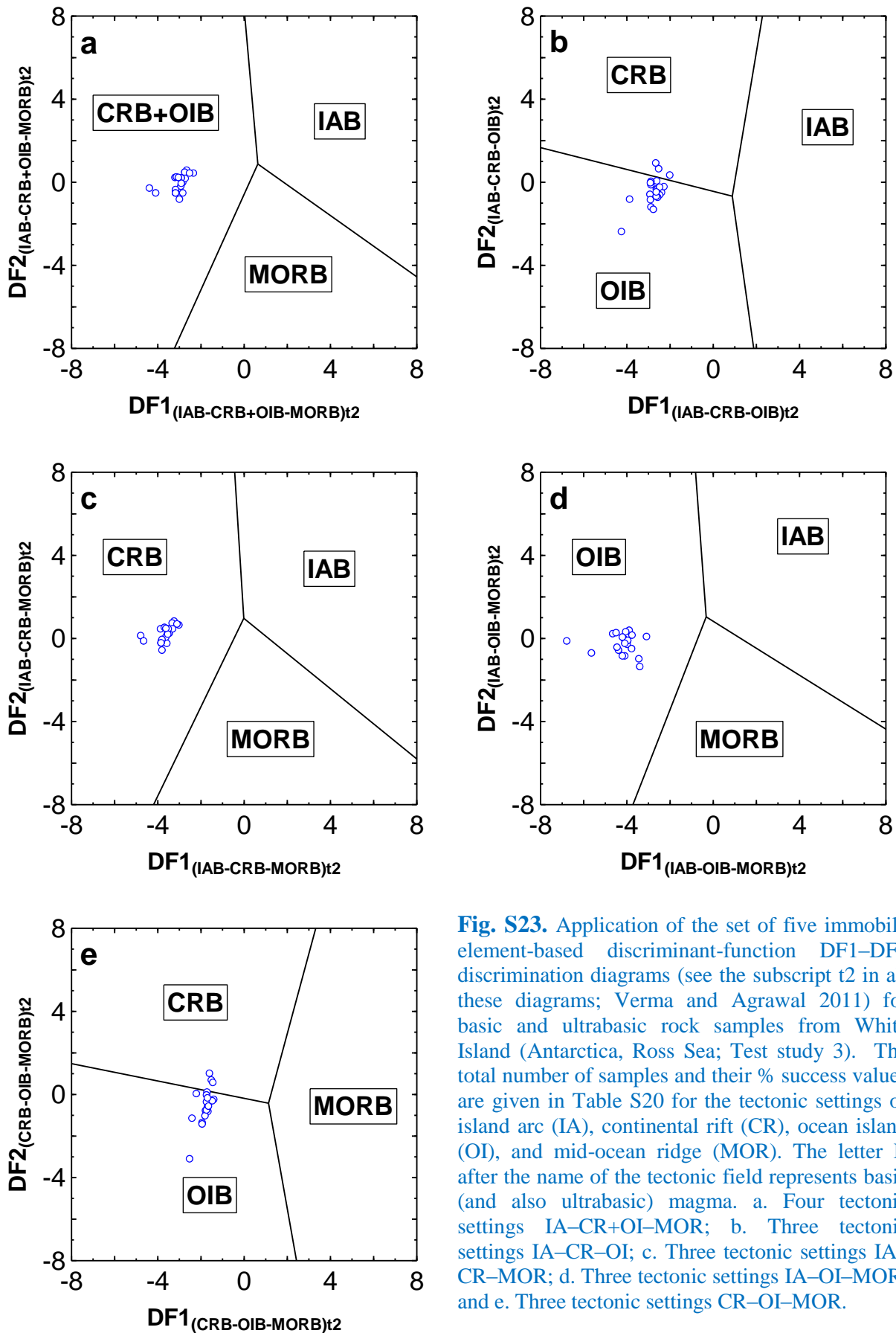


**Fig. S23.** Application of the set of five immobile element-based discriminant-function DF1–DF2 discrimination diagrams (see the subscript t2 in all these diagrams; Verma and Agrawal 2011) for basic and ultrabasic rock samples from White Island (Antarctica, Ross Sea; Test study 3). The total number of samples and their % success values are given in Table S20 for the tectonic settings of island arc (IA), continental rift (CR), ocean island (OI), and mid-ocean ridge (MOR). The letter B after the name of the tectonic field represents basic (and also ultrabasic) magma. a. Four tectonic settings IA–CR+OI–MOR; b. Three tectonic settings IA–CR–OI; c. Three tectonic settings IA–CR–MOR; d. Three tectonic settings IA–OI–MOR; and e. Three tectonic settings CR–OI–MOR.

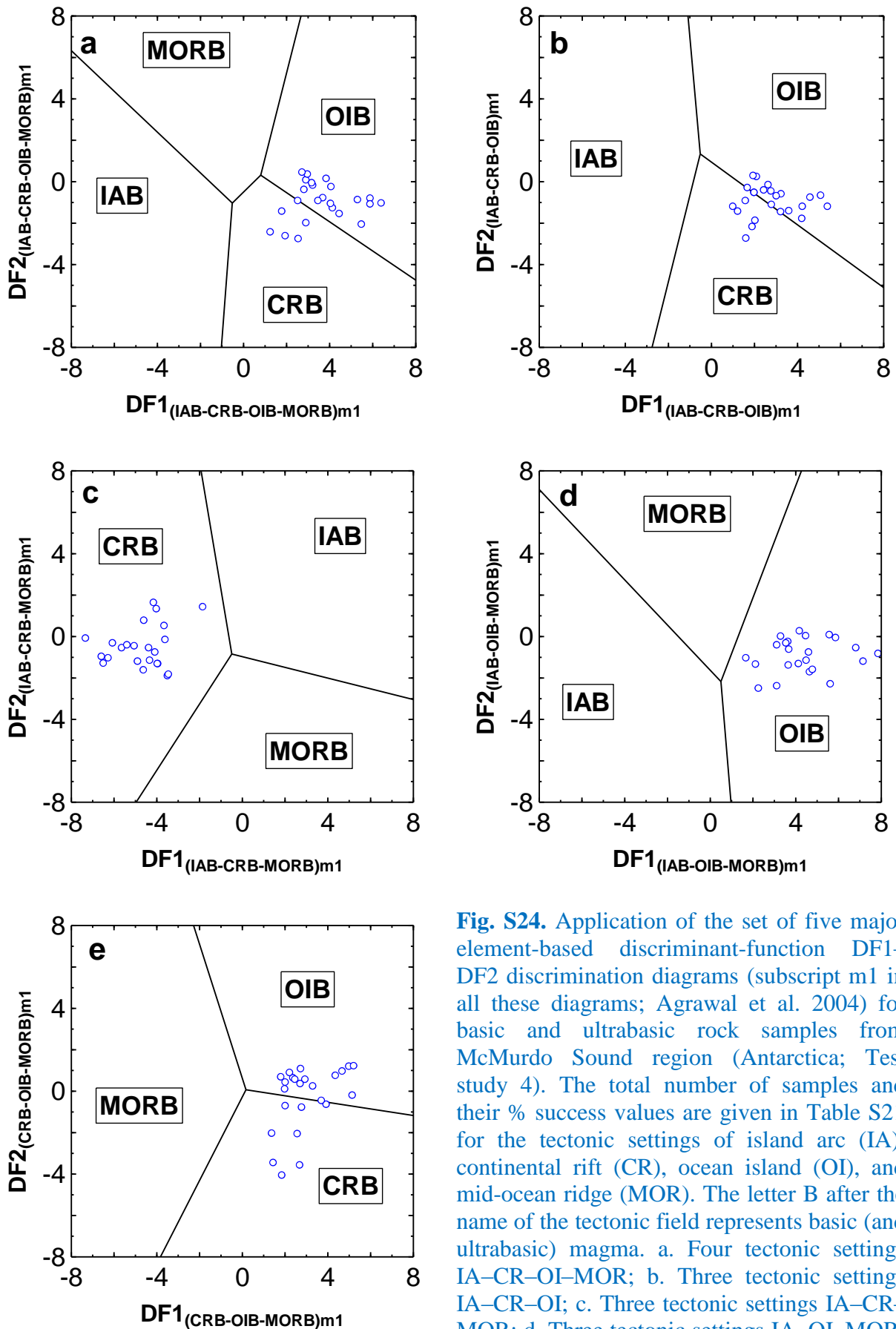


**Fig. S24.** Application of the set of five major element-based discriminant-function DF1–DF2 discrimination diagrams (subscript m1 in all these diagrams; Agrawal et al. 2004) for basic and ultrabasic rock samples from McMurdo Sound region (Antarctica; Test study 4). The total number of samples and their % success values are given in Table S21 for the tectonic settings of island arc (IA), continental rift (CR), ocean island (OI), and mid-ocean ridge (MOR). The letter B after the name of the tectonic field represents basic (and ultrabasic) magma. a. Four tectonic settings IA–CR–OI–MOR; b. Three tectonic settings IA–CR–OI; c. Three tectonic settings IA–CR–MORB; d. Three tectonic settings IA–OI–MORB; and e. Three tectonic settings CR–OI–MORB.

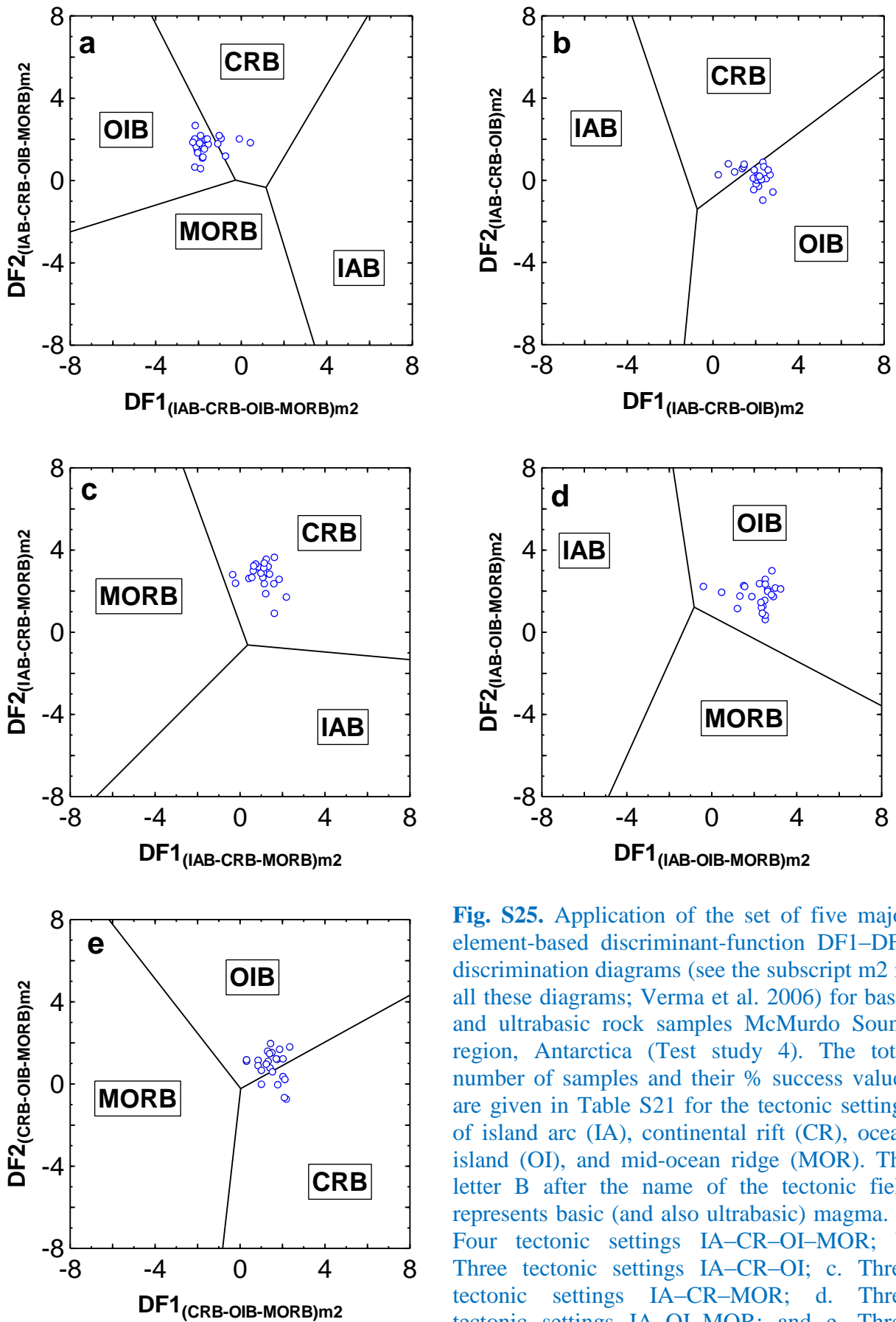


**Fig. S25.** Application of the set of five major element-based discriminant-function DF1–DF2 discrimination diagrams (see the subscript m2 in all these diagrams; Verma et al. 2006) for basic and ultrabasic rock samples McMurdo Sound region, Antarctica (Test study 4). The total number of samples and their % success values are given in Table S21 for the tectonic settings of island arc (IA), continental rift (CR), ocean island (OI), and mid-ocean ridge (MOR). The letter B after the name of the tectonic field represents basic (and also ultrabasic) magma. a. Four tectonic settings IA–CR–OI–MOR; b. Three tectonic settings IA–CR–OI; c. Three tectonic settings IA–CR–MOR; d. Three tectonic settings IA–OI–MOR; and e. Three tectonic settings CR–OI–MOR.

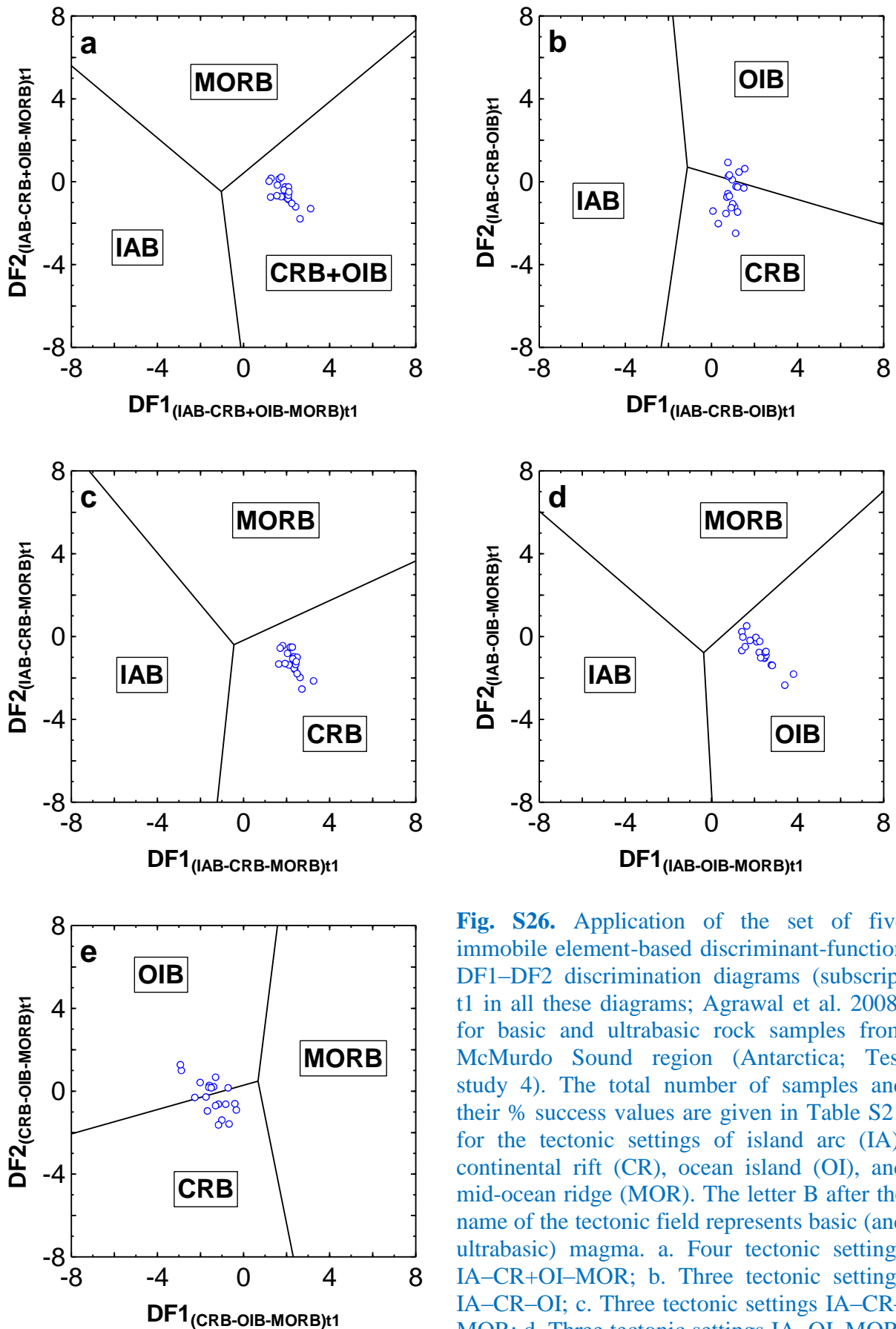


**Fig. S26.** Application of the set of five immobile element-based discriminant-function DF1-DF2 discrimination diagrams (subscript t1 in all these diagrams; Agrawal et al. 2008) for basic and ultrabasic rock samples from McMurdo Sound region (Antarctica; Test study 4). The total number of samples and their % success values are given in Table S21 for the tectonic settings of island arc (IA), continental rift (CR), ocean island (OI), and mid-ocean ridge (MOR). The letter B after the name of the tectonic field represents basic (and ultrabasic) magma. a. Four tectonic settings IA-CR+OI-MOR; b. Three tectonic settings IA-CR-OI; c. Three tectonic settings IA-CR-MOR; d. Three tectonic settings IA-OI-MOR; and e. Three tectonic settings CR-OI-MOR.

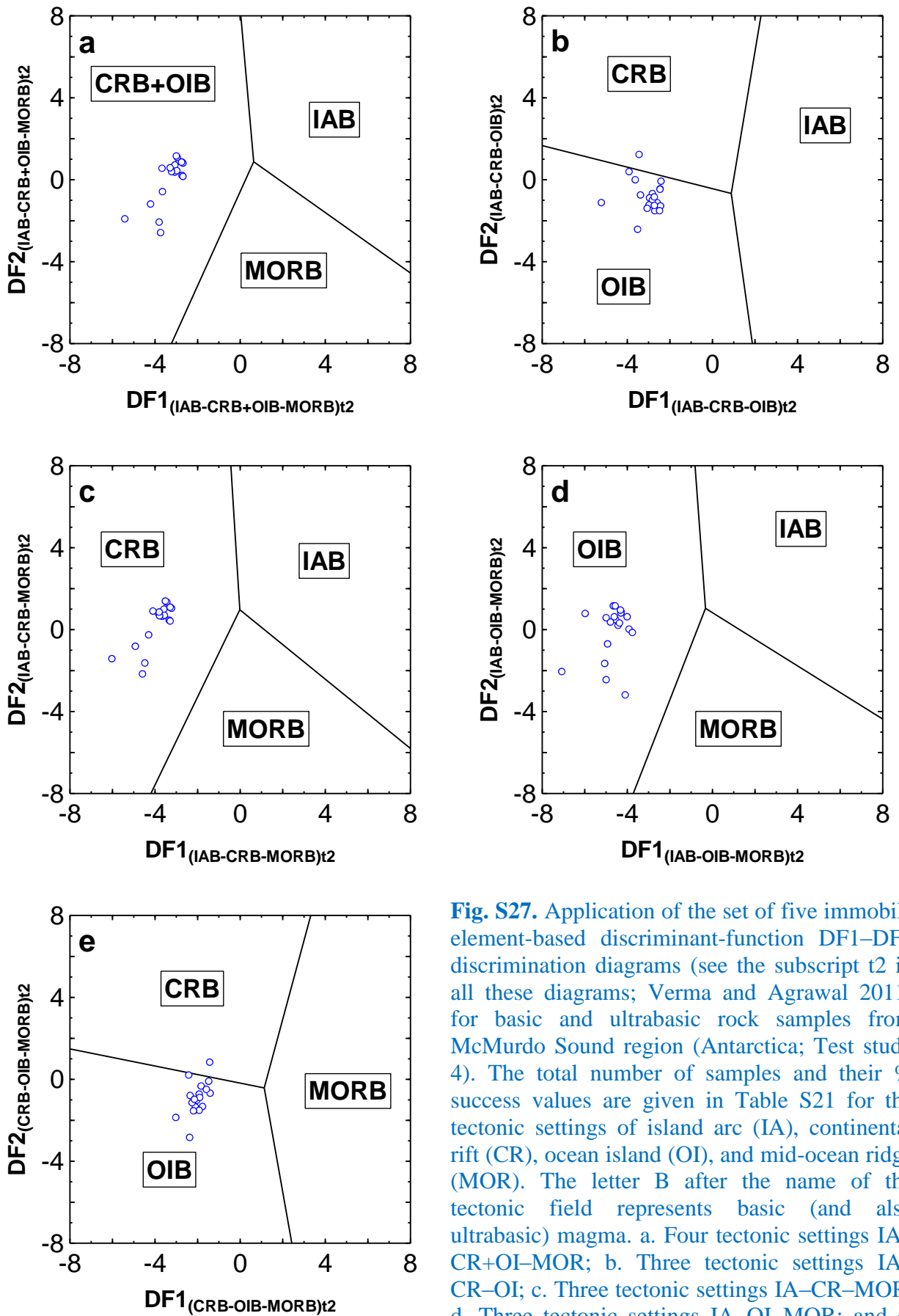


**Fig. S27.** Application of the set of five immobile element-based discriminant-function DF1–DF2 discrimination diagrams (see the subscript t2 in all these diagrams; Verma and Agrawal 2011) for basic and ultrabasic rock samples from McMurdo Sound region (Antarctica; Test study 4). The total number of samples and their % success values are given in Table S21 for the tectonic settings of island arc (IA), continental rift (CR), ocean island (OI), and mid-ocean ridge (MOR). The letter B after the name of the tectonic field represents basic (and also ultrabasic) magma. a. Four tectonic settings IA–CR+OI–MOR; b. Three tectonic settings IA–CR–OI; c. Three tectonic settings IA–CR–MOR; d. Three tectonic settings IA–OI–MOR; and e. Three tectonic settings CR–OI–MOR.

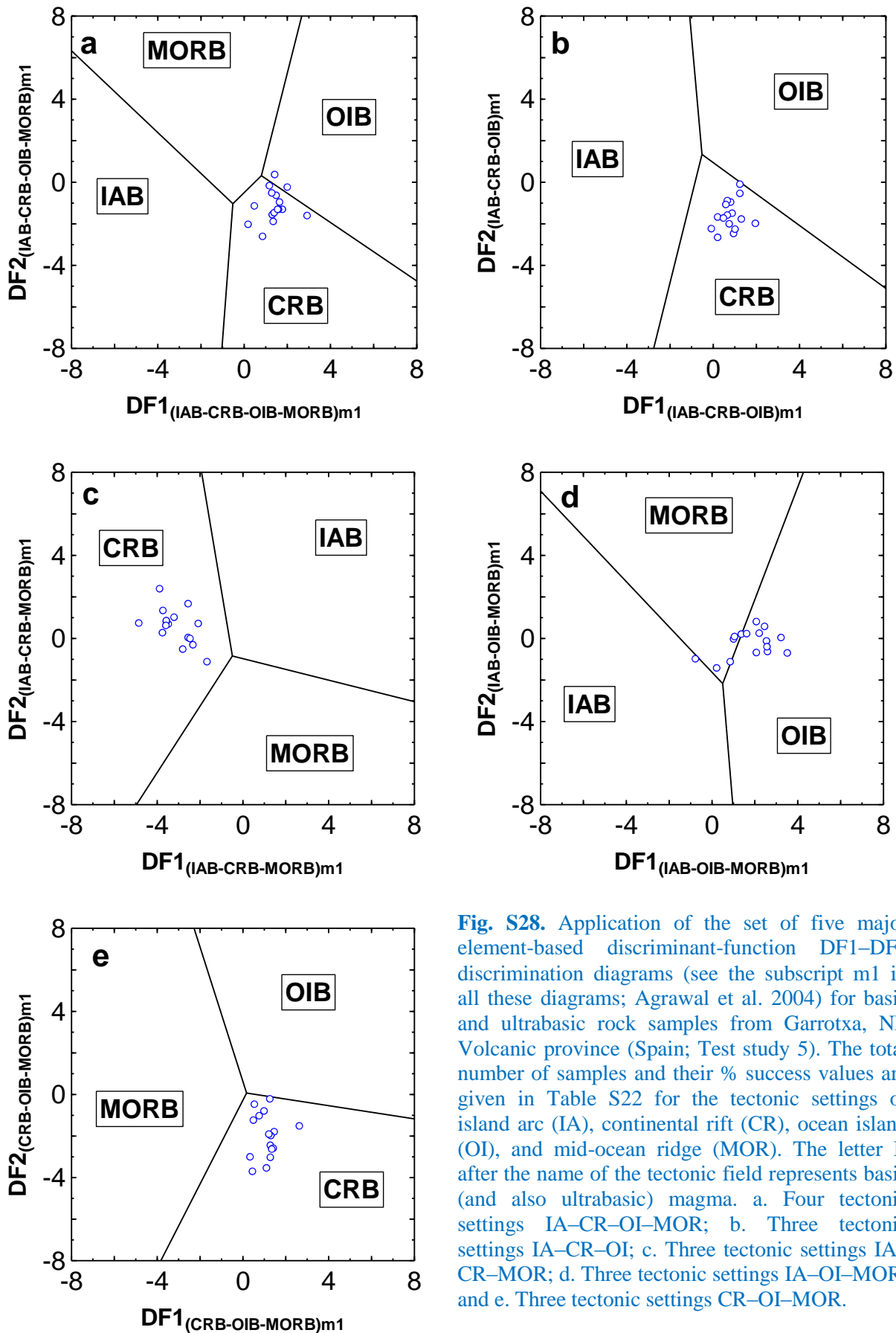


**Fig. S28.** Application of the set of five major element-based discriminant-function DF1–DF2 discrimination diagrams (see the subscript m1 in all these diagrams; Agrawal et al. 2004) for basic and ultrabasic rock samples from Garrotxa, NE Volcanic province (Spain; Test study 5). The total number of samples and their % success values are given in Table S22 for the tectonic settings of island arc (IA), continental rift (CR), ocean island (OI), and mid-ocean ridge (MOR). The letter B after the name of the tectonic field represents basic (and also ultrabasic) magma. a. Four tectonic settings IA–CR–OI–MOR; b. Three tectonic settings IA–CR–OI; c. Three tectonic settings IA–CR–MOR; d. Three tectonic settings IA–OI–MOR; and e. Three tectonic settings CR–OI–MOR.

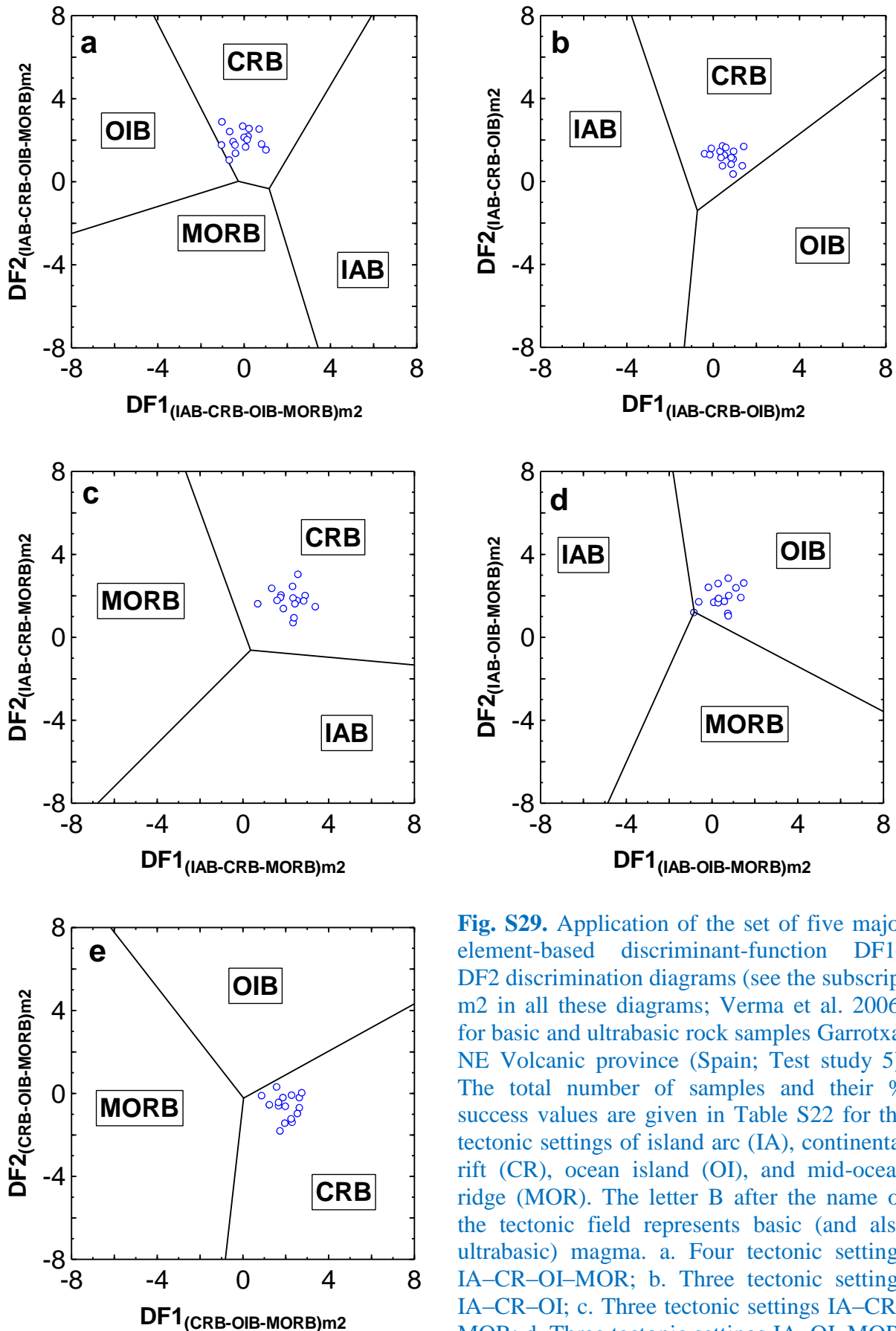


**Fig. S29.** Application of the set of five major element-based discriminant-function DF1–DF2 discrimination diagrams (see the subscript m2 in all these diagrams; Verma et al. 2006) for basic and ultrabasic rock samples Garrotxa, NE Volcanic province (Spain; Test study 5). The total number of samples and their % success values are given in Table S22 for the tectonic settings of island arc (IA), continental rift (CR), ocean island (OI), and mid-ocean ridge (MOR). The letter B after the name of the tectonic field represents basic (and also ultrabasic) magma. a. Four tectonic settings IA–CR–OI–MOR; b. Three tectonic settings IA–CR–OI; c. Three tectonic settings IA–CR–MOR; d. Three tectonic settings IA–OI–MOR; and e. Three tectonic settings CR–OI–MOR.

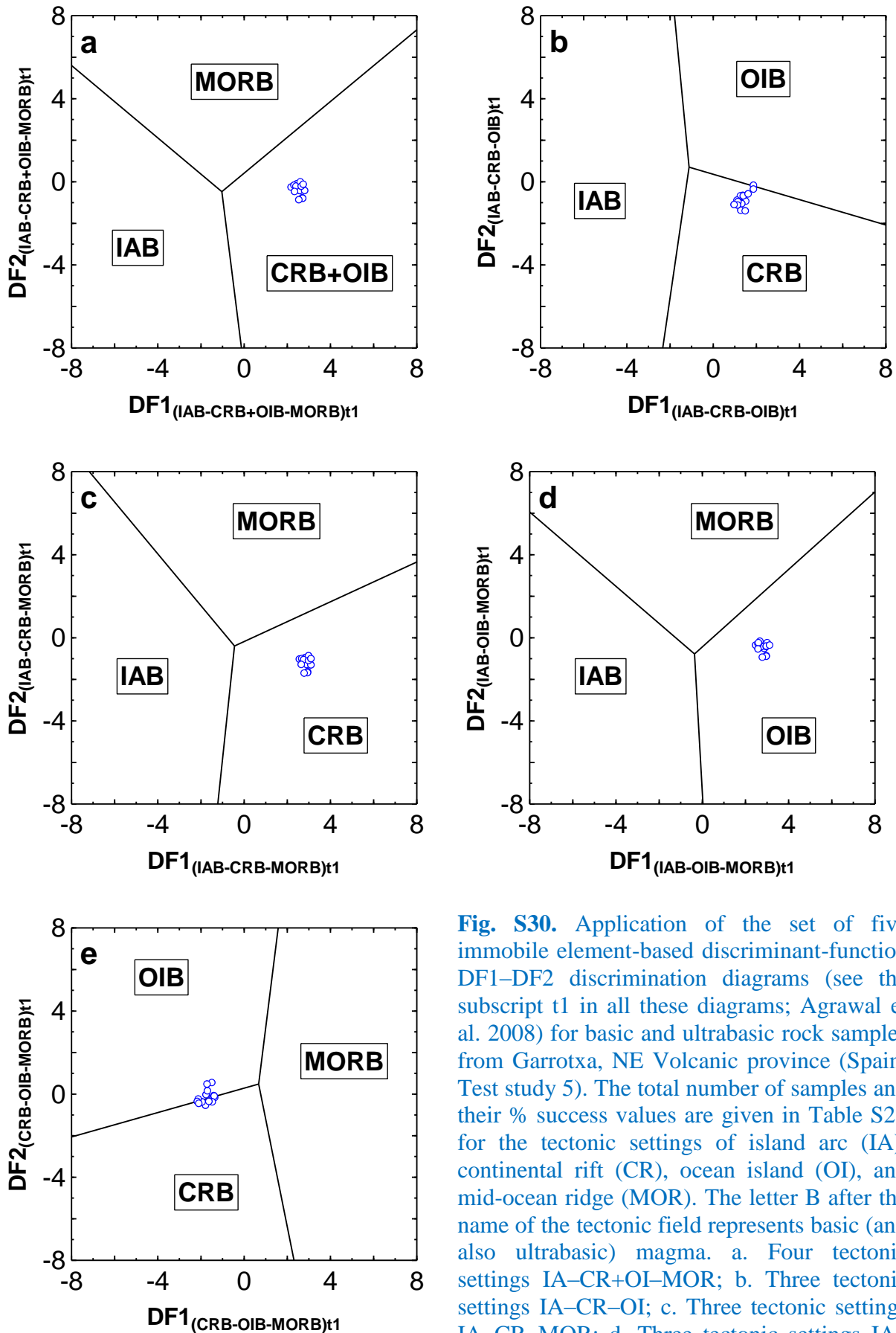


**Fig. S30.** Application of the set of five immobile element-based discriminant-function DF1-DF2 discrimination diagrams (see the subscript t1 in all these diagrams; Agrawal et al. 2008) for basic and ultrabasic rock samples from Garrotxa, NE Volcanic province (Spain; Test study 5). The total number of samples and their % success values are given in Table S22 for the tectonic settings of island arc (IA), continental rift (CR), ocean island (OI), and mid-ocean ridge (MOR). The letter B after the name of the tectonic field represents basic (and also ultrabasic) magma. a. Four tectonic settings IA-CR+OI-MOR; b. Three tectonic settings IA-CR-OI; c. Three tectonic settings IA-CR-MOR; d. Three tectonic settings IA-OI-MOR; and e. Three tectonic settings CR-OI-MOR.

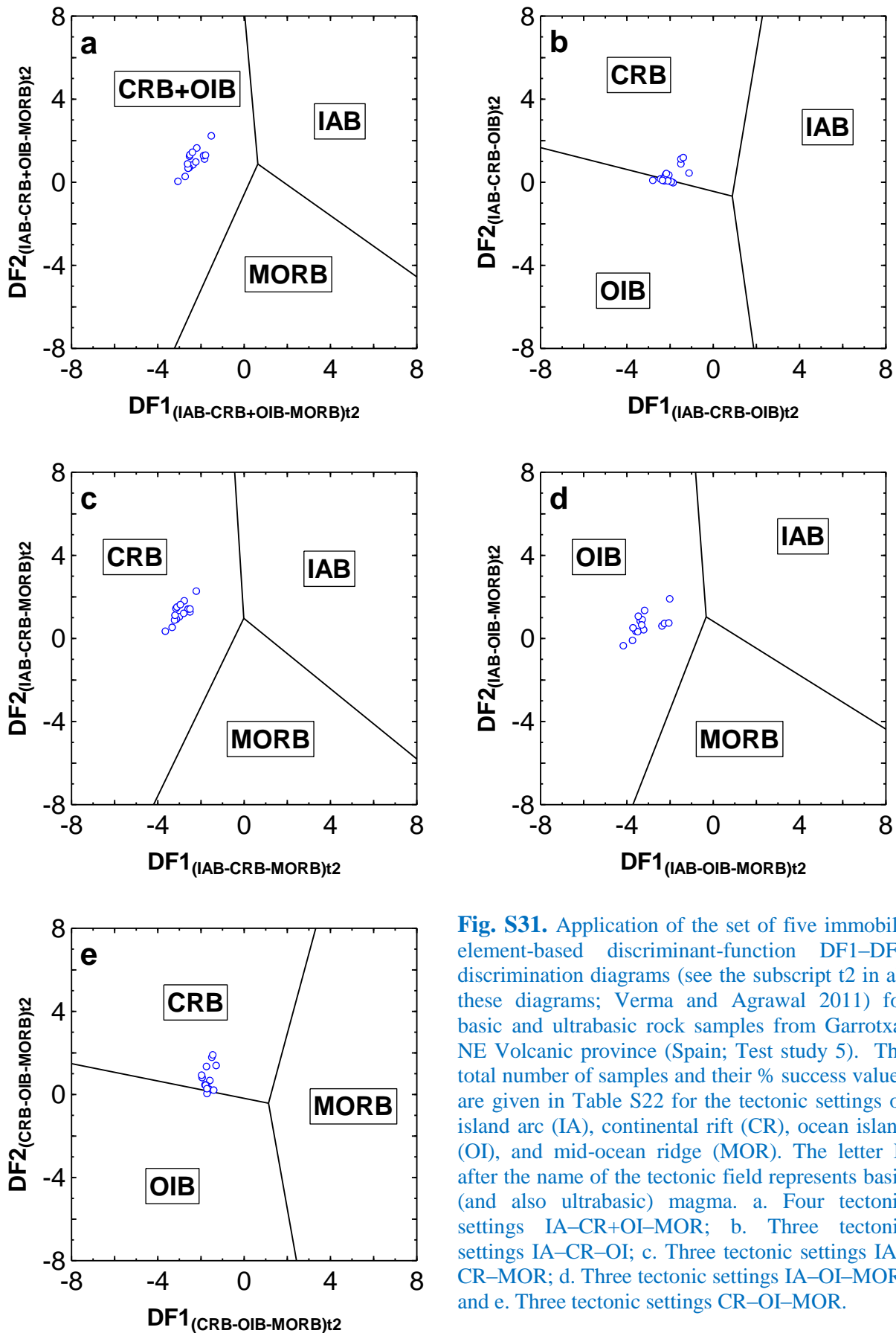


**Fig. S31.** Application of the set of five immobile element-based discriminant-function DF1–DF2 discrimination diagrams (see the subscript t2 in all these diagrams; Verma and Agrawal 2011) for basic and ultrabasic rock samples from Garrotxa, NE Volcanic province (Spain; Test study 5). The total number of samples and their % success values are given in Table S22 for the tectonic settings of island arc (IA), continental rift (CR), ocean island (OI), and mid-ocean ridge (MOR). The letter B after the name of the tectonic field represents basic (and also ultrabasic) magma. a. Four tectonic settings IA–CR+OI–MOR; b. Three tectonic settings IA–CR–OI; c. Three tectonic settings IA–CR–MOR; d. Three tectonic settings IA–OI–MOR; and e. Three tectonic settings CR–OI–MOR.

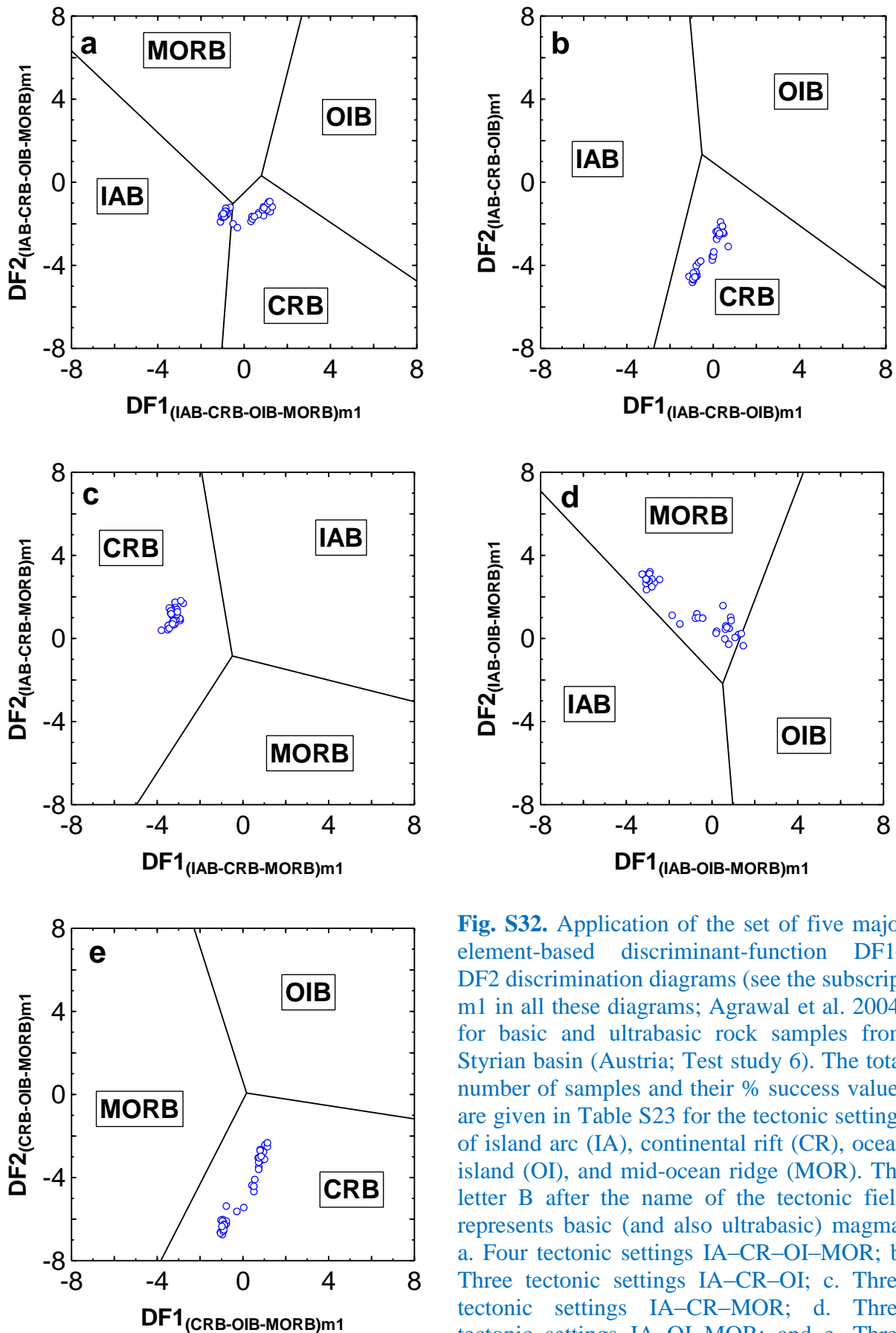


**Fig. S32.** Application of the set of five major element-based discriminant-function DF1–DF2 discrimination diagrams (see the subscript m1 in all these diagrams; Agrawal et al. 2004) for basic and ultrabasic rock samples from Styrian basin (Austria; Test study 6). The total number of samples and their % success values are given in Table S23 for the tectonic settings of island arc (IA), continental rift (CR), ocean island (OI), and mid-ocean ridge (MOR). The letter B after the name of the tectonic field represents basic (and also ultrabasic) magma. a. Four tectonic settings IA–CR–OI–MOR; b. Three tectonic settings IA–CR–OI; c. Three tectonic settings IA–CR–MOR; d. Three tectonic settings IA–OI–MOR; and e. Three tectonic settings CR–OI–MOR.

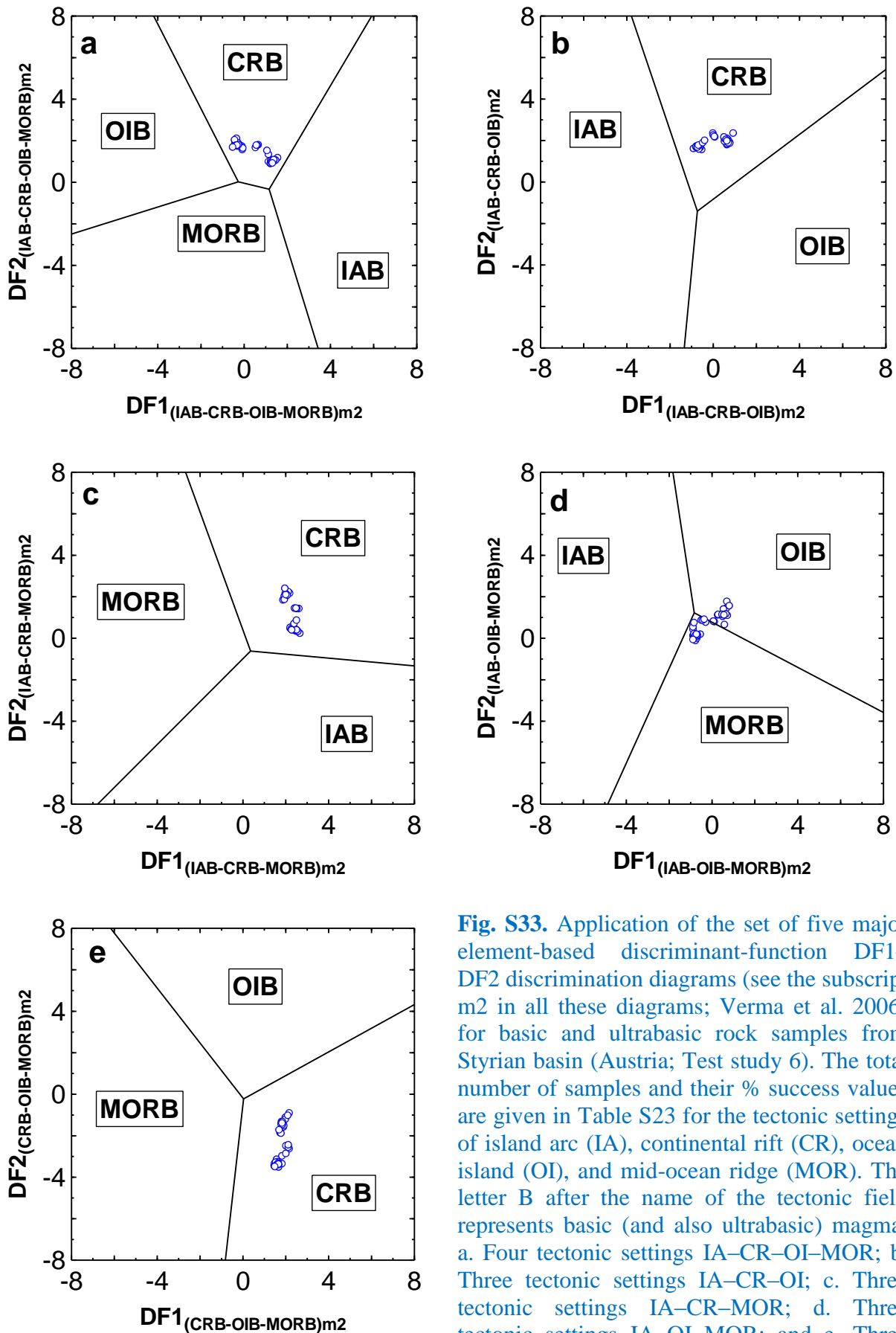


**Fig. S33.** Application of the set of five major element-based discriminant-function  $DF1-DF2$  discrimination diagrams (see the subscript m2 in all these diagrams; Verma et al. 2006) for basic and ultrabasic rock samples from Styrian basin (Austria; Test study 6). The total number of samples and their % success values are given in Table S23 for the tectonic settings of island arc (IA), continental rift (CR), ocean island (OI), and mid-ocean ridge (MOR). The letter B after the name of the tectonic field represents basic (and also ultrabasic) magma. a. Four tectonic settings IA–CR–OI–MOR; b. Three tectonic settings IA–CR–OI; c. Three tectonic settings IA–CR–MOR; d. Three tectonic settings IA–OI–MOR; and e. Three tectonic settings CR–OI–MOR.

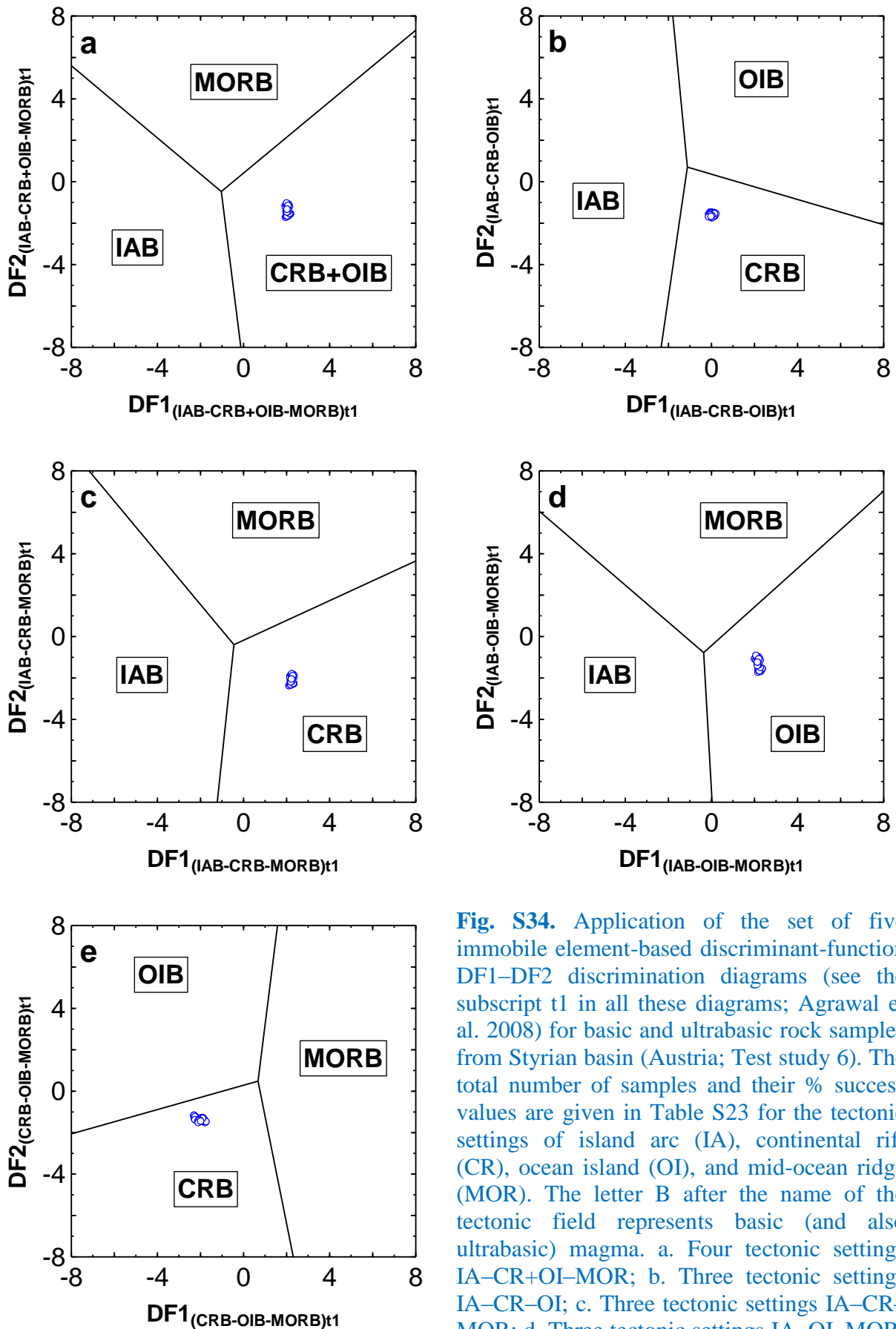


**Fig. S34.** Application of the set of five immobile element-based discriminant-function DF1-DF2 discrimination diagrams (see the subscript t1 in all these diagrams; Agrawal et al. 2008) for basic and ultrabasic rock samples from Styrian basin (Austria; Test study 6). The total number of samples and their % success values are given in Table S23 for the tectonic settings of island arc (IA), continental rift (CR), ocean island (OI), and mid-ocean ridge (MOR). The letter B after the name of the tectonic field represents basic (and also ultrabasic) magma. a. Four tectonic settings IA-CR+OI-MOR; b. Three tectonic settings IA-CR-OI; c. Three tectonic settings IA-CR-MOR; d. Three tectonic settings IA-OI-MOR; and e. Three tectonic settings CR-OI-MOR.

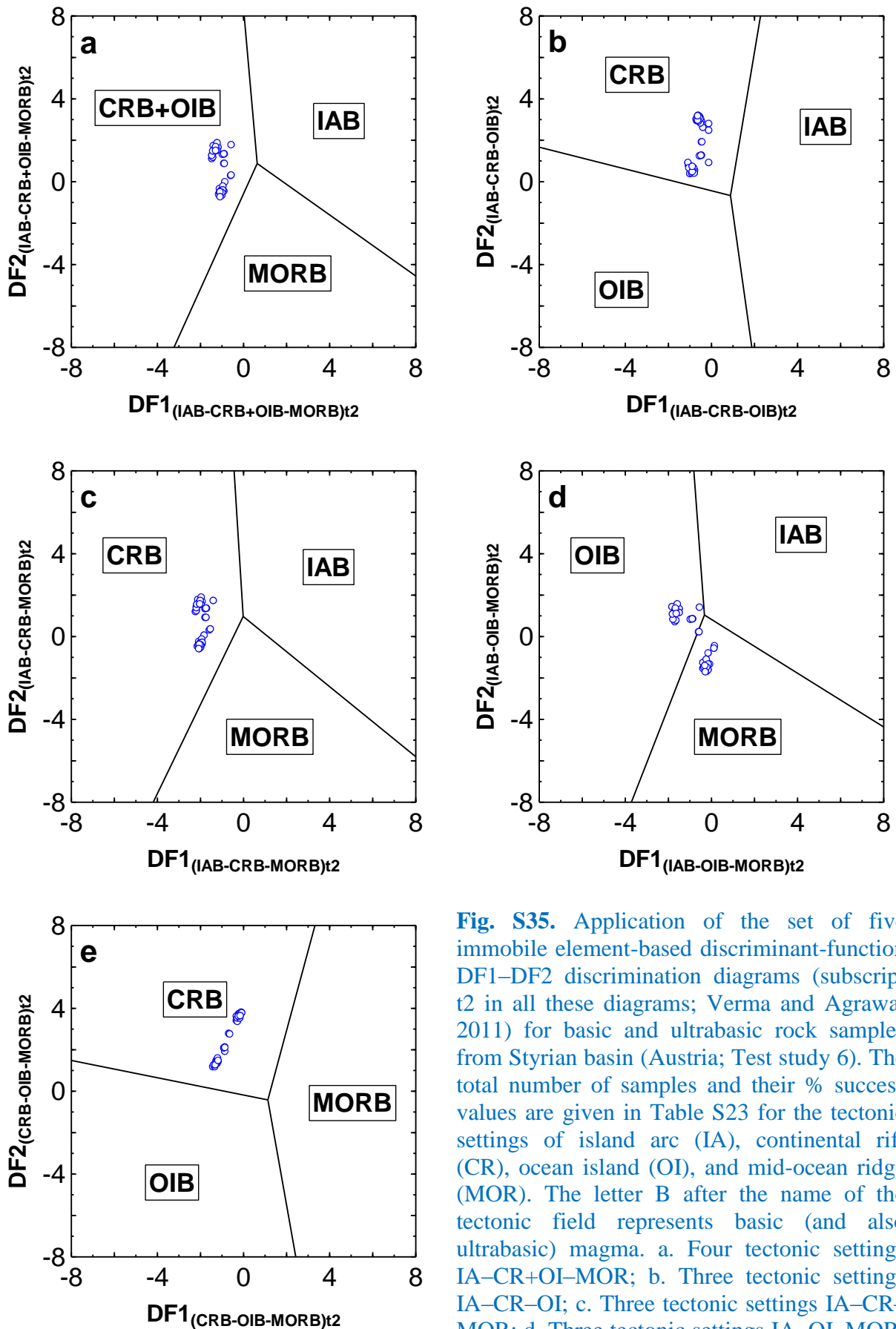


**Fig. S35.** Application of the set of five immobile element-based discriminant-function DF1-DF2 discrimination diagrams (subscript t2 in all these diagrams; Verma and Agrawal 2011) for basic and ultrabasic rock samples from Styrian basin (Austria; Test study 6). The total number of samples and their % success values are given in Table S23 for the tectonic settings of island arc (IA), continental rift (CR), ocean island (OI), and mid-ocean ridge (MOR). The letter B after the name of the tectonic field represents basic (and also ultrabasic) magma. a. Four tectonic settings IA-CR+OI-MOR; b. Three tectonic settings IA-CR-OI; c. Three tectonic settings IA-CR-MOR; d. Three tectonic settings IA-OI-MOR; and e. Three tectonic settings CR-OI-MOR.

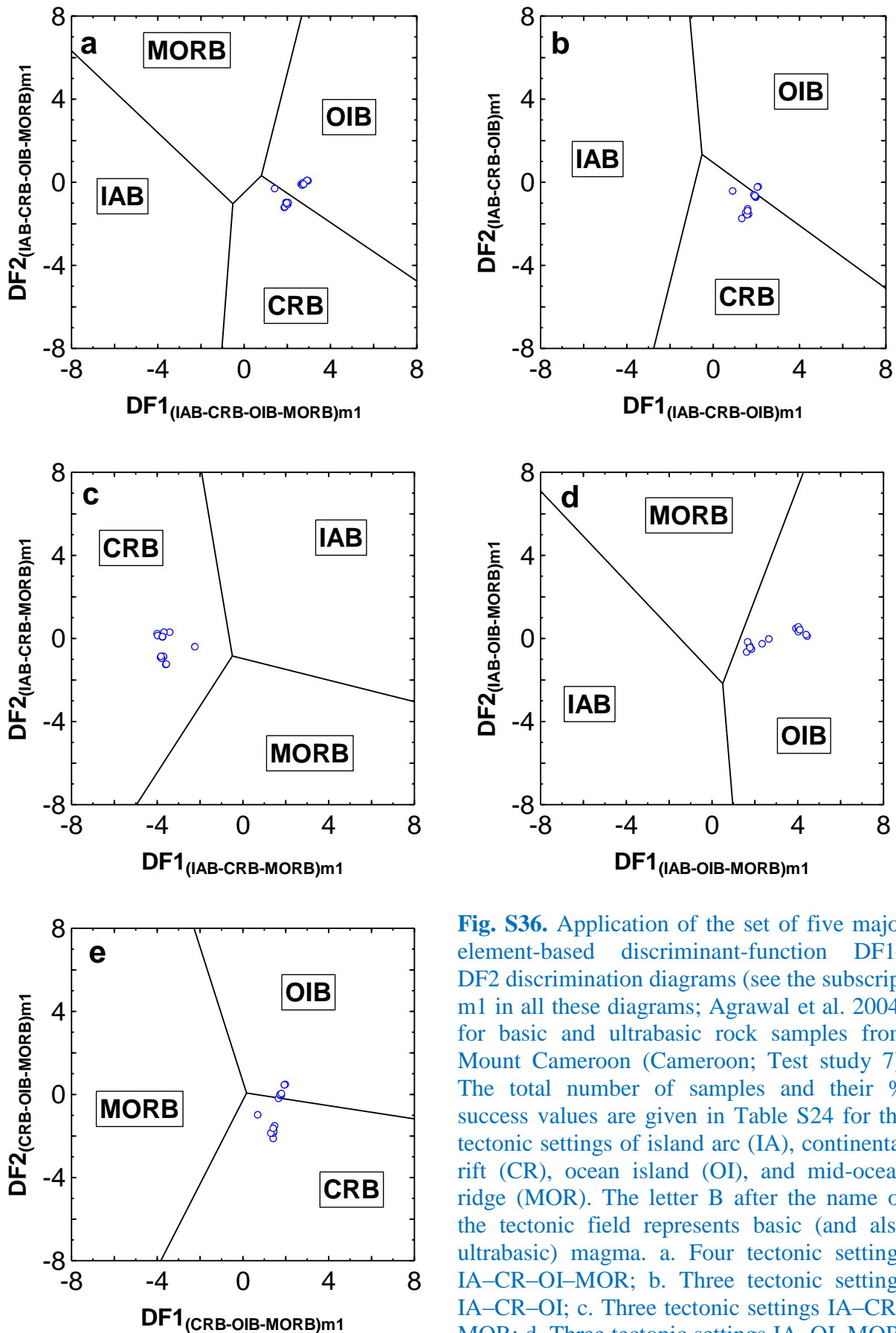


**Fig. S36.** Application of the set of five major element-based discriminant-function  $DF_1$ – $DF_2$  discrimination diagrams (see the subscript m1 in all these diagrams; Agrawal et al. 2004) for basic and ultrabasic rock samples from Mount Cameroon (Cameroon; Test study 7). The total number of samples and their % success values are given in Table S24 for the tectonic settings of island arc (IA), continental rift (CR), ocean island (OI), and mid-ocean ridge (MOR). The letter B after the name of the tectonic field represents basic (and also ultrabasic) magma. a. Four tectonic settings IA–CR–OI–MOR; b. Three tectonic settings IA–CR–OI; c. Three tectonic settings IA–CR–MOR; d. Three tectonic settings IA–OI–MOR; and e. Three tectonic settings CR–OI–MOR.

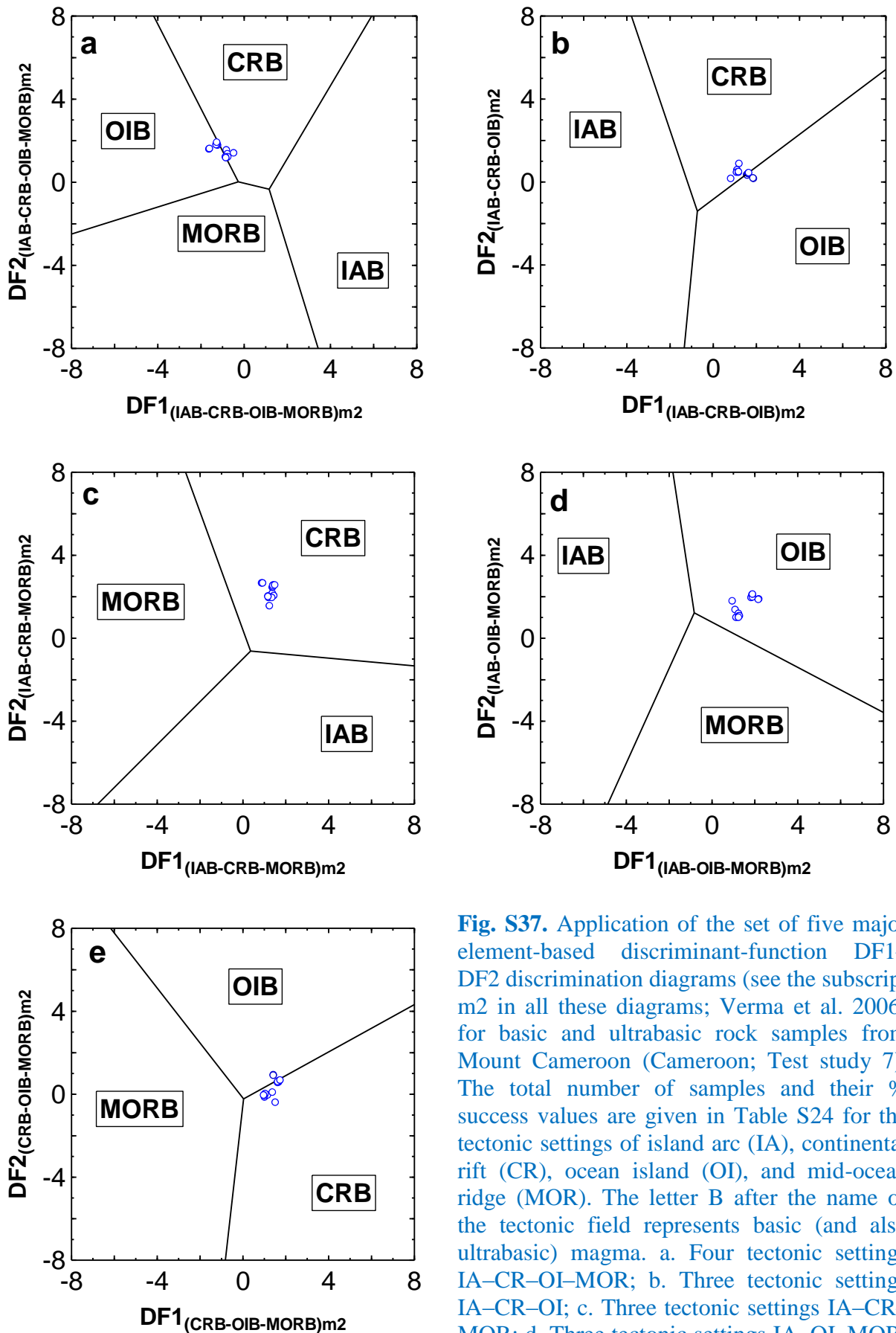


**Fig. S37.** Application of the set of five major element-based discriminant-function  $DF1-DF2$  discrimination diagrams (see the subscript m2 in all these diagrams; Verma et al. 2006) for basic and ultrabasic rock samples from Mount Cameroon (Cameroon; Test study 7). The total number of samples and their % success values are given in Table S24 for the tectonic settings of island arc (IA), continental rift (CR), ocean island (OI), and mid-ocean ridge (MOR). The letter B after the name of the tectonic field represents basic (and also ultrabasic) magma. a. Four tectonic settings IA–CR–OI–MOR; b. Three tectonic settings IA–CR–OI; c. Three tectonic settings IA–CR–MOR; d. Three tectonic settings IA–OI–MOR; and e. Three tectonic settings CR–OI–MOR.

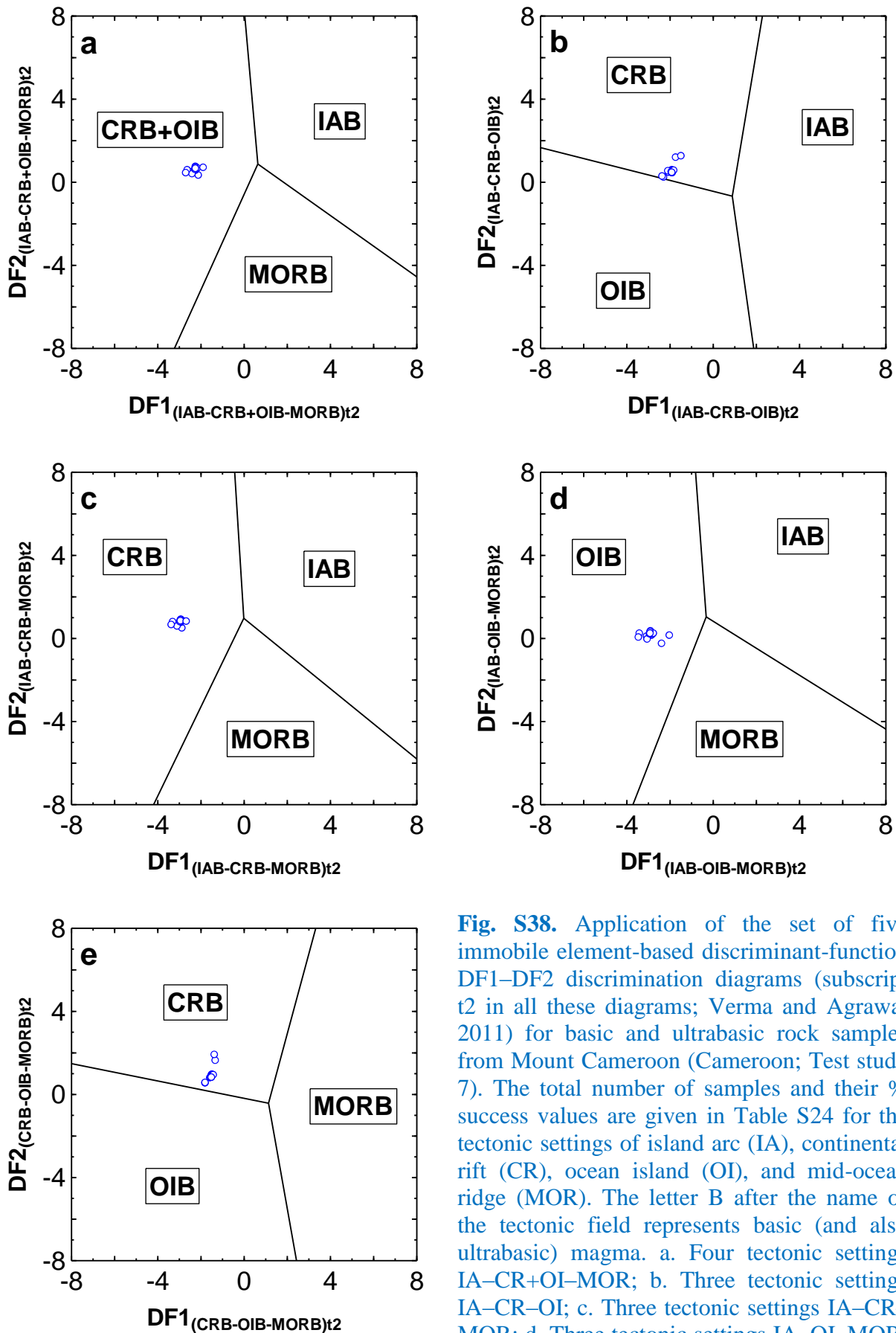


**Fig. S38.** Application of the set of five immobile element-based discriminant-function DF1-DF2 discrimination diagrams (subscript t2 in all these diagrams; Verma and Agrawal 2011) for basic and ultrabasic rock samples from Mount Cameroon (Cameroon; Test study 7). The total number of samples and their % success values are given in Table S24 for the tectonic settings of island arc (IA), continental rift (CR), ocean island (OI), and mid-ocean ridge (MOR). The letter B after the name of the tectonic field represents basic (and also ultrabasic) magma. a. Four tectonic settings IA-CR+OI-MOR; b. Three tectonic settings IA-CR-OI; c. Three tectonic settings IA-CR-MOR; d. Three tectonic settings IA-OI-MOR; and e. Three tectonic settings CR-OI-MOR.

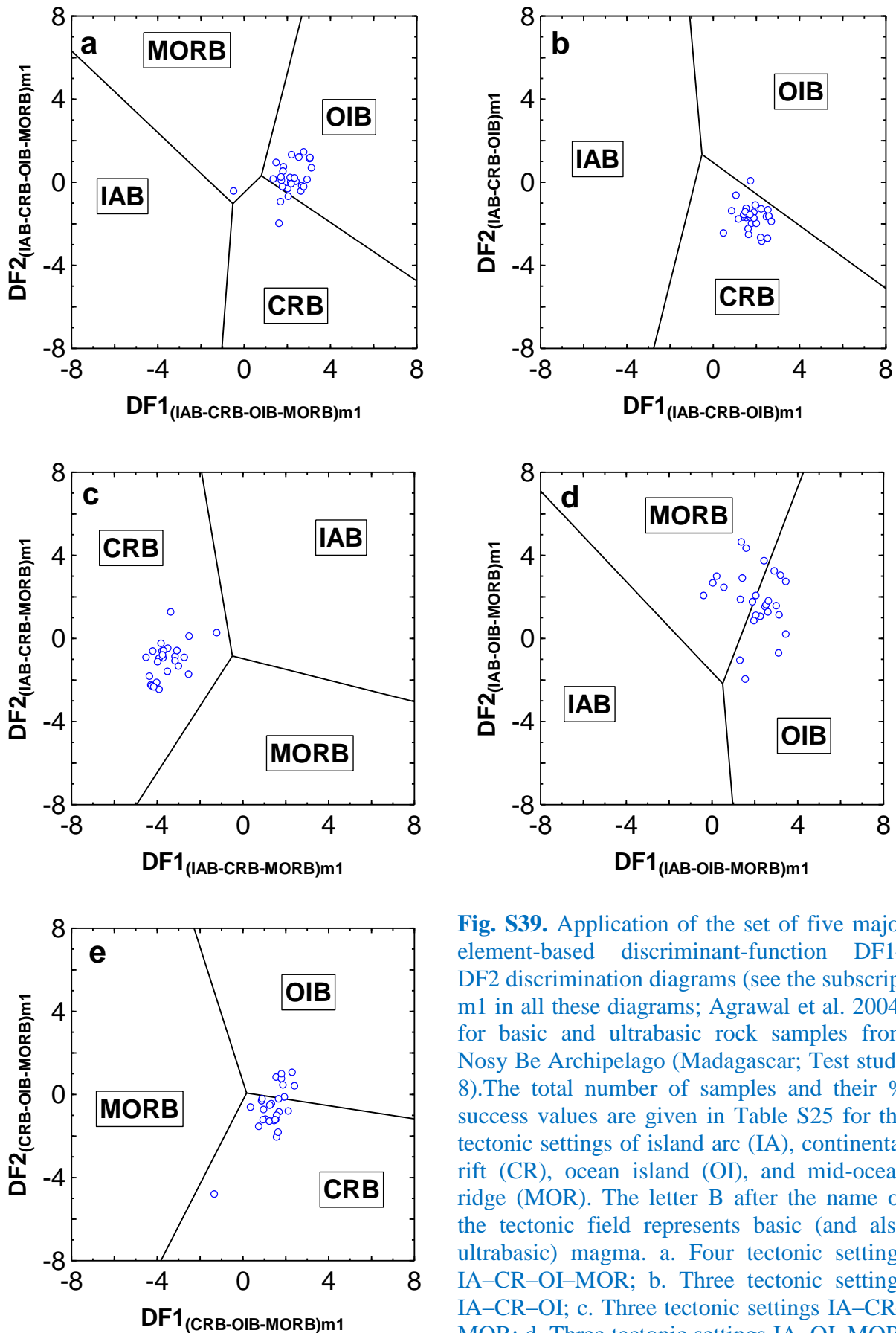


**Fig. S39.** Application of the set of five major element-based discriminant-function DF1–DF2 discrimination diagrams (see the subscript m1 in all these diagrams; Agrawal et al. 2004) for basic and ultrabasic rock samples from Nosy Be Archipelago (Madagascar; Test study 8). The total number of samples and their % success values are given in Table S25 for the tectonic settings of island arc (IA), continental rift (CR), ocean island (OI), and mid-ocean ridge (MOR). The letter B after the name of the tectonic field represents basic (and also ultrabasic) magma. a. Four tectonic settings IA–CR–OI–MOR; b. Three tectonic settings IA–CR–OI; c. Three tectonic settings IA–CR–MOR; d. Three tectonic settings IA–OI–MOR; and e. Three tectonic settings CR–OI–MOR.

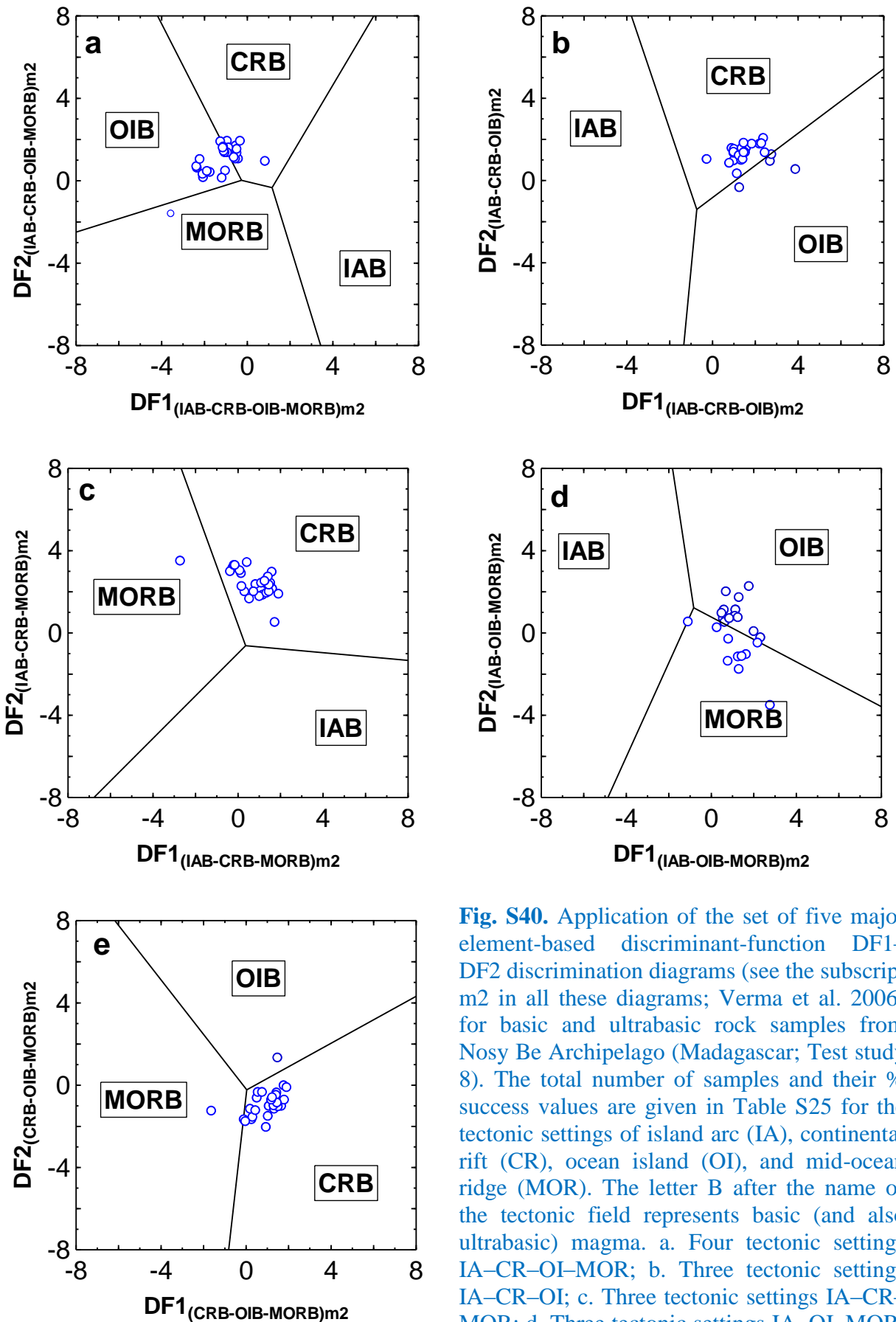


**Fig. S40.** Application of the set of five major element-based discriminant-function  $DF_1$ – $DF_2$  discrimination diagrams (see the subscript m2 in all these diagrams; Verma et al. 2006) for basic and ultrabasic rock samples from Nosy Be Archipelago (Madagascar; Test study 8). The total number of samples and their % success values are given in Table S25 for the tectonic settings of island arc (IA), continental rift (CR), ocean island (OI), and mid-ocean ridge (MOR). The letter B after the name of the tectonic field represents basic (and also ultrabasic) magma. a. Four tectonic settings IA–CR–OI–MOR; b. Three tectonic settings IA–CR–OI; c. Three tectonic settings IA–CR–MORB; d. Three tectonic settings IA–OI–MORB; and e. Three tectonic settings CR–OI–MORB.

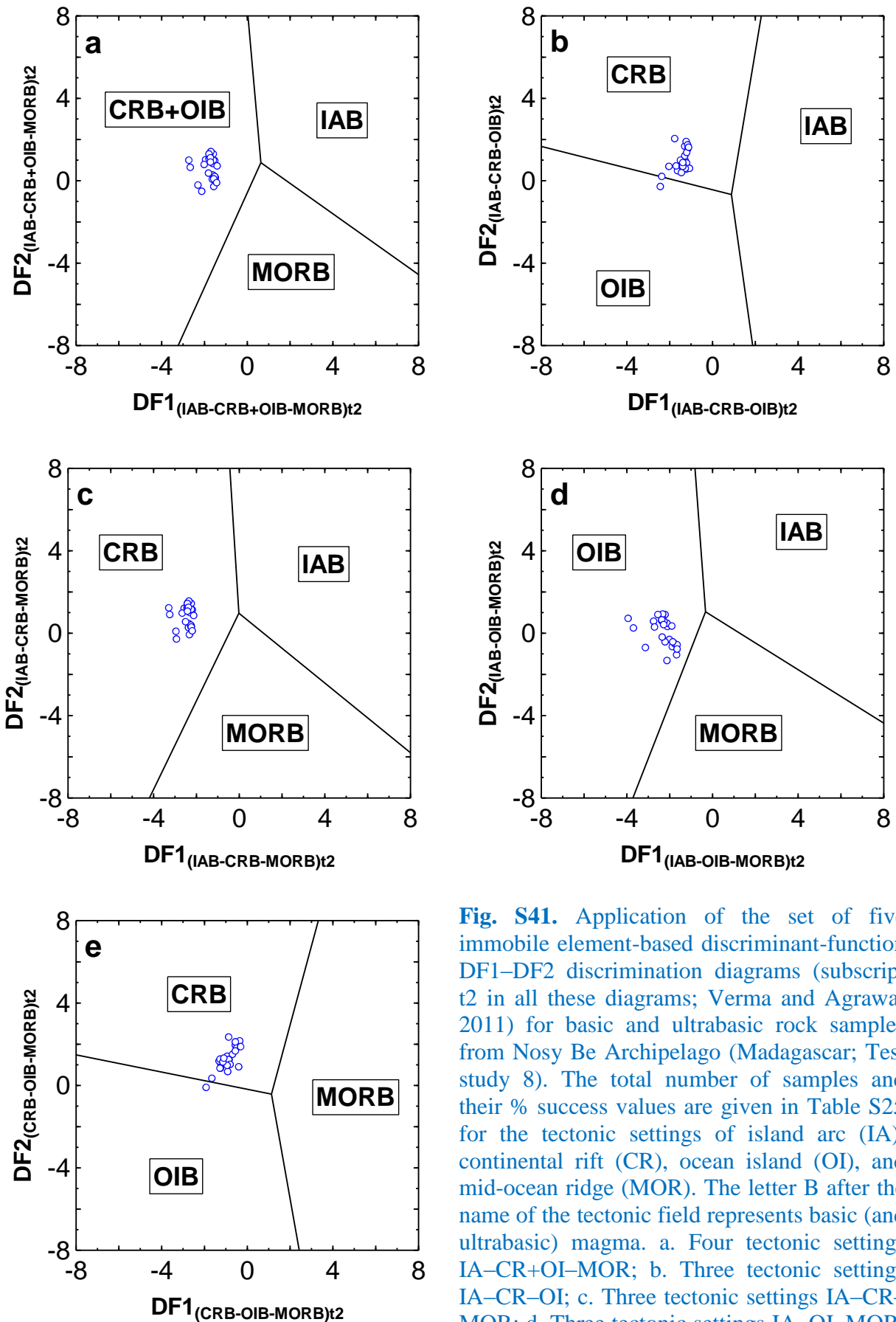


**Fig. S41.** Application of the set of five immobile element-based discriminant-function DF1–DF2 discrimination diagrams (subscript t2 in all these diagrams; Verma and Agrawal 2011) for basic and ultrabasic rock samples from Nosy Be Archipelago (Madagascar; Test study 8). The total number of samples and their % success values are given in Table S25 for the tectonic settings of island arc (IA), continental rift (CR), ocean island (OI), and mid-ocean ridge (MOR). The letter B after the name of the tectonic field represents basic (and ultrabasic) magma. a. Four tectonic settings IA–CR+OI–MOR; b. Three tectonic settings IA–CR–OI; c. Three tectonic settings IA–CR–MOR; d. Three tectonic settings IA–OI–MOR; and e. Three tectonic settings CR–OI–MOR.

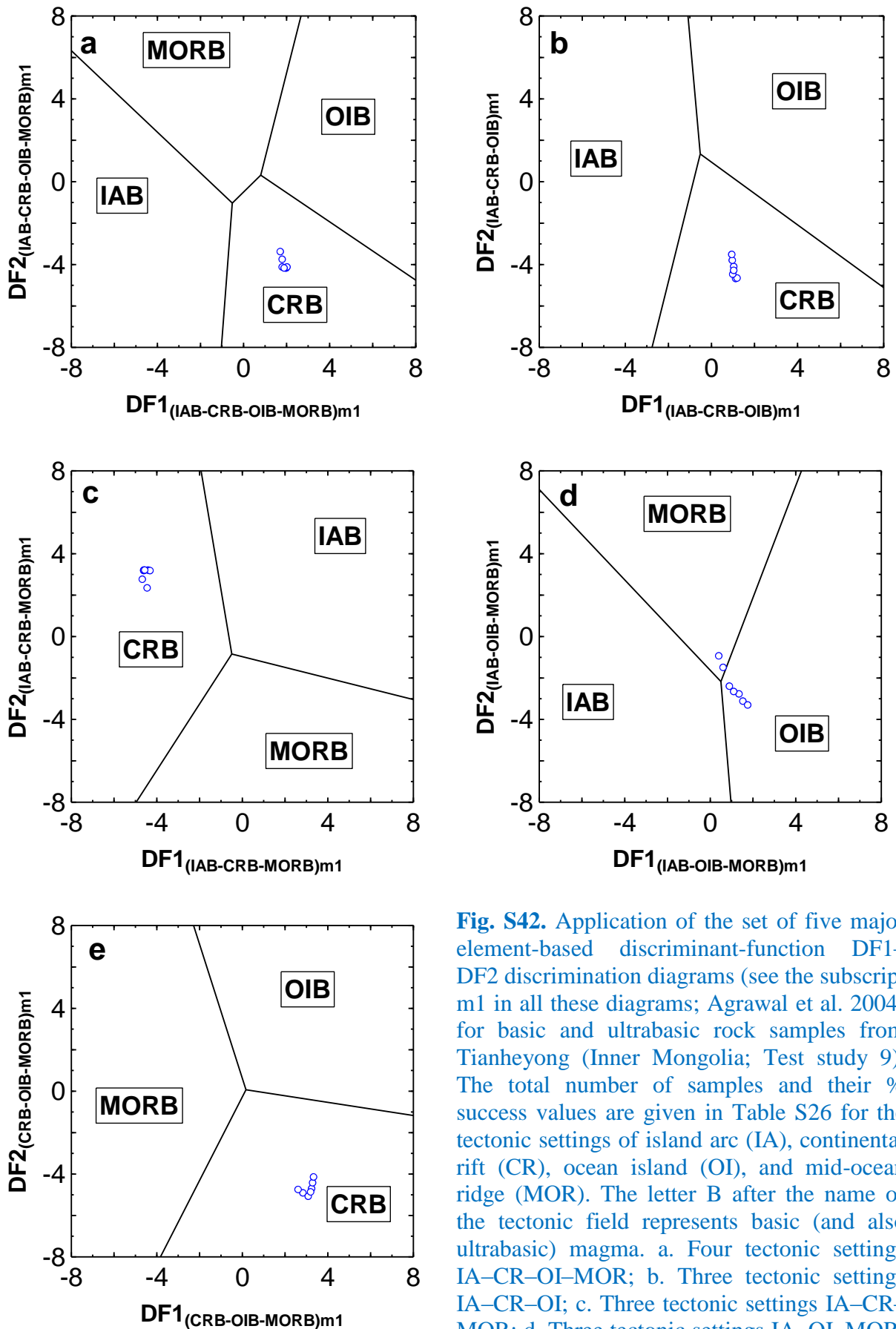


**Fig. S42.** Application of the set of five major element-based discriminant-function DF1–DF2 discrimination diagrams (see the subscript m1 in all these diagrams; Agrawal et al. 2004) for basic and ultrabasic rock samples from Tianheyong (Inner Mongolia; Test study 9). The total number of samples and their % success values are given in Table S26 for the tectonic settings of island arc (IA), continental rift (CR), ocean island (OI), and mid-ocean ridge (MOR). The letter B after the name of the tectonic field represents basic (and also ultrabasic) magma. a. Four tectonic settings IA–CR–OI–MOR; b. Three tectonic settings IA–CR–OI; c. Three tectonic settings IA–CR–MOR; d. Three tectonic settings IA–OI–MOR; and e. Three tectonic settings CR–OI–MOR.

ciii

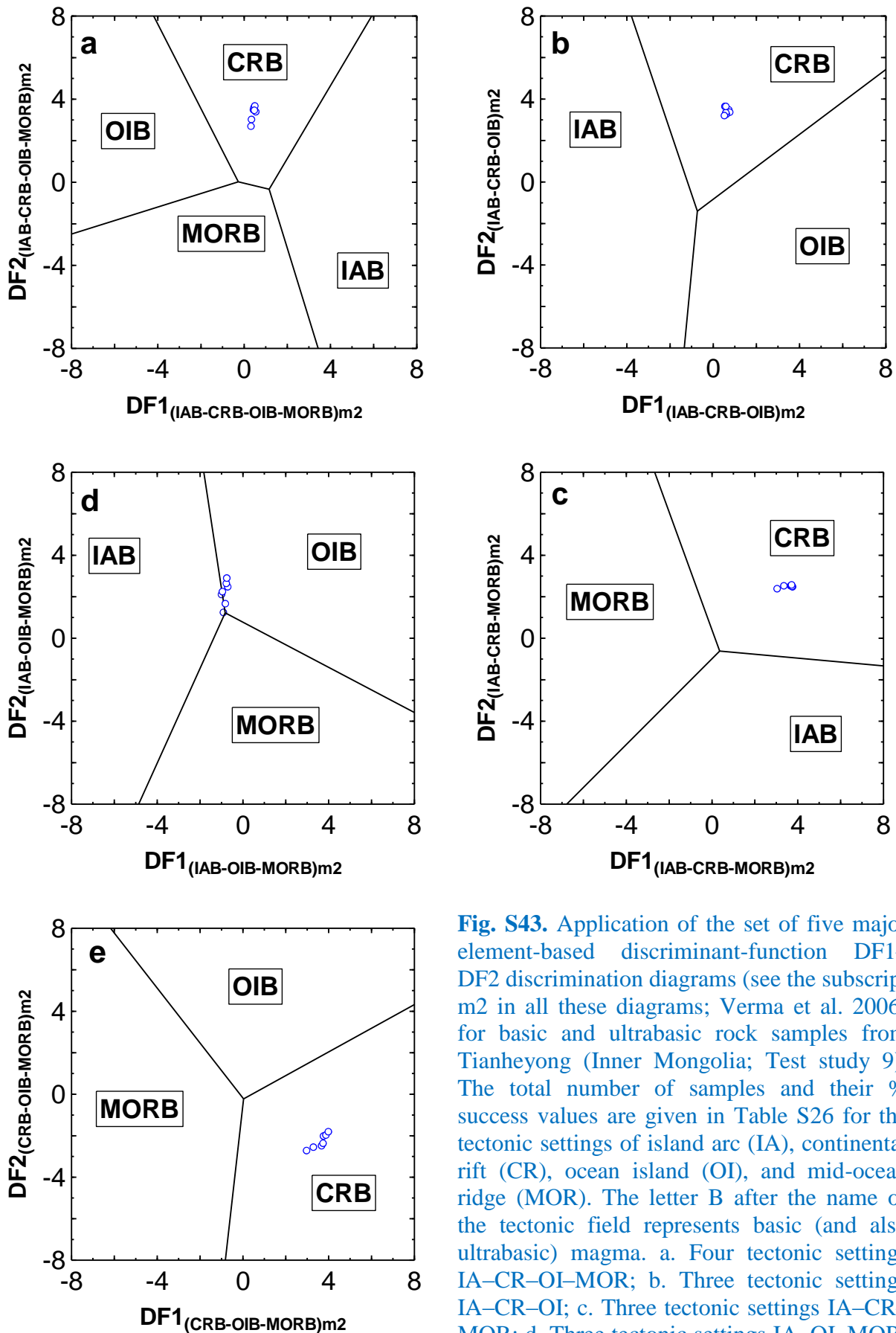


**Fig. S43.** Application of the set of five major element-based discriminant-function  $DF1-DF2$  discrimination diagrams (see the subscript m2 in all these diagrams; Verma et al. 2006) for basic and ultrabasic rock samples from Tianheyong (Inner Mongolia; Test study 9). The total number of samples and their % success values are given in Table S26 for the tectonic settings of island arc (IA), continental rift (CR), ocean island (OI), and mid-ocean ridge (MOR). The letter B after the name of the tectonic field represents basic (and also ultrabasic) magma. a. Four tectonic settings IA–CR–OI–MOR; b. Three tectonic settings IA–CR–OI; c. Three tectonic settings IA–CR–MOR; d. Three tectonic settings IA–OI–MOR; and e. Three tectonic settings CR–OI–MOR.

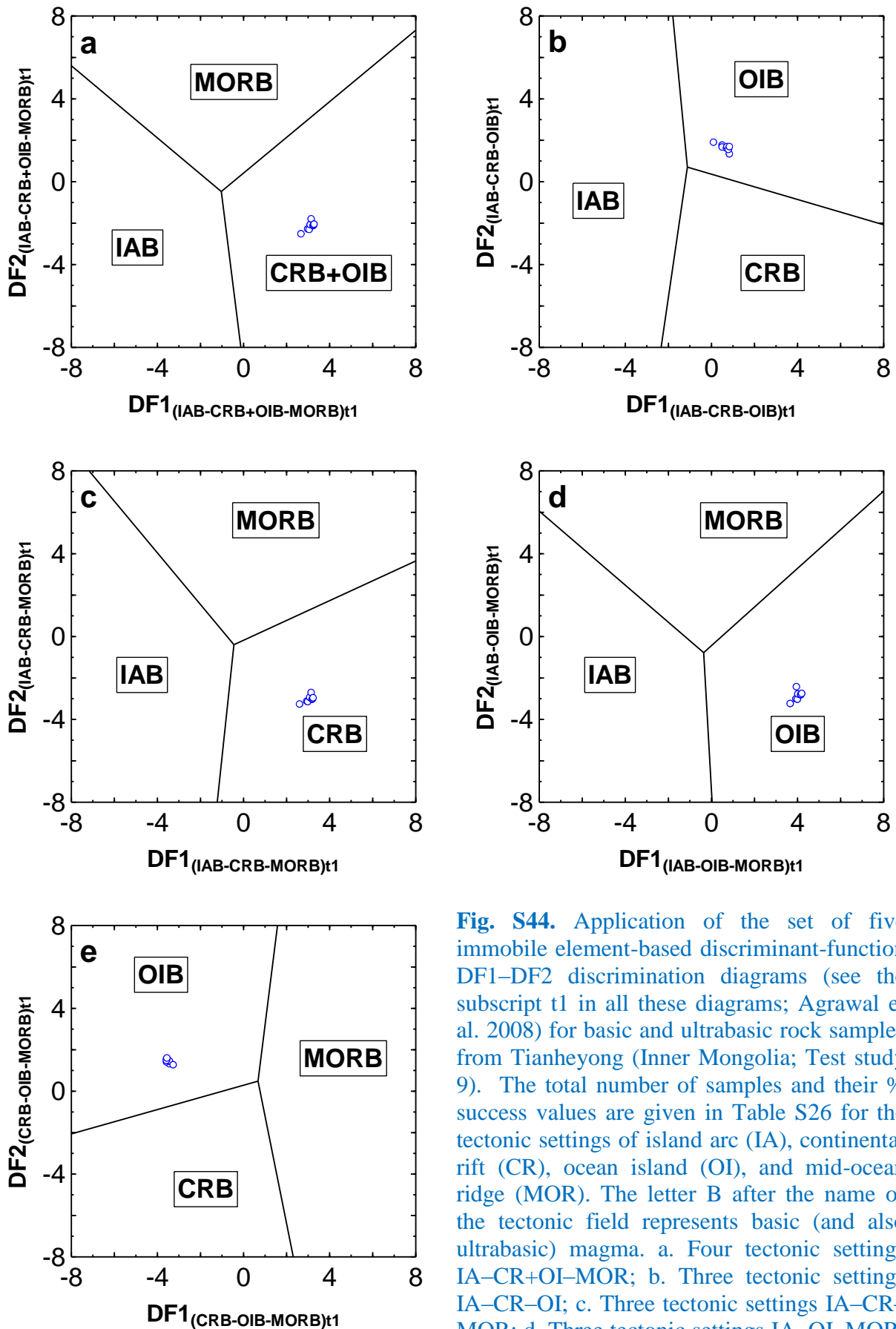


**Fig. S44.** Application of the set of five immobile element-based discriminant-function DF1-DF2 discrimination diagrams (see the subscript t1 in all these diagrams; Agrawal et al. 2008) for basic and ultrabasic rock samples from Tianheyong (Inner Mongolia; Test study 9). The total number of samples and their % success values are given in Table S26 for the tectonic settings of island arc (IA), continental rift (CR), ocean island (OI), and mid-ocean ridge (MOR). The letter B after the name of the tectonic field represents basic (and also ultrabasic) magma. a. Four tectonic settings IA-CR+OI-MOR; b. Three tectonic settings IA-CR-OI; c. Three tectonic settings IA-CR-MOR; d. Three tectonic settings IA-OI-MOR; and e. Three tectonic settings CR-OI-MOR

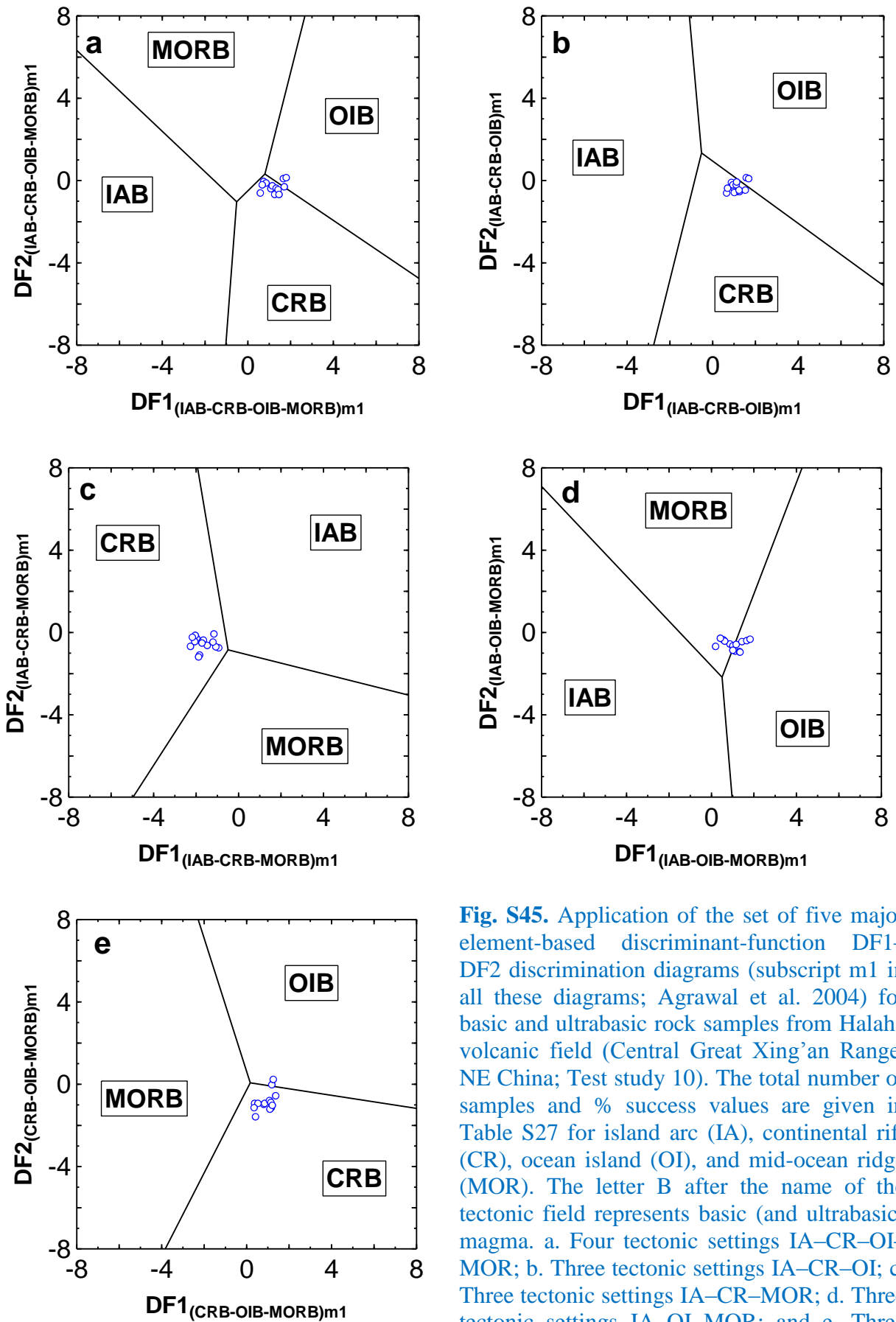


**Fig. S45.** Application of the set of five major element-based discriminant-function DF1–DF2 discrimination diagrams (subscript m1 in all these diagrams; Agrawal et al. 2004) for basic and ultrabasic rock samples from Halaha volcanic field (Central Great Xing'an Range, NE China; Test study 10). The total number of samples and % success values are given in Table S27 for island arc (IA), continental rift (CR), ocean island (OI), and mid-ocean ridge (MOR). The letter B after the name of the tectonic field represents basic (and ultrabasic) magma. a. Four tectonic settings IA–CR–OI–MOR; b. Three tectonic settings IA–CR–OI; c. Three tectonic settings IA–CR–MOR; d. Three tectonic settings IA–OI–MOR; and e. Three tectonic settings CR–OI–MOR.

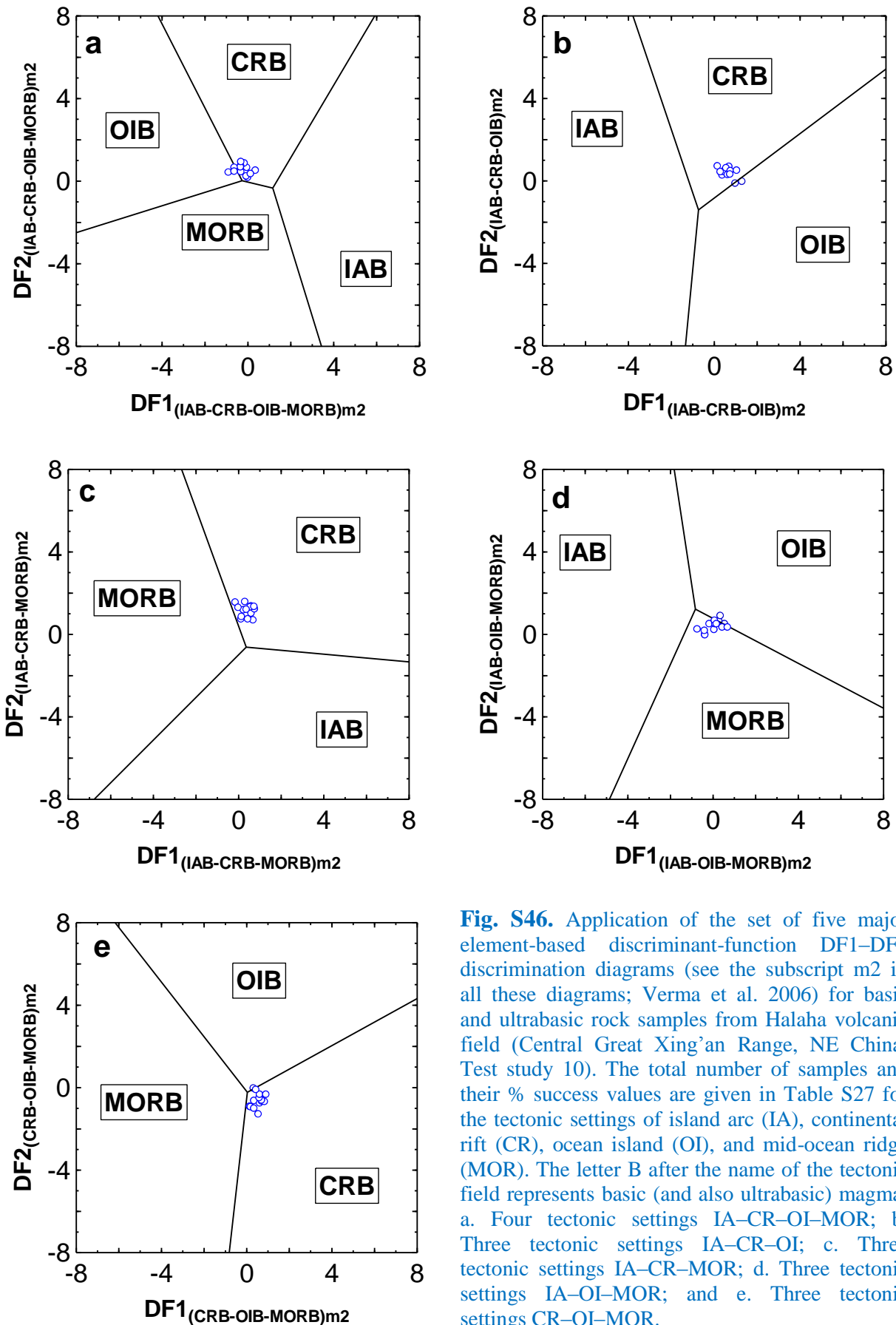


**Fig. S46.** Application of the set of five major element-based discriminant-function DF1-DF2 discrimination diagrams (see the subscript m2 in all these diagrams; Verma et al. 2006) for basic and ultrabasic rock samples from Halaha volcanic field (Central Great Xing'an Range, NE China; Test study 10). The total number of samples and their % success values are given in Table S27 for the tectonic settings of island arc (IA), continental rift (CR), ocean island (OI), and mid-ocean ridge (MOR). The letter B after the name of the tectonic field represents basic (and also ultrabasic) magma.

- Four tectonic settings IA-CR-OI-MOR;
- Three tectonic settings IA-CR-OI;
- Three tectonic settings IA-CR-MOR;
- Three tectonic settings IA-OI-MOR;
- Three tectonic settings CR-OI-MOR.

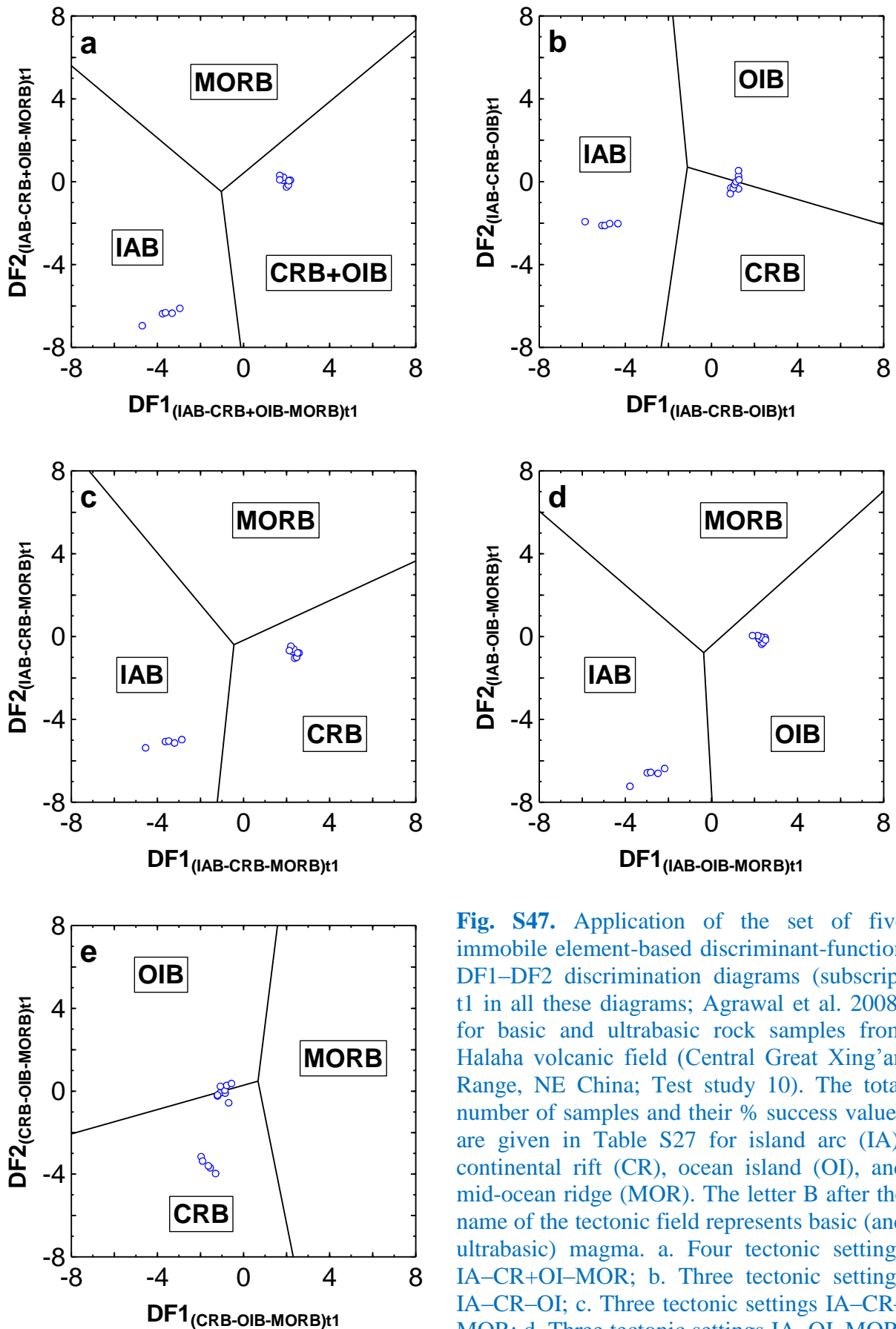


**Fig. S47.** Application of the set of five immobile element-based discriminant-function DF1-DF2 discrimination diagrams (subscript t1 in all these diagrams; Agrawal et al. 2008) for basic and ultrabasic rock samples from Halaha volcanic field (Central Great Xing'an Range, NE China; Test study 10). The total number of samples and their % success values are given in Table S27 for island arc (IA), continental rift (CR), ocean island (OI), and mid-ocean ridge (MOR). The letter B after the name of the tectonic field represents basic (and ultrabasic) magma. a. Four tectonic settings IA-CR+OI-MOR; b. Three tectonic settings IA-CR-OI; c. Three tectonic settings IA-CR-MOR; d. Three tectonic settings IA-OI-MOR; and e. Three tectonic settings CR-OI-MOR.

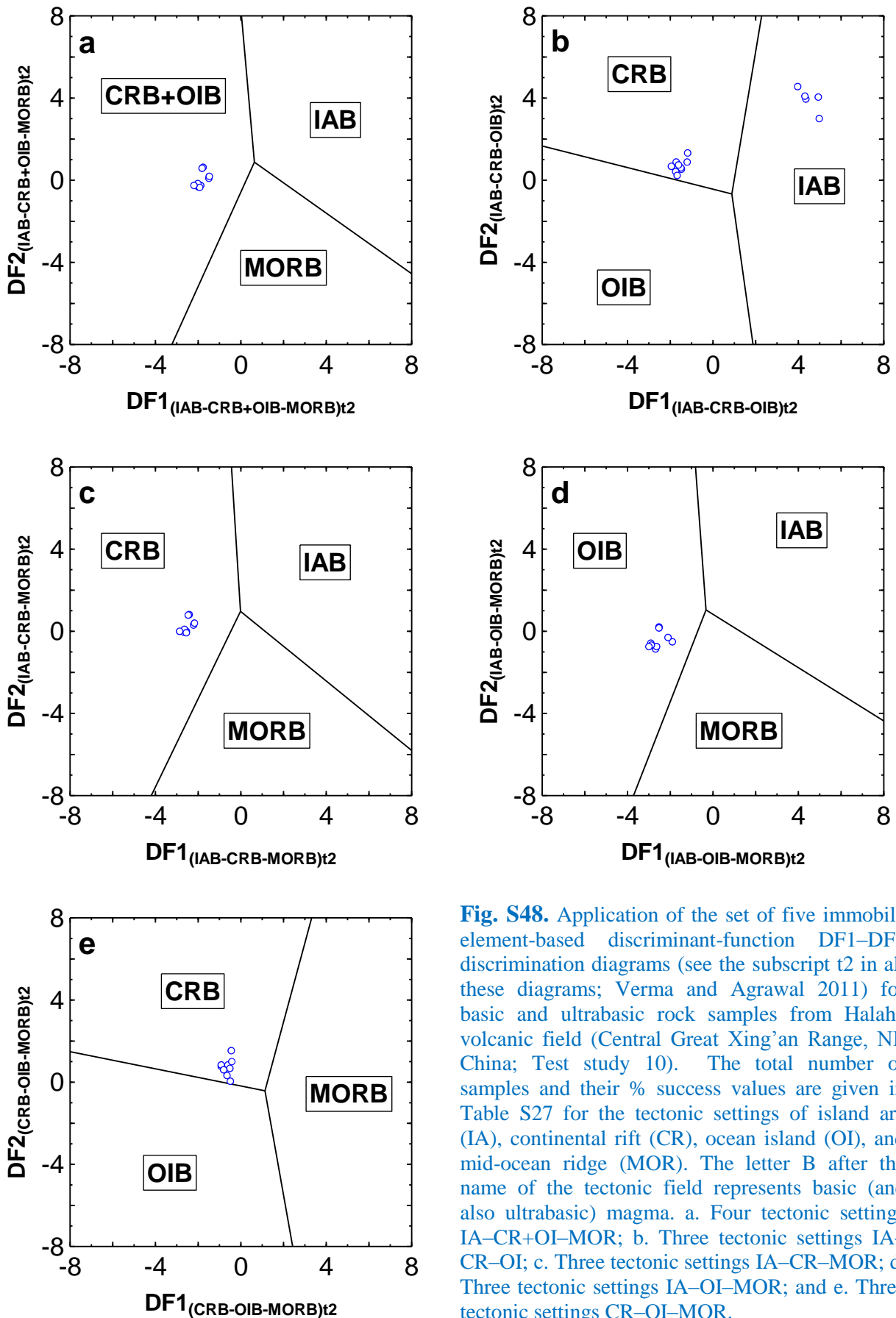


**Fig. S48.** Application of the set of five immobile element-based discriminant-function DF1-DF2 discrimination diagrams (see the subscript t2 in all these diagrams; Verma and Agrawal 2011) for basic and ultrabasic rock samples from Halaha volcanic field (Central Great Xing'an Range, NE China; Test study 10). The total number of samples and their % success values are given in Table S27 for the tectonic settings of island arc (IA), continental rift (CR), ocean island (OI), and mid-ocean ridge (MOR). The letter B after the name of the tectonic field represents basic (and also ultrabasic) magma. a. Four tectonic settings IA-CR+OI-MOR; b. Three tectonic settings IA-CR-OI; c. Three tectonic settings IA-CR-MOR; d. Three tectonic settings IA-OI-MOR; and e. Three tectonic settings CR-OI-MOR.

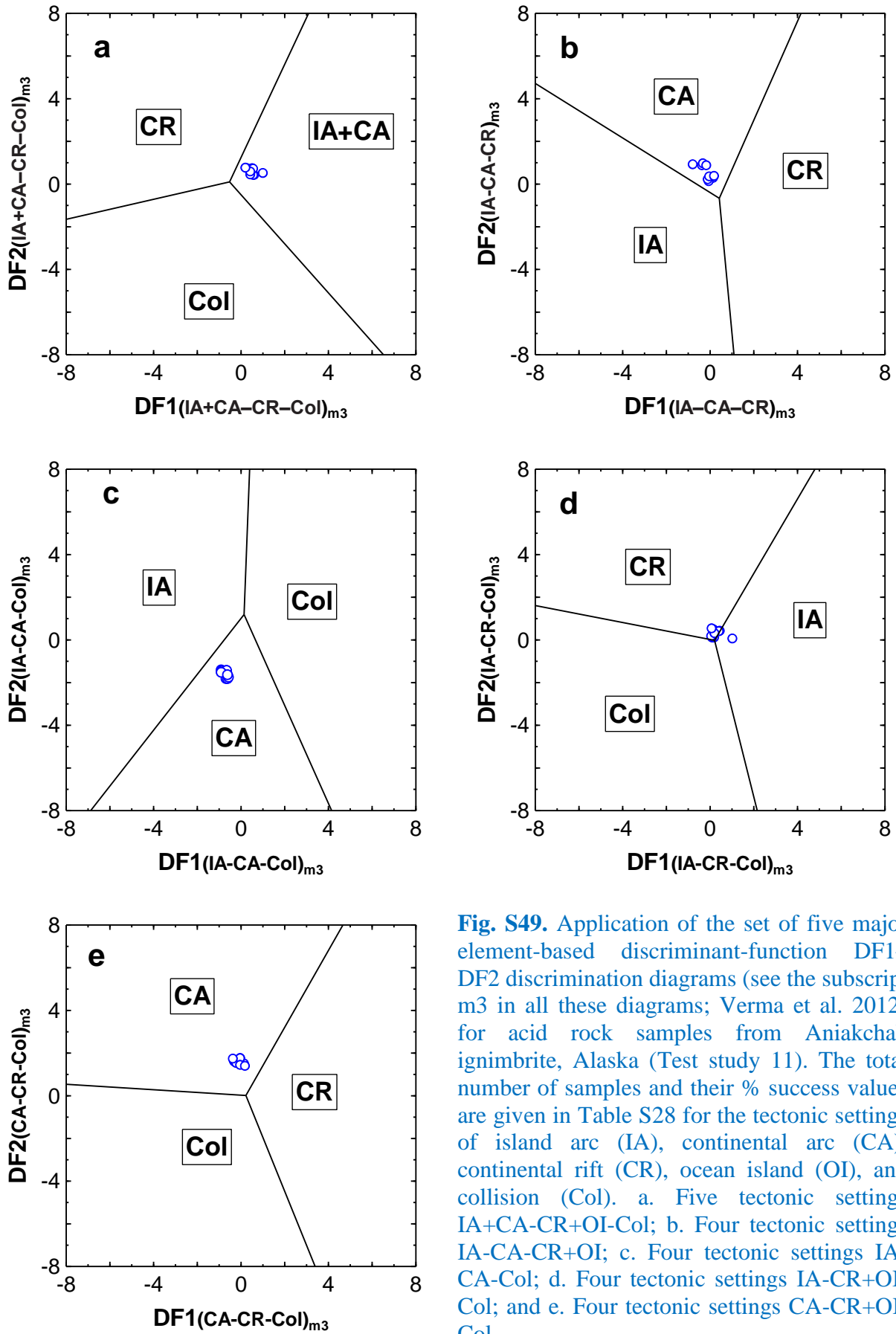


**Fig. S49.** Application of the set of five major element-based discriminant-function DF1–DF2 discrimination diagrams (see the subscript  $\text{m}^3$  in all these diagrams; Verma et al. 2012) for acid rock samples from Aniakchak ignimbrite, Alaska (Test study 11). The total number of samples and their % success values are given in Table S28 for the tectonic settings of island arc (IA), continental arc (CA), continental rift (CR), ocean island (OI), and collision (Col). a. Five tectonic settings IA+CA-CR+OI-Col; b. Four tectonic settings IA-CA-CR+OI; c. Four tectonic settings IA-CA-Col; d. Four tectonic settings IA-CR+OI-Col; and e. Four tectonic settings CA-CR+OI-Col.

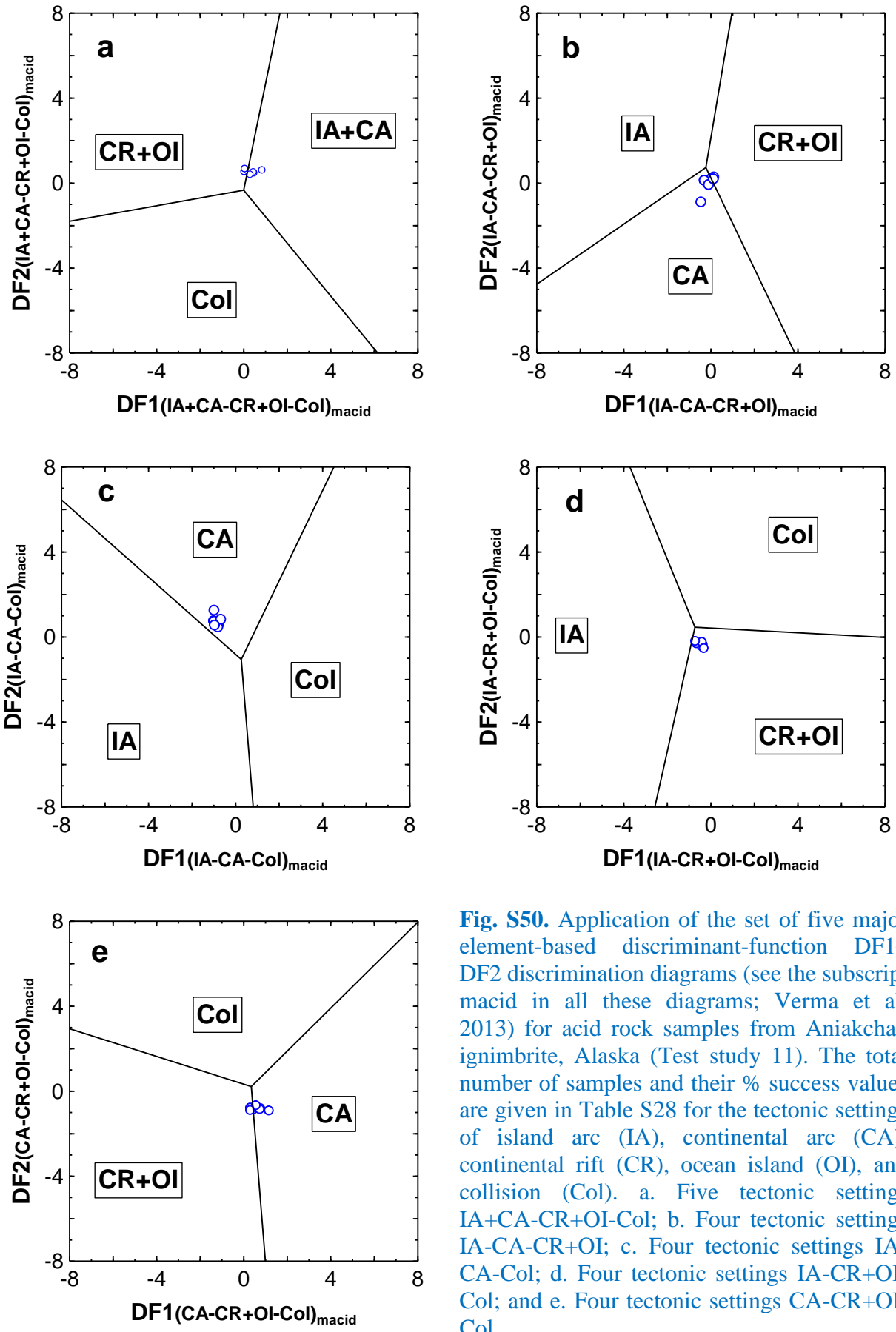


**Fig. S50.** Application of the set of five major element-based discriminant-function DF1–DF2 discrimination diagrams (see the subscript macid in all these diagrams; Verma et al. 2013) for acid rock samples from Aniakchak ignimbrite, Alaska (Test study 11). The total number of samples and their % success values are given in Table S28 for the tectonic settings of island arc (IA), continental arc (CA), continental rift (CR), ocean island (OI), and collision (Col). a. Five tectonic settings IA+CA-CR+OI-Col; b. Four tectonic settings IA-CA-CR+OI; c. Four tectonic settings IA-CA-Col; d. Four tectonic settings IA-CR+OI-Col; and e. Four tectonic settings CA-CR+OI-Col.

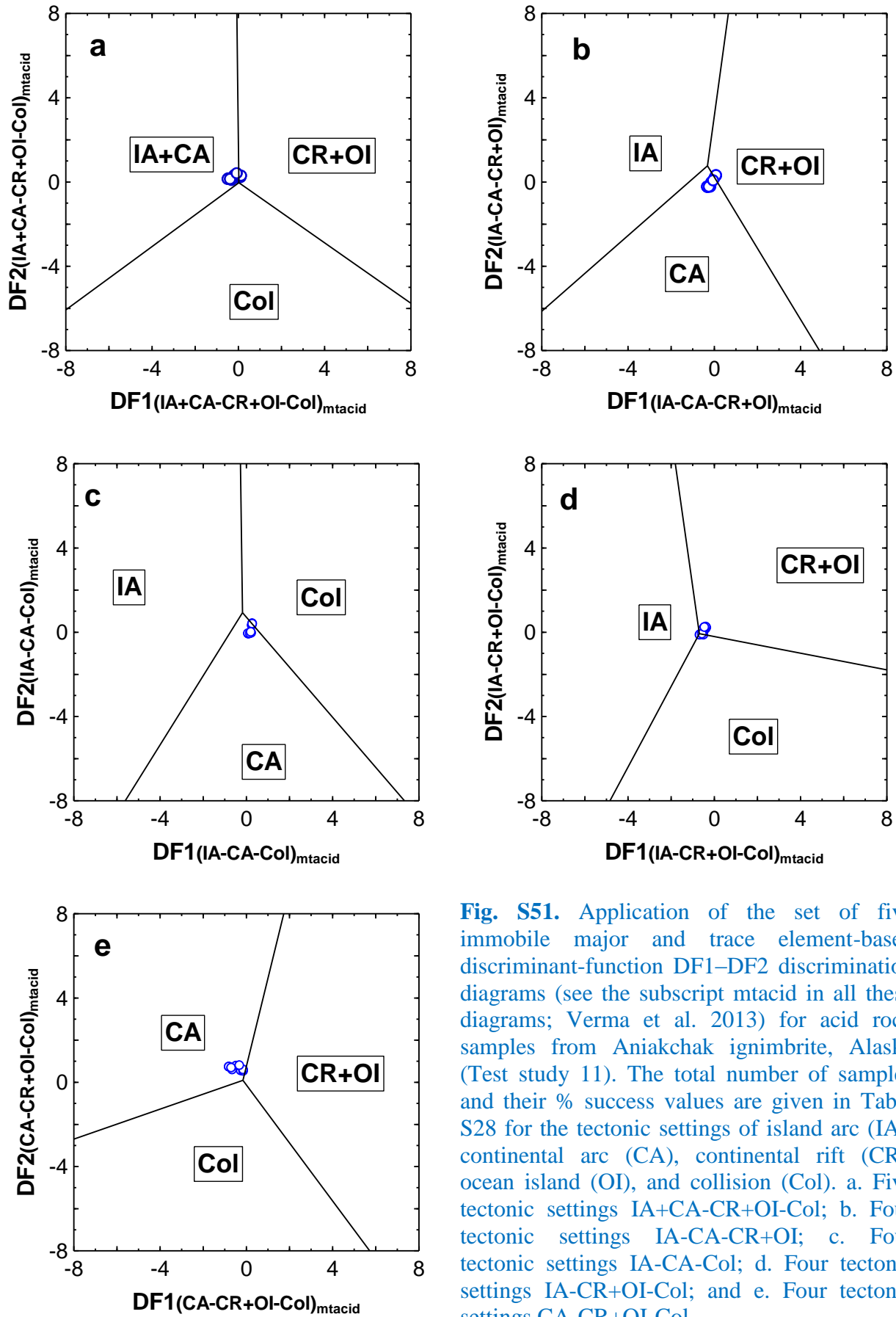


**Fig. S51.** Application of the set of five immobile major and trace element-based discriminant-function DF1–DF2 discrimination diagrams (see the subscript mtacid in all these diagrams; Verma et al. 2013) for acid rock samples from Aniakchak ignimbrite, Alaska (Test study 11). The total number of samples and their % success values are given in Table S28 for the tectonic settings of island arc (IA), continental arc (CA), continental rift (CR), ocean island (OI), and collision (Col). a. Five tectonic settings IA+CA-CR+OI-Col; b. Four tectonic settings IA-CA-CR+OI; c. Four tectonic settings IA-CA-Col; d. Four tectonic settings IA-CR+OI-Col; and e. Four tectonic settings CA-CR+OI-Col.

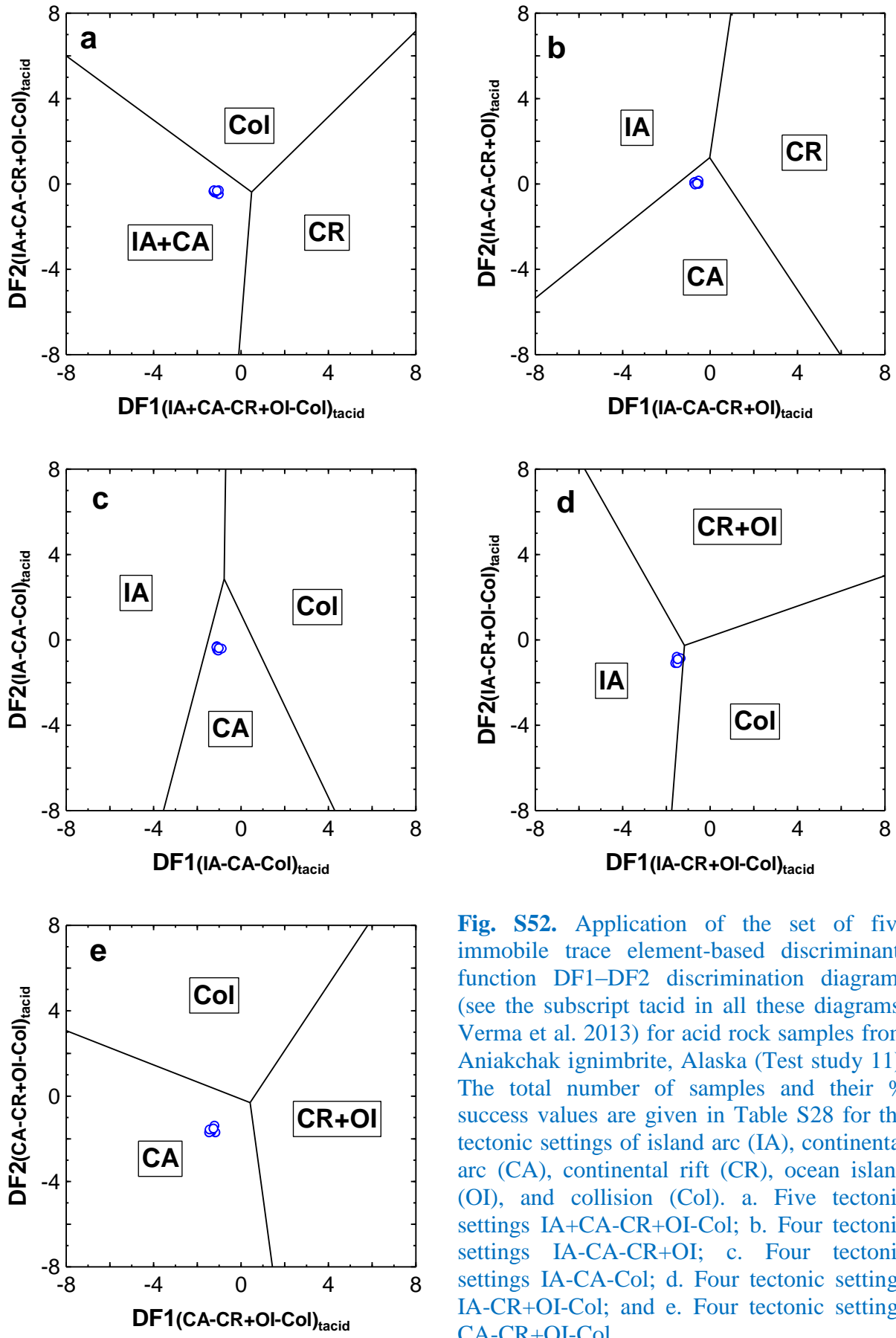


**Fig. S52.** Application of the set of five immobile trace element-based discriminant-function DF1–DF2 discrimination diagrams (see the subscript tacid in all these diagrams; Verma et al. 2013) for acid rock samples from Aniakchak ignimbrite, Alaska (Test study 11). The total number of samples and their % success values are given in Table S28 for the tectonic settings of island arc (IA), continental arc (CA), continental rift (CR), ocean island (OI), and collision (Col). a. Five tectonic settings IA+CA-CR+OI-Col; b. Four tectonic settings IA-CA-CR+OI; c. Four tectonic settings IA-CA-Col; d. Four tectonic settings IA-CR+OI-Col; and e. Four tectonic settings CA-CR+OI-Col.